

MICROCOPY RESOLUTION TEST CHART
NATIONAL BUREAU OF STANDARDS-1963-A

AD-A172 236

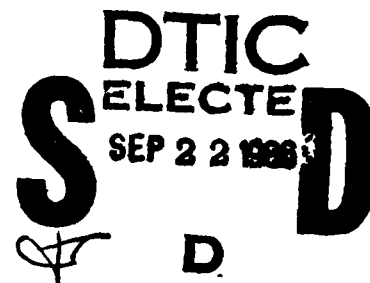
AFWAL-TR-86-4033



2

FAILURE ANALYSIS OF COMPOSITE STRUCTURE MATERIALS

Brian Smith
Ray Grove
Thomas Munns
Boeing Military Aircraft Company
P.O. Box 3707 M/S 73-43
Seattle, WA 98124



May 1986
Interim Report for 18 July 1984 to 1 October 1985

Approved for public release; distribution is unlimited.

MATERIALS LABORATORY
AIR FORCE WRIGHT AERONAUTICAL LABORATORIES
AIR FORCE SYSTEMS COMMAND
WRIGHT-PATTERSON AIR FORCE BASE, OH 45433-6533

86 9 19 001

ORIGINAL FILE COPY

REPORT DOCUMENTATION PAGE

AD-A172 236

1a. REPORT SECURITY CLASSIFICATION <p align="center">UNCLASSIFIED</p>			1b. RESTRICTIVE MARKINGS										
2a. SECURITY CLASSIFICATION AUTHORITY			3. DISTRIBUTION/AVAILABILITY OF REPORT <p align="center">Approved for public release; distribution is unlimited.</p>										
2b. DECLASSIFICATION/DOWNGRADING SCHEDULE													
4. PERFORMING ORGANIZATION REPORT NUMBER(S)			5. MONITORING ORGANIZATION REPORT NUMBER(S) <p align="center">AFWAL-TR-86-4033</p>										
6a. NAME OF PERFORMING ORGANIZATION <p align="center">Boeing Military Airplane Co.</p>		6b. OFFICE SYMBOL (if applicable)	7a. NAME OF MONITORING ORGANIZATION <p align="center">Air Force Wright Aeronautical Laboratory, Materials Laboratory, Systems Support Division (AFWAL/MLSE)</p>										
6c. ADDRESS (City, State and ZIP Code) <p align="center">P.O. Box 3707 MS 73-43 Seattle, WA 98124</p>			7b. ADDRESS (City, State and ZIP Code) <p align="center">Wright Patterson AFB, OH 45433-6533</p>										
8a. NAME OF FUNDING/SPONSORING ORGANIZATION		8b. OFFICE SYMBOL (if applicable) <p align="center">AFWAL/MLSE</p>	9. PROCUREMENT INSTRUMENT IDENTIFICATION NUMBER <p align="center">Contract No. F33615-84-C-5010</p>										
8c. ADDRESS (City, State and ZIP Code) <p align="center">WPAFB, OH 45433-6533</p>			10. SOURCE OF FUNDING NOS. <table border="1" style="width:100%; border-collapse: collapse; margin-top: 5px;"> <thead> <tr> <th style="width:25%;">PROGRAM ELEMENT NO.</th> <th style="width:25%;">PROJECT NO.</th> <th style="width:25%;">TASK NO.</th> <th style="width:25%;">WORK UNIT NO.</th> </tr> </thead> <tbody> <tr> <td align="center">62102F</td> <td align="center">2418</td> <td align="center">04</td> <td align="center">31</td> </tr> </tbody> </table>			PROGRAM ELEMENT NO.	PROJECT NO.	TASK NO.	WORK UNIT NO.	62102F	2418	04	31
PROGRAM ELEMENT NO.	PROJECT NO.	TASK NO.	WORK UNIT NO.										
62102F	2418	04	31										
11. TITLE (Include Security Classification) <p align="center">Failure Analysis of Composite Structure Materials (U)</p>													
12. PERSONAL AUTHOR(S) <p align="center">Brian Smith, Ray Grove, Thomas Munns</p>													
13a. TYPE OF REPORT <p align="center">Interim</p>		13b. TIME COVERED FROM 18 July 84 TO 1 Oct. 85		14. DATE OF REPORT (Yr., Mo., Day) <p align="center">May 1986</p>	15. PAGE COUNT <p align="center">225</p>								
16. SUPPLEMENTARY NOTATION													
17. COSATI CODES <table border="1" style="width:100%; border-collapse: collapse; margin-top: 5px;"> <thead> <tr> <th style="width:33%;">FIELD</th> <th style="width:33%;">GROUP</th> <th style="width:33%;">SUB GR.</th> </tr> </thead> <tbody> <tr> <td align="center">11</td> <td align="center">04</td> <td></td> </tr> </tbody> </table>			FIELD	GROUP	SUB GR.	11	04		18. SUBJECT TERMS (Continue on reverse if necessary and identify by block number) <p align="center">Composites, composite structure, failure analysis, fractography, graphite/epoxy, stress analysis, non-destructive evaluation, materials characterization</p>				
FIELD	GROUP	SUB GR.											
11	04												
19. ABSTRACT (Continue on reverse if necessary and identify by block number) <p>The objectives of the Failure Analysis for Composite Structural Materials program are to develop analytical and diagnostic techniques that can be used for determining the causes of failure in composite materials and to incorporate these results into a compendium of procedures which may be used as a reference manual when conducting a postfailure analysis of a composite structure, given the failed part as the starting point of the investigation. Such techniques include flowcharts describing the logical arrangement of investigative operations along with diagnostic procedures that will reveal the cause and mechanism of failure. To achieve these objectives, this program is divided into five tasks. (Continued on next page.)</p>													
20. DISTRIBUTION/AVAILABILITY OF ABSTRACT UNCLASSIFIED/UP LIMITED <input checked="" type="checkbox"/> SAME AS RPT. <input type="checkbox"/> DTIC USERS <input type="checkbox"/>				21. ABSTRACT SECURITY CLASSIFICATION <p align="center">UNCLASSIFIED</p>									
22a. NAME OF RESPONSIBLE INDIVIDUAL <p align="center">Frank Fechek</p>		22b. TELEPHONE NUMBER (Include Area Code) <p align="center">513/255-7483</p>		22c. OFFICE SYMBOL <p align="center">AFWAL/MLSE</p>									

REPORT DOCUMENTATION PAGE

19. ABSTRACT (Continue on reverse if necessary and identify by block number)

(Continued)

- Task 1 - Literature search and diagnostic technique selection
- Task 2 - Specimen production and test
- Task 3 - Diagnostic technique evaluation
- Task 4 - Creation of a failure analysis compendium
- Task 5 - Evaluation and demonstration of techniques

This interim report summarizes the progress and findings of activities carried out for Tasks 1 through 3 which identified, organized, and examined a variety of postfailure analysis methods for composite materials. Because such failures may arise from a wide variety of causes, analysis techniques examined included four basic disciplines: nondestructive evaluation (NDE), stress analysis, fractography, and materials characterization.

SUMMARY

The objectives of the Failure Analysis for Composite Structural Materials program are to develop analytical and diagnostic techniques that can be used for determining the causes of failure in composite materials and to incorporate these results into a compendium of procedures which may be used as a reference manual when conducting a postfailure analysis of a composite structure, given the failed part as the starting point of the investigation. Such techniques include flowcharts describing the logical arrangement of investigative operations along with diagnostic procedures that will reveal the cause and mechanism of failure. To achieve these objectives, this program is divided into five tasks.

- o Task 1—Literature search and diagnostic technique selection;
- o Task 2—Specimen production and test;
- o Task 3—Diagnostic technique evaluation;
- o Task 4—Creation of a failure analysis compendium; and
- o Task 5—Evaluation and demonstration of techniques.

This interim report summarizes the progress and findings of activities carried out for Tasks 1 through 3 which identified, organized, and examined a variety of postfailure analysis methods for composite materials. Because such failures may arise from a wide variety of causes, analysis techniques examined included four basic disciplines: nondestructive evaluation (NDE), stress analysis, fractography, and materials characterization.

In Task 1, each of these disciplines was reviewed, and specific methods valuable to the postmortem analysis of failed composite structures were identified. This investigation was accomplished by reviewing available literature in each diagnostic area and by visiting experts throughout the United States.

The literature search revealed that there were well-developed capabilities applicable to postfailure analysis using the techniques of nondestructive evaluation and materials characterization. The techniques of fractography and stress analysis were also identified in the literature, but were found to be not sufficiently developed for direct incorporation into the program compendium. At the conclusion of Task 1, detailed flowcharts were developed outlining a logical, sequential procedure for conducting a postfailure analysis of composite materials.



Codes	
Dist	Avail and/or Special
A-1	

In Tasks 2 and 3, specimens were fabricated, tested, and examined to evaluate fractographic analysis methods for composites.

Fractographic analysis was evaluated as a technique for identifying the load state, direction, and origin of fracture under both singular and multiple, more complex conditions of failure. Specimens for these examinations were made from Hercules 3501-6/AS4, and tested under Task 2. For this reporting period, these tests included controlled delamination of laminates under modes 1 and 2 in a variety of environmental conditions, and translaminar fracture under conditions of tension and compression.

Examinations of these specimens under Task 3 revealed several methods for identifying the load state, direction, and origin of fracture.

- o Mode 1 interlaminar fractures were identified by their flat fracture morphology. The direction of crack growth could be established by examining the direction of river mark coalescence or resin microflow.
- o Mode 2 interlaminar fractures were identified by their rough, hackled fracture morphology. In some cases, crack growth was identified by the direction of hackle tilting.
- o Translaminar tension fractures were identified by a rather rough fracture morphology with conditions of fiber pullout and undamaged fiber-end fracture. The direction of crack propagation could be determined by mapping the direction of fiber-end fractures.
- o Translaminar compression fractures were identified by a flat overall fracture surface with fiber-end fracture and fiber microbuckling. The direction of crack propagation could not be conclusively identified, but was observed to be parallel to the fiber fracture neutral axis.

FOREWORD

This report documents work performed under Contract F33615-C-5010 from July 6, 1984, through October 15, 1985. This contract with the Boeing Military Airplane Company, Seattle, Washington, is monitored by AFWAL/MLSE under the direction of Mr. F. Feчек, Air Force Wright Aeronautical Laboratories, Materials Laboratory, Wright-Patterson Air Force Base, Ohio 45433-6533.

The program is being conducted by the Materials Technology organization of the Boeing Commercial Airplane Company. Mr. L. P. Clark is the program Manager, and Mr. B. W. Smith is the principal investigator with technical support from co-principal investigator, Mr. R. A. Grove.

Other contributors to this report are Mr. T. E. Munns, Mr. R. E. Smith, and Dr. A. G. Miller of the Boeing Materials Technology Group. In-situ fracture analysis studies were performed at Texas A&M by Dr. W. Bradley.

The authors wish to thank Mr. F. Feчек and Ms. P. Stumpff of AFWAL/MLSE for their inputs and guidance. The assistance of Dr. C. Chamis of NASA, Dr. B. Pipes of the University of Delaware, Mr. R. Kar of Northrop, Mr. D. Robertson of Ford, and Mr. H. Chou of McDonnell Douglas in Task 1 is also greatly appreciated. In addition, the authors would like to express their thanks to the numerous publishing houses and authors who granted permission to include their works in the literature review section.

TABLE OF CONTENTS

<u>Section</u>	<u>Page</u>
1.0 INTRODUCTION AND OBJECTIVES	1
2.0 APPROACH	5
3.0 RESULTS	7
3.1 Technical Progress and Results	7
3.1.1 Task 1--Literature Search and FALN Development	7
3.1.2 Task 2--Production of Specialized Test Specimens	8
3.1.3 Task 3--Diagnostic Technique Evaluation	9
3.2 Findings and Conclusions	10
4.0 TASK 1: LITERATURE SEARCH AND DIAGNOSTIC TECHNIQUE SELECTION	11
4.1 Organization and Status	11
4.2 Literature Search Intent and Terms	11
4.3 Literature Search--Fractography	12
4.4 Literature Search--Stress Analysis	27
4.5 Literature Search--Nondestructive Evaluation	46
4.6 Literature Search--Materials Characterization	53
4.7 Meetings with Experts in Composite Failure Analysis	65
5.0 FAILURE ANALYSIS LOGIC NETWORKS	79
5.1 Objective and Status	79
5.2 Overall Failure Analysis Logic Network	79
5.3 Nondestructive Evaluation FALN	83
5.4 Materials Verification and Configuration FALN	84
5.5 Fractography FALN	90
5.6 Stress Analysis FALN	94
6.0 TASK 2: SPECIMEN FABRICATION AND TESTING	98
6.1 Objective and Status	98
6.2 General Approach to Task 2	98
6.3 Material Pedigree	103
6.4 Specimen Fabrication	103
6.5 Environmental Moisture Preconditioning	106
6.6 Interlaminar Mode 1 (Tension) Testing	110
6.7 Interlaminar Mode 2 (Shear) Testing	112
6.8 Mode 1 Translaminar Tension and Compression Testing	115
6.9 Mode 2 Translaminar Shear Testing	118
7.0 DIAGNOSTIC TECHNIQUE EVALUATION	119
7.1 Objectives	119
7.2 Approach	119
7.3 Interlaminar Fractures	121
7.3.1 Interlaminar Mode 1, Tension, 21°C (70°F)	121
7.3.2 Interlaminar Mode 2, Shear, 21°C (70°F)	140
7.3.3 Environmental Effects on Interlaminar Mode 1 and 2 Fracture Features	159

TABLE OF CONTENTS (cont'd)

<u>Section</u>		<u>Page</u>
7.4	Translaminar Fractures	172
7.4.1	Translaminar Mode I Tension, 21°C (70°F)	181
7.4.2	Translaminar Mode I, Compression, 21°C (70°F)	187
8.0	SUMMARY AND CONCLUSIONS	194
9.0	REFERENCES	197
10.0	ACRONYMS	224

LIST OF ILLUSTRATIONS

<u>Number</u>	<u>Title</u>	<u>Page</u>
1-1	Program Task Interrelationships	3
1-2	Boeing's Detailed Failure Analysis Logic Network (FALN)	4
4-1	Fractography Literature Search Summary	13
4-2	Fiber Pullout Under Uniaxial Tension	17
4-3	Fiber Pullout as a Function of Temperature and Absorbed Moisture	18
4-4	Radial Fiber Fracture Topography	19
4-5	Hackle Resin Fracture Features	21
4-6	Hackle Formation Through Resolved Tension Cracking	22
4-7	Hackle Formation Through Secondary Cracking Due to Bending Behind the Crack Tip	23
4-8	Cleavage Steps and Resin Texturing	24
4-9	Comparison of Fractography Literature Review Findings to Failure Analysis	25
4-10	Stress Analysis Literature Search Breakdown	28
4-11	Stress Transformation Equations	29
4-12	Comparison of Yield Criteria for Glass- and Graphite-Epoxy	32
4-13	Predicted Versus Actual Failure Pressure for Laminated Cylinders	33
4-14	Stress Gradients Resulting from Edge Effects	35
4-15	Through Thickness Tensor Polynomial Distributions for Curing Stresses and Stresses at First Failure in $(+0)_s$ Laminates	36
4-16	Tensor Polynomial Distributions Along the Interface of $(+0)_s$ Laminates for First Failure Under Tensile Strain with Curing Stresses	37
4-17	Fracture Toughness of Various Layups	38
4-18	Strength Reduction of Uniaxially Loaded Plate with Circular Hole, According to Average Stress Criterion	39
4-19	Strength Reduction of Uniaxial Loaded Hole According to Point Failure Stress Criteria	40

LIST OF ILLUSTRATIONS (cont'd)

<u>Number</u>	<u>Title</u>	<u>Page</u>
4-20	Strength Reduction as a Function of Hole Radius for (0/ +45/-45/90-Degree) _s Graphite-Epoxy Plates with Circular Holes under Uniaxial Tensile Loading	40
4-21	Effect of Impact Damage on the Compressive Strength of a Quasi-Isotropic Laminate	41
4-22	Stress Analysis Methods Identified in Literature Search	44
4-23	Nondestructive Evaluation Techniques	50
4-24	Test Parts	51
4-25	Method Selection (Listed in Order of Preference)	52
4-26	Impact Damage Detection Capability	53
4-27	Delamination/Disbond Defect Detection Capability	54
4-28	Cracks in Gr-Ep Specimen	56
4-29	LC Chromatogram of Narmco Resin Matrix Showing Major Peak Assignment	58
4-30	Diagram of GPC Technique	59
4-31	GPC Chromatogram of Narmco Neat Resin Showing Major Peak Assignment	59
4-32	DSC Thermogram for 3501-6 Resin	60
4-33	DR-FTIR Spectra of Graphite/Epoxy (AS/3501-5) Composite Before and After Thermal Aging	62
4-34	Elastic Modulus Versus Temperature, Narmco Matrix, Showing Variation with Hardener Content	63
4-35	DSC Results for Cured Fibredux	64
4-36	Materials Characterization Literature Survey Summary	66
4-37	Northrop Aircraft's FALN	69
4-38	SEM Photomicrographs of Mode I Fracture Surface	75
5-1	Simplified Investigative Framework	81
5-2	Detailed Investigative Framework	82
5-3	Nondestructive Evaluation	84

LIST OF ILLUSTRATIONS (cont'd)

<u>Number</u>	<u>Title</u>	<u>Page</u>
5-4	Failure Analysis Technique - Nondestructive Evaluation	85
5-5	Method Selection (Listed in Order of Preference)	86
5-6	Material Cure Configuration Verification Diagnostic Technique	88
5-7	Failure Analysis Techniques - Cured Material Identification	89
5-8	Failure Analysis Techniques - Degree-of-Cure Analysis	89
5-9	Failure Analysis Techniques - Uncured Material Identification	89
5-10	Sample Fingerprinting of Various Systems via X-Ray Fluorescence	90
5-11	Pyrolysis Gas Chromatography (PGC) of Two Different Resin Systems	91
5-12	Fractography FALN	93
5-13	Failure Analysis Techniques - Fractography	94
5-14	Failure Analysis Techniques - Fracture Surface Material and Chemical Characterization for Fractography	95
5-15	Stress Analysis FALN	96
5-16	Computer Analysis Programs	97
6-1	Singular- and Multiple-Failure-Condition Test Specimen Matrix	99
6-2	Basic Modes of Loading Involving Different Crack Types and Surface Displacements (Interlaminar and Translaminar)	102
6-3	Vendor Certification Records	104
6-4	Laminate/Sandwich Cure Cycle	105
6-5	Panel Layup Stacking Order	106
6-6	Panel Warpage, Splitting, and Delamination over FEP Insert Areas: Panel #3, Original Layup Sequence	107
6-7	Typical TTU Plan View of Specimen No. 7-2	107
6-8	Cross Section A-A (Figure 6-7) of TTU Identified Defect, Showing Localized Voids in Laminate	108

LIST OF ILLUSTRATIONS (cont'd)

<u>Number</u>	<u>Title</u>	<u>Page</u>
6-9	Glass Transition Temperature Values, Thermomechanical Analysis-Flexure Mode	109
6-10	NASA Moisture Absorption Data of Composite Materials Following Worldwide Outdoor Exposure	109
6-11	Environmental Conditioning	110
6-12	DCB Test Fixture During Trial Testing	111
6-13	100% Mode 2 Interlaminar Shear - Asymmetric Cantilever Beam Geometry	112
6-14	Interlaminar Mode 2 (Shear) Test Configuration	114
6-15	ENF Test Fixture During Trial Testing	115
6-16	Translaminar Tension Specimen in Test	116
6-17	Translaminar Compression Specimen in Test	117
6-18	Translaminar Shear Specimen After Test	118
7-1	Optical Photomicrographs of Intended Fracture Plane Between 0/0-Degree Plies, DCB 21°C (70°F) Specimen	122
7-2	SEM Fractographs of Mode 1 Delamination Between 0/0-Degree Plies	124
7-3	Photomicrograph Illustrating Adhesive Areas of Fiber/Matrix (F) Separation and Textured Microflow (T)	125
7-4	Optical Photomicrographs of Intended Fracture Plane Between 0/90-Degree Plies, DCB 21°C (70°F) Specimen	127
7-5	SEM Photomicrographs of Mode 1 Delamination Between 0/90-Degree Plies	129
7-6	Optical Photomicrographs of Intended Fracture Plane Between +45/-45-Degree Plies, DCB 21°C (70°F)	130
7-7	SEM Fractographs of Mode 1 Delamination Between +45/-45-Degree Plies	131
7-8	Fracture Surface	131

LIST OF ILLUSTRATIONS (cont'd)

<u>Number</u>	<u>Title</u>	<u>Page</u>
7-25	Fractographs of Mating Fracture Surfaces Produced Under Mode 2 Between +45/-45-Degree Plies (Hackle Separation Occurs by Mechanism A, in which Hackles (H) Are Retained on One Side, Tilted Coincident with the Direction of Crack Growth)	155
7-26	Optical Photomicrographs of Intended Fracture Plane Between 0/45-Degree Plies, ENF 21°C (70°F) Specimen	156
7-27	SEM Fractographs Illustrating Delamination Produced Between 0/+45-Degree Plies Under Mode 2 Loading	157
7-28	Optical Photomicrographs of Intended Fracture Plane Between 0/90-Degree Plies, ENF 21°C (70°F) Specimen	160
7-29	SEM Fractographs of Mode 2 Delamination Produced for 90/90-Degree Specimen (Separation Occurred Along Either the Adjacent 0- and 90-Degree Interface or Within the 0-Degree Ply)	161
7-30	Low Magnification Series of Characteristic 0/0-Degree Interface Mode 1 Fractures at Each Environmental Condition	163
7-31	Higher Magnification Series of 0/0-Degree Interface Mode 1 Fractures Presented in Figure 7-30 Showing Features of Fiber/Matrix (F) Separation and River Markings (R)	164
7-32	Low Magnification Series of Characteristic +45/-45-Degree Interface Mode 1 Fractures at Each Environmental Condition	165
7-33	Higher Magnification Series of +45/-45-Degree Interface Mode 1 Fractures Presented in Figure 7-32 Showing Features of Fiber/Matrix (F) Separation and River Markings (R)	166
7-34	Low Magnification SEM Series of Characteristic 0/90-Degree Mode 1 (Tension) Fractures at Each Environmental Condition	167
7-35	Higher Magnification Series of 0/90-Degree Interface Mode 1 (Tension) Fractures Presented in Figure 7-34 Showing Features of Fiber/Matrix (F) Separation and River Markings (R)	168
7-36	Low Magnification SEM Series of Characteristic 0/45-Degree Interface Mode 1 Fractures at Each Environmental Condition	169
7-37	Higher Magnification SEM Series of 0/45-Degree Interface Mode 1 Fractures Presented in Figure 7-36 showing Features of Fiber/Matrix (F) Separation and River Markings (R)	170

LIST OF ILLUSTRATIONS (cont'd)

<u>Number</u>	<u>Title</u>	<u>Page</u>
7-38	Low Magnification SEM Series of Characteristic 0/0-Degree Interface Mode 2 (Shear) Fractures at Each Environmental Condition	173
7-39	High Magnification SEM Series of 0/0-Degree Interface Mode 2 (Shear) Fractures Presented in Figure 7-38 Showing Features of Fiber/Matrix (F) Separation and River Markings (R)	174
7-40	Low Magnification SEM Series of Characteristic 0/90-Degree Interface Mode 2 Fractures at Each Environmental Condition	175
7-41	Higher Magnification SEM Series of 0/90-Degree Interface Mode 2 (Shear) Fractures Presented in Figure 7-40 Showing Features of Fiber/Matrix (F) Separation and River Markings (R)	176
7-42	Low Magnification SEM Series of Characteristic +45/-45-Degree Interface Mode 2 Fractures at Each Environmental Condition	177
7-43	Higher Magnification SEM Series of +45/-45-Degree Interface Mode 2 (Shear) Fractures Presented in Figure 7-42 Showing Features of Fiber/Matrix (F) Separation and River Markings (R)	178
7-44	Low Magnification SEM Series of Characteristic 0/45-Degree Mode 2 (Shear) Fractures at Each Environmental Condition	179
7-45	Higher Magnification SEM Series of 0/-45-Degree Mode 2 (Shear) Fractures Presented in Figure 7-44 Showing Features of Fiber/Matrix (F) Separation and River Markings (R)	180
7-46	Translaminar Tension Fractures; 0/90-Degree Laminate	182
7-47	Translaminar Tension Fractures; +45/-45-Degree Laminate	185
7-48	Translaminar Tension Fractures; Quasi-Isotropic Laminate	186
7-49	Translaminar Compression Fractures; Unidirectional 0-Degree Laminate	188
7-50	Translaminar Compression Fractures; 0/90-Degree Laminate	189
7-51	Translaminar Compression Fractures; +45/-45-Degree Laminate	190
7-52	Translaminar Compression Fractures; Quasi-Isotropic Laminate	191
7-53	Typical Fiber End Fracture; Representative of Fiber Flexure Fracture	192

1.0 INTRODUCTION AND OBJECTIVES

The need to develop a comprehensive postfailure analysis capability for composite materials has become apparent in recent years. With the increasing use of these materials in aerospace applications, unanticipated failures under full-scale test conditions as well as in service are more likely to occur. This likelihood makes it necessary to develop the technology (or capability) to identify the causes and understand the circumstances of such failures, so that improvements to future designs can be made or appropriate corrective actions taken.

The steps for determining the causes of component failure in metallic structures are well established. Not only do postfailure investigators have a well-established protocol, but they can also draw on a battery of recognized analytical methods. Unfortunately, that is not the case with composite materials. Neither a well-accepted protocol (failure analysis logic network, or FALN) nor a set of analysis methods exists to determine failure causes for composite materials.

This program is specifically aimed at correcting that situation. The objective is to establish a widely disseminated and generally accepted "Composites Structure Failure Analysis Handbook"—or the equivalent for composite materials of such metals books as the Air Force electron fractography and the American Society for Metals (ASM) fractography and failure prevention handbooks. While this program will not produce the handbook, it will produce the *Compendium of Postfailure Analysis Techniques for Composite Materials*, which should provide the basis for the handbook.

To provide the basic technology required for successfully carrying out a composites postfailure analysis investigation, this program consists of three primary objectives:

- o Establish, verify, compile, and demonstrate techniques and procedures for the postfailure analysis of graphite-epoxy structures
- o Define a logical investigative sequence, using the above procedures, that identifies the starting point, mode, and reason for in-service failures
- o Establish a compendium that summarizes the techniques and investigative procedures defined above.

To achieve these objectives Boeing's existing FALN has been structured as follows:

- o Task 1—Literature Search and Diagnostic Technique Evaluation
- o Task 2—Specimen Production and Test
- o Task 3—Diagnostic Technique Evaluation
- o Task 4—Creation of a Failure Analysis Compendium
- o Task 5—Evaluation and Demonstration of Techniques

These tasks and their interrelationships are schematically illustrated in Figure 1-1, and Boeing's FALN is shown in Figure 1-2. Tasks 1 through 3 address the compilation and review of the various diagnostic techniques and protocols available, then select and evaluate their overall utility and effectiveness on test specimens made to fail under controlled conditions. The resulting compendium (Task 4) will provide a listing of the techniques and procedures found to be applicable in Tasks 1 through 3. This compendium will be presented in an instructional format and will include example data/information as well as appropriate FALNs to guide investigators along a logical analysis path. In Task 5 this compendium will be applied by Boeing to three failed components selected and submitted by the Air Force.

This interim report covers activities completed in Tasks 1 through 3. Significant features are:

- o A review of existing literature
- o Detailed failure analysis logic networks (FALNs)
- o Detailed descriptions of specimens fabrication and test procedures
- o Fractographic analysis findings for specimens failed under simple, singular-failure conditions.

Uncompleted activities in Tasks 2 through 5 will be documented in the final report at the conclusion of the programs' technical effort.

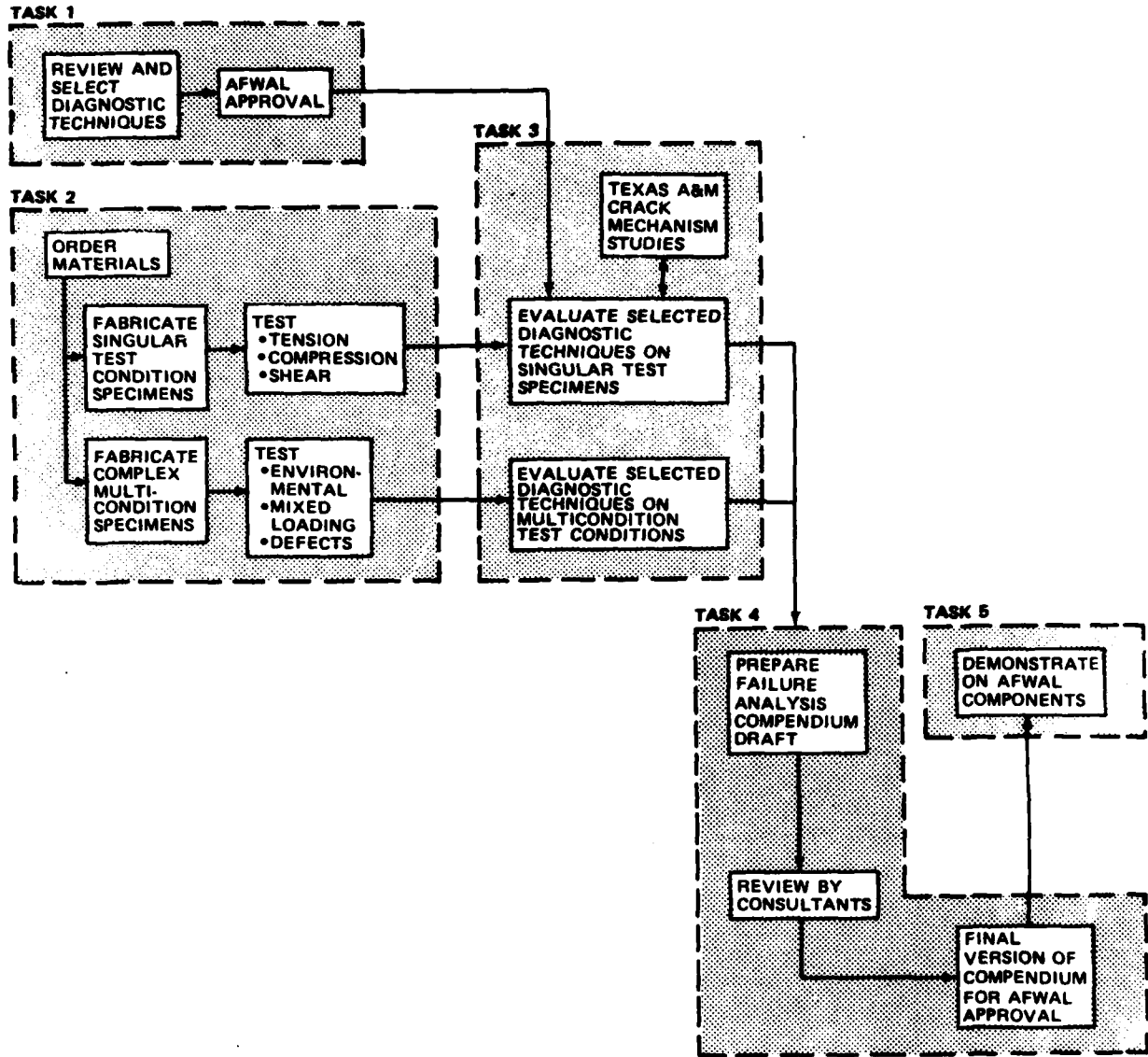


Figure 1-1. Program Task Interrelationships

2.0 APPROACH

This program has been structured to produce a Compendium of Postfailure Analysis Techniques for Composite Materials—along with several supporting examples of its application and effectiveness. The fundamental approach is to use Boeing's existing expertise and pertinent scientific literature, and then through a series of five tasks to identify, evaluate, summarize and demonstrate the techniques and procedures necessary for a rudimentary failure analysis. The tasks are as follows:

- o Task 1—Literature Search and Diagnostic Technique Evaluation
- o Task 2—Specimen Production and Test
- o Task 3—Diagnostic Technique Evaluation
- o Task 4—Creation of a Failure Analysis Compendium
- o Task 5—Evaluation and Documentation of Techniques

Figure 1-1 illustrates the specific interrelationships of these tasks, with Boeing's experience forming the basic foundation at program start. In general, comprehensive failure analysis has been hampered by a lack of clearly defined information requirements. Research, while moving forward, has not always addressed large-scale in-service failures or the needs of the failure analyst. Since Boeing has been involved in composite failure analyses since 1977, that experience and FALN (see Figure 1-2) have produced an initial model defining the necessary requirements, techniques, and procedures.

Tasks 1 through 3 systematically identify, review and evaluate the diagnostic techniques necessary for a failure analysis.

Task 1 compiles diagnostic techniques from the available literature for: (1) direct incorporation into the final compendium, (2) additional study, or (3) elimination. Since many of the techniques for performing a failure analysis may already exist, this literature review represents a logical starting point; it includes nondestructive evaluation, stress analysis, materials characterization and fractographic analysis techniques. Task 1 also involved on-site visits with specific experts to further define existing capabilities.

Those techniques selected for further study in Tasks 2 and 3 were evaluated by examining pedigree specimens that failed under tightly controlled conditions. These studies were carried out on a model state-of-the-art carbon fiber/350°F curing epoxy system in order to provide standard baseline data.

Information generated by Tasks 1 through 3 should provide the majority of information necessary to establish a Compendium of Postfailure Analysis Methods for Composite Materials (Task 4). This compendium will assemble the diagnostic techniques and FALNs into an instructionally oriented failure analysis form. Use of the compendium will be evaluated by an exercise involving analysis of three failed components. The exercise will evaluate the investigative sequence, as well as the fractographic, nondestructive, and materials characterization techniques examined and developed in this program. Because of the complex nature of these parts, detailed stress analyses will not be performed.

3.0 RESULTS

3.1 TECHNICAL PROGRESS AND RESULTS

During performance of Tasks 1, 2, and 3, considerable progress has been made toward achieving the program objectives.

3.1.1 Task 1—Literature Search and FALN Development

The objectives of this task were twofold: first, to review existing diagnostic techniques and identify those of potential value for composite materials failure analysis; and second, to organize these techniques into a logical framework describing their sequence of use. The framework considers the type of information obtainable by each technique, its value, and its relationship to other techniques.

Literature published from 1978 to the present was reviewed to identify existing diagnostic techniques for composite failure analysis. These documents addressed four general areas: nondestructive evaluation, stress analysis, fractography, and materials characterization. A total of 286 abstracts were identified, and 58 papers were examined.

Well-developed diagnostic techniques were identified for both nondestructive evaluation and materials characterization. In both these areas, there were many techniques that were sufficiently mature for direct incorporation into the "Compendium of Postfailure Analysis Techniques for Composite Materials." However, in fractography and stress analysis, the information available was insufficiently developed or documented for direct incorporation.

In the case of stress analysis, most of the surveyed literature focused on simple specimens failed under idealized conditions. Such techniques generally assumed relatively simple failure criteria and were capable only of roughly approximating the load at failure. Consequently, while it is reasonable to assume that these techniques might be improved to deal adequately with in-service failures, the accuracy, documentation, and degree of detail in current stress analysis literature is inadequate for direct incorporation into a useful compendium.

In the area of fractography, the situation was similar. Again, a significant portion of the literature reviewed relatively small coupons failed under ideal conditions, although some documents dealt with methods for analyzing larger, full-scale coupons. In general, while the available literature on fractography makes an important contribution to the understanding of fractures, it did not appear sufficiently complete to be directly incorporated into the final compendium.

Under Task 1, Boeing's initial FALN was reviewed, updated, and expanded. This FALN delineates the logical sequence of investigative operations required for carrying out a failure analysis, and describes when and where to employ nondestructive evaluation, stress analysis, materials characterization, and fractography. Because this FALN applies these techniques on a broad scale, four sub-FALNs were developed to describe the logical flow of analysis in greater detail for each major discipline. To aid investigators in selecting the best techniques for these sub-FALNs, supporting charts were also developed under Task 1. The charts (contained in this interim report) describe the uses, attributes, and drawbacks of the most useful analysis techniques.

3.1.2 Task 2—Production of Specialized Test Specimens

The primary objective of Task 2 was to design, fabricate, and test specimens that failed under a single failure mode with a known crack direction or under complex, multiple conditions. The task was divided into two subtasks, 2A and 2B. The first of these subtasks examined the simpler conditions of failure, whereas subtask 2B examined multiple, complex conditions.

During this report period, all of the specimens for each of the two subtasks were designed and produced. In accordance with Boeing procedures, these specimens were cured at 177°C (350°F), and employed Hercules 3501-6 resin with AS-4 fibers. Vendor tests of the materials were performed prior to fabrication to establish the pedigree of the material.

In addition to design and fabrication, specimen tests were completed for the subtask 2A (singular failure mode) specimens during this report period. Four specimen configurations were tested, each of which was designed to provide control over the mode and direction of crack propagation. In the case of interlaminar fractures, failures were produced under mode 1 (tension) conditions, using a double cantilever beam specimen configuration. Failures under mode 2 (shear) conditions were produced using an end-notch flexural

specimen geometry. Controlled fractures through the laminate thickness (translaminar) were generated using notched-beam flexure for mode 1 (tension and compression) and notched rails for mode 2 (shear). As part of subtask 2A, specimens were also tested at -54°C (-65°F), 21°C (70°F), 21°C (70°F) wet, 82°C (180°F), 82°C (180°F) wet, 132°C (270°F), and 132°C (270°F) with, as well as without, prior environmental moisture conditioning.

3.1.3 Task 3—Diagnostic Technique Evaluation

This task established and evaluated fractographic techniques for identifying the direction and mode of crack propagation, and contributing conditions such as environment, defects, etc., involved in failure. During this reporting period, interlaminar modes 1 and 2, and translaminar mode 1 tension and compression failures were examined. For each of these fractures, a variety of analytical methods for identifying the direction and mode of failure were evaluated. Consistent with the failure analysis logic networks developed under Task 1, this task employed both optical and scanning electron microscope (SEM) analysis methods for examining these relatively simple singular failure conditions.

Detailed examinations of interlaminar and translaminar singular failures revealed significant differences in fracture characteristics.

Interlaminar mode 1 fractures were relatively easy to identify and analyze. For this mode of failure, the direction of crack propagation can be discerned by examining the direction of cumulative river mark coalescence or detailed resin microflow. Mode 1 failures are easily identified by their consistently flat fracture topography.

Interlaminar mode 2 shear fractures typically exhibit a rougher and more complex appearance than those noted under mode 1 (tension). Because of their more complex appearance, it is more difficult to determine the crack propagation direction of mode 2 fractures. For cross-ply layups (ply orientations other than 0/0-degree), the tilt of the fractured epoxy platelets or hackles are aligned in the direction of crack propagation. However, for 0/0-degree ply layups, the hackles are aligned roughly parallel to the crack, but are oriented both toward and away from the direction of crack propagation, and therefore do not reliably indicate crack growth direction.

Translaminar mode I fractures are easily identified by extensive fiber pullout and the distinctly radial morphology of the fractured fiber ends. This radial morphology indicates the local direction of fiber-end fracture. The cumulative direction of these individual fiber-end fractures corresponds to the direction of crack growth.

Translaminar compression fractures typically exhibit extensive fracture surface damage and fiber microbuckling. Though this mode is relatively easy to identify, no combination of discrete features was found that can be used to determine clearly the direction of crack propagation.

3.2 FINDINGS AND CONCLUSIONS

In summary, the results obtained in Task 3 indicated that several distinct fractographic features exist that are useful in determining the direction, and thereby the origin and load state, of fracture. Interlaminar and translaminar tension failures were relatively straightforward, but interlaminar shear and translaminar compression failures were more complex.

Although the latter two fracture types appeared fairly easy to identify, determining the direction of crack growth was considerably more difficult. Under conditions of compression, difficulty resulted from extensive fracture surface damage. For interlaminar shear, difficulties arose from the random orientation of features to crack growth.

In these latter cases, further study within Task 3 is necessary to resolve concerns and improve the techniques so that they are useful for widespread application.

4.0 TASK 1—LITERATURE SEARCH AND DIAGNOSTIC TECHNIQUE SELECTION

4.1 ORGANIZATION AND STATUS

This task encompassed two activities. In the first, literature on the subject of composites failure analysis was collected and reviewed. In the second, Boeing's previously established failure analysis logic networks (FALNs) were reviewed and then expanded to develop a comprehensive guideline for the failure analyst. Both activities have been completed. Findings from the literature search are reviewed in Section 4.0. Section 5.0 presents comprehensive failure analysis logic networks that have been developed for each of the four investigative disciplines.

4.2 LITERATURE SEARCH INTENT AND TERMS

The literature search was carried out in the disciplines of fractography, stress analysis, materials characterization, and nondestructive evaluation because they are the four basic procedures used in the failure analysis of metal and unreinforced polymer systems. While a developed failure analysis procedure does not exist for composites, the basic concerns in performing a postmortem analysis were judged to be similar for all material systems, and include failures due to process and fabrication errors, design errors, and service conditions.

The objective of this task was to review available literature and identify technologies that are useful for analyzing failures in composite materials.

An authoritative document, with a comprehensive listing of these technologies and their relationship to the analysis of failed components, does not exist. However, in recent years composite materials have been the subject of considerable research and testing, and many of the technologies necessary to carry out a failure analysis have been established. Consequently, the collection and review of existing relevant information was a logical starting point from which to develop a compendium of methods for the failure analyst.

Accomplishing this task served several purposes. Gathering the information provided an accurate listing of sources for techniques that relate to analyzing composite materials. Much of the information provided direct reference data and a good listing of analysis techniques and attributes for the "Compendium of Postfailure Analysis Techniques for Composite Materials." Shortcomings and inadequacies in analysis techniques were also

identified, revealing some methods of potential value that have not been sufficiently developed. Identifying these techniques provided a clearer picture of many concerns and problems that must be addressed in Task 3 or in subsequent follow-on activities.

The four analytic disciplines are considered necessary to assess the extent of damage, to reconstruct the sequence of failure, to identify anomalous fabrication conditions, and to evaluate the criticality of service-generated defects and flaws.

A computerized literature search in each of these disciplines was performed on documents published from 1978 to the present employing the NTIS and NASA data bases. The literature was searched using a list of key words: chemical analysis, cure, curing, composite materials, degree of cure, delamination, dynamic mechanical analysis, environmental fractures, failure analysis, fractography, fracture, fracture mode, graphite-epoxy composites, materials characterization, microcracking, neutron radiography, nondestructive evaluation, nondestructive inspection, nondestructive testing, optical microscopy, scanning electron microscopy, thermomechanical, ultrasonics, and X-ray radiography.

The listed words were selected based on Boeing's estimation of techniques or topics related to the analysis of failed composites. Approximately 365 abstracts were obtained. Based on evaluation of these abstracts, 109 articles were ordered for detailed review, and the review evaluated each article for its theoretical foundation, supporting data or models, experimental validity, and value in performing a failure analysis.

4.3 LITERATURE SEARCH-FRACTOGRAPHY

Reviewing the available literature on the fractographic aspects of failed composite materials from 1978 to the present reveals that the subject has been investigated by a significant number of researchers. Notable contributors to this body of information and their articles are listed in the reference section of this report. As illustrated in Figure 4-1, these investigations covered a wide variety of layups, specimen configurations, imposed fracture environments, and load conditions.

In reviewing the research, it is important to recognize that the majority of fractographic examinations carried out in a postfailure analysis will be directed toward determining the sequence of fracture events. Secondly, these examinations will also be aimed at identifying the load states involved in fracture, as well as factors such as environment,

LOAD STATE	LAYUP, deg	AUTHORS/PAPER ¹	CRACK DIRECTION	ENVIRONMENT	FIBER FRACTURE FEATURES ²	RESIN FRACTURE FEATURES ²
Uniaxial tension	(0), (90) (+45/-45)	Liechti (ref. 7)	Uncontrolled	21°C (70°F), dry	<ul style="list-style-type: none"> Radial pattern on individual fiber ends Resin adhering to fibers 	<ul style="list-style-type: none"> Both hackles and river marks on delamination surfaces
Uniaxial tension	(0), (0/90)	Miller, Wingert (ref. 1)	Uncontrolled	-54°C (-65°F), dry and wet 21°C (70°F), dry and wet 132°C (270°F), dry and wet	<ul style="list-style-type: none"> Increased fiber pull out with increased temperature and moisture Reduced resin adhering to fibers with increased temperature and moisture Radial pattern on individual fiber ends 	
Uniaxial tension	(+45/-45) (0, +45/-45), (0, +45/-45), 90)	Kline, (ref. 8)	Controlled	21°C (70°F), dry		<ul style="list-style-type: none"> Hackles on delamination surfaces
Uniaxial tension	(0), (7), (10) (15), (20) (30), (45) (90)	Purslow (ref. 3)	Uncontrolled	21°C (70°F), dry		<ul style="list-style-type: none"> River marks on delaminations normal to applied loads Hackles on delamination surfaces with shear loading Hackle formation related to resolved tensile cracks
Uniaxial tension	(+5/-5), (+15/-15) (+30/-30), (+45/-45)	Johannesson, (ref. 10)	Uncontrolled	21°C (70°F), dry	<ul style="list-style-type: none"> General fiber pull out Resin adhering to fibers 	<ul style="list-style-type: none"> Hackles on delamination surfaces Hackle formation related to resolved tensile cracks
Uniaxial tension	(0), (+45/-45) (90)	Morris (ref. 5)	Controlled	21°C (70°F), dry		<ul style="list-style-type: none"> Hackles on delamination surfaces Hackle formation related to secondary cracks due to crack tip opening Hackle angle shown to indicate crack direction

¹ References contained in Section 8.0.

² Comment represents author's interpretation of findings.

Figure 4-1. Fractography Literature Search Summary (Page 1 of 3)

LOAD STATE	LAYUP, deg	AUTHORS/PAPER ¹	CRACK DIRECTION	ENVIRONMENT	FIBER FRACTURE FEATURES ²	RESIN FRACTURE FEATURES ²
Uniaxial tension	(0 ₂ , +5/-5), (0 ₂ , +15/-15), (0 ₂ , +30/-30), (0 ₂ , 90 ₂), Tested at 0, 5, 10, 15 30, 45, 60 75, 90	Sinclair (ref. 13)	Uncontrolled	21°C (70°F), dry	<ul style="list-style-type: none"> 0° to 5° test angle produced tiered fiber fracture 	<ul style="list-style-type: none"> Hackles on delamination surface produced at test angles from 5- to 30-deg Both hackles and river marks on delamination surfaces produced at test angles from 30- to 45-deg River marks on delamination surfaces produced at test angles from 45- to 90-deg
Uniaxial tension	0 0 Post-cured	Clements (ref. 2)	Uncontrolled	21°C (70°F), dry and wet 96°C (204.8°F), dry and wet	<ul style="list-style-type: none"> Increased fiber pull out with increased temperature and moisture Reduced resin adhering to fibers with increased temperature and moisture Flat areas of fiber fracture at origin Cleavage steps between groups of fibers indicating crack direction 	
Uniaxial compression	N/A	Purslow (ref. 3)	Uncontrolled	21°C (70°F), dry	<ul style="list-style-type: none"> Fiber microbuckling with neutral axis, tension and compression features 	
Uniaxial compression	N/A	Line, Chang (ref. 8)	Uncontrolled	21°C (70°F), dry		<ul style="list-style-type: none"> Both hackles and river marks on delamination surfaces
Uniaxial compression	(90) (± 45) (0, ± 45, 90),	Liechti (ref. 7)	Uncontrolled	21°C (70°F), dry	<ul style="list-style-type: none"> Fiber microbuckling for (+45/-45-deg) and (0-, +45-, 90-deg), lay-ups 	<ul style="list-style-type: none"> Both hackles and river marks on delamination surfaces
Uniaxial compression	N/A	Freeman (ref. 5)	Uncontrolled	21°C (70°F), dry	<ul style="list-style-type: none"> Fiber microbuckling 	

¹ References contained in Section 8.0.

² Comment represents author's interpretation of findings.

Figure 4-1. Fractography Literature Search Summary (Page 2 of 3)

LOAD STATE	LAYUP, deg	AUTHORS/PAPER ¹	CRACK DIRECTION	ENVIRONMENT	FIBER FRACTURE FEATURES ²	RESIN FRACTURE FEATURES ²
Uniaxial tension	(0)	Morris (ref. 6)	Controlled	21°C (70°F), dry		<ul style="list-style-type: none"> • Hackles on delamination surface • Formation related to secondary cracks due to crack tip opening • Hackle angle shown to indicate crack direction
	(0)	Liechti (ref. 7)	Controlled	21°C (70°F), dry		<ul style="list-style-type: none"> • River marks and fine resin feathering on delamination surface for mode 1 • Hackles on delamination surfaces for mode 2 • Hackle formation related to resolved tensile cracks
Interlaminar mode 1 (toughness)	(0)	Kline, (ref. 8)	Controlled	21°C (70°F), dry		<ul style="list-style-type: none"> • Fine triangular void areas • River marks on delamination surface
Interlaminar mode 1 and mode 2 (toughness)	(0)	Donaldson (ref. 11)	Controlled	21°C (70°F), dry		<ul style="list-style-type: none"> • River marks under 100% mode 1 • Hackles under 100% mode 2 • Hackle formation related to resolved tensile cracks
Interlaminar mode 1 (toughness)	(0)	Robertson (ref. 12, 13)	Controlled	21°C (70°F), dry		<ul style="list-style-type: none"> • River marks, hackles and fine textured feathering • Hackles related to crack plain twisting
Flexure (bending)	(0)	Purslow (ref. 3)	Uncontrolled	21°C (70°F), dry	Macroscopic areas of compression and tensile fiber fracture separated by neutral axis line	
Flexure (short-beam shear)		Browning (ref. 14)	Uncontrolled	21°C (70°F), dry		Hackles on delamination surfaces
Flexure (bending)	(0)	Liechti (ref. 7)	Uncontrolled	21°C (70°F), dry		Hackles on delamination surfaces

¹ References contained in Section 8.0.

² Comment represents author's interpretation of findings.

Figure 4-1. Fractography Literature Search Summary (Page 3 of 3)

defects, or material anomalies that may have contributed to crack initiation or growth. In reviewing the literature, particular attention has been given to those fractographic features that investigators may use to define:

- o The direction and origin of fracture
- o The fracture load state (e.g., tension, shear, compression)
- o Features associated with defect (material anomaly or environmentally aided fracture).

The following authors' works have been cited in the literature search. Their names are followed by numbers, in parentheses, which correspond to the number in References, (Section 9.0). In the literature for fractography, the works of the following investigators are cited: Miller and Wingert (1), Clements (2), Purslow (3), Adams (4), Freeman (5), Morris (6), Liechti (7), Kline (8), Sinclair (9), Johannesson (10), Donaldson (11), Robertson (12), Robertson (13), and Browning (14). Authors cited in the literature for stress analysis are: Craddock (15), Crossman (16), Herakovich (17), Chamis (18), Bathias (19), McGarry (20), Awerbuch (21), Daniel (22), Mikulas (23), O'Brien (24), Webster (25), Wilson (26), Starnes (27), Wu (28), and McLaughlin (29). Those cited in the nondestructive evaluation portion of this study are: Phelps (30), Reynolds (31), Schramm (32), Ulman (33), Bar-Cohen (34), Moran (35), Baumann (36), Sendckyj (37), Reifsnider (38), Soni (39), Gibbons (40), Teagle (41), Bar-Cohen (42), Raatz (43), and Duke (44). In the materials characterization section, the investigators cited are: Wickham (45), May (46), Crozier (47), Rogers (48), Tung and Dynes (49), Chen and Hunter (50), Carpenter (51), Sewell (52), Mones (53), Stark (54), Carpenter (55), Munns and Seferis (56), Chu and Seferis (57), Young (58), Burroughs (59), Chu and Seferis (60), Baumgartner and Lemming (61), Putter (62), Jackson (63) and Chang (59).

The following discussion has been divided into two main sections covering fiber-dominated and resin-dominated fracture features. This division reflects both the binary phase structure of composites and the tendency of researchers to examine one of these structures in particular detail.

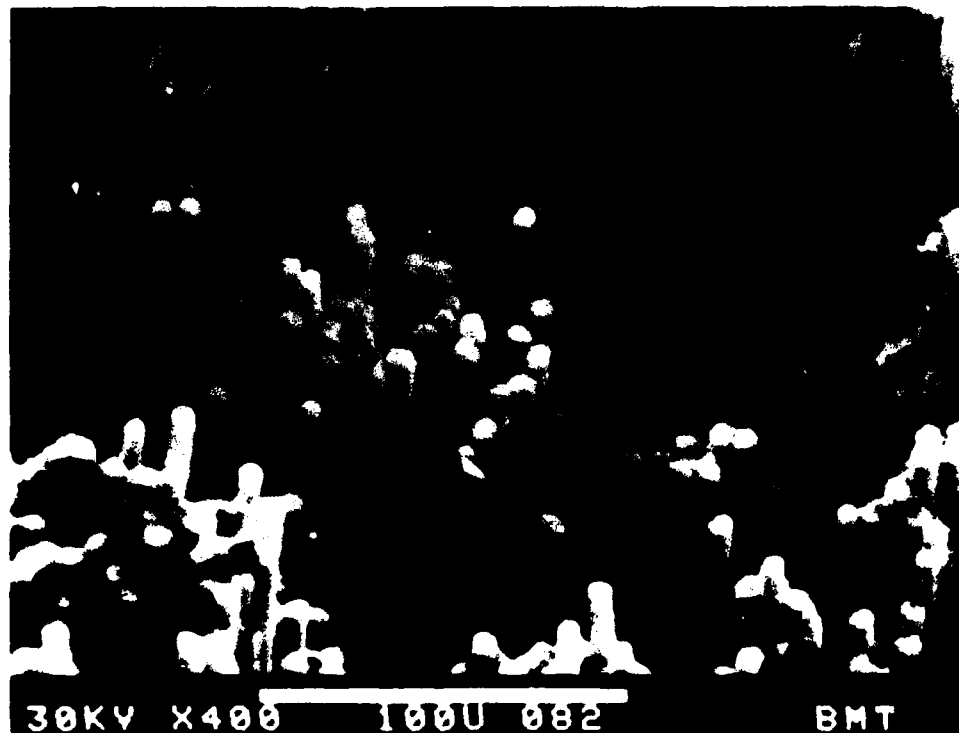
In the area of fiber-dominated fractures, investigators have examined the relationship of fiber pullout to test environment, absorbed moisture, and defect conditions. The characteristics of individual fibers fractured under tension, compression, and flexure loading and their relationship to the direction of crack propagation were also studied.

Resin fracture morphologies that have been examined include two main features: hackles (serrated platelets of fracture resin), and river markings (often referred to as cleavage steps).

Fiber-Dominated Fractures

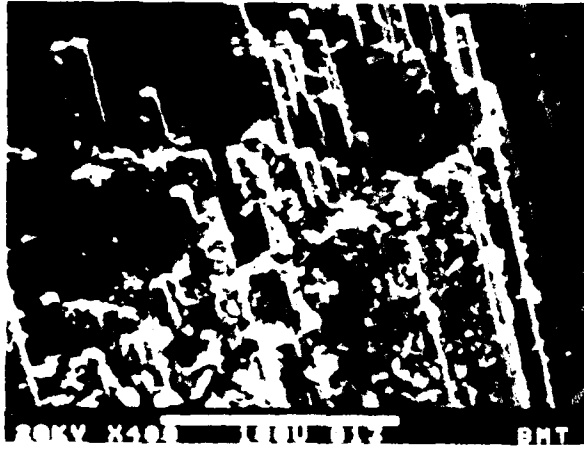
Most authors agree about the fracture appearance of individual fibers under a variety of conditions. Miller, Clements, and Purslow have characterized the fracture surface features of graphite fibers in detail.

Various authors have described the existence of discrete fibers (or bundles of fibers) pulled from the surrounding matrix under uniaxial tension (see Figure 4-2). This characteristic was perhaps most extensively investigated by Miller, in his examination of 0-degree and 0/90-degree tensile coupons fabricated from three material systems and failed in a variety of environmental conditions. As illustrated in Figure 4-3, and generally supported in the work of Clements, little pullout occurs in cold temperatures or with low amounts of absorbed moisture (-54°C (-65°F) dry & wet, 21°C (70°F) dry). However, with elevated temperature and/or moisture absorption, a significant increase in the degree of fiber pullout tends to occur. Miller argues that this tendency arises from decreased

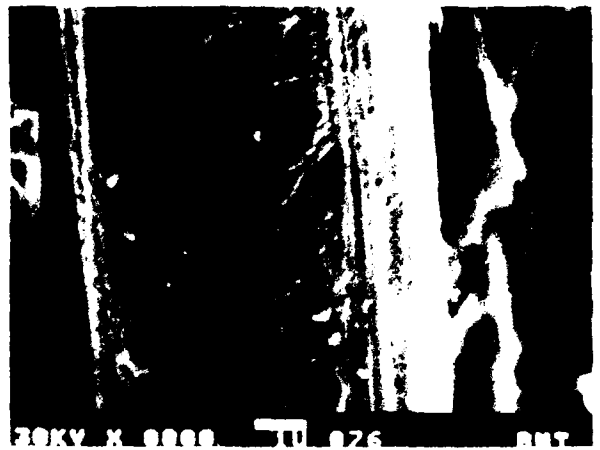
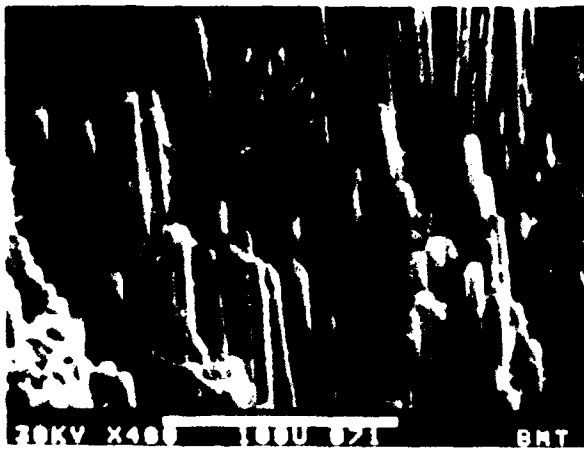


(Ref. 1 Copyright © ASTM; Reprinted with Permission)

Figure 4-2. Fiber Pullout Under Uniaxial Tension



-54°C (-65°F) Dry



21°C (70°F) Wet



132°C (270°F) Wet

(Ref. 1 Copyright © ASTM, Reprinted with Permission.)

Figure 4-3. Fiber Pullout As a Function of Temperature and Absorbed Moisture

fiber/matrix adhesion combined with increased ductility of the overall matrix system at elevated temperatures and absorbed moisture levels. Miller cites as evidence for the first portion of this argument the pronounced decrease in residual matrix resin adhering to the fiber at elevated temperature and moisture conditions (Figure 4-3). Clements also presents this argument; however, she places more emphasis on the increased ductility of the matrix in reducing the overall sensitivity of the tested laminate to flaws and individual fiber fractures prior to ultimate separation. Both investigators demonstrated some of the general morphological characteristics of tensile fiber fracture and the effect of the environment on these features.

On a more detailed level, all of the above researchers observed the features of individual or groups of fiber ends fractured under uniaxial tension. As illustrated in Figure 4-4, Miller and Purslow have demonstrated that fibers fractured under longitudinal tension exhibit a distinct radial topography; these radial patterns were shown to originate from a variety of sources, including internal and surface flaws as well as adjacent fiber fractures. This latter condition is particularly well demonstrated in Figure 4-4, derived from Miller and Wingert's work, both of whom claim that radial patterns illustrate the direction of individual fiber fracture. In Miller's studies, the orientation of individual fiber fractures is said to be extremely localized. As a result, it was reported that the direction of overall crack propagation could not be identified through examination of these features. However, in Purslow's work radial fiber features are shown to have an overall orientation sufficient to establish a global direction of crack propagation. This discrepancy between Miller and Purslow may reflect Miller's use of 0-degree (rather than cross-ply) layups, which are prone to axial-shear splitting. In general, this splitting tends to break the



(Ref 6 Copyright © ASTM, Reprinted with Permission)

Figure 4-4. Radial Fiber Fracture Topography

sample into a series of parallel sections, promoting multiple origins and local crack directions. Another possibility is that the resin system explored by Miller may have been less defect sensitive, retarding the establishing of a unified crack direction. In any event, Purslow's work suggests that mapping individual fiber radials may provide a reasonable means of establishing the direction of crack propagation for fiber-dominated fracture surfaces. However, in light of Miller's findings the applicability of this methodology may have significant limitations governed by layup, material, and failure environment.

While the foregoing discussions were concerned with tension-induced failure, several authors (particularly Purslow) have examined the appearance of fractures generated under compression and flexure. Purslow, Adams, and Freeman have illustrated that under uniaxial compression loading, groups of fibers fracture due to microbuckling. Fibers or groups of fibers are reported to fracture at the maximum point of flexure as the fiber is driven out of axial alignment. The resultant fracture surface exhibits individual fiber fractures with both compressive and tensile failure regions, separated by a central, neutral axis fracture line. The orientation of the neutral axis is said to indicate the direction of local microbuckling, and in Purslow's work is suggested as a possible means for determining the direction of crack growth. However, Purslow also indicates that areas of microbuckling may occur prior to, during, or after the main fracture event--possibly precluding the use of these features for crack mapping. In view of Purslow's comments, it is only possible to speculate if these features may in fact be useful in identifying the direction of crack growth.

Purslow performed what is perhaps the best work illustrating a macroscopic morphology unique to fracture under flexural loading. In his work he observed that flexure produces an overall fracture topography somewhat similar to that noted for individual compressive fiber fractures. The tensile and compressive loads applied during flexure generate relatively large-scale areas of compressive and tensile fiber fracture, separated by a distinct neutral axis line. While Purslow does not indicate how to determine the direction of crack growth of such fractures, he does suggest that the position of the neutral axis may be of value in reconstructing the loading conditions of flexure at the time of failure.

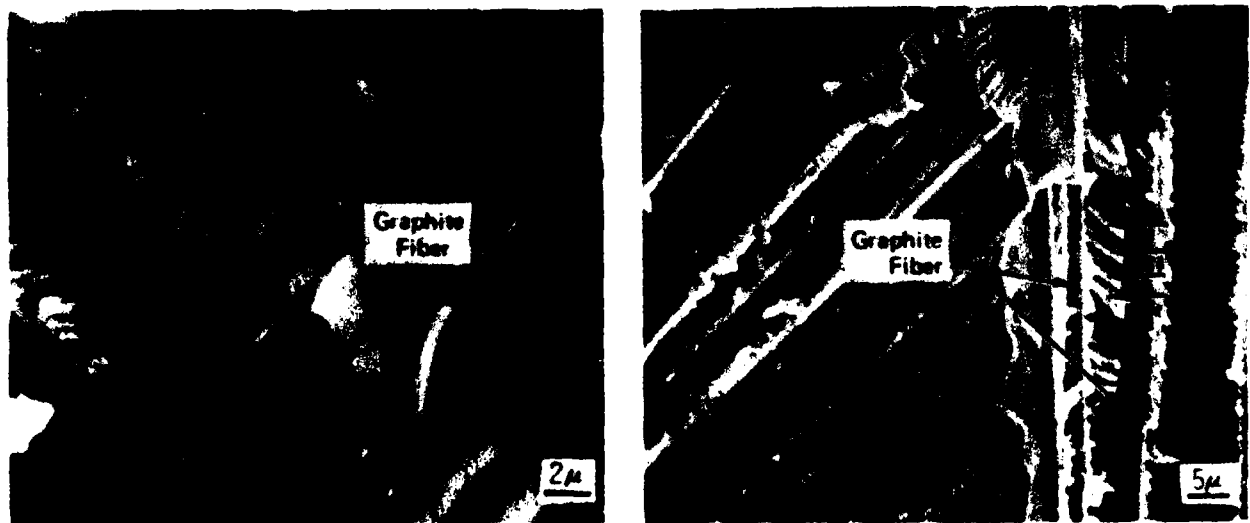
Resin-Dominated Fractures

Numerous investigators have examined resin-dominated graphite-epoxy composite fractures generated under a variety of test conditions. The literature search performed for

this report revealed that some disagreement exists between authors. Discrepancies center around the specific load states associated with the formation of certain features and the interpretation of these features with respect to the direction of crack propagation. Since the state of stresses that exist for an anisotropic material depend strongly upon layup, edge proximity, and the internal position examined, it is likely that many of these differences arise from investigators examining differing fracture surfaces generated under the same ostensible test conditions.

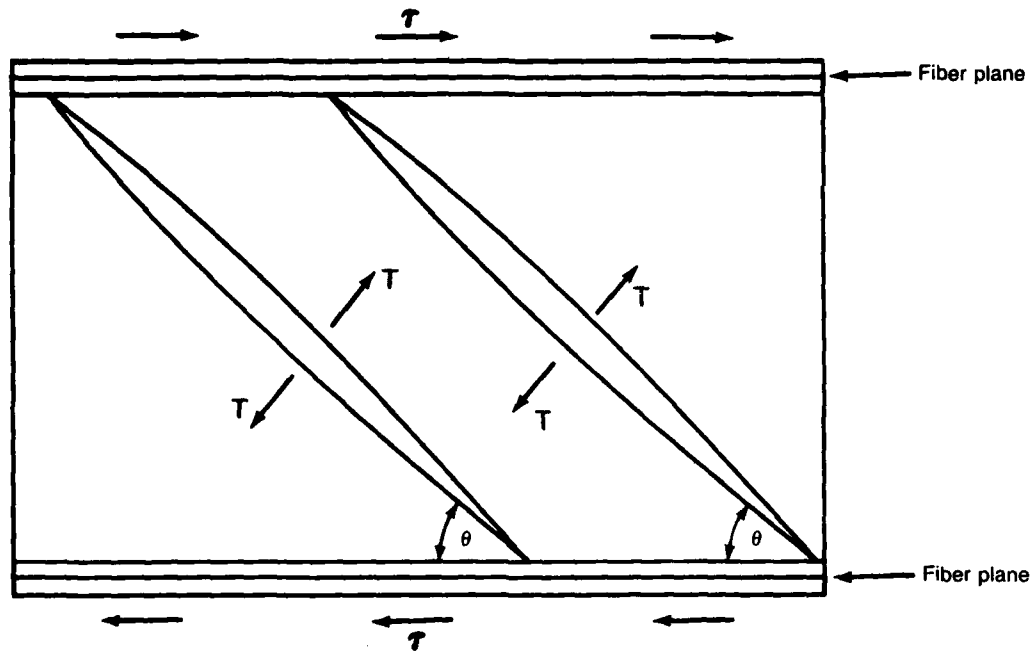
The majority of investigators (Purslow, Morris, Liechti, Kline, Sinclair, Johannesson) identified two features characteristic of matrix fracture: hackles and river markings.

Hackles are numerous platelets of fractured epoxy distributed in rows between fibers (Figure 4-5). Hackles have been observed under a variety of failure conditions including both interlaminar and intralaminar delaminations, as well as pulled-out fibers under uniaxial tension. Because these features have been observed under poorly defined load states, it is difficult to ascertain the exact load state responsible for the feature formation. Perhaps the most convincing research is found in the works of Purslow, Johannesson, Sinclair, and Donaldson, where hackles have been observed in great numbers under conditions of applied shear. Each of these authors proposed that hackles occur through the formation of numerous microcracks under resolved tension as illustrated in Figure 4-6. However, none of these authors indicates how such features or such a mechanism could be used to identify the direction of crack propagation.



(Ref. 6 Copyright © ASTM, Reprinted with Permission)

Figure 4-5. Hackle Resin Fracture Features

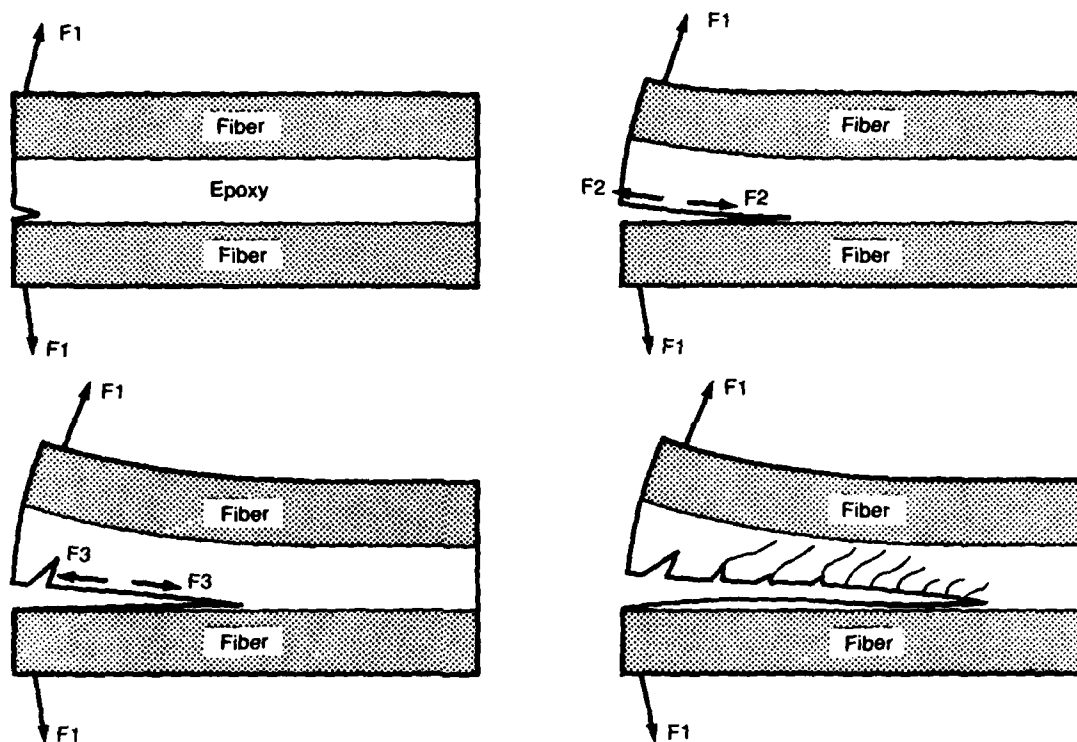


(Ref. 7)

Figure 4-6. Hackle Formation Through Resolved Tension Cracking

At variance with the above findings, Morris and Robertson have observed hackle structures under conditions of applied interlaminar tension. Morris advances an explanation for his observation by identifying a mechanism that forms hackles as a result of secondary cracks generated by continued flexure behind the crack tip (Figure 4-7). In this model, there is an indication that secondary cracks initiate and grow at an angle in the direction of overall crack growth. This indication gives rise to Morris' proposed method of determining the direction of crack growth by drawing arrowheads on a photograph of the specimen such that the arrowheads appear to be inserted into the open crack tips; the arrowheads then indicate the direction of propagation. This model gives no explanation for the tendency of cracks to grow at an inclined angle. Furthermore, Morris observes the existence of hackles inclined in opposing directions on mating fracture surfaces, which would seem to preclude the use of his proposed model to determine a clear direction of crack growth. As a result, it is difficult to evaluate the effectiveness of Morris' model based on the information available.

River markings, often referred to as cleavage lines or cleavage steps, are the second major feature noted by most investigators. As presented by Robertson in Figure 4-8, these features exhibit a distinct branched structure identical to that found in the fracture



(Ref 6 Copyright © ASTM; Reprinted with Permission)

Figure 4-7. Hackle Formation Through Secondary Cracking Due to Bending Behind the Crack Tip

of brittle metals. Purslow, Liechti, Sinclair, Donaldson, and Robertson have observed river markings on fracture surfaces oriented transversely to the applied tensile direction. In composites, these features appear to be unique to tension loading. Although river markings have been identified by many investigators, the concept of using them to determine the direction of crack growth has been advanced only by Purslow and Liechti. Both authors indicate that these features parallel the direction of microscopic crack growth. Purslow proposes that the direction of river markings can be used to reconstruct the global direction of crack growth when used in conjunction with the direction of radial fiber fractures.

In addition to river marks and hackles, investigators Robertson, and Liechti have observed a feathered or textured resin fracture morphology under tensile loading. Robertson notes that this textured morphology tends to be extremely fine—on the order of 350 nm (See Figure 4-8). As a result, it tends to be visible in the scanning electron microscope only when viewed at pronounced tilt. Robertson suggests this fine film texture arises from



(Ref 13. Copyright © Elsevier Applied Science Publishers, Ltd., Reprinted with Permission)

Figure 4-8. Cleavage Steps and Resin Texturing

meniscus instability of the crack front. Such an instability would give rise to multiple crack fingers spaced approximately 350 nm (3.94×10^{-8} in) apart. According to Robertson, the separations resulting from these fingers would produce a fine series of steps and an overall textured or feathered appearance. Both authors observed that this feature occurs coincident with the direction of localized crack growth. Consequently the textured or feathered morphology appears to be an additional method to determine the direction of crack progression by fractographic examination.

Discussion

For the failure analyst, fractographic characterization—the examination and interpretation of fracture surfaces generated during failure—is one of the most important tasks in an investigation. It is therefore relevant to summarize how the published literature on this topic relates to the actual analysis of failed structures.

In a failure analysis, the purpose of fractography is to define the fracture sequence and the conditions that contribute to failure. This objective can be broken down into the identification of: the direction of crack propagation and its point of origin, the load state

at fracture, and contributory factors to crack growth such as defects or environmental conditions. With respect to these tasks, it is significant that the literature reviewed contains some findings directly applicable to these objectives (see Figure 4-9). Basic morphologies have been sufficiently characterized to identify some simple modes of failure and contributory conditions. However, only a limited amount of useful research has addressed the determination of crack propagation direction, and in this area, substantial disagreements exist. Consequently, while the fracture surfaces of composites have been characterized in some detail, the available information addresses the total capability required to perform a failure analysis only to a small degree.

Identification of Load State

The easiest fractographic task is that of identifying the load state under which fracture occurred, and the literature on this subject presents a straightforward set of

TASK	CONDITION	METHOD OF IDENTIFICATION	AUTHORS
Identification of load condition	Translaminar tension	Exhibits distinct fiber pullout, little fracture surface damage, and radial fracture pattern on individual fibers	<ul style="list-style-type: none"> ● Miller (ref. 1) ● Liechti (ref. 7) ● Purslow (ref. 3) ● Johannesson (ref. 10) ● Clements (ref. 2)
	Translaminar compression	Exhibits general fracture surface damage and fiber microbuckling with areas of tension and compression divided by a neutral axis line on each fiber	<ul style="list-style-type: none"> ● Purslow (ref. 3) ● Liechti (ref. 7) ● Freeman (ref. 5)
	Translaminar flexure	Exhibits macroscopic areas of compression and tensile fiber fracture divided by a neutral axis line	<ul style="list-style-type: none"> ● Purslow (ref. 3)
	Interlaminar tension	Exhibits river marks and fine resin texturing	<ul style="list-style-type: none"> ● Liechti (ref. 7) ● Kline (ref. 8) ● Donaldson (ref. 11) ● Robertson (ref. 13)
			Exhibits hackled resin platelets
Identification of load state	Interlaminar shear	Exhibits hackled resin platelets	<ul style="list-style-type: none"> ● Purslow (ref. 3) ● Johannesson (ref. 10) ● Sinclair (ref. 9) ● Liechti (ref. 7) ● Donaldson (ref. 11) ● Browning (ref. 14)
Identification of crack direction and origin	Uniaxial tension	Crack direction indicated by cumulative direction of fiber radial fractures	<ul style="list-style-type: none"> ● Purslow (ref. 3)
	Interlaminar tension	Crack direction indicated by direction of river mark coalescence	<ul style="list-style-type: none"> ● Purslow (ref. 3) ● Liechti (ref. 7) ● Kline (ref. 8)
		Crack direction indicated by finely textured pattern	<ul style="list-style-type: none"> ● Robertson (ref. 13) ● Liechti (ref. 7)
		Crack direction indicated by hackle tilt	<ul style="list-style-type: none"> ● Morris (ref. 6)
Identification of contributory factors	Environment and absorbed moisture	Elevated temperature and moisture produce fiber pullout and decreased fiber/matrix adhesion	<ul style="list-style-type: none"> ● Miller (ref. 1) ● Clements (ref. 2)

Figure 4-9. Comparison of Fractography Literature Review Findings to Failure Analysis

characteristics to identify several of the simple failure modes. For translaminar failures, these characteristics involve the fracture morphology of individual fiber ends; however, macroscopic differences—such as the degree of fiber pullout or fracture surface damage—can also be used to identify overall load states. The literature review indicated that tension-generated fractures can be identified by the distinct radial appearance of individual fractured fibers and by pronounced pulling-out of fiber from the surrounding matrix. Fractures generated under compression and flexure are easily distinguished from those generated under tension. Compression fractures show no fiber pullout whatsoever, but exhibit extensive fracture surface damage and individual fiber ends that show a distinct morphology characteristic of microbuckling. Flexure fractures typically exhibit a distinct macroscopic fracture mode evidenced by discrete areas of compression and tension fracture separated by a line that corresponds to the neutral axis.

The available literature indicates that load states for interlaminar fractures are somewhat more difficult to analyze. Most investigators agree that hackles represent interlaminar shear, and that river marks and fine texturing indicate interlaminar tension. However, Robertson has observed some hackle formation under conditions of interlaminar tension and Morris has reported observing only hackles under conditions of interlaminar tension. While some general trends exist in the observations of these characteristic features, there is by no means an overwhelming agreement on the correspondence of these features with the load state of failure.

Identifying Crack Directions and Origins

Only a small number of authors has examined fracture features as they relate to determining the direction of crack propagation. As a result, well-documented methodologies in this critical area are notably lacking. In these investigations, the least controversy exists on determining the direction of crack growth for translaminar fractures. Purslow contends that the direction of tension fractures can be identified by examining the cumulative direction of individual fiber and fractures; however, he is the only individual who has reported this technique.

Defining the direction of crack growth for interlaminar fractures presents an even more complex situation. Several authors indicate that the direction of crack growth can be identified for interlaminar tension fractures by examining the direction of river mark coalescence or resin feathering. However, as pointed out earlier, not all authors agree on

the features characteristic of interlaminar tension and shear fractures. Morris identified hackles—as opposed to river marks—as the predominant feature of interlaminar tension. He also proposed that the direction of crack propagation for mode I fractures could be determined by examining hackle tilt. The situation is further complicated by the fact that a means for determining the direction of propagation for shear failures—where hackles generally predominate—has not been developed by any of the investigators. As a result, the situation for interlaminar fractures is confused in that no analytic methods exist for shear failures and general disagreement exists over tension failures.

Identifying Contributory Factors

Identifying factors that contribute to failure is one of the most difficult areas of investigation; the problem arises from the large number of factors that must be considered. The only contributory factors examined in the literature are those that deal with the effect of temperature or absorbed moisture; several investigators note that such conditions can be identified based on the amount of fiber pullout and reduced fiber/matrix adhesion. The general trend observed is of increasing fiber pullout and decreased fiber/matrix adhesion with increasing temperature or absorbed moisture content.

4.4 LITERATURE SEARCH—STRESS ANALYSIS

An examination of the literature available on stress analysis revealed more information has been published on this subject than for any of the other disciplines. The depth of detail and approaches covered in these articles ranged from relatively simple equations to extremely complex analytic methods. In some cases, the level of complexity reflected the audience each author chose to address. In other cases, the level of complexity corresponded to the level of accuracy the author attempted to achieve in predicting the onset of failure. The simplest investigations reviewed general laminate theory with the prediction of failure onset based on exceeding material strength. Investigators also examined semi-empirical approaches in which material toughness properties are used to predict residual strength. At the most complex level, investigators attempted to combine a multitude of failure prediction approaches with detailed finite element analyses into an integrated computer program.

For the failure investigator, the literature clearly illustrates that a number of methods exist for predicting the strength of composites. However, each author's work presents

only the methods that focus on the specific specimen geometry examined. At the simplest level, the specimens were pressurized cylinders without edge effects. More complex specimens were bolted joints and finite-width plates, with and without moisture conditioning. Consequently, it is difficult to determine how easily the techniques reviewed can be translated into a relatively complex, real-world structure that has poorly defined environmental exposure and load conditions.

To perform a detailed review, the literature was broken down into two broad categories of failure criteria: individual-ply, and laminate-level failure. These two categories and their subdivisions (illustrated in Figure 4-10) reflect a basic division in the level of detail involved in each approach.

On a gross level, analyses are carried out on the complete laminate. This methodology employs an approach similar to that used for homogeneous isotropic materials such as metals. In these analyses, characteristics of material toughness are used in conjunction with specimen geometry to predict component residual strengths.

At the finest level, prediction of failure onset is achieved using individual-ply failure criteria where ply-by-ply stresses are considered and evaluated against material strengths. Because of the complexity of these analytic methods, failure prediction is

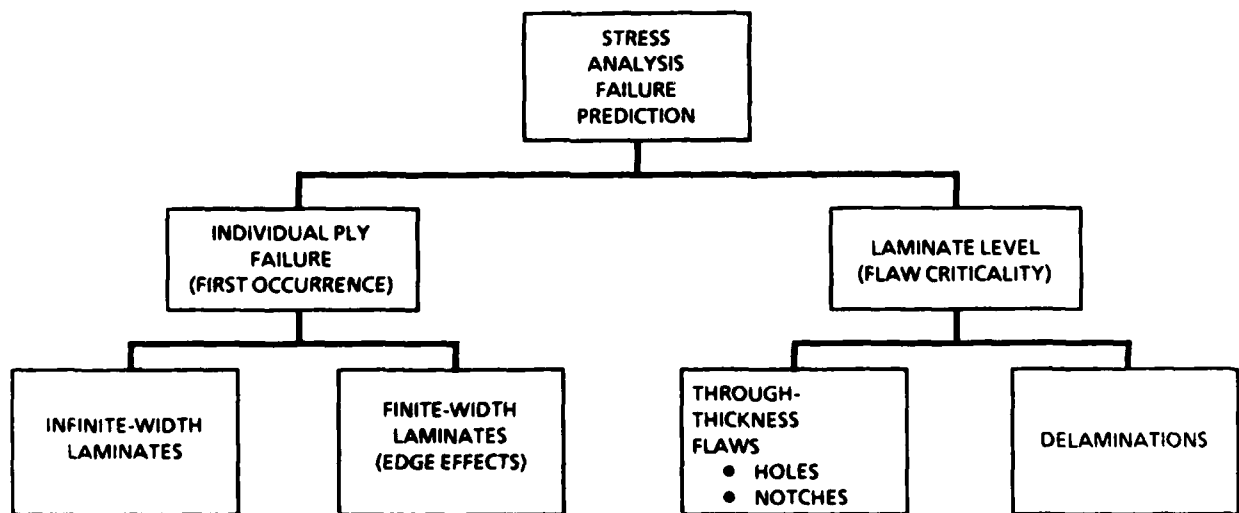


Figure 4-10. Stress Analysis Literature Search Breakdown

usually carried out only for the first occurrence of ply failure rather than for full-specimen failure. Details of each author's investigation into these methodologies are discussed below.

Individual Ply Failure Criteria

When performing stress analyses on individual plies, particular emphasis has been placed, within the literature, on developing criteria to identify the first occurrence of ply failure. In investigating this methodology, researchers examined both finite- and infinite-width specimens. The principal difference between these configurations is the degree to which free edge effects are considered. Of the two, infinite-width panels are simpler to analyze.

In Craddock's article, standard laminate theory methods to calculate individual-ply stresses are reviewed, and several different failure criteria for infinite-width panels are evaluated. In this review, applied stresses are transformed into on-axis ply stresses (or strains) using the stress transformation equations commonly employed in lamination theory (Figure 4-11). A detailed review of this theory can be found in any standard textbook on composites. For these transformed stresses or strains, a variety of criteria for the onset of first-ply failure were evaluated. For each criterion, failure is defined as the point at which the conditions of transformed stress exceed the individual ply's strength envelope. The definition of this envelope is the most basic difference between the various criteria examined. In Craddock's work, five criteria were evaluated:

1. Maximum Stress Theory

Failure occurs when material strength is exceeded along any of the principal laminate orientations. This condition is described in the following equation where failure occurs

	σ_1	σ_2	σ_6
σ_x	m^2	n^2	$2mn$
σ_y	n^2	m^2	$-2mn$
σ_s	$-mn$	mn	$m^2 - n^2$

$$m = \cos \theta, n = \sin \theta$$

Figure 4-11. Stress Transformation Equations

when the applied stresses are equal to or greater than the tension, compression or shear strength of the material:

$$\begin{aligned} & \sigma_1 \geq X^t \text{ or } \sigma_1 \geq X^c \\ \text{or } & \sigma_2 \geq Y^t \text{ or } \sigma_2 \geq Y^c \\ \text{or } & \sigma_{12} \geq S \end{aligned}$$

where

- σ_1 = stress along the fiber direction
- σ_2 = stress transverse to fiber direction
- σ_{12} = in-plane shear stress
- X^t, Y^c = tension and compression strength along the fiber direction
- Y^t, Y^c = tension and compression strength transverse to fiber direction
- S = in-plane shear strength

2. Hill's Criterion

A form of Von Mises' Distortional Energy Criterion where failure occurs when:

$$\left(\frac{\sigma_1}{X^1}\right)^2 + \frac{\sigma_1\sigma_2}{(X^1)^2} + \left(\frac{\sigma_2}{Y^1}\right)^2 + \left(\frac{\sigma_{12}}{Y^1}\right)^2 = 1$$

where $\sigma_1, \sigma_2, \sigma_{12}$, and X^t, Y^t , and S have the same meaning as noted above. For this equation, the failure strength in tension is assumed to be identical to that for compression.

3. Azzi-Tsai Criterion

A form of Hill's criterion where different tension and compression strengths are allowed. Failure occurs when:

$$\left(\frac{\sigma_1}{X^1}\right)^2 - \frac{\sigma_1\sigma_2}{(X^1)^2} + \left(\frac{\sigma_2}{Y^1}\right)^2 + \left(\frac{\sigma_{12}}{S}\right)^2 = 1$$

where $X^1 = X^t$ when X^1 is positive and $X^1 = X^c$ when X^1 is negative, and similarly, $Y^1 = Y^t$ when Y^1 is positive and $Y^1 = Y^c$ when Y^1 is negative. For the equation above, X^t, X^c, Y^t , and Y^c have the same meanings as denoted previously.

4. Hoffman's Criterion

A further generalized criterion where failure occurs when:

$$\frac{\sigma_1^2 - \sigma_1\sigma_2}{X^t X^c} + \frac{\sigma_2^2}{Y^t Y^c} + \frac{X^c - X^t}{X^c X^t} \sigma_1 + \frac{Y^c - Y^t}{Y^c Y^t} \sigma_2 + \frac{\sigma_{12}^2}{S^2} = 1$$

where $\sigma_1, \sigma_2, \sigma_{12}$, and X^t, X^c, Y^t, Y^c , and S have the same meanings as in the above criteria.

5. Tsai-Wu's Criterion

The most commonly used where tensors are used to describe material strength. Failure occurs when:

$$F_i \sigma_i + F_{ij} \sigma_i \sigma_j = 1 \quad i, j = 1, 6$$

where F_i, F_{ij} are strength tensors, and

$$F_1 = \frac{1}{X^t} - \frac{1}{X^c}$$

$$F_2 = \frac{1}{Y^t} - \frac{1}{Y^c}$$

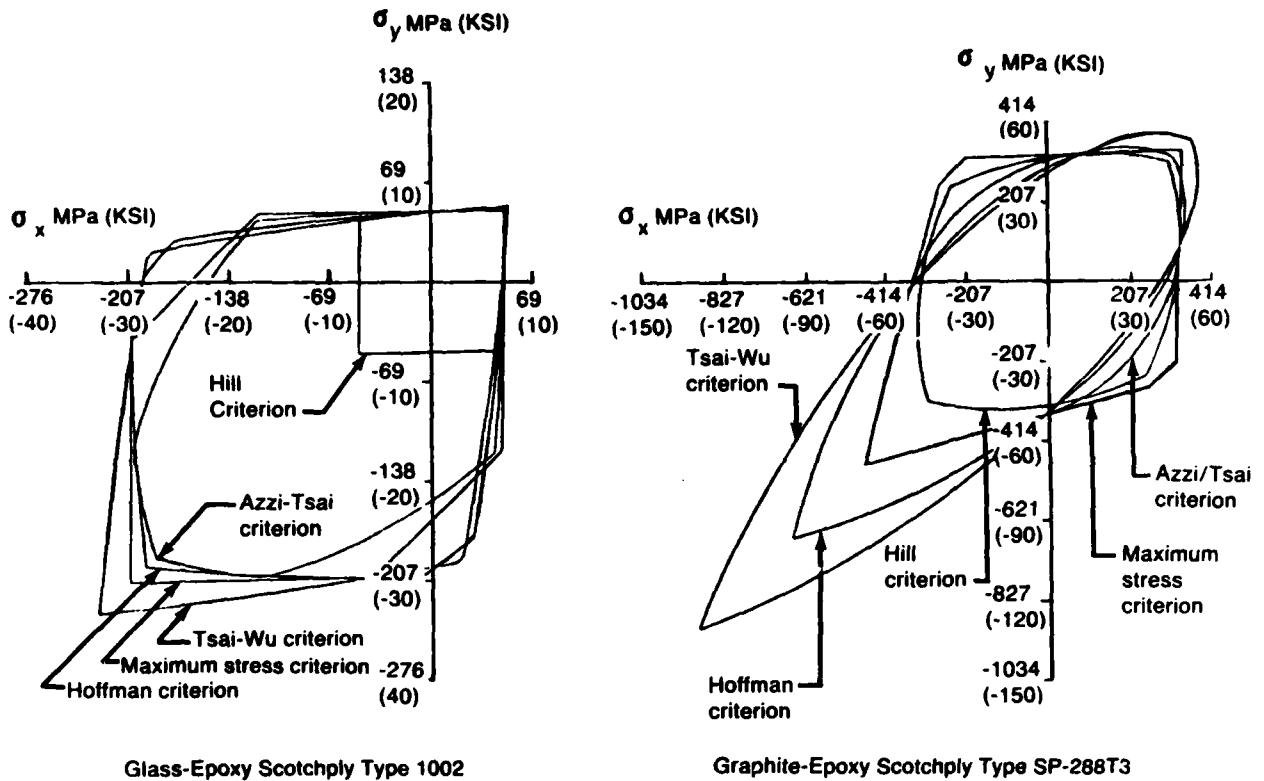
$$F_{11} = \frac{1}{X^t X^c}$$

$$F_{22} = \frac{1}{Y^t Y^c}$$

$$F_{66} = \frac{1}{S^2}$$

where X^t, X^c, Y^t, Y^c , and S have the same meanings as denoted previously.

Many of these failure theories are adaptations of the energy distortion failure theories commonly employed in predicting the onset of failure in metals (Von Mises' Theory). As noted in Craddock's work, the failure envelopes predicted by these criteria vary widely. Figure 4-12 illustrates the laminate failure envelopes predicted by each criteria for fiberglass and graphite-epoxy laminated tubes. To a large extent, the variations reflect

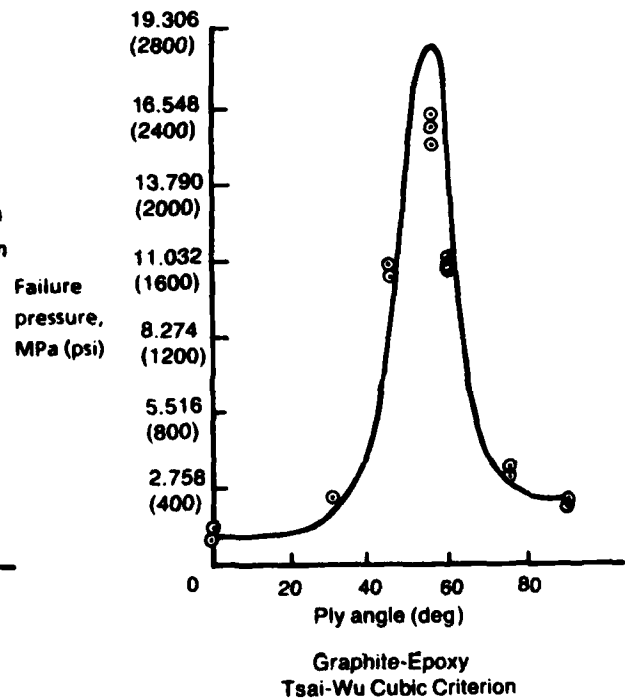
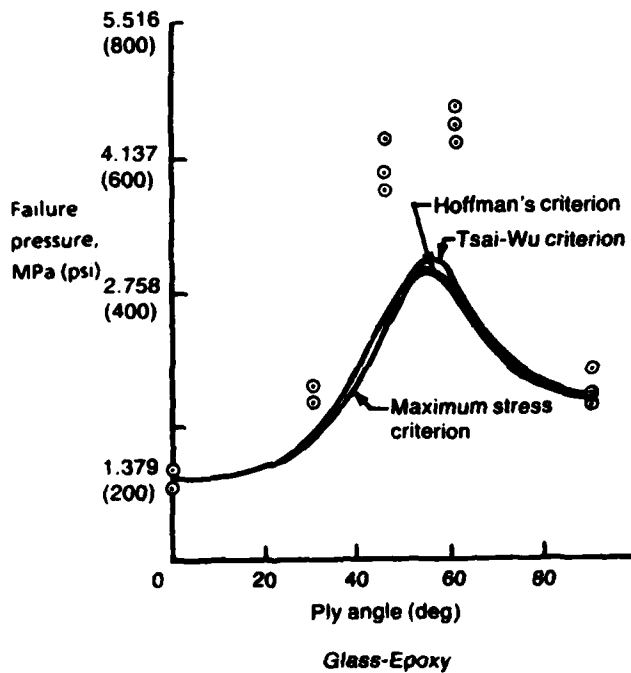
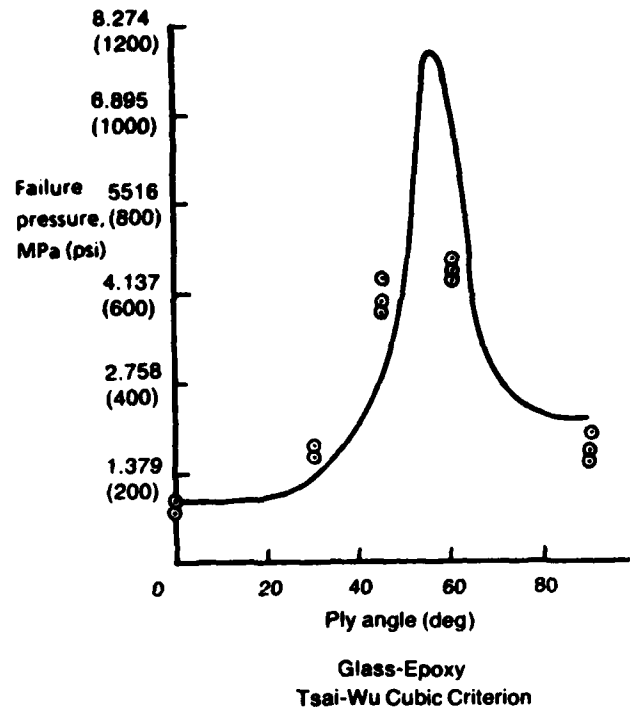
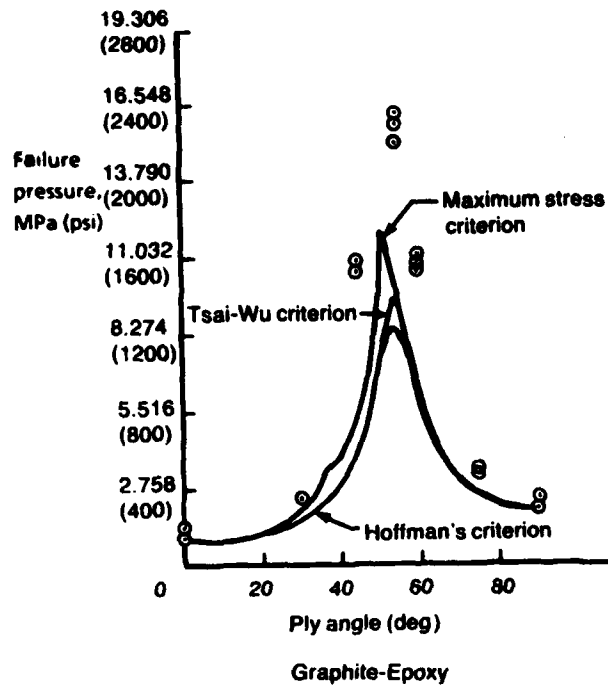


(Ref. 15. Copyright © American Institute of Aeronautics & Astronautics; Reprinted with Permission)

Figure 4-12. Comparison of Yield Criteria for Glass- and Graphite-Epoxy

the extent to which each criteria accounts for anisotropy in material strength. More significant than these differences, however, is the ability of each theory to predict the actual point of failure onset. As presented by Craddock, a comparison of the actual with the predicted onset of failure for relatively simple laminates reveals substantial differences (Figure 4-13). While the criteria indicate general trends in failure stresses, they do not appear capable of predicting failure onset with much accuracy. This situation reflects the difficulty in applying an analytical model to variable material strengths. Another potential contributor to this inaccuracy is the fact that each criterion predicts the occurrence of failure at an individual-ply level rather than at the laminate level, where measurable failure occurs. In either case, the great differences in accuracy and predicted envelopes highlight some of the major problems with attempts to analytically predict the point of failure.

While Craddock examined the use of relatively simple cylindrical tubes, other investigators examined specimens with finite-width effects both with and without environmental and cure stress considerations. These investigations represent the next level of



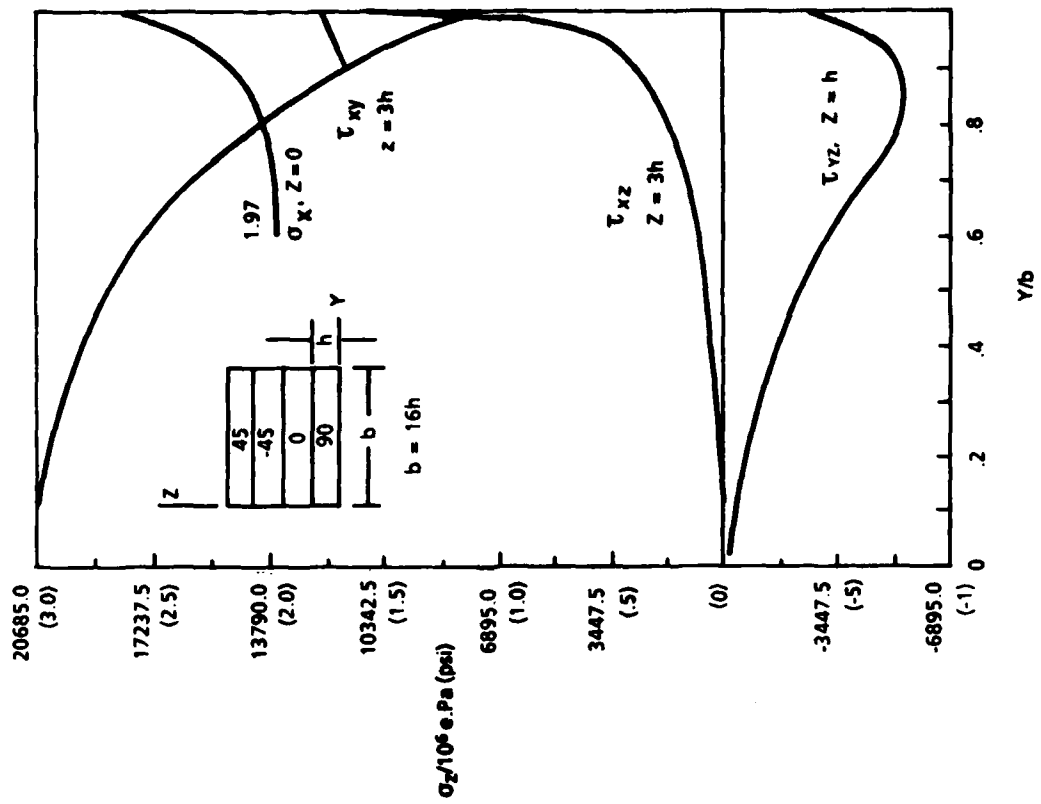
(Ref. 15. Copyright © American Institute of Aeronautics & Astronautics; Reprinted with Permission.)

Figure 4-13. Predicted Versus Actual Failure Pressure for Laminated Cylinders.

complexity in predicting failure onset using individual-ply failure criteria. For the failure analyst, these works are useful in that they embody considerations likely to be necessary with real-world structures. Both Crossman and Herakovich observed that significant variations in stresses and strains can occur at the free edge of specimens. Both authors show the magnitude of these stresses for relatively simple layups and specimen geometries. Generally, the most significant stresses are those developed near the specimen's free edge. In analyzing these stresses, both authors employed two-dimensional finite-element grids arranged along the specimen cross-section. Using these grids illustrates the degree of complexity involved in determining the stresses (or strains) in microscale with such design details. As noted by Crossman, particularly large gradients can occur in both Z and Y directions (Figure 4-14). Regarding the application of individual-ply failure criteria, the large increase in σ_z , σ_x , and τ_{xz} stresses near the edge of the specimen are particularly significant, since laminate theory methods would have ignored these increases.

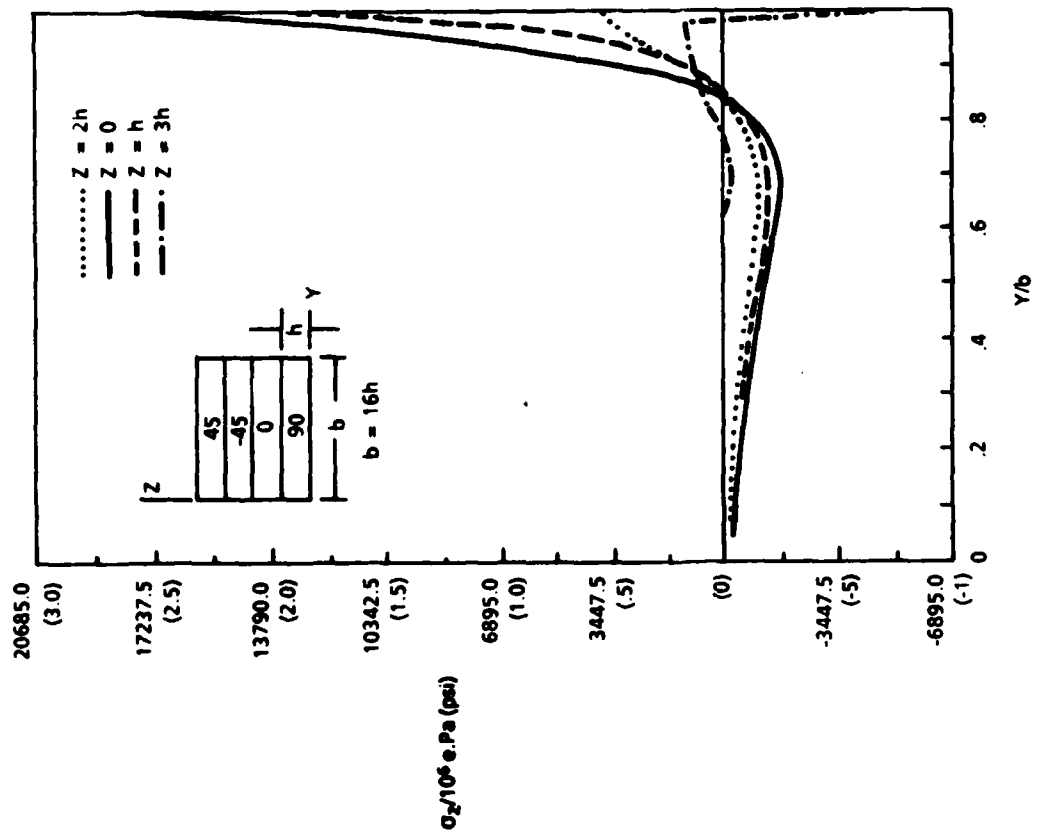
Both Crossman and Herakovich predicted that stresses would be further influenced by internal cure stress, test temperature, and conditions of moisture absorption or desorption (Figure 4-15). In Herakovich's work, the relationship of these stresses to failure prediction were considered. Since his finite-element model examined stresses along three dimensions, it was necessary to observe a fully three-dimensional failure criterion. Herakovich used the tensor polynomial criteria advanced by Tsai-Wu, in which strength tensors are given in terms of material principal strengths. As illustrated in Figure 4-16, Herakovich predicted that the onset of failure depends quite strongly on edge stresses, particularly for small ($+0$) laminate angles. While not verified against actual test data, these results, when considered with Crossman's, clearly indicate that both edge and environmental stress effects must be carefully evaluated in predicting the onset of failure for whichever individual-ply criteria are employed.

Perhaps the farthest advancement of first-ply failure criteria as a method of prediction has been made by Chamis. In attempting to predict the defect growth and damage of composite materials subjected to load, Chamis developed an integrated computer program called CODSTRAN. Within this program, a detailed finite-element grid is constructed and evaluated for failure using both individual first-ply failure criteria and laminate-level fracture criteria. In the case of individual-ply failures, Chamis' program incorporates both general quadratic and modified distortional energy (Von Mises') criteria to predict the occurrence of failure for each element of the overall finite-element model. What is



Variations stress distributions along several ply interfaces in (+45/-45/0/90 - degrees)_s

(Ref. 16. Copyright © Sighthoff and Noordhoff International Publishers, reprinted with permission.)



Distributions along each ply interface for (+45/-45/0/90 - degree)_s

Figure 4-14. Stress Gradients Resulting From Edge Effects

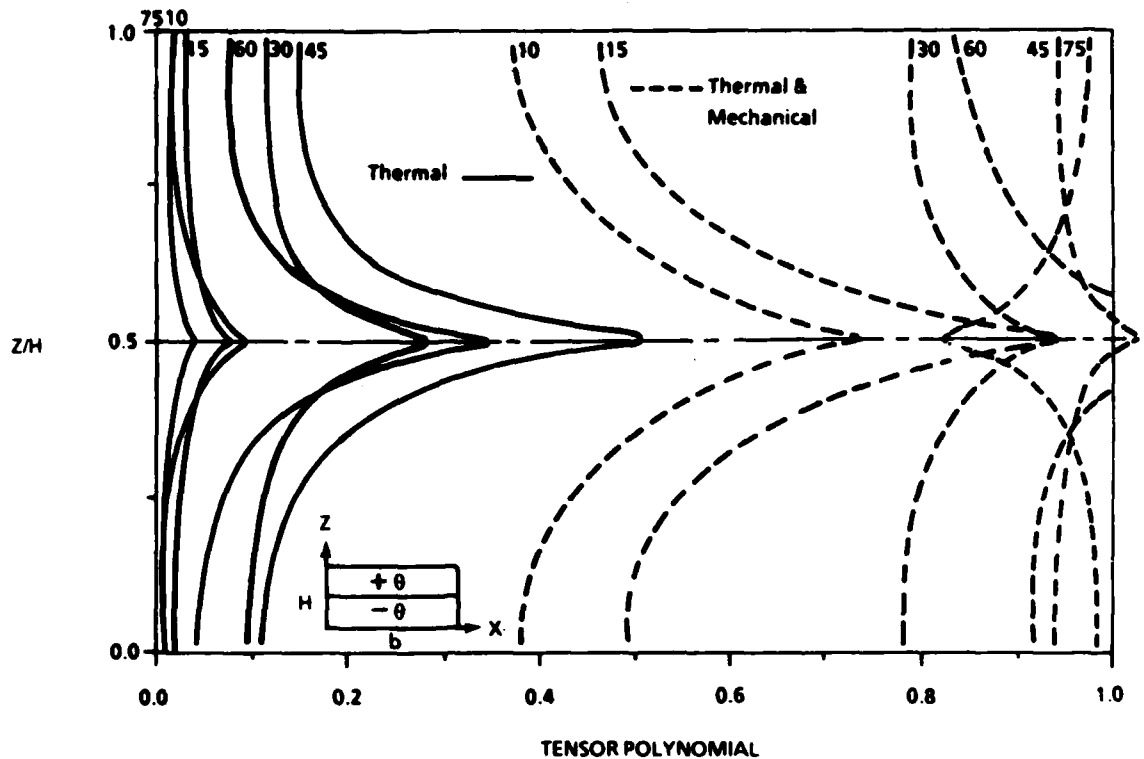


Figure 4-15. Through Thickness Tensor Polynomial Distributions For Curing Stresses and Stresses at First Failure in $[\pm\theta]$, Laminates

unique about Chamis' work, however, is that failed-ply elements are eliminated, and the analysis process is reiterated. As a result, CODSTRAN describes the sequence of events leading to failure, and an approximate prediction of the load at failure.

Laminate Failure Criteria

The results of the literature search in the second major area of stress analysis, laminate failure criteria, revealed a number of approaches for predicting the onset of specimen failure. These investigations examined the relationship of damage, cracks, holes, or internal delaminations on residual strength. Most of the analytic techniques reviewed employed semi-empirical approaches similar to the fracture toughness methods commonly used with metal structures. These methods typically involve the experimental determination of an intrinsic material property related to crack growth—such as material fracture toughness. This value, when considered with the size and geometry of the flaw, allows the stress at fracture to be calculated.

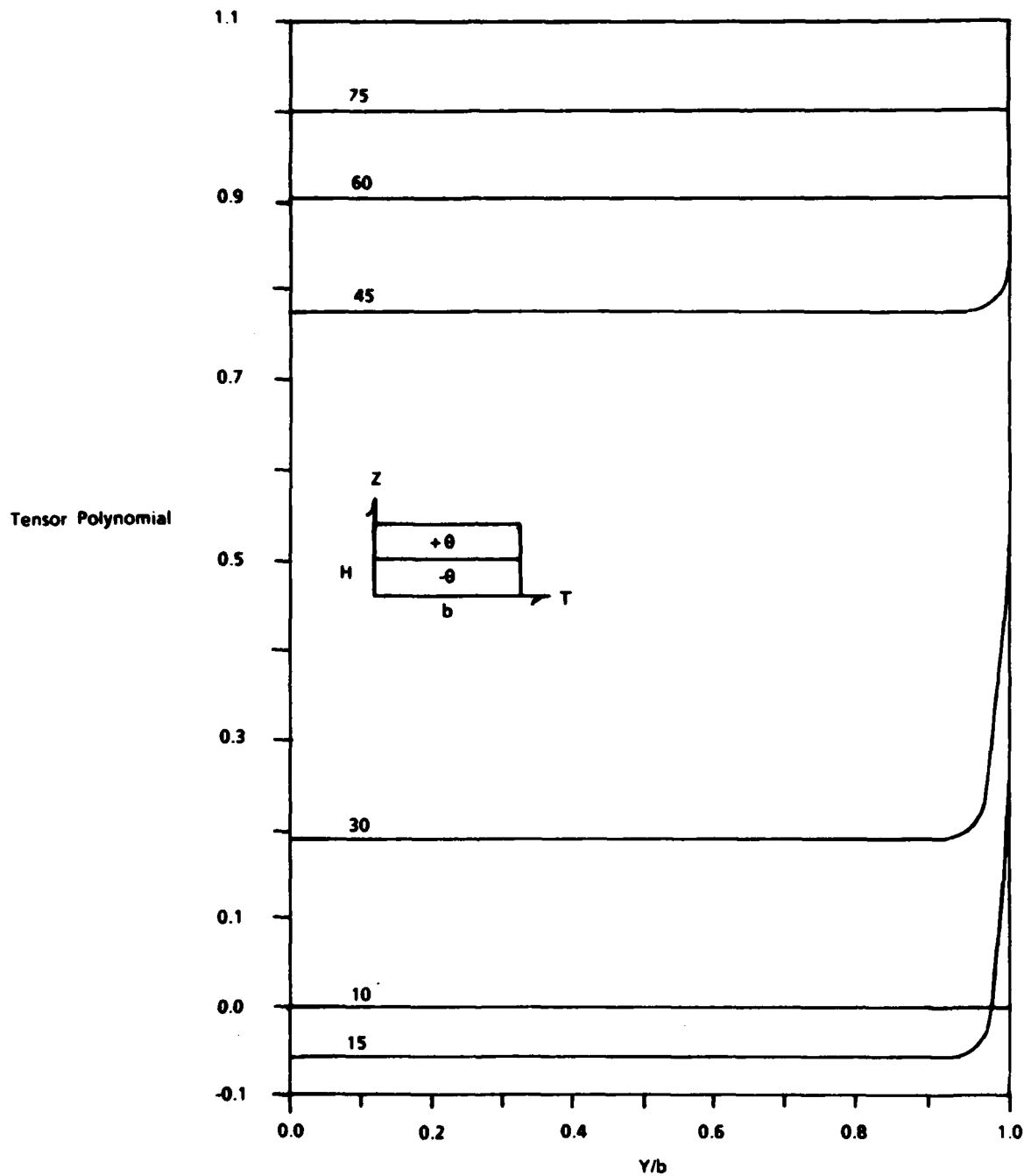


Figure 4-16. Tensor Polynomial Distributions Along the Interface of $[\pm\theta]_5$ Laminates for First Failure Under Tensile Strain With Curing Stresses

The easiest-to-understand methodologies for determining laminate failure are those adapted directly from metals fracture toughness analyses. These analyses predict the onset of component fracture through the experimental determination of a characteristic K_C fracture toughness value. In these cases, K_C indicates the stress intensity factor at which fracture occurs based on the initial crack length and maximum load at failure. (For reference, this value is often referred to as $K_{apparent}$ in metals fracture toughness.) In works by Bathias, McGarry, and Awerbuch, K_C values have been determined for a variety of layups. In measuring values, these researchers used specimens adapted directly from traditional metals toughness testing, such as compact tension coupons or large center-crack tension panels. In Bathias' work, K_C values were measured for a variety of layups. As illustrated in Figure 4-17, values ranging from 16 to 43 $\text{MPa}\sqrt{\text{m}}$ were measured, and demonstrated a clear dependence on the ply stacking sequence and orientations examined. (For 7075-T7351 aluminum, K_C typically equals 80 to 90 $\text{MPa}\sqrt{\text{m}}$). Each author suggests that knowledge of this material property for a layup can be used to estimate the stress at fracture instability for a given crack and component geometry.

This point of instability can be defined by using the equation:

$$K_C = Y\sigma \sqrt{\pi a}$$

where Y is a geometric factor related to the crack length and location within the component being examined, σ equals the stress at instability, a equals the full crack length, and K_C equals the material fracture toughness. A more detailed review of this technology can be found in any of several texts dealing with the fracture behavior of metals.

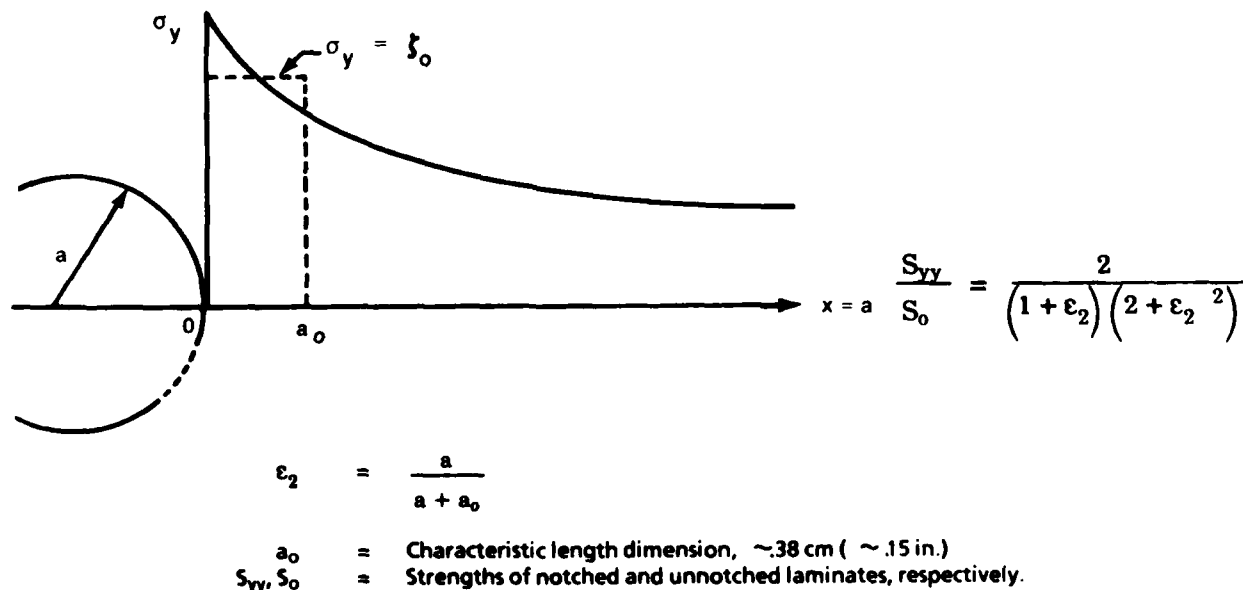
Numerous researchers have also attempted to predict the criticality of holes, cracks, and damage by empirically measuring other characteristic fracture properties--in much the same way as is done with fracture toughness. The most noteworthy of these efforts

		LAYUP (DEGREES)		
FRACTURE TOUGHNESS ($\text{mPa}\sqrt{\text{m}}$)		0/45/90/135/90/45/0 16 plies	0/30/60/90/120/150/0 13 plies	0/45/135/0/135/45/0 16 plies
	K_C	29-43	23-35	16-22

(Ref. 19. Copyright © Butterworth Scientific Ltd.; Reprinted with Permission.)

Figure 4-17. Fracture Toughness of Various Layups

include two failure criteria which assume failure occurs when the stress at some distance away from the flaw reaches the ultimate material strength. These two are the average stress, and the point stress failure criteria models. As described in Daniel's paper, the average stress failure criterion proposes that failure occurs when the average stress over a characteristic material dimension (a_0) equals the material strength. This criterion is illustrated in Figure 4-18, where a_0 represents the length dimension of a particular layup and material. Similarly, the point-stress failure criterion presented by Mikulas predicts that panel failure occurs when the axial stress at some distance (d_0) from the hole boundary equals the strength of the unnotched laminate as shown in Figure 4-19. Daniel, Mikulas, and other investigators measured both a_0 and d_0 for a variety of layups and found a relatively good correspondence of predicted and measured strengths for open holes (Figure 4-20). Of particular concern to the failure analyst, however, is the ability to predict failure onset for flaw conditions such as through-cracks or impact damage. In this area, Mikulas examined the applicability of the point failure criteria; for the case of a



(Ref 22 Reprinted with the permission from "ICCM II," by B.R. Noton, et al., The Metallurgical Society, 420 Commonwealth Drive, Warrendale, Pennsylvania 15086.)

Figure 4-18. Strength Reduction of Uniaxially Loaded Plate With Circular Hole, According to Average Stress Criterion

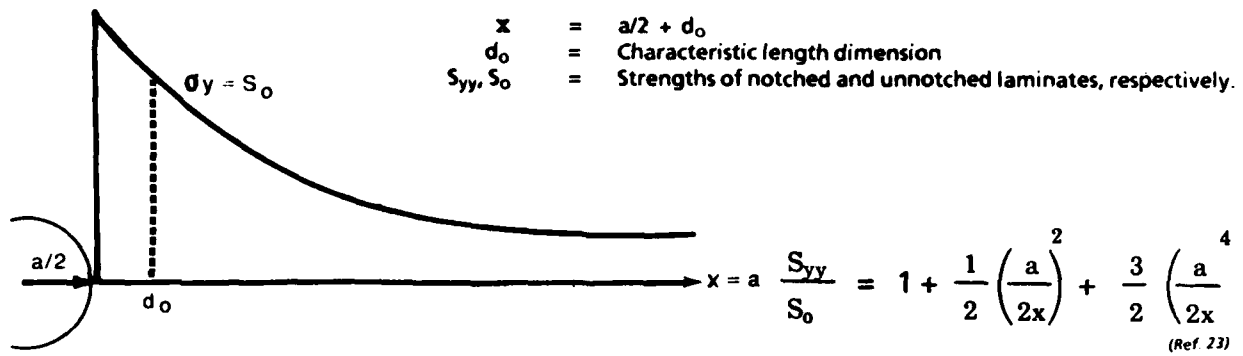
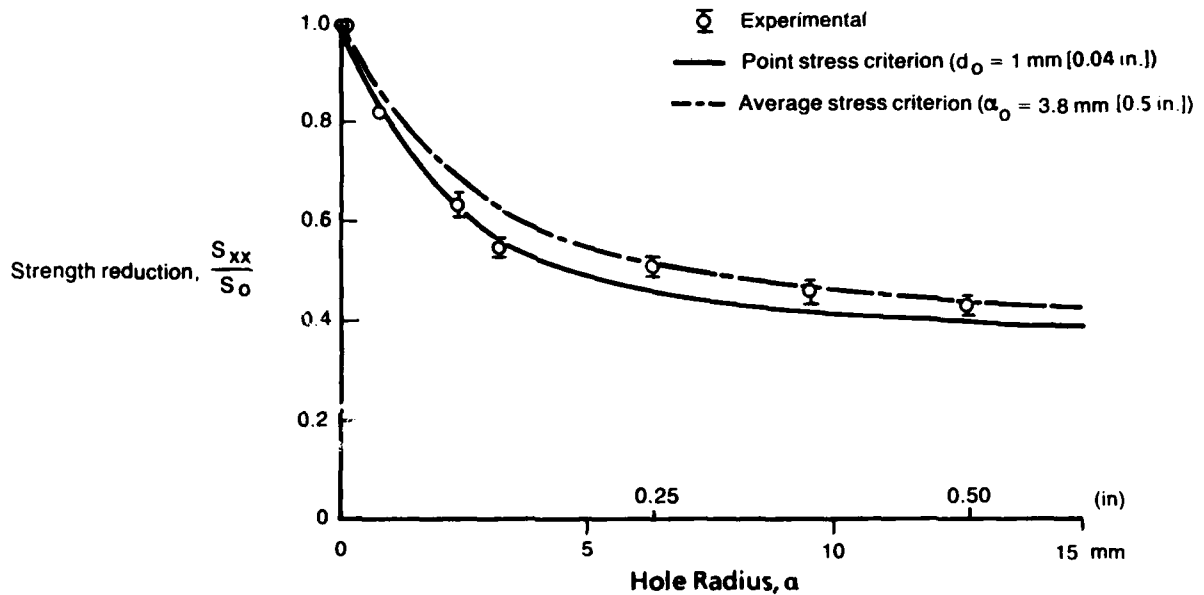


Figure 4-19. Strength Reduction of Uniaxial Loaded Hole According to Point Failure Stress Criteria



(Ref. 22. Reprinted with the permission from "ICCM II", by B. R. NOTON, et al., The Metallurgical Society, 420 Commonwealth Drive, Warrendale, Pennsylvania 15086)

Figure 4-20. Strength Reduction as a Function of Hole Radius for (0/ + 45/- 45/90-Degree), Graphite-Epoxy Plates With Circular Holes Under Uniaxial Tensile Loading

through-crack, stress as a function of distance from the crack was expressed as:

$$\frac{\sigma_y}{\sigma_\infty} = \frac{X}{\sqrt{X^2 - \left(\frac{a}{2}\right)^2}}$$

where: $x = x_1 + \frac{a}{2}$

- X = distance along the x-axis, away from the crack
- a = crack length
- σ_∞ = stress at infinite distance from crack
- σ_y = stress in the y direction

As a result, Mikulas indicated that the residual strength for a given crack of size a can be determined if X is set equal to d_0 .

With respect to impact damage, Mikulas reported that the characteristic length d_0 depends on the toughness of the resin system examined. As illustrated in Figure 4-21, a relatively good correlation exists for tough resin chemistries, but not for brittle, delamination-prone resin systems. These observations indicate that the accuracy of failure predictions will depend strongly on the resin system used, and the configuration of damage examined.

While the work discussed above examined the criticality of through-thickness flaws (except for impact), other investigators have considered the ability to predict failure with

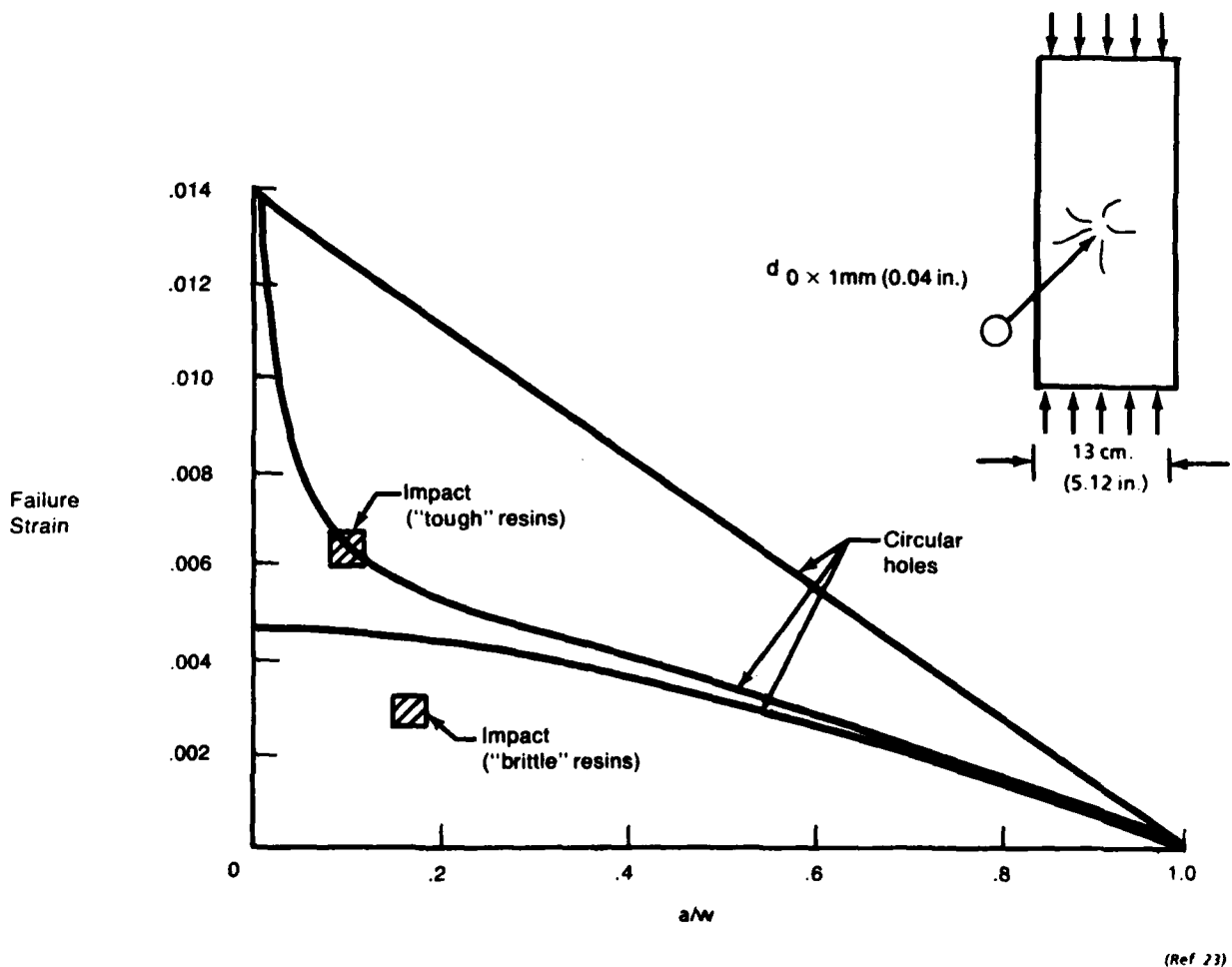


Figure 4-21. Effect of Impact Damage on the Compressive Strength of a Quasi-Isotropic Laminate.

in-plane interlaminar flaws. Research on this condition, however, has not been as extensive as in other areas, and has only been performed fairly recently. Investigations in this area have been performed principally by two researchers, O'Brien and Webster. In O'Brien's studies, the stability of delaminations under tension loading were examined; the onset of instability was determined by expressing the strain energy release rate, G , of a relatively simple delaminated coupon as an equation. The strain energy release rate, G , in a similar manner to K in metals, can be used to describe the stress intensity of a crack tip. In O'Brien's study, G_C , a value characteristic of material toughness, was expressed in generic form as:

$$G_C = \frac{P^2}{2b} \cdot \frac{dC}{dA}$$

where

- b = width of crack
- G = strain energy release rate
- C = compliance
- A = area of fracture
- P = load

Given this material toughness value, O'Brien's study developed an equation to describe the magnitude of G developed in the simple coupon examined. The equation was found to equal a constant dependent only on the number and location of delaminated plies. O'Brien's work indicates that by knowing the value of these constants in conjunction with G_C for a particular material system, the load at instability (P) can be calculated fairly readily, providing an approximate prediction of failure onset.

Webster has also examined the stability of simple interlaminar flaws; however, in this researcher's work, the stability of flaws was partly considered under the more difficult condition of axial compression. Webster examined the load at which a near-surface circular delamination begins to buckle out of plane. Webster indicates that after predicting buckle onset, instability of the delamination should be determined by examining when the potential energy stored in the buckle equals the strain energy release rate (G_C) necessary to produce crack growth. Unfortunately, while Webster's investigation alludes to an actual derivation of these relationships, none was derived. Consequently, it is difficult to determine the extent to which this method works, or what its limitations might be.

Discussion

In Section 4.4 of this report, literature on stress analysis is reviewed in detail. While these writings by no means encompass the entire field of stress analysis, they provide perspective on the techniques and procedures available for composite materials. Before discussing the application of these techniques, however, it is important to recognize the role of stress analysis in a postfailure investigation.

Most components are subjected to detailed stress analyses as part of their initial design. Consequently, in the as-designed configuration, failure should not occur as long as the component is operated within its design life and envelope. However, real-world experience indicates that component fractures do occur in service. Common causes of such failures include:

- o **Design Deficiencies** such as insufficient assessment of loads and stresses; either of design details or individual plies. Also included is the oversimplification of loads, load paths, and the combined effects of load, damage, and environment.
- o **Manufacturing and Process Discrepancies** such as mismachined radii, ply layup errors, and mislocated or misdrilled fastener holes.
- o **Service Damage** including foreign object impact, subcritical cracking, and improper maintenance or repair.

For each case, the objective in analyzing stress is to determine if the occurrence of a failure not predicted during initial design can be explained and understood. While techniques such as fractography may be able to identify the origin and mode of fracture, it is stress analysis that most often determines the cause of failure.

The stress analysis to investigate part failure can be relatively complex, but from the point of view of the failure analyst, the process involved can be divided into two discrete tasks, thus making the review of available literature more straightforward. The two tasks are:

- o **Assessment of the component strength in the as-fabricated condition**

- o Assessment of component residual strength considering flaws, damage, and sub-critical cracks.

Figure 4-22 illustrates the relationship between the methods identified in the literature and these two tasks. The first task, assessing the part strength in the as-fabricated

ANAL. TASK	METHOD	DESCRIPTION	AUTHORS	COMMENTS
Assessment of as-fabricated strength	Laminate theory and first ply failure criteria	Laminate theory is used to identify two-dimension stresses; one of several failure criteria are applied to define occurrence of first-ply failure	<ul style="list-style-type: none"> ● Chamis (ref. 18) ● Craddock (ref. 15) ● McLaughlin (ref. 29) 	<ul style="list-style-type: none"> ● Valuable for simple prediction of ply failure ● Laminate theory requires knowledge of local stresses ● Laminate theory cannot handle edge effects/complex geometries ● Predicted failure stresses vary widely with criterion used ● Failure criterion not accurate ● Does not predict full failure
	Finite element analysis and first ply failure criteria	Finite element analysis is used to define stresses in three dimensions for edge effects/environments/bolted joint configurations; one of several criteria are applied to define occurrence of first-ply failure	<ul style="list-style-type: none"> ● Crossman (ref. 16) ● Herakovich (ref. 17) ● Wu (ref. 28) 	<ul style="list-style-type: none"> ● Valuable for simple prediction of ply failure ● Finite element techniques can be used to define local stresses ● Method accounts for edge effects, environment, complex geometries ● Predicted failure stresses vary widely with criterion used ● Failure criterion not accurate ● Does not predict full failure
	Point or average failure stress criteria	A semi-empirical method for describing the strength of open or filled holes; failure occurs when point or average stress at a characteristic distance from hole equals material strength	<ul style="list-style-type: none"> ● Mikulas (ref. 23) ● Wilson (ref. 26) ● Daniel (ref. 22) 	<ul style="list-style-type: none"> ● Valuable for prediction of strength with holes ● Requires knowledge of characteristic distances for material ● Requires knowledge of stress distribution around hole
Assessment of residual strength	Point failure stress criterion	Adapted semi-empirical method from predicting strength with holes; failure occurs when stress at a characteristic distance from damage radius equals material strength	<ul style="list-style-type: none"> ● Mikulas (ref. 23) ● Starnes (ref. 27) 	<ul style="list-style-type: none"> ● Valuable for predicting residual strength with impact of through-thickness cracks ● Requires knowledge of characteristic distance for material ● Requires knowledge of stress distribution around hole ● Requires estimation of initial damage size to predict strength
	K_{Ic} fracture toughness	Fracture toughness method commonly used with metals	<ul style="list-style-type: none"> ● Bathias (ref. 19) ● McGarry (ref. 20) ● Averbuch (ref. 21) 	<ul style="list-style-type: none"> ● Valuable for predicting residual strength with through-thickness cracks under tension loads ● Requires knowledge of K_{Ic} for material layup ● Requires estimation of initial crack size to predict strength
	G strain energy release rate	Predicts onset of delamination instability based on G_{Ic} for material and G level generated by applied load	<ul style="list-style-type: none"> ● O'Brien (ref. 24) ● Webster (ref. 25) 	<ul style="list-style-type: none"> ● Valuable for predicting delamination instability ● Requires knowledge of G for material/layup ● Requires calculation of buckle stability for compression case ● At present, can handle only very simple geometries
	CODSTRAN	Integrated computer program that incorporates finite element model, first-ply failure, and point average failure criteria; program is iterative, allowing prediction of failure sequence and residual strength	<ul style="list-style-type: none"> ● Chamis (ref. 18) 	<ul style="list-style-type: none"> ● Attempts to meld various techniques discussed above ● Requires expert computer programmer ● Requires material data, as described above ● Inaccurate prediction of strength

Figure 4-22. Stress Analysis Methods Identified in Literature Search

condition, evaluates stresses at a greater level of detail than during initial design. In most cases, this assessment focuses on the crack origin, with special attention to discrepant manufacturing and production conditions. Principal techniques at this level of assessment likely to be of value include individual-ply, point, and average-failure criteria.

The individual-ply failure criterion examines stresses at the individual ply level and establishes the onset of first-ply failure. The chief benefit of this analysis method to failed structures is its ability to predict the point of initial failure on a microscale. This ability is particularly significant since most initial design analyses consider stresses on a gross-average basis. However, even though there is potential value in this methodology, some drawbacks exist. The most significant of these is that to examine edge-effect stresses the individual-ply failure criterion requires a knowledge of plan view stress distributions (surface stress flow) and detailed finite-element grids. For companies with experts in stress analysis, neither of these factors is a limitation. More significantly, however, the individual-ply failure criterion predicts failure initiation, not full failure. It also exhibits significant inaccuracies when correlated with test data. Consequently, failure onset cannot be meaningfully determined based on the individual-ply failure criterion. As a result, prediction of the stress required for full failure is more likely to be calculated by gross area stress calculations with fine, finite-element grid structures placed in the area of failure origin.

Other considerations in estimated gross area stress are the point- and average-failure stress criteria. As described in the works of Daniel and Mikulas on laminate failure criteria, the stress at failure can be determined for any hole, given the characteristic length dimension (d_0) for the particular material and layup. Based on results reported in these researchers' works, this method appears to work relatively well, its only apparent constraints being that it requires empirical measurement of d_0 and knowledge of the plan view stresses for the area of interest. In actual application, neither of these constraints should be significant; however, additional concerns that must be addressed include the effects of environment, absorbed moisture, and resin formulation on the validity of a single value used as a characteristic material property.

Figure 4-22 depicts the second major task involved in the stress analysis of a failed component—assessing its residual strength. Considerable investigation has been done that can be directly translated to the analysis of through-thickness flaws. Unfortunately, the characterization of flaw criticality in delaminations was relatively limited and immature.

For through-thickness cracks, the situation is more encouraging. Either the K_{IC} fracture toughness or point-stress failure criterion appear to work well for predicting the onset of crack instability. The limit in applying either of these methodologies lies in the ability of disciplines such as fractography to identify and define the size of original damage. Given this measurement, establishing the point of stress necessary to cause failure requires only that values for d_0 or K_{IC} be known. The literature shows that these values have been measured for a variety of layups. However, these characteristic material properties may vary with resin system and environment, making the calculation of residual strength more difficult.

Methods for analyzing delamination are not nearly as mature as those for measuring through-thickness flaws. Very simple models have been examined for both tension- and compression-loaded plates. Results showed some promise of being able to predict the onset of delamination growth under tension. However, the sole researcher who examined delamination stability under compression only alluded to its calculation using G , the strain energy release rate. As a result, one must conclude that calculating the flaw criticality of such in-plane defects is extremely difficult, and not yet practical for general use.

In summary, reviewing the stress analysis literature revealed several techniques for assessing the strength of failed components either as-fabricated, or with through-thickness damage or fracture. These techniques, their value and their limitations are summarized in Figure 4-22. Certain of these techniques are somewhat inaccurate, or may require measured properties not readily available; however, at the very least, the techniques define the applicable methodologies and their attributes.

4.5 LITERATURE SEARCH—NONDESTRUCTIVE EVALUATION

In the broadest sense, nondestructive evaluation (NDE) includes any examination that assesses material integrity without damaging or destroying a part, and it is used for a variety of tasks such as: in-process quality control, in-situ test monitoring, and fleet service inspection. For failure analysis, nondestructive evaluations are useful for identifying conditions of nonvisible fracture for documentation, and for planning subsequent destructive evaluations. Since nonvisible fracture conditions (such as delaminations) are particularly common in composite materials, nondestructive evaluation methods are particularly important for the composite failure analyst.

Nondestructive evaluation techniques described in the literature reviewed for this project can be grouped into three broad categories that reflect the methods used to identify nonvisible damage conditions. The categories are: ultrasonics, eddy current, and X-ray radiography.

Ultrasonic Testing

Composite materials can be probed ultrasonically using a variety of techniques. All of the techniques are similar in that they apply an ultrasonic waveform to a specimen and then monitor resonance, attenuation, or return echos as signs of internal damage. In the literature reviewed, specific methods that employed this technique include:

Ultrasonic Through-Transmission. This method received the widest consideration in the literature. Researchers who considered this method include Phelps, Reynolds, Schramm, and Ulman. Ultrasonic through-transmission uses two yoke-mounted transducers that are positioned on opposite sides of the part acoustically coupled to the surface of the part using oil, grease, gels, or water columns. Streams of water issue from the transducers and impinge on the part; ultrasonic sound waves from the sending transducer are transmitted through the water column, through the part, and continue along the water column on the opposite side to the receiving transducer. Fractures in the panel cause a reduction in sound transmission, allowing for relatively easy identification of flaws. In studies by Phelps, this method has been shown to be particularly sensitive to in-plane damage such as delaminations.

Single-Sided Harmonic Bond Testers. This technique has also been investigated by a number of researchers. The method uses standing waves to sense changes in laminate panel thickness; since delaminations produce a change in the effective thickness of bonded plies, a change in harmonic resonance occurs. As indicated in the works of Reynolds and Phelps, this change in resonance can be used to identify delaminations when a set of harmonic resonance calibration curves for laminates of different thicknesses is provided. In Reynolds' work, successful measurements of flaws as small as 10 mm (0.39 in.) have been made on laminates up to 4 mm (0.16 in.) thick.

Single-Sided Ultrasonic Angle Beams (Backscatter). This method uses backscattered ultrasound pulses to detect internal flaws. In most instances, this technique employs separate transmitting and receiving transducers housed in a single surface probe. As

described by Bar-Cohen and Moran a complex wave front is created in the structure by the transmitter, and is continuously monitored by the receiving transducer. With this system, delaminations create both a phase and amplitude change, allowing their detection. Because the inputted ultrasonic signal is angled with respect to the specimen surface, this particular technique has enhanced sensitivity to cracks oriented in the through-the-thickness direction.

Pulse Echo. Many of the investigators who examined through-thickness methods have also examined pulse echos generated by reflections of an ultrasonic wave. Test equipment puts an ultrasonic pulse into the part and measures the time and amplitude of the reflected sound wave. This technique relies on the identification of sound reflected from distinct internal flaws such as delaminations. By measuring the reflected signal with respect to time, the position of internal flaws in the part can be determined.

Eddy Current. This technique is commonly used in metals, and several researchers explored its use for composite materials. As described by Phelps, eddy current relies on the conductivity of graphite fiber. In this kind of testing, an alternating magnetic field is applied to the part by an AC-powered test instrument coil. This alternately expanding and collapsing magnetic field induces an eddy current in the specimen, and the eddy current creates its own magnetic field. The interaction of this magnetic field with the test instrument varies as internal flaws and fractures are encountered. In works by both Phelps and Reynolds, eddy current methods have been shown to be somewhat satisfactory for identifying internal fractures in composites made with fabric materials; however, using this method for tape materials has generally proved unsatisfactory.

X-ray Radiography. X-ray radiographic methods have been examined in the works of Phelps, Baumann, and Sendcky. Examinations were carried out by transmitting a beam of X-ray radiation through the part, and recording the amount of penetrating radiation on photosensitive film. The beam is partially absorbed by the material it passes through, and discontinuities or voids that cause a reduction in total part thickness result in less absorption and more exposure of the photosensitive film. Several investigators note that since this method relies on a reduction in material thickness, it tends to be relatively insensitive to delaminations. However, it readily detects through-thickness fractures.

Radio-Opaque Penetrant Radiography. This technique, examined by several researchers, uses the same radiographic method described above, but incorporates the use of an X-ray

attenuating dye applied prior to examination. The dye dramatically enhances many defects that are not normally visible, and aids considerably in their detection. This method has, by far, the best resolution of any of the techniques available; however (as noted by Phelps) debris, grease, and fluid must be cleaned from the part, and some form of access for the penetrant to enter delaminated areas is required. In addition, some of the available penetrants are toxic.

Edge Replication. This technique has been explored by several investigators such as Riefsnider; it uses standard metals replica techniques to record microscopic cracking along the free edges of the component. An acetate film that has been softened with acetone is firmly applied to the edge, then allowed to dry. The result is a mirror image of the edge that can be examined at higher magnification to assess nonvisible damage. This technique provides an easily handled copy of the specimen which can be examined without component damage or sectioning, but caution is advised since the acetone solvent can react with the resin system and actually create artifacts and/or permanent component damage.

Discussion

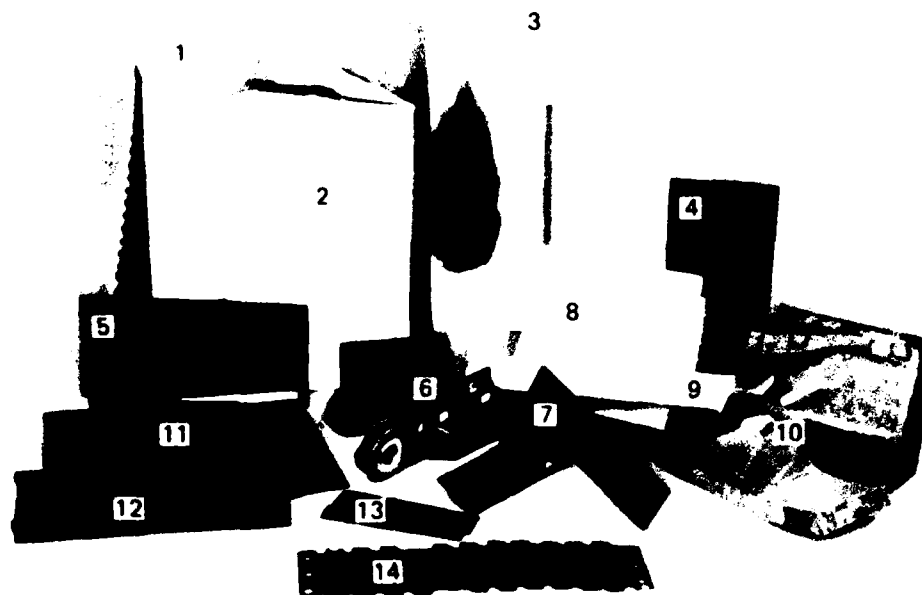
A wide variety of nondestructive evaluation methods have been examined in the literature reviewed for this project. These techniques and the types of defects they can detect are summarized in Figure 4-23. The differences and advantages of various techniques are best discussed in studies performed by Phelps and Reynolds. In Phelps' study, each of the techniques listed in Figure 4-23 were evaluated and compared on panels fabricated with known or induced defect conditions. Figure 4-24 illustrates the panels and conditions examined. In evaluating techniques, Phelps placed primary importance on the suitability of each technique for in-service field inspections. As a result, the most often-recommended techniques were those that were portable and readily available (Figure 4-25). However, in examining Phelps' test data, through-transmission ultrasonics appears the best choice for identifying nearly all the defect conditions illustrated in Figures 4-26 and -27. Through-transmission ultrasonics was able to identify well over 90% of the defects examined. This finding is confirmed in Reynold's work in which a variety of non-United States fabricators indicated that C-scan ultrasonics was the most sensitive technique (with the exception of dye penetrant X-ray radiography) for detecting internal voids and delaminations.

TASK	METHOD	DESCRIPTION	AUTHORS
Identify in-place delaminations, disbonds and identify through-thickness cracking	Thought-transmission ultrasonics	Thought-transmission ultrasonics	Phelps (ref. 30) Schramm (ref. 32) Raatz (ref. 43) Reynolds (ref. 31) Duke (ref. 44) Gibbons (ref. 40) Ulman (ref. 33) Teagle (ref. 41)
	Pulse echo	Measures reflected sound from defect surface	Phelps (ref. 30) Bar-Cohen (ref. 42) Raatz (ref. 43) Reynolds (ref. 31) Ulman (ref. 33)
	Harmonic bond testers	Measures resonant frequency of laminate	Phelps (ref. 30) Reynolds (ref. 31)
	Eddy current	Measures eddy current induced by test probe	Phelps (ref. 30) Reynolds (ref. 31) Sendekyj (ref. 37) Baumann (ref. 36)
	Dye penetrant radiography (fabric)	Measures X-ray attenuation which is enhanced by using radio-opaque dye penetrant	Phelps (ref. 30) Reynolds (ref. 31) Baumann (ref. 36)
	X-ray radiography*	Measures X-ray attenuation	

Figure 4-23. *Nondestructive Evaluation Techniques*

Other ultrasonic techniques, such as pulse echo, harmonic bond testing, and single-sided angle beams appear capable of detecting roughly one-half to two-thirds of the defects identifiable by through-transmission ultrasonics. As indicated in Figures 4-26 and -27 the sensitivity of these techniques to a variety of defects depends strongly on the type of instrument used. Of the instruments examined by Phelps, harmonic bond testers appear to be somewhat more sensitive to most defects than pulse-echo or single-sided ultrasonic methods.

While not covered in Figures 4-26 or -27, X-ray radiography was found by both Phelps and Reynolds to be an excellent nondestructive evaluation tool, particularly when used with radio-opaque dye penetrants. As shown by Phelps, radiography without enhancement illustrates fractures running through the specimen thickness with relative clarity (Figure 4-28). As noted by both authors, this result reflects the localized reduction in material thickness associated with such fractures. However, visualization of internal delaminations (as shown in Figure 4-28) was found to require DIB radio-opaque dye penetrant enhancement.



Key	Description	Defects
1	Gr-Ep laminate/Nomex honeycomb skin and rib structure, mechanically fastened, painted two sides. B727 element or section	Impact damage, fastener hole damage, water-in-honeycomb, rib flange cracks
2	Gr-Ep laminate and Nomex honeycomb painted one side	Delamination/disbond defects and impact damage defects in honeycomb, laminate, and transition areas
3	Wedge shape, Gr-Ep skin—Nomex honeycomb painted two sides	Impact damage, lightning damage, burn damage
4	Gr-Ep laminate plates, painted one side	Delamination/disbond and impact damage defects, simulated surface cracks
5	Unidirectional Gr-Ep laminate	Simulated surface cracks
6	Gr-Ep laminate lug and thick sections	Fracture in lug, simulated hole cracks
7	Gr-Ep honeycomb panel mechanically fastened to Gr-Ep I-stiffened skin structure	Complete failure (fracture) in flange at one hole
8	Curved Gr-Ep skin and Nomex honeycomb	Impact damage
9	Kevlar and Gr-Ep skin and Nomex honeycomb	Impact damage
10	Kevlar and Gr-Ep skin and septumized Nomex honeycomb—B767 landing gear door sections	Delamination/disbond defects
11	Gr-Ep laminate and aluminum honeycomb or titanium plate	Delamination/disbond defects
12	Gr-Ep laminate I-stiffened skin panel	Impact damage
13	Gr-Ep laminate stepped-thickness X-ray and ultrasonic test part	Varied thicknesses
14	Gr-Ep laminate fatigue specimens	Cracks and hole damage

(Ref. 30)

Figure 4-24. Test Parts

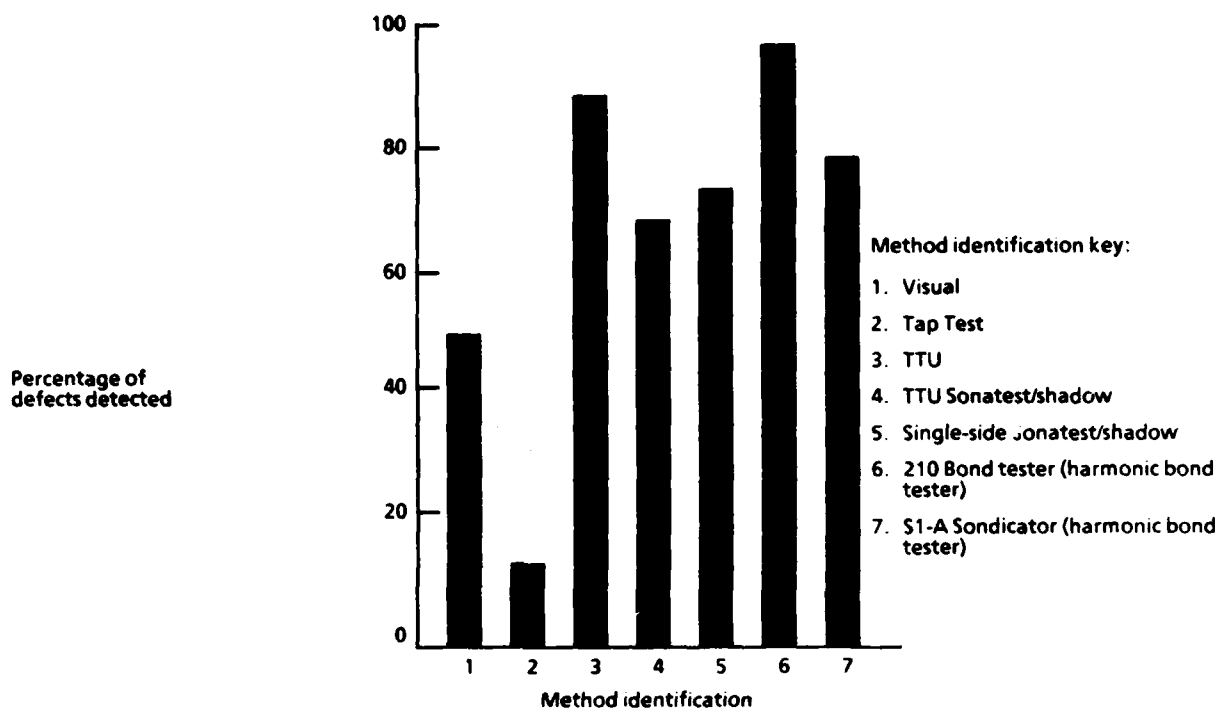
STRUCTURES		DEFECTS									
		DELAMINATION/ DISBOND	IMPACT DAMAGE	FASTENER HOLE DAMAGE	LIGHTNING DAMAGE	BURN DAMAGE	FRACTURES, SURFACE	FRACTURES, SUBSURFACE AND SUBSTRUCTURE	INTERNAL STRUCTURE DAMAGE—ACCESS THROUGH DOORS	INTERNAL STRUCTURE DAMAGE—INACCESSIBLE	WATER-IN- HONEYCOMB
LAMINATED SKIN		1)D,E 2)D,E	1)A,B 2)B,C, D,E,G	1)A,B 2)B,H,G	1)A,B 2)B,E,D	1)A,B 2)B,E,D	1)A,B,H 2)H,D,F	1)H,D,F 2)B,F, G,E,H	1)B 2)B,F, G,E,H	1)F 2)F	
SKIN/HONEYCOMB PANEL		1)E,D 2)E,D	1)A,B 2)A,D E,H,G	1)A,B 2)B,H,G	1)A,B 2)B,E, D,F	1)A,B 2)B,E, D,F	1)A,B,H 2)B,H,I	1)B 1)H,D,F	1)F 2)B,F E,H	1)F 2)F	1)F,E 2)F,E
SKIN-TO-STIFFENER JOINT		1)D,E 2)D,E	1)A,B 2)B,D E,H,G	1)A,B 2)B,H,G	1)A,B 2)B,D E,F	1)A,B 2)B,D E,F			1)B 2)B,I		
SKIN-TO-METAL JOINT		1)D,E 2)D,E	1)A,B 2)B,D E,H,G	1)A,B 2)B,H,G	1)A,B 2)B,D, E,F	1)A,B 2)B,D, E,F			1)B 2)B,I		
SKIN-TO-SKIN TRAILING EDGE JOINT		1)C,E,D 2)B,D,I	1)A,B 2)B,C, D,H,I	1)A,B 2)B,H, G,I	1)A,B 2)B,C, D,E	1)A,B 2)B,D, C,E					1)C,E, D,F 2)C,E, D,F
HONEYCOMB RIBS, SPARS, AND SKIN STIFFENERS				1)A,B 2)B,H,G	1)A,B 2)B,D,E	1)A,B 2)B,D,E		1)F 2)F	1)B 2)B,F, G,H,E	1)F 2)F	1)F 2)F
LAMINATED RIBS, SPARS, AND SKIN STIFFENERS				1)A,B 2)B,H,G	1)A,B 2)B,D,E	1)A,B 2)B,D,E		1)F 2)F	1)B 2)B,F, G,E,H	1)F 2)F	
FULL-DEPTH HONEYCOMB		1)E,C,D 2)E,C,D	1)A,B 2)B,D, E,H,G		1)A,B 2)B,E,D	1)A,B 2)B,E,D	1)A,B,H 2)B,H,I	1)F 2)F		1)C,E, D,F 2)C,E, D,F	1)F,C,E 2)F,C,E
SEPTUMIZED HONEYCOMB		1)E,C,D 2)D,E,C	1)A,B 2)B,D, E,H,G		1)A,B 2)B,E,D	1)A,B 2)B,E,D	1)A,B,H 2)B,H,I	1)F 2)F		1)D,C, E,F 2)D,C, E,F	
LUGS AND THICK SECTIONS		1)D,F,G 2)G,F,G		1)D,F,G 2)D,F,G	1)D,F,G 2)D,F,G	1)D,F,G 2)D,F,G	1)A,B,H 2)B,H,I	1)D,F 2)D,F		1)F 2)F	1)F,D,E 2)F,D,E

Key:

Inspection method:	C	Ultrasonic TTU	H	Eddy current
A	D	Ultrasonic pulse echo	I	Penetrant
B	E	Bondtester	Task:	
	F	Low KV X-ray	1)	Detection
	G	DIB enhanced X-ray	2)	Evaluation

(Ref 30)

Figure 4-25. Method Selection (Listed in Order of Preference)



(Ref. 30)

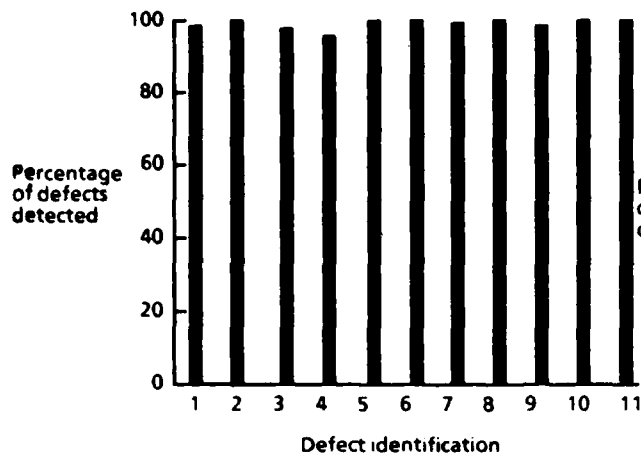
Figure 4-26. Impact Damage Detection Capability

Phelps' extensive investigation into eddy current methods suggests that some defects in fabrics can be readily identified. However, both Reynolds and Phelps note that test instruments used in this technique must operate in the proper frequency range and be properly adjusted. Phelps' study suggests that the detection capability of this method is below that of through-transmission ultrasonics, and is likely equivalent to pulse-echo and single-sided ultrasonic methods.

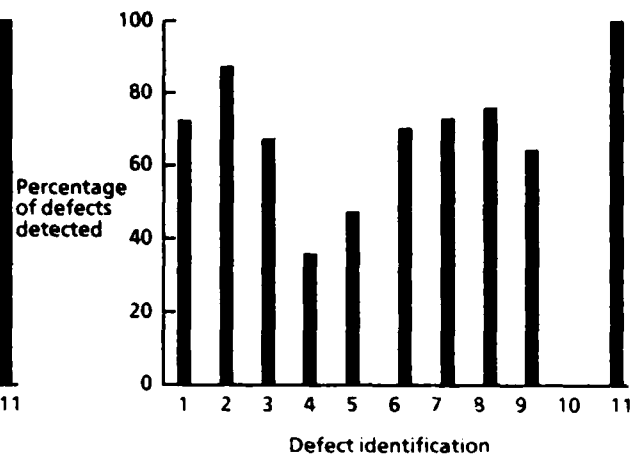
4.6 LITERATURE SEARCH—MATERIALS CHARACTERIZATION

The characterization of materials involved in component failure is aimed at identifying errors in their fabrication and/or processing. Material properties such as strength, stiffness, and environmental durability can be dramatically affected by processing and fabrication errors. As part of this project, a comprehensive literature search was undertaken to identify techniques available for characterizing composite materials.

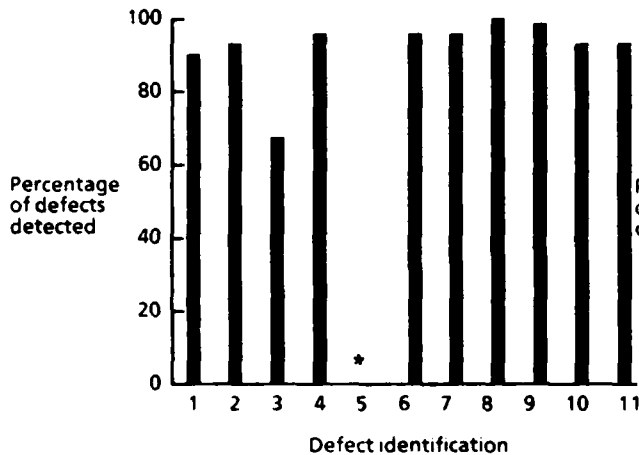
A variety of techniques for evaluating composite materials was identified in the literature examined. Most investigators developed and evaluated test methods to verify the



a) THROUGH-TRANSMISSION ULTRASONIC (TTU)

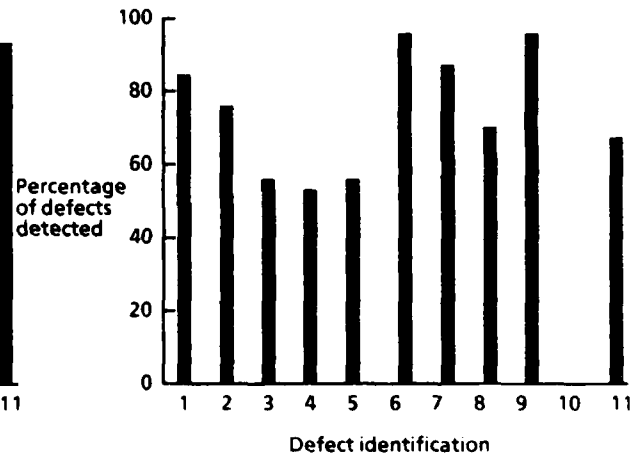


b) PULSE-ECHO TRANSMISSION



c) TTU SONATEST/SHADOW

* Omitted—temporary yoke could not accommodate the transition area



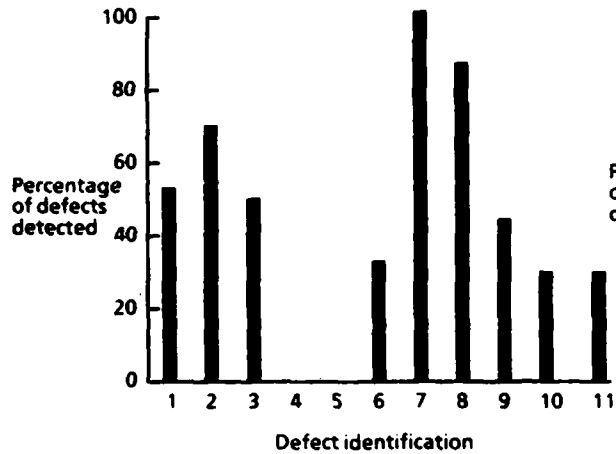
d) SINGLE-SIDE SONATEST/SHADOW

Defects Detected—Key:

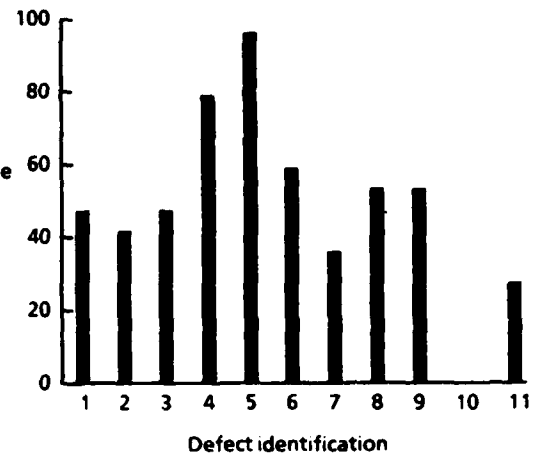
- | | |
|-------------------------------|---|
| 1. Total defects | 6. First eight plies |
| 2. Small defects | 7. Nine plies or more |
| 3. Edge defects | 8. Rough side |
| 4. Laminate/honeycomb defects | 9. Tool side |
| 5. Transition zone defects | 10. Graphite-epoxy-aluminum honeycomb defects |
| | 11. Graphite-epoxy-titanium plate defects |

(Ref 30)

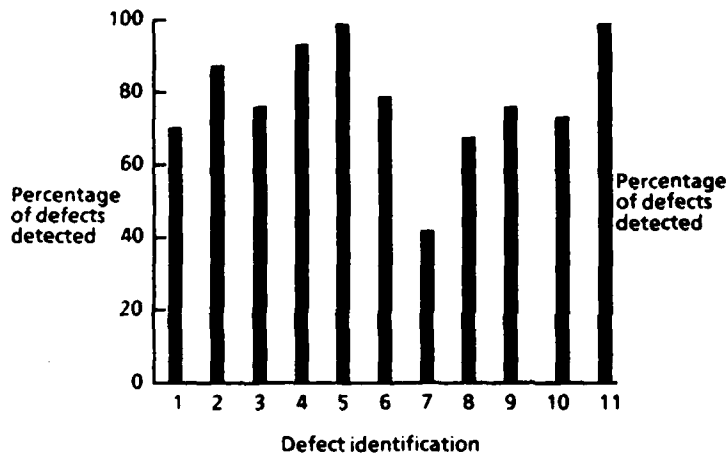
Figure 4-27. Delamination/Disbond Defect Detection Capability (Page 1 of 2)



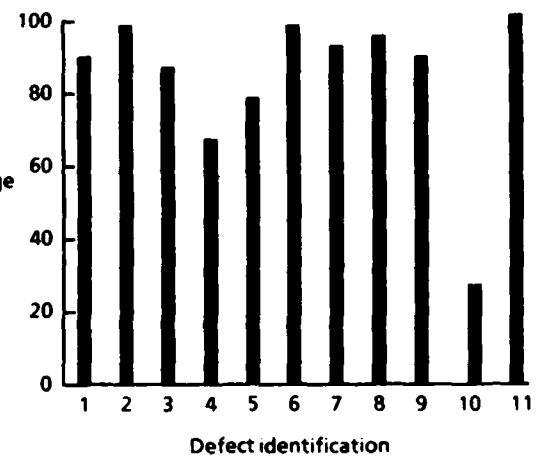
e) ULTRASONIC THICKNESS GAGE (PULSE ECHO)



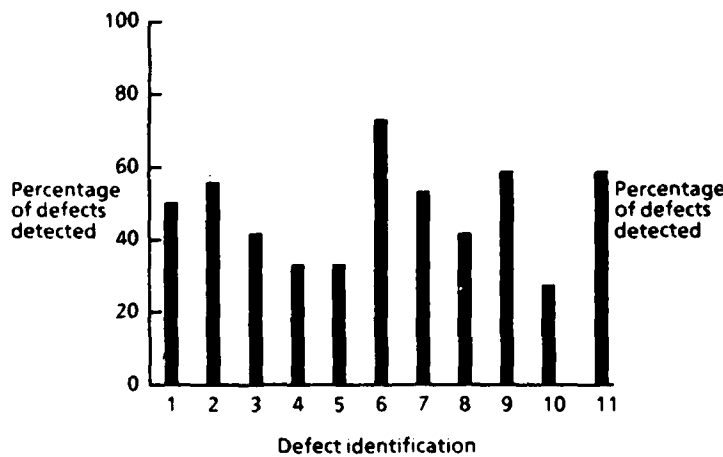
f) ANGLE BEAM ULTRASONIC (SINGLE SIDED)



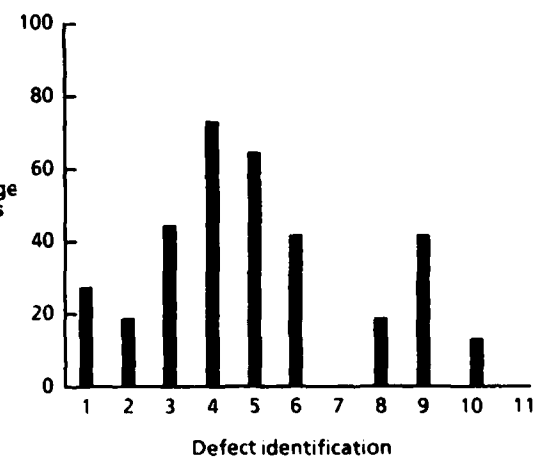
g) SONDICATOR S-1A (HARMONIC BOND TESTER)



h) 210 BOND TESTER (HARMONIC)



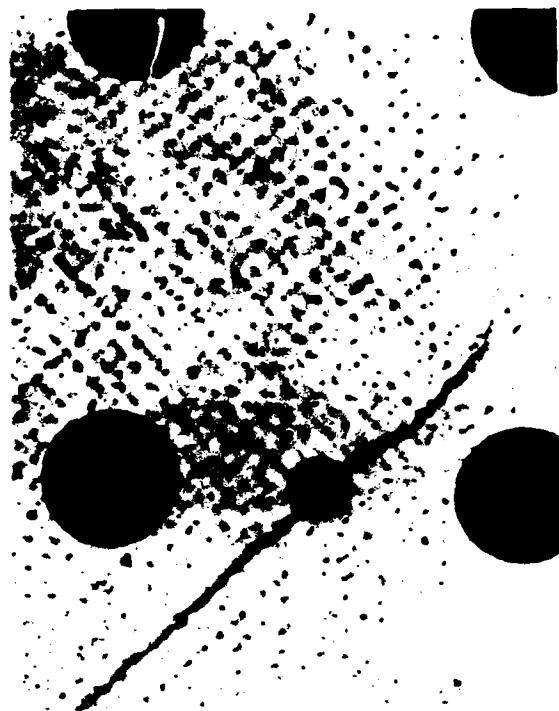
i) OTHER BOND TESTERS



j) TAP TEST

(Ref. 30)

Figure 4-27. Delamination/Disbond Defect Detection Capability (Page 2 of 2)



a) NO ENHANCEMENT



b) DIB-ENHANCED

(Ref 30)

Figure 4-28. Cracks in Gr-Ep Specimen

conformance of materials and processes to specification. They also studied degradation resulting from environmental exposure. In these studies, the examination of composite materials was divided into two categories: uncured and cured material evaluations.

Uncured Material Evaluations

Evaluation techniques for uncured epoxies are well established and extensively documented. To characterize the constituents and formulation of uncured prepreg, methods such as high pressure liquid chromatography (HPLC), gel permeation chromatography (GPC), infrared spectroscopy, differential scanning calorimetry (DSC), wet chemical analysis, and atomic absorption spectroscopy were examined by a number of researchers. However, though these techniques are well developed, they are seldom used in failure analysis because the prepreg materials used to fabricate the failed parts are not generally available to analysis. Several studies, including those by Wickham, May, Crozier, Rogers, Tung and Dynes, and Chen and Hunter, describe the analytical techniques available for complete chemical characterization of uncured epoxies. Carpenter provides characterization techniques for the particular resin (Hercules 3501-6) used in this program.

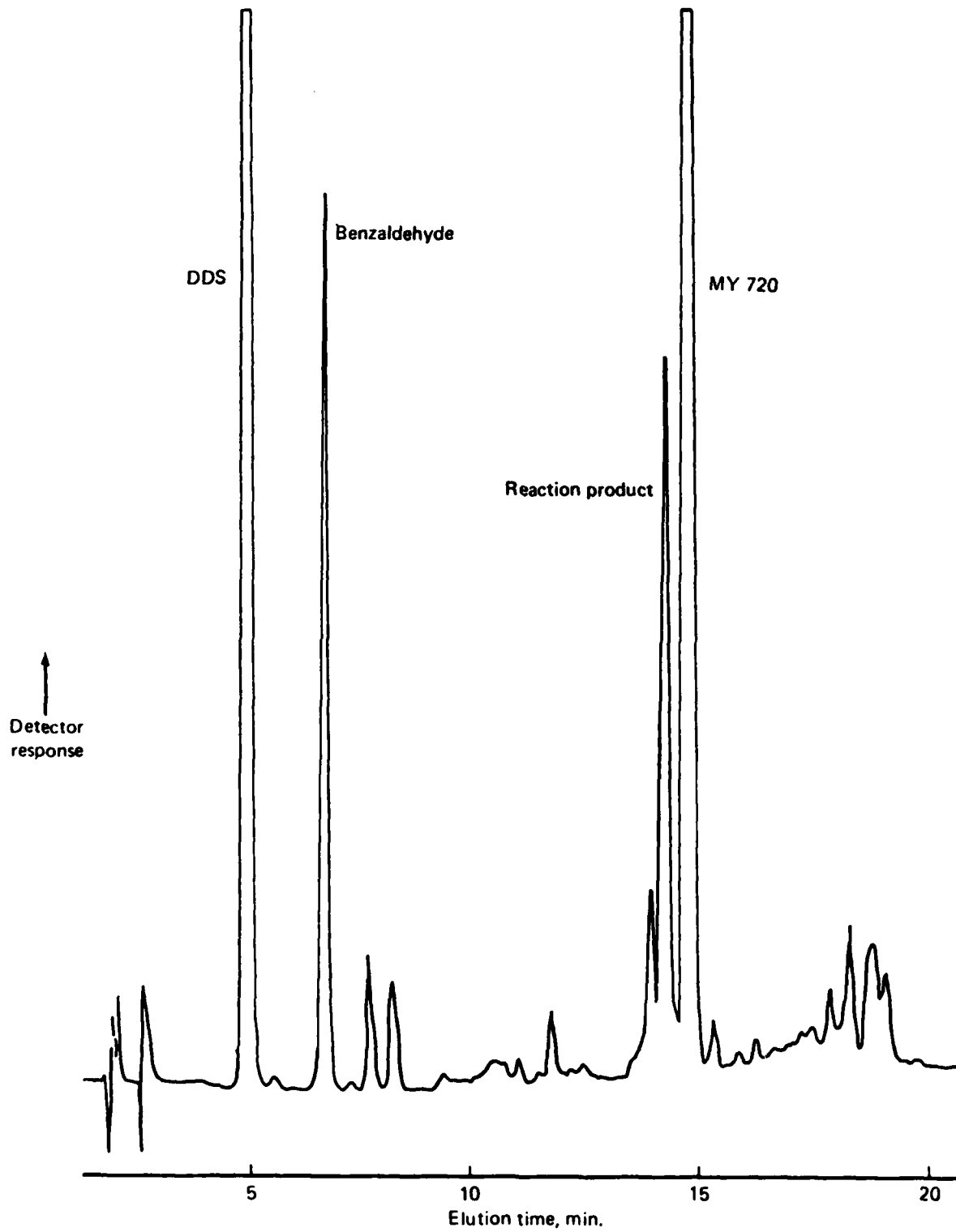
High pressure liquid chromatography (HPLC) separates individual resin components according to their size or solubility. Components can be identified by comparing the peak position on a chromatogram to a reference standard. Peak areas can be used to determine relative concentrations. Several researchers describe their determining the presence and concentration of the primary epoxy, the secondary epoxy, the unreacted amine hardener and reaction products during staging. A typical LC chromatogram is shown in Figure 4-29. Sewell describes detailed HPLC test procedures for the Hercules 3501-6 epoxy system.

Gel Permeation Chromatography (GPC) separates resin components by passing them through a gel with controlled pore sizes. The larger components are detained by the gel (Figure 4-30). The presence and concentration of resin constituents and reaction products can be detected using GPC. A typical GPC chromatograph is shown in Figure 4-31. GPC was found to be less informative than HPLC for low-molecular-weight components.

Infrared (IR) spectroscopy measures the absorption of incident infrared radiation, and is used to verify matrix resin formulation by identifying functional groups. IR spectroscopy is especially useful in determining the DDS hardener content by detecting the presence of sulfonyl groups. Other resin components may also be analyzed. Mones describes techniques for detailed characterization of epoxy curing reactions using quantitative IR spectroscopy techniques.

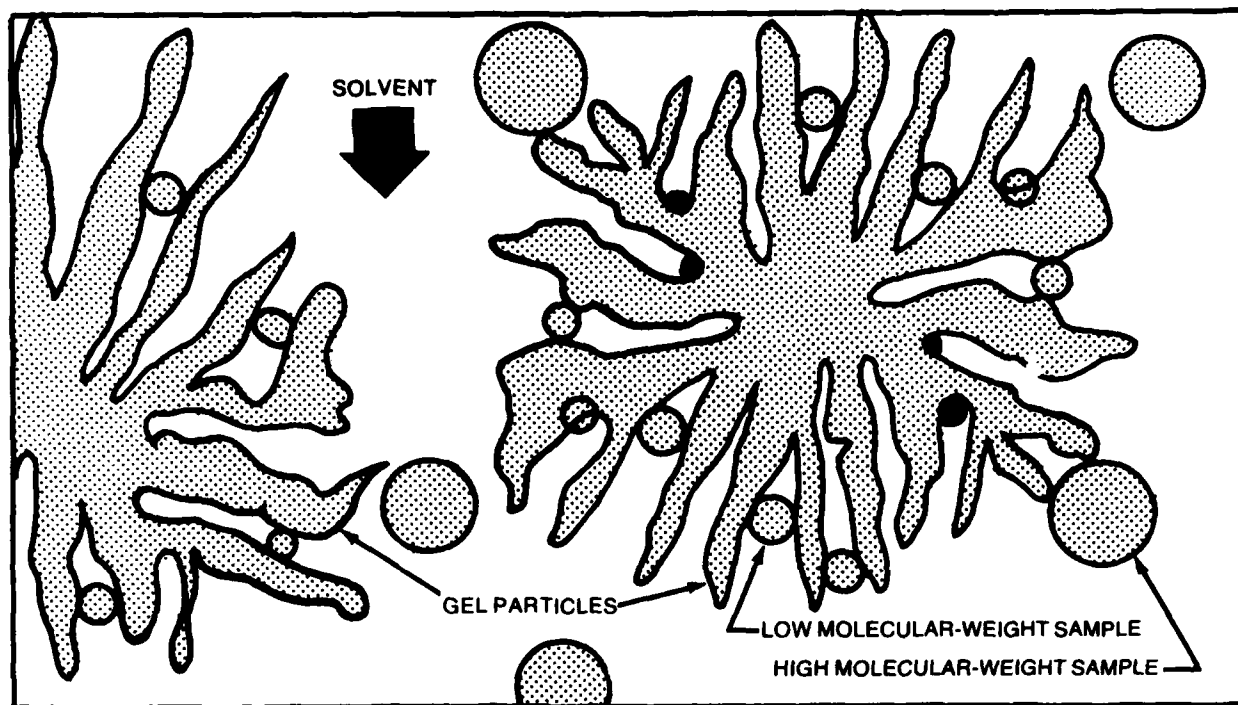
Differential scanning calorimetry (DSC) characterizes an uncured epoxy matrix by measuring the heat evolved versus temperature from the exothermic cure reactions. A typical DSC thermogram is shown in Figure 4-32 for Hercules 3501-6 epoxy; the total heat of reaction (the area between the thermogram peaks and baseline), the relative peak size, and reaction temperature can verify resin formulation. Stark provides a systematic analysis of DSC thermograms for cure reactions in uncatalyzed epoxies. Carpenter, and Munns and Seferis describe analyses of DSC thermograms for catalyzed epoxies.

Wet chemical titration techniques determine the total amount of epoxy or the amount of primary epoxy present in the resin formulation. Carpenter, and Chu and Seferis describe methods of determining epoxy equivalent weight through titration. Crozier and Rogers determine primary epoxy (MY-720) content by tertiary amine titration. Wet chemical techniques lose some of their utility because they can not detect groups reacted during staging.



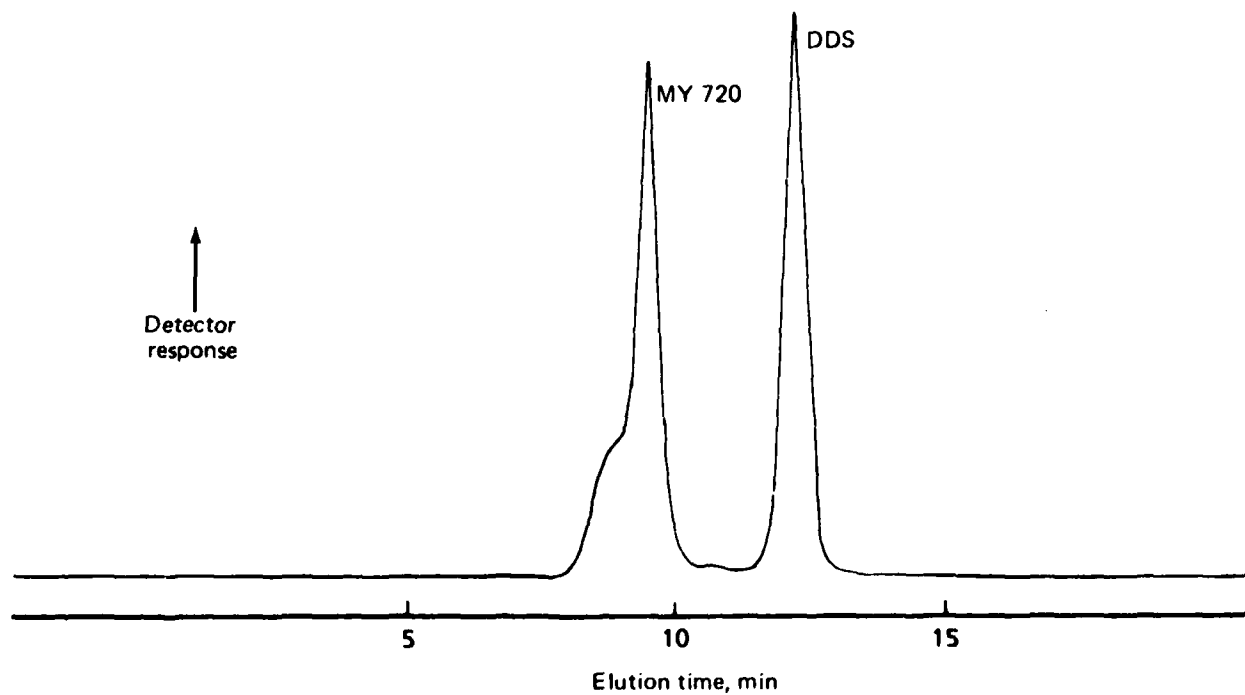
(Ref 50)

Figure 4-29. LC Chromatogram of Narmco Resin Matrix Showing Major Peak Assignment



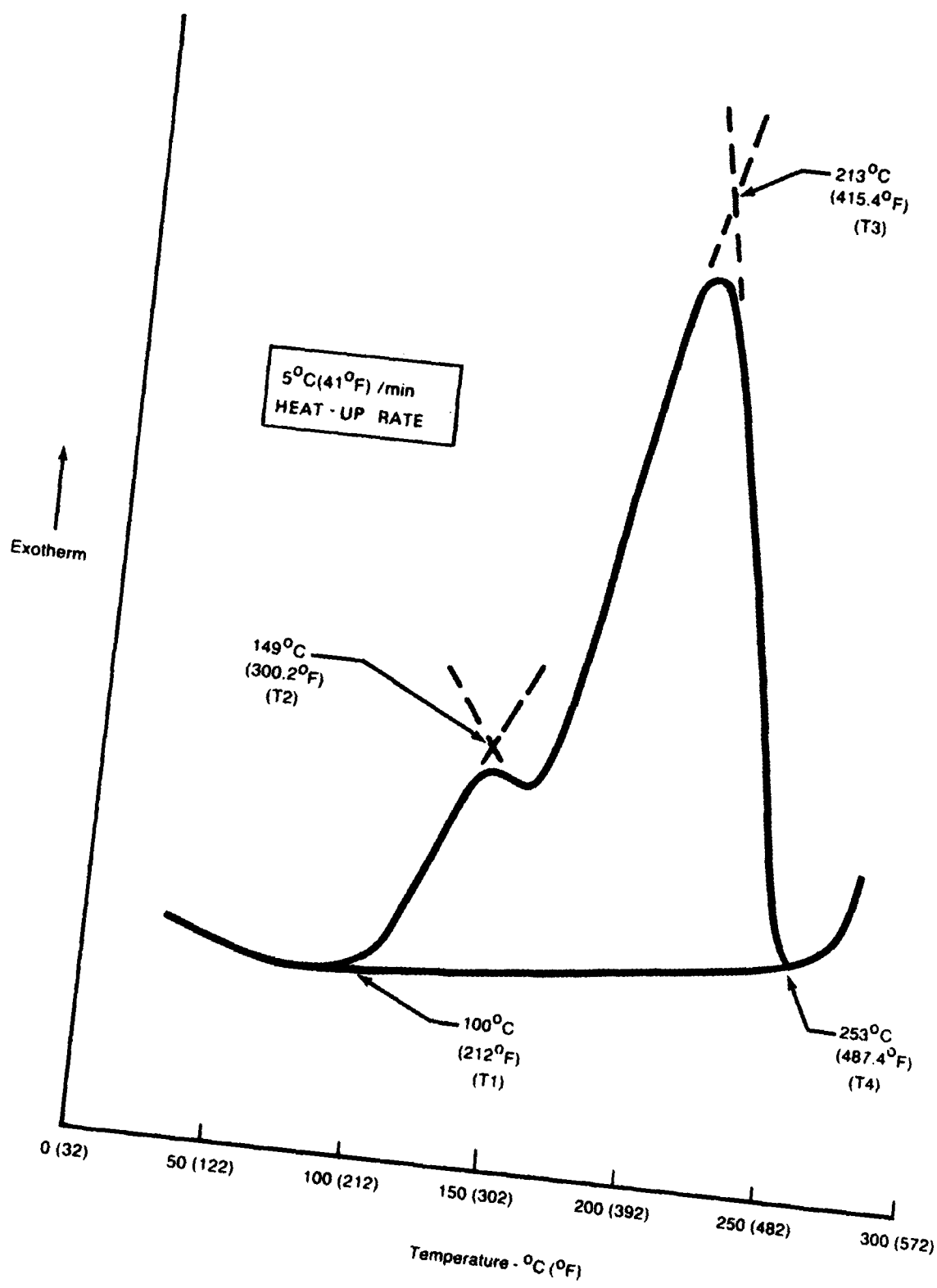
(Ref. 50)

Figure 4-30. Diagram of GPC Technique



(Ref. 50)

Figure 4-31. GPC Chromatogram of Narmco Neat Resin Showing Major Peak Assignment



(Ref 51. Copyright © SAMPE, reprinted with permission.)

Figure 4-32. DSC Thermogram for 3501-6 Resin

Atomic absorption spectroscopy determines the presence and concentration of catalyst in epoxy formulations. The concentration of BF_3 containing catalyst is determined by measuring boron content.

Cured Material Evaluation

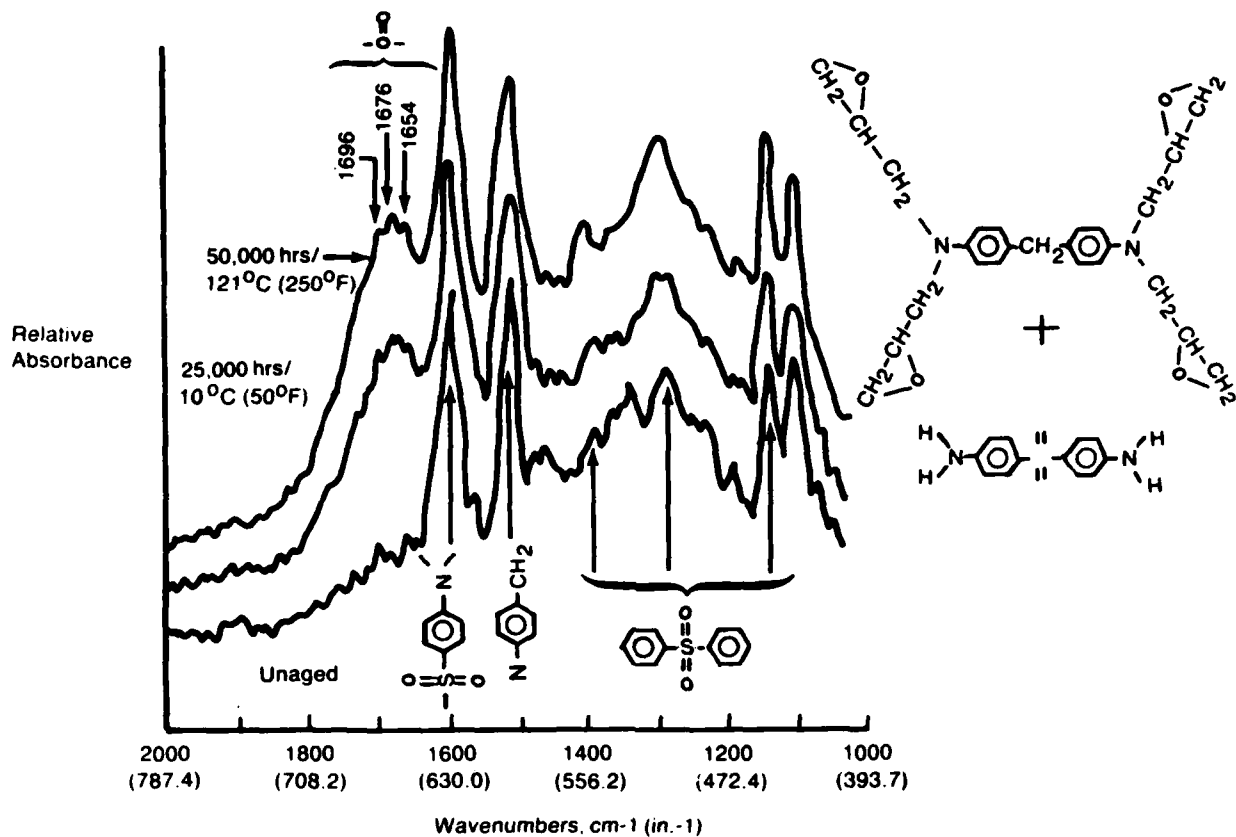
The evaluation of cured epoxy matrix resins is not as well established as uncured epoxy analysis methods, due to the cured epoxy network's intractability. Techniques such as diffuse reflectance infrared spectroscopy, dynamic mechanical analysis (DMA), and acid digestion can characterize the cured epoxy matrix. Processing verification methods such as thermomechanical analysis (TMA), DSC, DMA, and IR spectroscopy can verify proper material processing.

Diffuse reflectance-Fourier transform infrared spectroscopy (DR-FTIR) measures the absorption of radiation scattered from the cured resin sample. DR-FTIR allows IR spectroscopic techniques to be used on cured epoxies. Young discussed DR-FTIR techniques to verify resin formulation and detect thermal aging by comparing the peak heights and area ratios of specimen IR spectra to reference standards. Figure 4-33 shows how DR-FTIR was used to detect aging in Hercules 3501-5A epoxy.

Dynamic mechanical analysis (DMA) measures the change in viscoelastic properties with temperature. DMA provides information on matrix resin formulation as well as part processing and environmental exposure history. The works of Carpenter, Chen and Hunter, and Burroughs and Leckenby describe changes in dynamic mechanical properties with controlled changes in formulation. Figure 4-34 shows the changes in elastic modulus versus temperature for varied DDS hardener content. Chu and Seferis summarize the effect of mixing variables, formulation changes, and processing variables on dynamic mechanical properties. The effects of moisture exposure on dynamic mechanical response are discussed by Baumgartner and Lemming, and Putter.

Measuring composite fiber volume indicates if the prepreg was manufactured in accordance with specification. **Acid digestion** determines the fiber volume of a cured carbon-epoxy composite by dissolving the matrix resin and leaving the carbon fiber behind. Several digestion techniques were evaluated by Jackson.

The glass transition temperature of a cured epoxy network depends on the extent of crosslinking reaction. Measurement of composite glass transition temperature indicates the degree of resin cure when compared to a correctly cured standard. Glass transition

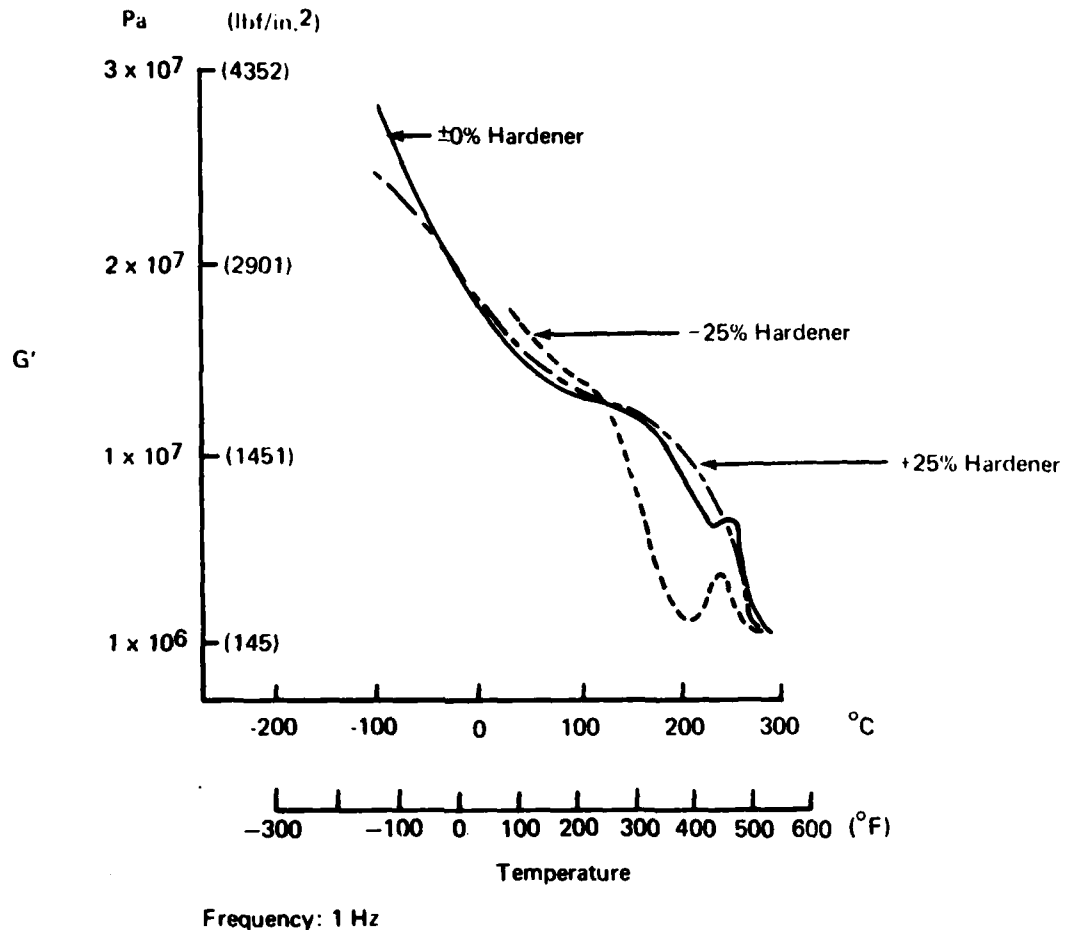


(Ref. 58. Copyright © SAMPE; Reprinted with Permission.)

Figure 4-33. DR-FTIR Spectra of Graphite/Epoxy (AS/3501-5) Composite Before and After Thermal Aging

temperature is generally measured using thermal analysis techniques such as **thermo-mechanical analysis (TMA)**, DMA and DSC. TMA measures the displacement of a probe as a function of temperature (thermal expansion). Burroughs and Leckenby describe TMA glass transition temperature measurement techniques for carbon-epoxy composites. Methods for determining glass transition temperature from DMA measurements were described by Carpenter, Burroughs and Leckenby, and Baumgartner and Lemming. Carpenter and Chang discuss glass transition measurement using DSC. TMA is the most common glass transition temperature measurement technique for failure analysis because of the small sample requirement and ease of determination.

Differential scanning calorimetry (DSC) determines the extent of reaction of a cured composite by measuring the residual heat of reaction. The area between the thermogram peak and a baseline is the residual heat of reaction for the matrix. By comparing the residual heat of reaction to the total expected heat of reaction measured on uncured



(Ref. 50)

Figure 4-34. Elastic Modulus Versus Temperature, Narmco Matrix, Showing Variation With Hardener Content

material, the extent of reaction can be determined. Burroughs and Leckenby, and Munns and Seferis describe techniques for determining extent of reaction from residual heat of reaction. The change in DSC thermograms with an increasing extent of cure is shown in Figure 4-35. Generally, DSC is used in failure analyses to show incomplete curing rather than to determine the exact extent of reaction. To determine the extent of reaction for a composite sample, corrections must be made for the weight of the carbon fibers, which is difficult because the fiber volume of the small sample required for DSC may not be indicative of the bulk fiber volume.

Infrared spectroscopy determines the number of unreacted functional groups in an incompletely cured epoxy network. The works of Mones and Chang include methods for determining the extent of reaction from IR peak intensity.

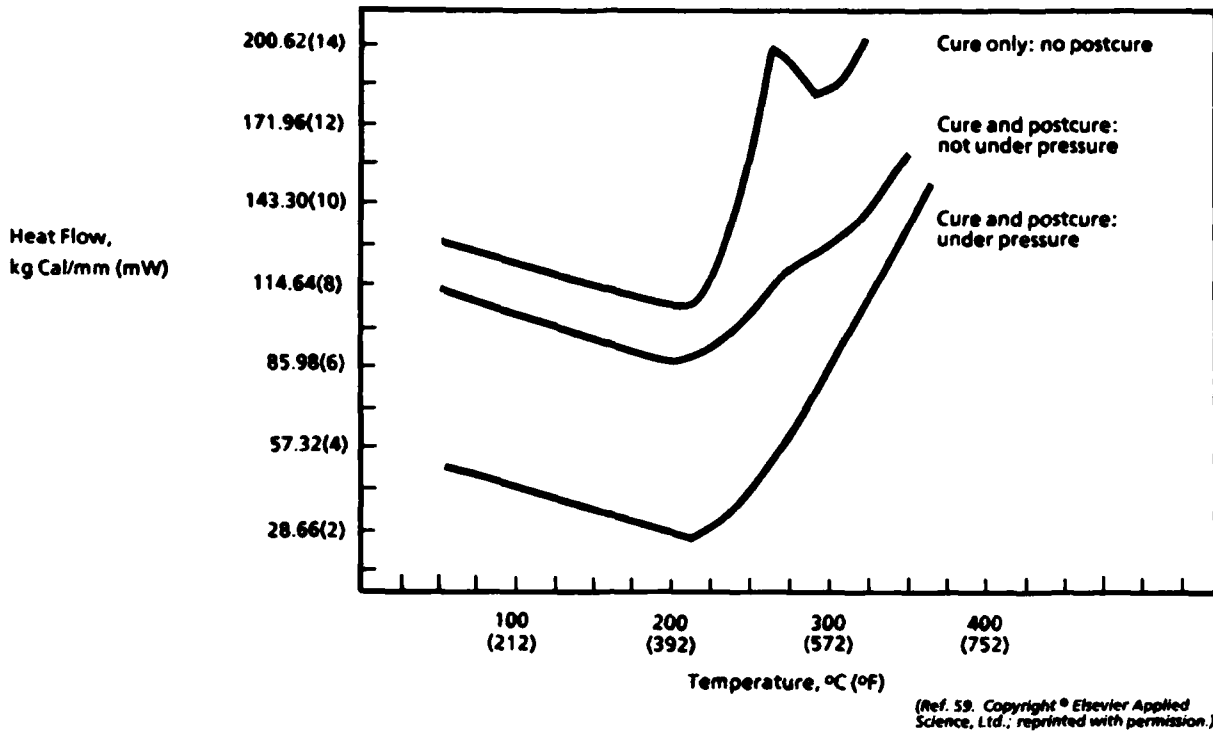


Figure 4-35. DSC Results For Cured Fibredux

Discussion

As noted above, analytical methods for evaluating uncured carbon-epoxy composites are fairly well established. A detailed summary of these methods and their descriptions is contained in Figure 4-36. Methods such as HPLC, GPC, IR spectroscopy, DSC, wet chemical, and atomic absorption can be combined to provide a detailed formulation analysis for prepreg. The methods are not often used in failure analysis because the prepreg is not available.

Evaluation of the cured carbon-epoxy material is required as part of any failure analysis. The most commonly used analysis tests the extent of cure of the matrix resin. Thermal analysis techniques such as TMA, DMA, and DSC are preferred because they are easy to apply and require small samples. Cured-matrix formulation characterization techniques such as DR-FTIR and DMA are used only if the cure analysis indicates material anomalies.

In general, the techniques identified in the literature review were created for materials development programs. Application of these techniques to failure analysis requires some modification or adaptation. Interpreting results may not be as straightforward for a material that has been subjected to actual service as it is for a material that has been tested only under well-controlled laboratory conditions.

4.7 MEETINGS WITH EXPERTS IN COMPOSITE FAILURE ANALYSIS

As part of Task 1, experts in the field of composite failure analysis from throughout the United States were visited. Interviews were conducted with individuals from industry, Government, and the academic community to gather information regarding diagnostic techniques and FALN systems and approaches. For diagnostic techniques, the primary interest was identifying state-of-the-art methods for the postmortem analysis of composites. When discussing the FALN, the objective was to have each expert review and understand the current program, and suggest changes or alterations based upon his expertise and experience. In gathering these inputs, specific emphasis was placed on evaluating each diagnostic technique and the FALN for theoretical foundation, supporting data or models, experimental data validity, and value to performing a failure analysis.

In each visit, the Failure Analysis for Composite Structure Materials project was reviewed and discussed to give each expert a clear understanding of the program's goals and scope, and to present the program FALN. The presentation was tailored to the specific interests and expertise of each consultee. For example, while visiting Dr. Ramesh Kar at Northrop, Dick Robertson at Ford, and Hsin-Nan Chou at McDonnell Douglas, the fractographic findings from Task 3 were reviewed in detail. At NASA-Lewis and the University of Delaware, more time was spent reviewing sub-FALNs and general diagnostic methodologies.

Most of the individuals visited were pleased with the program's overall scope and intent, and the approach received general approval. Several individuals commented that although Hercules 3501/AS-4 represents a logical starting point, thermoplastic matrices should be included in future follow-on studies. Most people were also curious about dissemination of information from the current program and the availability of either interim reports or the final compendium for their use. They were advised to contact Mr. Frank Feчек, the AFWAL/MLSE project engineer, regarding specifics on obtaining the desired information.

Most individuals had no further input regarding additional diagnostic techniques or FALN modifications, with the exception of Dr. Chris Chamis at NASA-Lewis and Dick Robertson at Ford.

Dr. Chamis gave specific inputs regarding NASA's perspective of stress analysis methods, state of the art, and view of postmortem failure analysis. As a result of this information,

ANALYSIS TASK	METHOD	DESCRIPTION	AUTHORS	COMMENTS
Uncured epoxy evaluation	High pressure liquid chromatography (HPLC)	Identify individual components by separating according to size or solubility	<ul style="list-style-type: none"> Wickham (ref. 45) May (ref. 46) Crozier (ref. 47) Rogers (ref. 48) Tung (ref. 49) Chen (ref. 50) Sewell (ref. 52) 	Detect presence/determine concentrations of: <ul style="list-style-type: none"> Epoxy monomers Unreacted amine hardener Reaction products
	Gel permeation chromatography (GPC)	Identify individual components by separating according to size	<ul style="list-style-type: none"> Wickham (ref. 45) Tung (ref. 49) Chen (ref. 50) 	Detect presence/determine concentrations of: <ul style="list-style-type: none"> Epoxy monomers Unreacted amine hardener Reaction products
	Infrared spectroscopy (IR)	Identify functional groups using IR spectra	<ul style="list-style-type: none"> Wickham (ref. 45) May (ref. 46) Crozier (ref. 47) Rogers (ref. 48) Carpenter (ref. 51) Monos (ref. 53) 	<ul style="list-style-type: none"> Detect DDS hardener content Identify resin components
	Differential scanning calorimetry (DSC)	Perform enthalpy measurements	<ul style="list-style-type: none"> Wickham (ref. 45) May (ref. 46) Tung (ref. 49) Chen (ref. 50) Stark (ref. 54) Carpenter (ref. 51) Munns (ref. 56) 	Verify formulation by: <ul style="list-style-type: none"> Measuring total heat of cure reaction Measuring size and location of exotherm peaks
	Wet chemical	Determine concentration of functional groups by titration	<ul style="list-style-type: none"> Carpenter (ref. 51) Chu (ref. 57) Crozier (ref. 47) Rogers (ref. 48) 	<ul style="list-style-type: none"> Determine epoxy equivalent weight Determine primary epoxy content
	Atomic absorption	Measure atomic absorption spectra	<ul style="list-style-type: none"> Wickham (ref. 45) Carpenter (ref. 51) 	Determine catalyst content (BF ₃)
Cured epoxy evaluation	Diffuse reflectance-fourier transform infrared spectroscopy (DR-FTIR)	Identify functional groups using IR analysis of scattered beam	<ul style="list-style-type: none"> Young (ref. 58) 	<ul style="list-style-type: none"> Identify resin components Identify thermal aging
	Dynamic mechanical analysis (DMA)	Measure change in viscoelastic properties with temperature	<ul style="list-style-type: none"> Chen (ref. 50) Carpenter (ref. 55) Burroughs (ref. 57) Baumgartner (ref. 61) 	<ul style="list-style-type: none"> Detect formulation variations Show moisture effects
	Acid digestion	Remove matrix resin by exposing to acid	<ul style="list-style-type: none"> Jackson (ref. 59) 	Determine fiber volume
	Thermomechanical analysis (TMA)	Measure probe displacement as a function of temperature	<ul style="list-style-type: none"> Burroughs (ref. 15) 	Determine glass transition/extent of reaction
	Differential scanning calorimetry (DSC)	Measure heat evolved as a function of temperature	<ul style="list-style-type: none"> Carpenter (ref. 55) Chang (ref. 64) Burroughs (ref. 59) Munns (ref. 56) 	<ul style="list-style-type: none"> Determine glass transition/extent of reaction Determine residual heat of reaction/extent of reaction
	Infrared spectroscopy	Identify unreacted functional groups using IR spectra	<ul style="list-style-type: none"> Monos (ref. 53) Chang (ref. 64) 	Determine extent of reaction from peak intensity

Figure 4-36. Materials Characterization Literature Survey Summary

a draft sub-FALN on this discipline was developed for inclusion into the final compendium.

Discussions with Dick Robertson focused on the observation of lamellar-type features under mode I loading conditions. As a result of these discussions, there was general agreement that lamellae may be due to alterations in the microscopic load state associated with fiber pullout. Mr. Robertson agreed to send Boeing some of his mode I samples for review under Task 3.

In general, most of the individuals visited agreed with the FALN, the proposed diagnostic techniques, and findings and interpretations offered. Most of these individuals have explored only a limited portion of the overall technology involved, and very little of their effort was aimed at the postmortem failure analysis of full-scale components. The consensus is that the current Air Force program is leading the industry in terms of technology and degree of effort.

A detailed account of the information obtained on each site visit is given below.

Northrop Aircraft Division
Dr. Ramesh Kar
Hawthorne, California

Mr. Ray Grove of Boeing visited Dr. Kar on September 11, 1985. Dr. Kar is Northrop's designated technical leader in composites postfailure analysis and fractography. Among the companies visited, Northrop stands as one of the few currently pursuing a capability aimed at analyzing large-scale in-service experimental components. Northrop's overall goals, areas of expertise, and approaches are aligned with the overall Air Force program. Because of their emphasis on component failure analysis, Northrop has developed a FALN and supporting diagnostic techniques. During the July, 1985, Air Force-sponsored International Conference on Postfailure Analysis Techniques for Fiber-Reinforced Composites, Northrop's techniques and FALN were presented and discussed along with an applied example. In visiting this company, a primary goal was to gain a more detailed understanding of these items and their relationship to the current Air Force program.

FALN - Northrop was well aware both of the scope and intent of the Air Force program, and of why such a methodology and program were necessary, and was in agreement with the current program approach and objectives. The FALN illustrated in Figure 4-37 describes Northrop's general approach and the steps involved in performing a failure analysis. The approach is oriented toward fractographic examinations and proceeds in a straightforward manner from low-magnification (global) examinations, towards more detailed and intensive techniques such as SEM, image analysis, and metallography. This approach is similar in many ways to portions of the current program FALN, and reflects Boeing and Northrop experience with metals failure analysis, standard metallurgical approaches, and experience with in-service and large-scale test components.

While portions of the Northrop and the current program FALNs appear similar, some substantial differences exist. In Northrop's approach NDE, macroscopic inspection, SEM/TEM examinations, and metallography are the only operations. Depending on the outcome of each examination, the investigator is directed towards either additional (unspecified) techniques, or the cause of failure. As presented, this approach relies exclusively on NDE, fractography, and metallography to direct and determine the cause of failure.

In Boeing's opinion, a potential problem with this approach is that it assumes all defective material conditions or design errors can be identified by these methods. However, very little (if any) experimental data or models exist describing how these conditions affect fractographic features. As a result, the theoretical foundation and utility of this approach appear to contain elements of risk.

In addition to this major difference in analytical approach, Northrop also departs from the current Air Force program in several other respects. These include:

1. Less detail regarding each operation. No stated goal for any operation. No decision steps involved in the use of an operation.
2. Only one decision step (located near the end of the FALN) to direct operations and subsequent analyses.
3. No evaluation of either material or drawing conformity unless indicated by NDE, fractography, or metallographic findings.

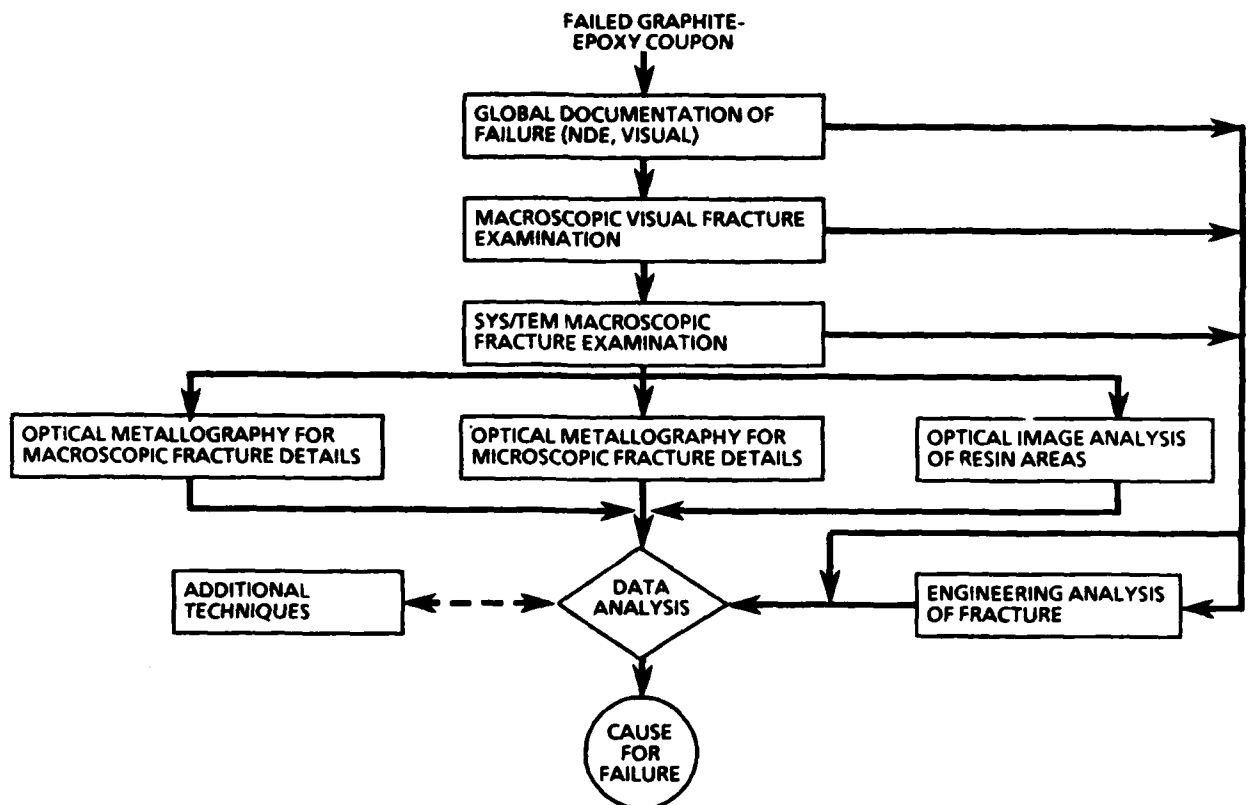


Figure 4-37. Northrop Aircraft's FALN

4. No assessment or evaluation of background data or service history.
5. No stress analysis of the part or its failure condition unless indicated by NDE, fractography, or metallographic findings.
6. No use of high-magnification optical fractography.

In discussing these differences, Dr. Kar indicated that background information and history are usually obtained and reviewed as one of the first operations in a failure analysis. Apparently, this step was omitted in the interest of simplifying their overall FALN. Dr. Kar felt differences noted in items 1, 2, 3, and 4 reflected the lack of detail in Northrop's FALN. Northrop indicated that a more detailed version of their FALN has not been developed. In general, Northrop had no problem with, or specific comments on, the more detailed FALN developed under the current Air Force program. However, it was unclear whether this input reflected Northrop's lack of familiarity with this level of FALN detail, or whether the existing FALN was in fact satisfactory. Regarding differences 5 and 6, Dr. Kar indicated that his group does not usually interact with groups doing stress

analysis nor do they use optical microscopy for crack-mapping purposes. In discussing this Dr. Kar indicated that both these areas may be viable operations in performing a failure analysis. However, Northrop has no specific experience with either.

While Northrop gave no inputs regarding the existing FALN, Boeing's review of their approach did reveal some logical changes. Northrop's FALN shows metallographic examinations as a separate operation. In the current Air Force FALN, this technique is buried as a sub-operation in fractographic examinations. As a result, the current program FALN is being updated to incorporate metallography as a separate and visible operation. This new version will be included in the annual report and will show metallography as an operational box associated with the identification of crack types and the examination of origin and propagation anomalies.

Diagnostic Techniques—In discussing techniques, Dr. Kar concentrated on his company's fractographic capabilities. Since Northrop's efforts were primarily aimed at the postfailure analysis of service and test components, their efforts in this area have been focused on identifying the origin and direction of crack propagation. In developing this methodology, Dr. Kar indicated that their efforts have fallen into two categories: the characterization of open hole compression coupons and of fractured test components.

Northrop has examined a large number of open hole compression coupons both metallographically and under the SEM. These examinations were performed on AS6/5245C and CE1200/5245 laminates which exhibited differing open hole compression properties. The intent in examining these specimens was to identify either the mode of failure or specific origin site involved in fracture. Fracture features characterized by these examinations included fiber buckling, intra-ply cracking, delaminations, hackles, and river markings. According to Dr. Kar, in examining these samples he was unable to establish any correspondence of failure initiation or growth with the direction of anticipated fracture from the hole. Dr. Kar indicated that Northrop's interpretation of river mark patterns generated inconsistent and varied crack directions.

Northrop has examined many fractured test components over the past several years. Dr. Kar's overview of these examinations was typified by the failure analysis of a five-stringer test panel. In this case, Northrop utilized the SEM to map river mark patterns and define the direction of crack propagation. The map was used to identify crack origin zones associated with each stringer. While Dr. Kar indicated that the origin of fracture had been identified, he also revealed that the analysis was limited to 11 localized areas.

Since most of the fracture surface was not mapped, it is unclear whether these origin zones constitute primary or secondary sites of initiation. The use of optical microscopy to cover more fracture surface area in a continuous manner was suggested; however, Dr. Kar indicated that optical microscopy was not used at Northrop as a fractographic analysis tool for mapping delamination surfaces. Without this technique, or more SEM sampling, the adequacy of their methodology appears questionable.

In discussing the above findings, Northrop indicated that river marks can be used to identify the direction of crack propagation. In this respect Dr. Kar agreed with the basic findings of Task 3 on mode 1 samples. However, Northrop has not tested interlaminar specimens with known crack directions, origins, and load states. Dr. Kar indicated that some asymmetric mixed mode (+45/0/0-45-degree)_s DCB specimens had been tested; however, he was unsure of the percentages of mode 1 and mode 2, and did not have any information suitable for presentation regarding fractographic features, experimental validity, or fracture models. Based on these observations, it appears that Northrop's capability in this area is based on existing metallurgical interpretations rather than on controlled testing and examination.

NASA-LEWIS

Dr. Christos Chamis and Ms. Carol Ginty
Cincinnati, Ohio

Mr. Brian Smith of Boeing, and Mr. Frank Fechek and Ms. Pat Stumpf, both of the U. S. Air Force, visited Dr. Chamis and Ms. Ginty on September 24, 1985. Dr. Chamis and Ms. Ginty were consulted because of industry-wide recognition for their expertise in composite materials stress analysis. Discussions at the Lewis Research Center centered on the state of stress analysis methods and a logical FALN approach for stress analysis. While NASA has studied the effect of load state on fracture morphology, this work was not discussed in any detail as it has been well documented and there is little question about their findings.

NASA is well aware of the current Air Force program scope and intent. NASA's emphasis in stress analysis and fractography has not been aimed at the postmortem analysis of full-scale components. Rather, its efforts are directed more toward coupon testing to understand the fundamental behavior of composite materials and their failure processes.

In assessing the state of the art for stress analysis techniques, Dr. Chamis related that some very good analysis methods exist; however, they are typically no more than 60% to 75% accurate in predicting failure. In most cases, these methods fall into three groups: those predicting first-ply failure, those predicting failure based on a combination of empirical data and laminate analysis methods, and those incorporating the latter method combined with hygrothermal effects. In discussing these, NASA indicated that a viable stress analysis technique for in-service failures should incorporate all of these methodologies and that a current NASA program called CODSTRAN should accomplish this objective.

In reviewing CODSTRAN, it was apparent that NASA has had some excellent results. However, with the program at its present level of completion, NASA has obtained only 70% accuracy in predicting failure. Dr. Chamis felt that accuracy may be improved as more detail is added to CODSTRAN. However, NASA's experience with composites was such that it felt that inaccuracies in test methods, aircraft load predictions, and component interactions would always leave some degree of inaccuracy in predicting failure. While some reports on CODSTRAN have been released, the program itself has not.

After reviewing CODSTRAN, the discussion turned to the investigative sequence for postmortem stress analysis of failed components. This conference was enlightening in that it provided inputs regarding a stress analysis FALN, and it helped clarify the logical position and relationship of various diagnostic techniques, including CODSTRAN. Dr. Chamis felt that the typical procedure for designing a component involves:

1. Assessment of the part configuration and loads
2. Development of an initial layup based on overall part requirements (i.e., stiffness, strain, buckling stability)
3. Definition of load paths and panel strains based on the initial layup configuration
4. Reiteration of 2 and 3

5. Point-design allowables testing
6. Full-scale structural testing.

Referring to the above procedure, Dr. Chamis pointed out that the most common sources for potential failures include inaccuracies in assumed loads, environment, damage, and errors in assessing load paths, and damage/defect criticalities. He also noted that a variety of manufacturing discrepancies, material faults or anomalous service conditions could also give rise to failure. In analyzing these causes, he felt that the stress analyst should gather inputs to direct his activities in accordance with the existing program FALN, but should also review initial design assumptions and analyses. In some cases examination of these analyses in greater detail may disclose critical failure conditions not revealed by the techniques in the program FALN. In carrying out this review, Dr. Chamis suggests that the stress analyst go back through his initial design steps asking these questions:

- o What additional loads or conditions could cause failure?
- o Are there any errors in the initial analysis?
- o Does a more detailed map of load paths (finite element) reveal a critical condition?
- o Have the criticalities of assumed flaws, defects, and damage been adequately accessed?

These inputs from NASA-Lewis were used to develop a flow chart illustrating a FALN for stress analysis. This flow chart is presented in Section 5.6. The procedure shown on this chart allows investigative stress analysis with or without inputs from other operations (such as fractography, etc.) within the overall FALN. One potential problem in this approach is that it can rely on assumptions or conjecture in the absence of information from the overall FALN. However, since some failure conditions may not be identifiable based solely on FALN inputs, such an approach appears unavoidable.

Ford Motor Company
Mr. Richard Robertson
Dearborne, Michigan

Mr. Frank Feчек and Ms. Pat Stumpf of the U. S. Air Force and Mr. Brian Smith of Boeing visited Mr. Robertson and several members of his staff on September 27, 1985. The intent in visiting Ford was to address Mr. Robertson's fractography findings on mode I tension fractures; he has reported seeing lamellae formations under mode I loading conditions, in addition to river markings and resin microflow.

In discussing the current Air Force program, Ford was enthusiastic about the U. S. Air Force developing a widely available handbook dealing with composite failure analysis. However, with the exception of Mr. Robertson's fractography work, Ford has not attempted to develop a failure analysis capability, and therefore had no specific inputs regarding the overall program goals or basic approach. In general, the people at Ford felt the current program was timely as well as logically organized.

Ford's fractographic studies were aimed at understanding the microscopic processes involved in fracture and energy absorption. It was felt that this approach would help develop materials with improved toughness. In these studies, Ford has not tested a large number of samples with strictly controlled load states; most of their fractures have been produced by hand loading small double cantilever beam specimens to failure. As illustrated in Figure 4-38, the fracture surfaces of these specimens exhibit: flat areas of resin fracture, localized areas of fiber pullout, and gross twisting of the fracture plane in local areas.

In reviewing these features, Mr. Smith and Mr. Robertson agreed that the flat areas of resin fracture appear similar to Air Force program mode I specimens and were not controversial. In the latter two areas, detailed inspection at 500X to 2000X revealed multiple plates of fractured matrix inclined at a relatively low angle to the fracture surface. Such features associated with fiber pullout have been observed in the current Air Force program under mode I loading on a relatively low density basis. These features are believed to reflect the occurrence of mode III loading along the fiber edge, when a significant portion of the fiber is being pulled out of the surrounding matrix. Mr. Robertson agreed that the stress state involved in fiber pullout may be complex, so that the mode II features identified under the Air Force's program may be observed under



(Ref. 12. Copyright © Chapman and Hall, Ltd.; reprinted with permission.)

Figure 4-38. SEM Photomicrographs of Mode 1 Fracture Surface

mode 1 due to localized re-orientation of the applied stress. The Boeing and Ford representatives agreed that the lamellar features observed probably occur normal to the direction of resolved tension, leading to the postulation that gross variations in the fracture plane and observed lamellar structure in these areas probably reflects a variation in the orientation of resolved tension. The exact cause of this re-orientation in Ford's samples was not discussed; however, such a condition could arise from either hand loading (introduction of some amount of mode 2 component), edge effects, or discontinuous cracking ahead of the main crack front.

To contribute to understanding and resolving the fracture morphology of these samples, Mr. Robertson agreed to provide this Air Force program with some of Ford's test specimens. When these specimens are examined, the emphasis will be on characterizing: the percentage of fiber pullout, flat and twisted areas, and the overall lamellar structure. Ford's observation of lamellae under mode 1 loading appears resolvable; both fiber pullout and hand loading offer viable and consistent arguments.

Because of Ford's research emphasis, the company has not explored any specific techniques for a crack mapping methodology in detail. However, Mr. Robertson's

published work indicates that river markings have been observed coincident with the direction of anticipated crack propagation. Mr. Robertson indicated that these features could be interpreted through traditional means and the direction of local fracture determined. Ford noted that a significant amount of variation in the direction of these river markings has been observed on unreinforced resin bend bar samples, but because the significance of these variations has not been determined, Mr. Robertson was unsure how well this technique would translate to large, complex structures.

University of Delaware, Center for Composite Materials

Dr. Byron Pipes

Newark, Delaware

Mr. Brian Smith of Boeing visited Dr. Pipes and his associates on September 28, 1985. Dr. Pipes is Dean of the engineering department at the University of Delaware, and he heads the Center for Composite Materials. Dr. Pipes' inputs regarding the overall FALN, as well as his perspective regarding the state of contemporary stress analysis techniques was of particular interest.

Dr. Pipes is one of three subcontractors under the current Air Force program. As a result, he is intimately familiar with the current program's goals, approach, and test methodology. The University of Delaware has been deeply involved--particularly in the area of test methodology--with mode 1 and mode 2 interlaminar toughness testing in recent years.

Dr. Pipes and his associates felt the selected specimens and approach for this program were logical and straightforward. He gave no inputs regarding the overall program FALN; however, in reviewing Dr. Chamis' input regarding stress analysis, Dr. Pipes felt that CODSTRAN was a long way from being applicable to actual in-service components. He believed the chief problem lay in the amount of computing time required to carry out an analysis, and in the assumptions that must be made for modeling composite behavior on a workable scale. Discussing the latter problem, Dr. Pipes stated that in order to be accurate, composite behavior should be considered on a relatively fine scale. Some of the

inaccuracies associated with CODSTRAN might be attributed to the definition of failure modes on a ply-by-ply level, rather than on a fiber, fiber/interface, and resin-interphase basis. Despite these concerns, Dr. Pipes had no specific comments regarding the stress analysis sub-FALN developed as a result of visiting Dr. Chamis. The overall approach (in which stress analyses are carried out with progressively increasing detail) seemed to fit with Dr. Pipes' general impression of how an analysis should be carried out. However, reflecting his reservations about CODSTRAN, he indicated that the concept of evaluating the criticality of defects, loads, and environments solely by analytical means was tenuous.

Additional discussions at the University of Delaware reviewed their fractographic findings on mode 1 and mode 2 interlaminar toughness coupons. In testing these samples, the university has done an extremely thorough job in characterizing toughness behavior and the effect of specimen geometry. Typically, examinations of these samples were aimed at defining the gross mechanisms of deformation associated with the toughness performance of various matrix systems. The results reviewed included both brittle epoxies, as well as state-of-the-art thermoplastic composite materials. Delaware's fractographic findings on epoxy matrices mirror those generated under the current Air Force program. Under mode 1, a relatively flat fracture morphology characterized by river marks and resin microflow was observed. On the other hand, mode 2 fractures typically exhibited numerous rows of hackles. Unfortunately, because of the university's investigative goals, no effort was made to examine the relationship of these features with the direction of crack propagation. As a result, inputs from the University of Delaware were limited to the load state/fracture morphology results described above.

McDonnell Douglas Aerospace Company

Mr. Hsin-Nan Chou

St. Louis, Missouri

Mr. Brian Smith of Boeing visited McDonnell Douglas Aerospace Company on September 29, 1985. McDonnell, along with Northrop and Boeing, is one of the few companies that, until recently, has actively pursued a failure analysis capability for composite materials; therefore its experiences and diagnostic techniques were of particular interest.

Unfortunately, Mr. Chou reported that McDonnell's activities in this area were discontinued around 1982. Mr. Gorman Morris was the principal investigator during these efforts; however he was unable to attend the meeting. As a result, no inputs were available on McDonnell's FALN or methodologies.

As Mr. Morris was unavailable, the current Air Force program was reviewed in detail with 25 to 35 engineers from both the aerospace and aircraft units of McDonnell Douglas. General interest was expressed in the availability of the current program compendium. In addition, several individuals in the aerospace company were particularly interested in future exploration into the behavior of thermoplastic matrices; however, because of McDonnell's lack of activity in this area no specific inputs were obtained.

5.0 TASK 1: FAILURE ANALYSIS LOGIC NETWORKS

5.1 OBJECTIVE AND STATUS

This section reviews the flow charts and supporting data tables developed within Task 1. The failure analysis logic network (FALN) flow charts were developed to provide investigators with guidelines delineating a logical sequence of investigative operations. Such guidelines have not been available previously due to the relative complexity of composite materials and their fairly recent use in industry. In developing these guidelines, specific objectives were incorporated to provide investigators a logical sequence that:

- o Considers a variety of potential causes including design or fabrication errors, anomalies, and in-service damage
- o Incorporates multiple analytical disciplines, such as nondestructive testing, fractography, stress analysis, and materials characterization
- o Avoids the premature destruction of evidence
- o Builds on gathered information and allows for redirected investigations.

In performing Task 1, Boeing's initially proposed FALN--which was aimed at satisfying these objectives--was updated and completed. In addition, detailed FALNs were developed for the areas of nondestructive testing, materials characterization, fractography and stress analysis. Detailed tables of support information were also completed for each of these areas delineating techniques described in each FALN.

5.2 OVERALL FAILURE ANALYSIS LOGIC NETWORK

Identifying the logical sequence of steps for carrying out a postfailure analysis is often a complex and difficult process. Sufficient information must be gathered and evaluated to determine the cause of fracture from positive supporting evidence rather than by a process of elimination. Developing positive evidence is often complex because numerous potential causes exist and multiple contributory factors may be involved. To accurately identify the cause of fracture, each potential cause and its contributory factors must be

taken into consideration using an organized investigation sequence. Developing such a plan is further complicated by the fact that some investigative steps destroy evidence. Consequently, existing evidence must be adequately documented and the logical flow of information from one analysis to another considered.

To assist investigators in developing a logical plan, an overall framework was developed during Task I based on well-established procedures used in failure analysis of metallic structures. The rationale of the framework considers a variety of potential causes, interrelationships, and the premature destruction of evidence. Because composite materials differ from metals in many respects, the analysis operations were modified to address composites. The approach simplifies and streamlines the number and complexity of analyses. The final framework consists of five basic investigative operations arranged around intermediate decision points:

- o Collection and review of background history and information
- o Nondestructive inspection
- o Evaluation of part conformity to specified requirements
- o Detailed fractographic examinations
- o Stress analysis.

The sequence of application for the five operations is illustrated in Figure 5-1. The sequence encourages the use of simple, inexpensive examinations initially, followed by progressively more detailed analyses. Through comprehensive Task I evaluations, a significant amount of detail has been added to the investigative framework illustrated in Figure 5-1. This version, shown in Figure 5-2, establishes a more accurate path for investigators, and delineates most of the widely used techniques, use points, and decisions involved in carrying out a postmortem analysis.

During the initial stages of investigation, information on fabrication, loads, environment, and service history is collected and reviewed with the intention of identifying areas of concern, and building a familiarity with the component, its operation, and its environment. After this initial stage, nondestructive inspections are performed to identify and define the extent and nature of fracture, and document it for later reference. This operation establishes the groundwork to plan more detailed examinations and destructive sectioning. After nondestructive examination, the part is evaluated for conformity with drawing, material, and process specifications. Each initial examination is directed toward

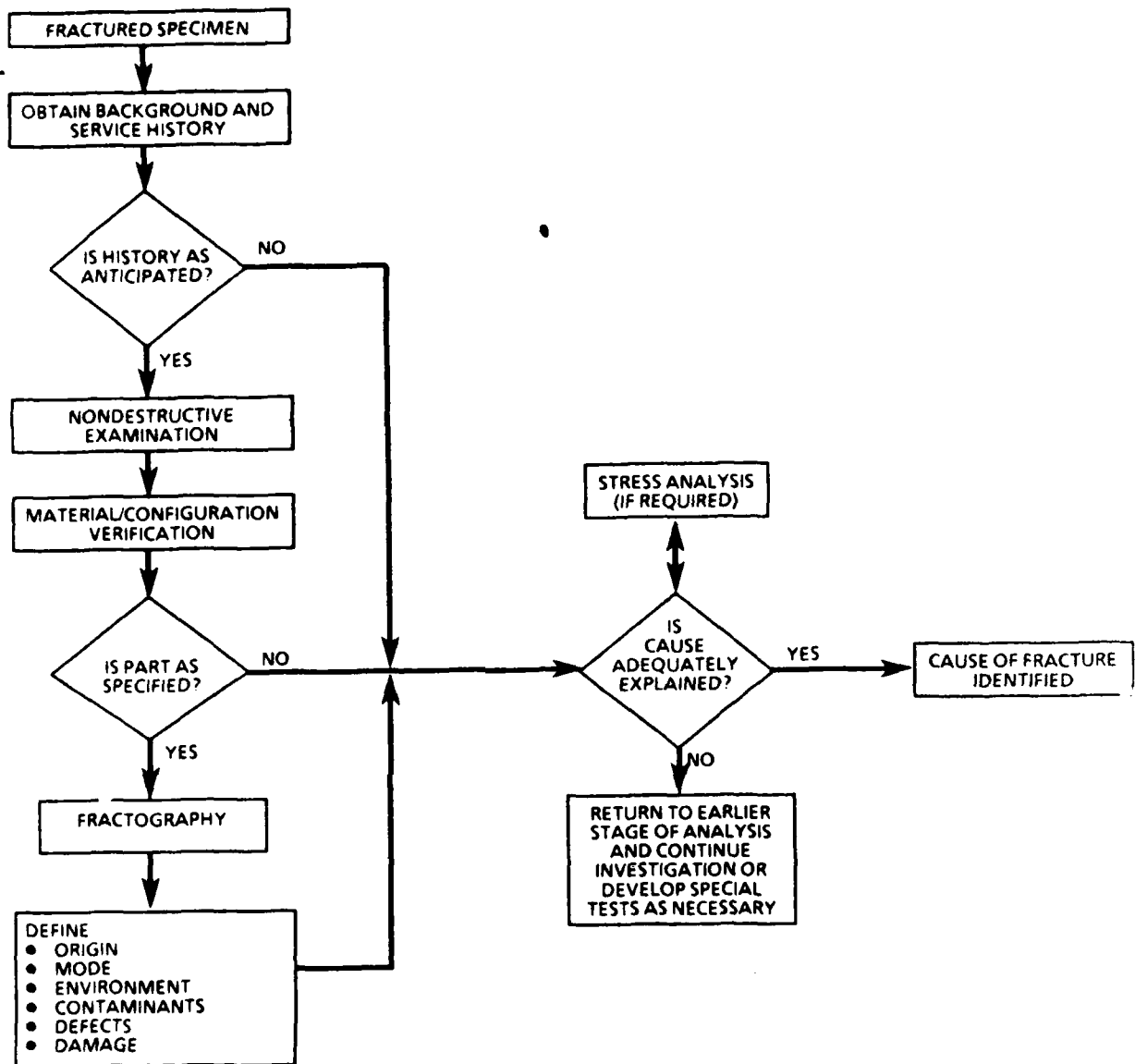
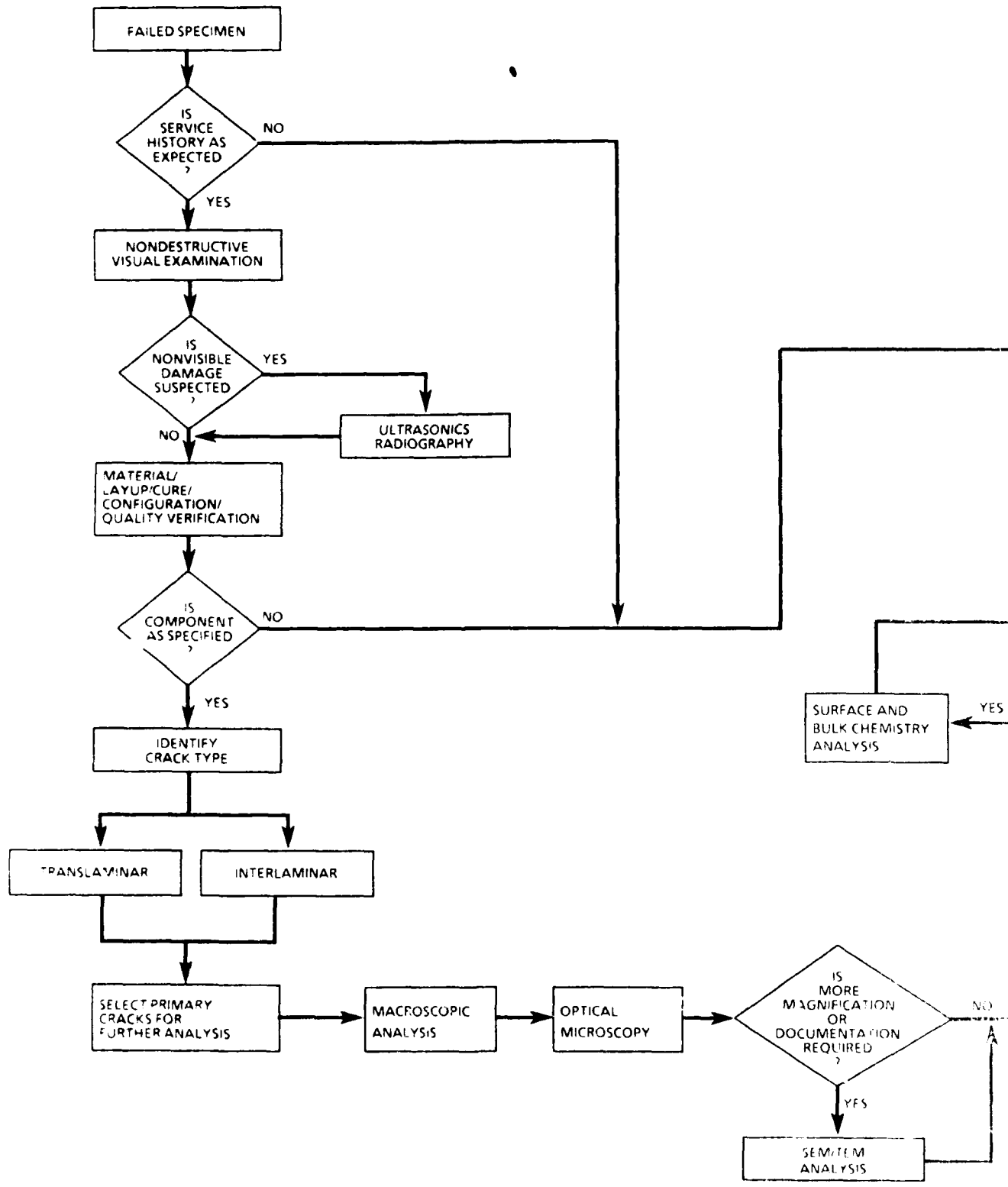


Figure 5-1. Simplified Investigative Framework

identifying items of significance early in the investigation. Through an iterative process the number of steps can be minimized and effort concentrated on items of interest.

Detailed fractographic and stress examinations are the next analytic steps. These operations identify more specific details and assess their significance. Typically, fractographic examinations are performed prior to detailed stress analyses. Fracture examinations are used principally to identify the origin and load conditions involved in failure. In many cases, the main benefit of fracture examination is the identification of material defects or anomalies. As such factors are identified, sufficient information may



AD-A172 236

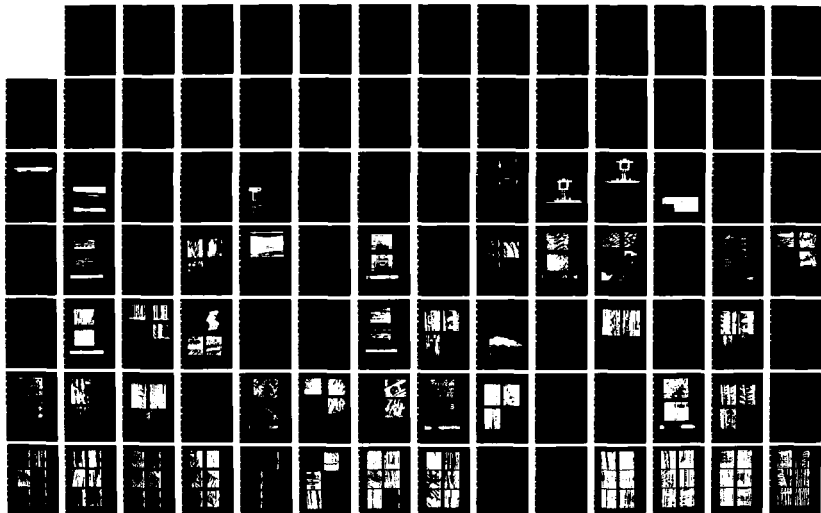
FAILURE ANALYSIS OF COMPOSITE STRUCTURE MATERIALS(U)
BOEING MILITARY AIRPLANE CO SEATTLE WA B SMITH ET AL.
MAY 86 AFWAL-TR-86-4033 F33615-84-C-5010

2/3

UNCLASSIFIED

F/G 11/4

NL





MICROCOPY RESOLUTION TEST CHART
NATIONAL BUREAU OF STANDARDS-1963-A

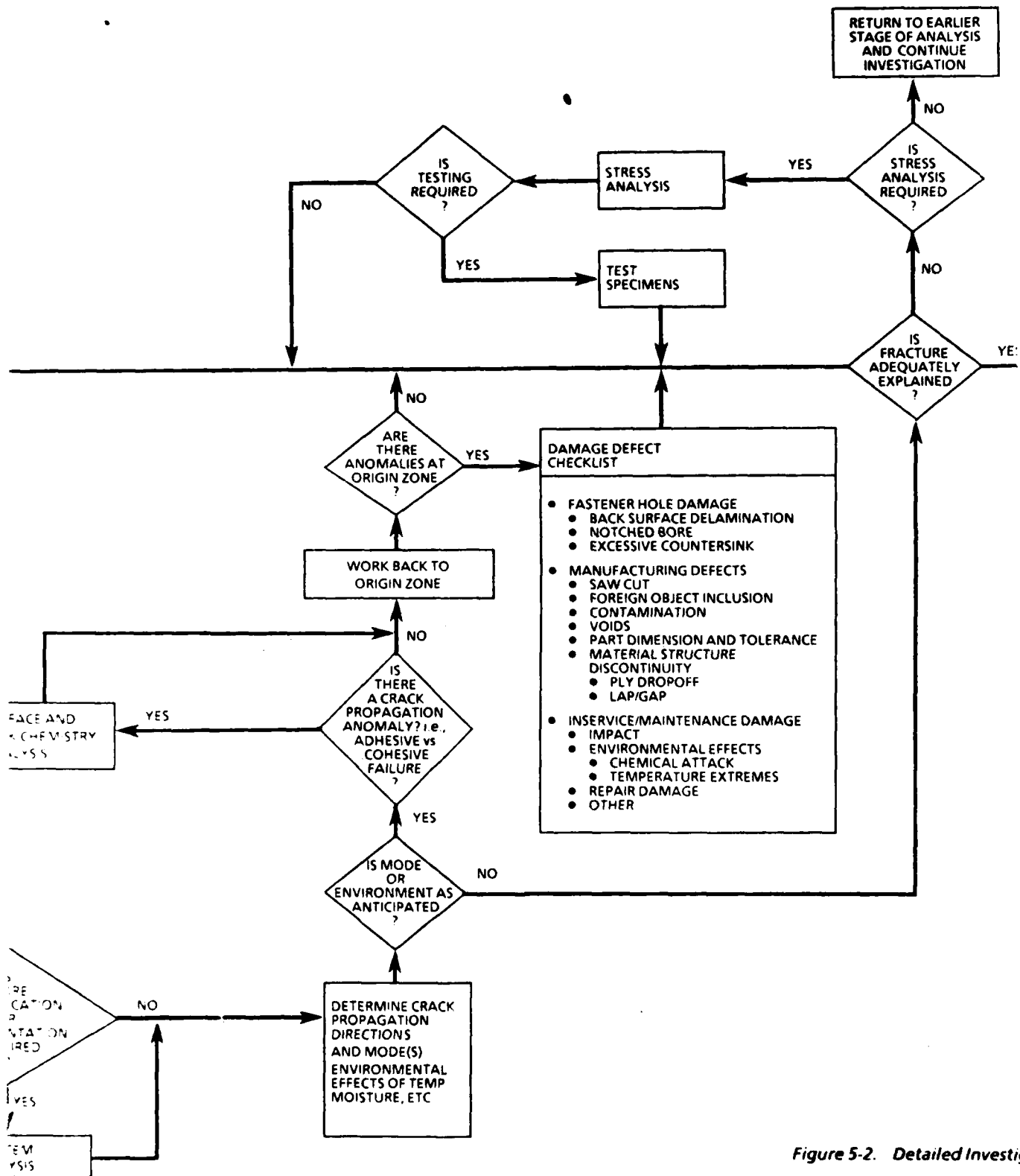


Figure 5-2. Detailed Investigation of Fracture

(2)

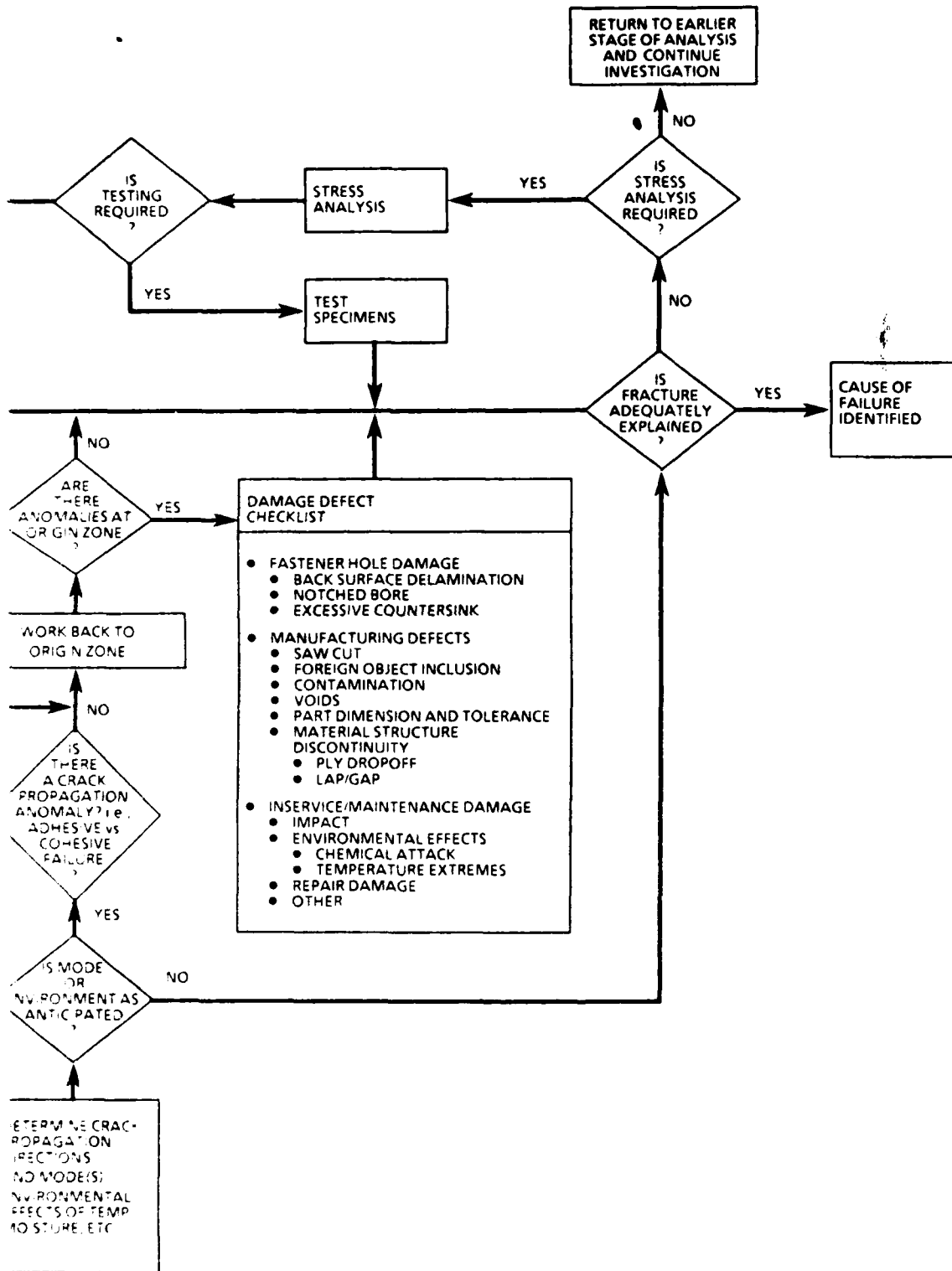


Figure 5-2. Detailed Investigative Framework

(3)

be developed to identify either a specific cause for failure or a point of interest (i.e., origin) for further analyses. After inputs from fractographic analysis have been developed, stress analyses may be performed to evaluate localized stress states, out-of-compliance conditions, or the critical nature of identified defects. In cases where questions may remain, additional specialized tests may be required to model previously indeterminate conditions.

5.3 NONDESTRUCTIVE EVALUATION FALN

Before performing more detailed analyses, nondestructive evaluations can be extremely useful to the failure investigator by revealing areas of fracture not readily discernable through visual examinations. Nondestructive evaluation is of particular importance with composite materials because of their predisposition to nonvisible internal delaminations, flaws, and conditions of damage. In addition to its primary benefits, nondestructive evaluation has several other notable advantages.

Providing adequate documentation prior to destructive sectioning is of particular importance in failure analysis. With many modern nondestructive analysis techniques available for composites (e.g., X-ray and through-transmission ultrasonics) a permanent record is made of both visible and nonvisible areas of fracture. This record, somewhat like optical photography, provides invaluable documentation for later perusal. Finally, since nondestructive testing is usually performed by a support specialist, the investigator is freed to establish a coherent plan for more detailed evaluation prior to destructive testing.

To provide the investigator with a better definition for the sequence of steps involved in the nondestructive evaluation of a part, the FALN in Figure 5-3 was developed. Several goals were considered in creating this FALN: the chart should provide the most basic information first, and the techniques should progress from the most easily interpreted to the more complex. The chart begins by documenting the fracture in general terms using relatively simple techniques. Next, two operations provide more plan view and cross-section information using more complex techniques.

Since many novice investigators may be unfamiliar with the variety of techniques shown, additional supporting information has been included in two figures. Figure 5-4 lists each technique, its description, general use, and value. Figure 5-5 shows a modified version of Mr. M. Phelps' recommended nondestructive evaluation techniques; note that the emphasis

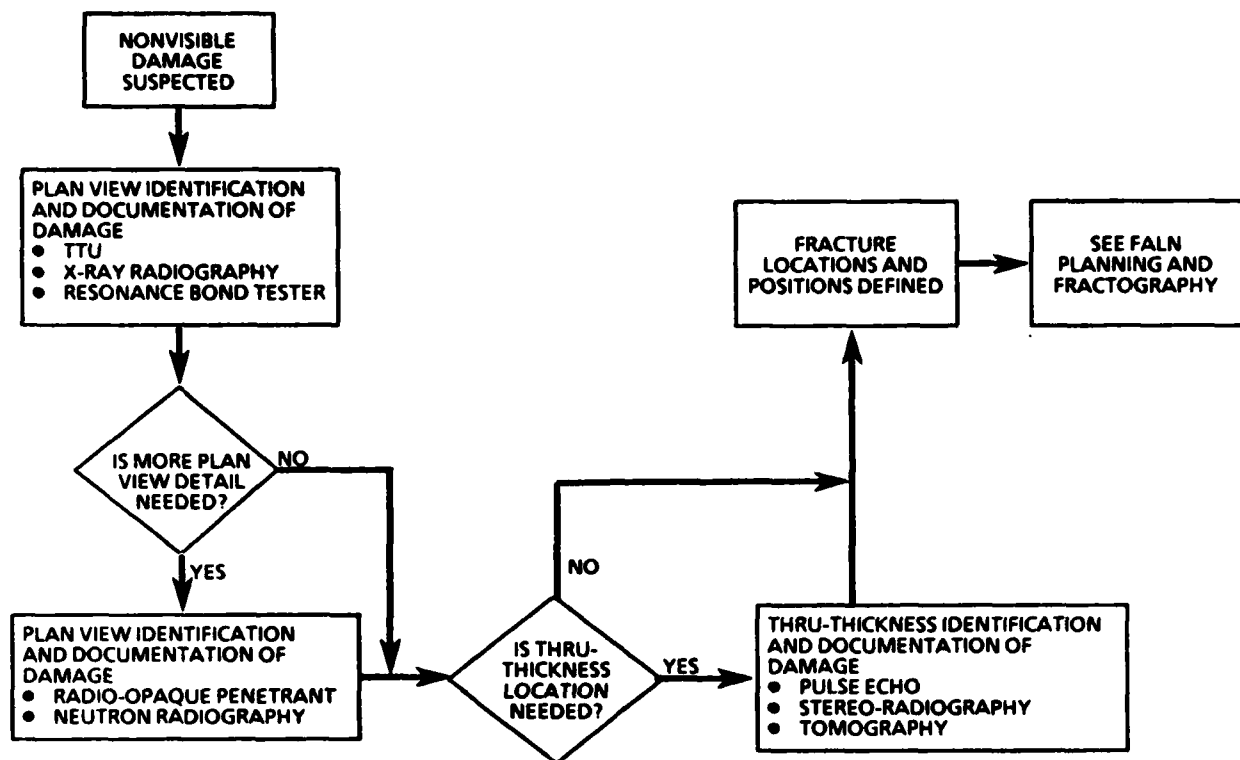


Figure 5-3. Nondestructive Evaluation

on defects and structures has been modified to reflect postfailure analysis rather than in-service inspection. Figure 5-5 also lists the preferred order of analysis application for differing structural configurations and fracture types based on Boeing's internal failure analysis experience.

5.4. MATERIALS VERIFICATION AND CONFIGURATION FALN

In most failure analyses, the examination of part material, configuration, and quality should be considered a routine procedure necessary to the accurate evaluation of the failure cause. These examinations should identify gross deficiencies that could have significant effect on material properties or the magnitude of local stresses within the part. For composite materials, items of concern include:

- o The wrong material
- o Undercure
- o Ply placement and orientation errors
- o Mismachined details, radii, holes, etc.
- o Improper fastener installation, joining, etc.

TECHNIQUE*	DESCRIPTION	USE	VALUE
Through-transmission ultrasonic (TTU) ● C-Scan	Measures ultrasonic sound attenuation ● C-Scan-plan-view presentation	Determines size and location of nonvisible damage, defects, fracture in plan view	<ul style="list-style-type: none"> ● Plan-view documentation of failure ● Plan-view assessment of part quality ● Planning analyses
Pulse ultrasonic ● B-Scan ● C-Scan	Measures ultrasonic sound reflection ● B-Scan – through-transmission view presentation ● C-Scan – plan-view presentation	Determines size and location of damage, defects, fracture in both a plan and through-thickness view	<ul style="list-style-type: none"> ● Plan-view documentation of failure ● Through-thickness view documentation of failure ● Plan-view assessment of part quality ● Through-thickness assessment of part quality ● Planning analyses
Resonance bond testers ● Bondscope 2100 ● Sondicator ● Acoustic flaw detector ● MIA 3000	Measures mechanical resonance changes caused by defects, meter, or CRT display	Determines size and location of nonvisible damage	<ul style="list-style-type: none"> ● Determining of size and location of part damage ● Method can be used when only one side is accessible
X-ray radiography (tomography)	Measures X-ray attenuation plan-view presentation	<ul style="list-style-type: none"> ● Determines size and location of translaminar fractures and radio-opaque defects – plan-view presentation ● Delamination size and location determined with radio-opaque penetrant ● Through-thickness position determined by stereo-radiography or X-ray tomography 	<ul style="list-style-type: none"> ● Plan-view documentation of failure ● Plan-view assessment of part quality and defects ● Planning analyses
Neutron radiography	Measures neutron attenuation plan-view presentation	<ul style="list-style-type: none"> ● Determines size and location of translaminar fractures and neutron opaque defects – plan-view presentation ● Delamination size and locations determined with neutron-opaque penetrant ● Used often where metal structure overlays composite material – neutrons are not as attenuated by metal as X-ray, and are relatively sensitive for polymers with hydrogen 	<ul style="list-style-type: none"> ● Plan-view documentation of failure ● Plan-view assessment of part quality and defects ● Planning analyses
Eddy current	Measure conditions which interrupt the flow of eddy current induced in the part	Determines differences between paint scratches and surface cracks in Gr/Ep fabric structures	<ul style="list-style-type: none"> ● Plan-view documentation of fracture with single-side access ● Planning analyses

* Techniques are listed in order of preference, based on applicability, reliability, cost, and sample requirements.

Figure 5-4. Failure Analysis Technique – Nondestructive Evaluation

STRUCTURES		DEFECTS						
		DELAMINATION/ DISBOND	IMPACT DAMAGE	FASTENER HOLE DAMAGE	LIGHTNING DAMAGE	BURN DAMAGE	TRANSLAMINAR FRACTURES, SURFACE	TRANSLAMINAR FRACTURES, SUBSURFACE AND SUBSTRUCTURE
LAMINATED SKIN		C,D,E	A,C,D,E G	A,C,G,H	A,C,D,E	A,C,D,E	A,B	C,G,F, D,E
SKIN/HONEYCOMB PANEL		C,E,D	A,C,E,D	A,C,G,H	A,C,E,D	A,C,E,D	A,B	C,G,F D,E
SKIN-TO-STIFFENER JOINT		C,D,E	A,C,D,E G	A,C,G,H	A,C,D E	A,C,D E	A,B	C,G,F D,E
SKIN-TO-METAL JOINT		C,D,E	A,C,D, E	A,C,H	A,C,D E	A,C,D, E	A,B	C,I,D E
SKIN-TO-SKIN TRAILING EDGE JOINT		C,E,D	A,C,E D,G	A,C,G H	A,C,E, D	A,C,E, D	A,B	C,G, F,D,E
LAMINATED RIBS, SPARS, AND SKIN STIFFENERS		D,E	D,E, G	A,D, E,G,H	A,D,E G	A,D,E, G	A,B	C,G,F D,E
LUGS AND THICK SECTIONS		C,D,E	A,C,D,E	A,C,G H	A,C,D,E	A,C,D, E	A,B	C,G,F D,E

Key:

Inspection method

A	Visual	F	Low KV X-ray
B	Penetrant	G	DIB-enhanced X-ray
C	Ultrasonic TTU	H	Eddy current
D	Ultrasonic pulse echo	I	Neutron radiography
E	Bond tester		

Figure 5-5. Method Selection (Listed in Order of Preference)

These conditions are likely to be rare. However, since they require little effort to examine and have such a critical influence on failure, their inclusion in any complete analysis is a necessity. Configuration and materials verification examinations have been included in the overall FALN illustrated in Figure 5-2. Because of their potential impact

on subsequent operations, these examinations have been incorporated in the early stages of analysis. In many cases, identification of a major discrepancy (such as using the wrong material), may sufficiently explain the cause of fracture, thus shortening the entire investigative process.

In support of the overall FALN, a detailed flow chart for configuration and materials verification was developed and reviewed under Task 1. This FALN, illustrated in Figure 5-6, provides a detailed guideline for investigators to evaluate critical items such as configuration, ply layup, degree of cure, and the type of resin system used. This FALN employs relatively simple analysis techniques; more complex and difficult analyses occur at later stages. Because novice investigators may be unfamiliar with many of the techniques specified, Figures 5-7 through 5-9 were developed to review each technique, and give its description, use, and general value in performing a failure analysis.

In Figure 5-6, one of the more detailed areas of a configuration and materials verification study is illustrated. Once a material has cured, ascertaining its identity poses a relatively difficult problem arising from the generally similar chemical structure of cross-linked epoxy systems and the tendency of cured resins to resist yielding their identities by typical analytic methods. However, since many of the currently used epoxies exhibit nearly identical properties (within a cure-temperature family), identification of the exact resin system used may not be as crucial as identifying a material with its proper cure-temperature family. Through the combined use of Tg and residual heat of reaction measurements, the particular cure-temperature family of most materials can be established with some confidence.

For example, when fully cured, most epoxies exhibit no appreciable residual heat of reaction and the Tg's are at—or slightly above—the range of their original cure temperature. Thus, when little heat of reaction is observed, the measured glass transition temperature gives a fairly good indication of the cure temperature family of material used. However, in cases where some heat of reaction still exists, undercure is indicated. In these cases, this data in combination with the measured Tg may be sufficient to identify the specific cure-temperature family of the material. For example, a substantial residual heat of reaction combined with a Tg well below the specified cure temperature probably indicates the proper use of prepreg material but an insufficient degree of cure. In making these analyses, it is important to keep in mind that undercure can arise from several causes—only one of which may be an improper cure procedure. Alterations in

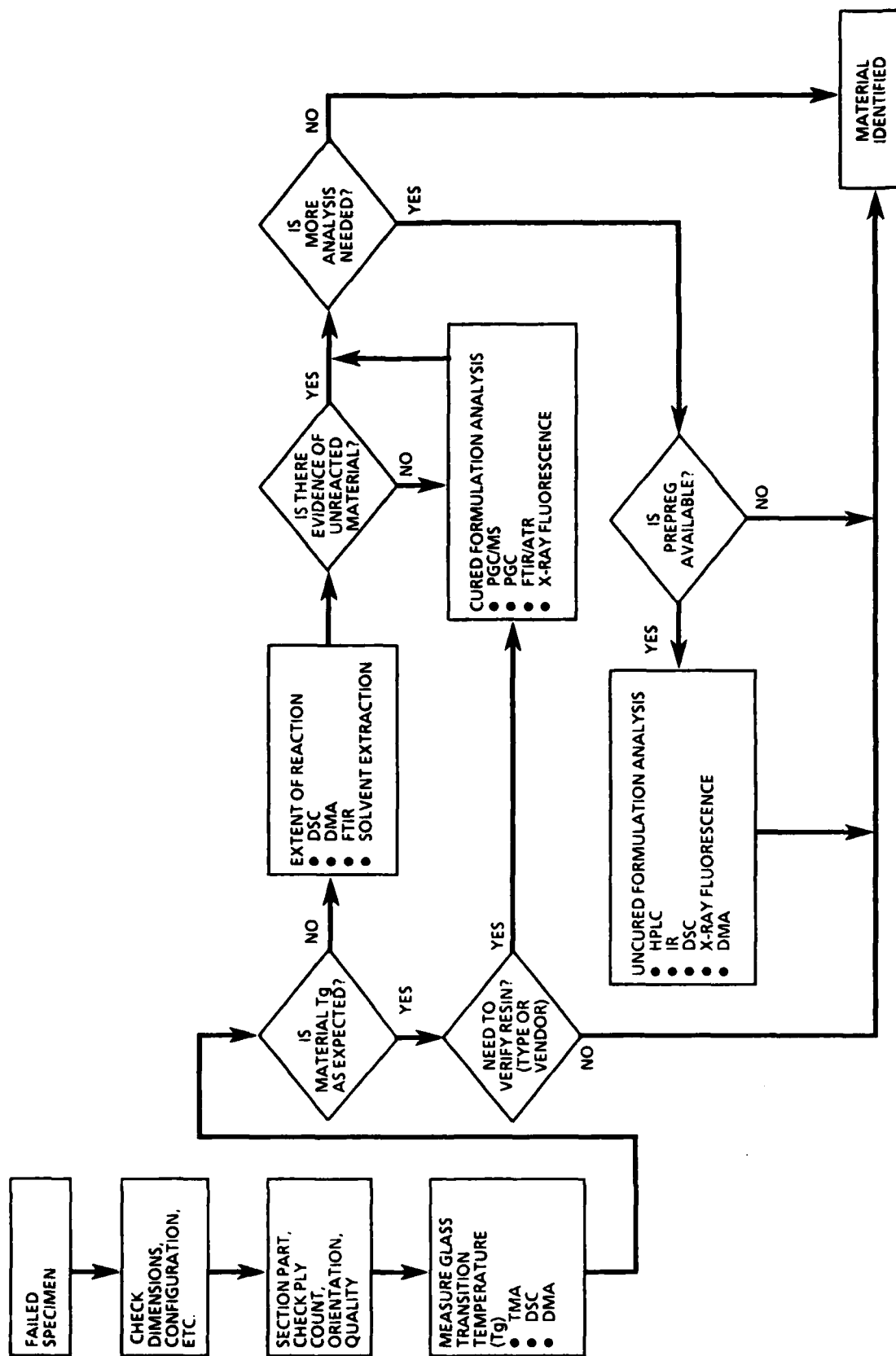


Figure 5-6. Material Cure Configuration Verification Diagnostic Technique

TECHNIQUE	DESCRIPTION	USE	VALUE
Pyrolysis – gas chromatography (PGC)	Determines gas chromatograms formed from nonvolatile organics by thermal decomposition	Qualitative and quantitative analysis of cured epoxy	Formulation/impurity verification
Pyrolysis – gas chromatography / mass spectroscopy (PGC/MS)	Allows mass spectrometer to act as a detector for the gas chromatograph	Qualitative and quantitative analysis of cured epoxy	Formulation/impurity verification
Infrared spectroscopy	Measures IR spectra	Functional group analysis	Formulation verification
X-ray fluorescence	Measures X-ray fluorescence spectra	Determines sulfur content	Hardener content
Thermomechanical analysis (TMA)	Measures material thermal-mechanical response	Determines glass transition	Identify general resin system

Figure 5-7. Failure Analysis Techniques – Cured Material Identification

TECHNIQUE	DESCRIPTION	USE	VALUE
Thermomechanical analysis (TMA)	Measure probe displacement as a function of sample temperature	Determines glass transition temperature	Indication of degree of cure or environmental effects
Differential scanning calorimetry (DSC)	Performs enthalpy measurements	<ul style="list-style-type: none"> • Determines glass transition temperature • Determines residual heat of reaction 	Indication of degree of cure or environmental effects
Dynamic mechanical analysis (DMA)	Measures mechanical response to oscillating dynamic loading	<ul style="list-style-type: none"> • Determines glass transition temperature • Observes mechanical transition due to additional crosslinking 	<ul style="list-style-type: none"> • Indication of degree of cure or environmental effects • Indication of undercured condition
Infrared spectroscopy	Measures IR spectrum	Distinguishes between reacted and unreacted functional groups	Indicates amount of unreacted functional groups to determine extent of cure
Solvent extraction	Exposure to an organic solvent	Removes unreacted material leaving reacted network behind	Indication of the degree of cure

Figure 5-8. Failure Analysis Techniques – Degree-of-Cure Analysis

TECHNIQUE	DESCRIPTION	USE	VALUE
High-pressure liquid chromatography (HPLC)	Produces liquid chromatograms of any soluble liquid	Identifies individual components of differing solubilities or size	Formulation verification
Infrared spectroscopy	Measures IR spectra	Identifies functional groups attached to carbon backbone	Formulation verification
Differential scanning calorimetry (DSC)	Performs enthalpy measurements	Determines heat of reaction	Formulation verification
X-ray fluorescence	Measures X-ray fluorescence spectra	Determines sulfur content	Hardener content

Figure 5-9. Failure Analysis Techniques – Uncured Material Identification

prepreg formulation can reduce reaction rates during cure. Therefore, when a sufficient degree of undercure is detected, it is generally recommended that additional tests be carried out on the original prepreg to verify its chemistry.

In some analyses, identifying the specific resin system used may be important; however, the investigator should be aware that extensive capabilities in this area are only partially developed. Sufficient differences exist in basic formulations so that relatively simple tests (such as X-ray fluorescence) may be used to identify different systems (Figure 5-10), but for the most part the ability to identify resin systems within the same temperature-cure family is relatively difficult. One of the potentially promising techniques is pyrolysis gas chromatography (PGC) in which the vaporized remains of a sample are separated in a column to form a unique fingerprint as shown in Figure 5-11.

5.5 FRACTOGRAPHY FALN

Some of the most extensive investigations in a failure analysis involve the examination of the fracture surfaces of failed parts. These surfaces may provide the only true physical

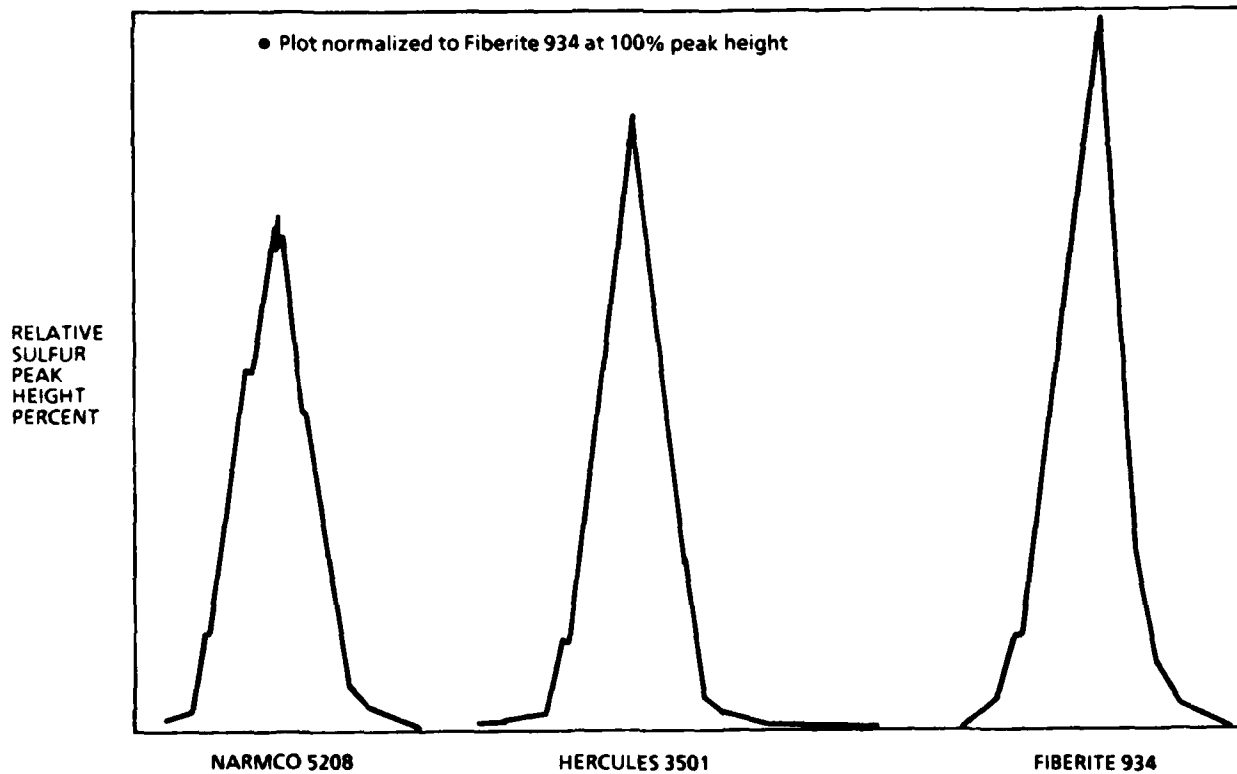


Figure 5-10. Sample Fingerprinting of Various Systems Via X-Ray Fluorescence

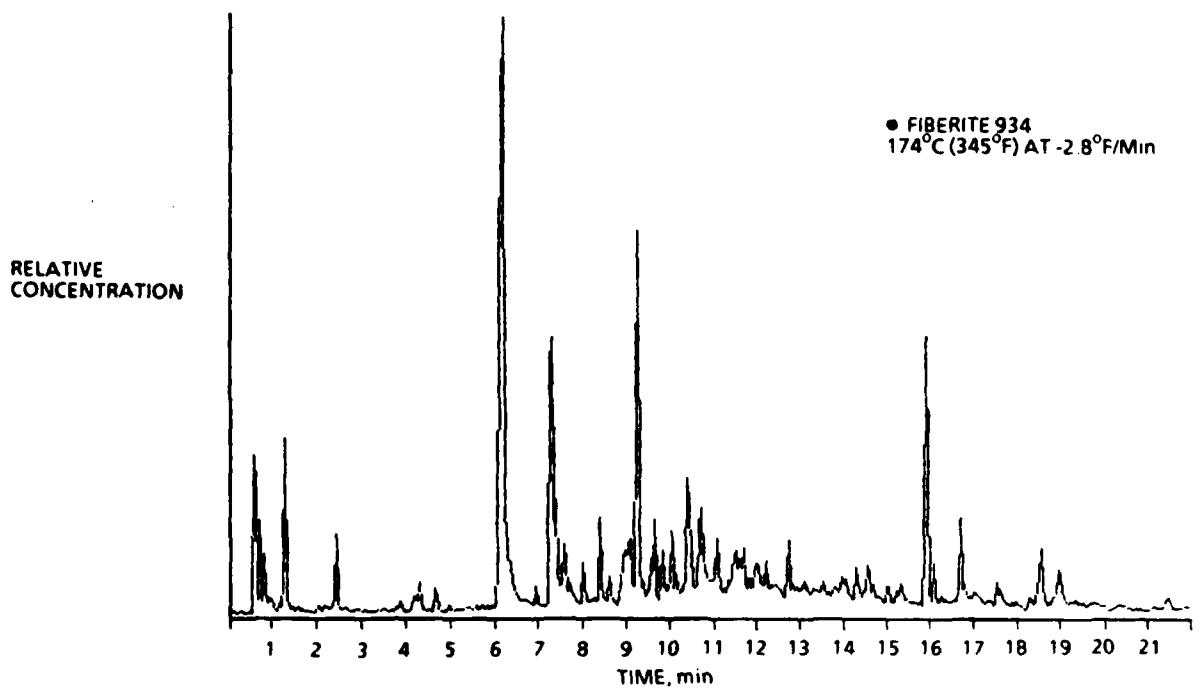
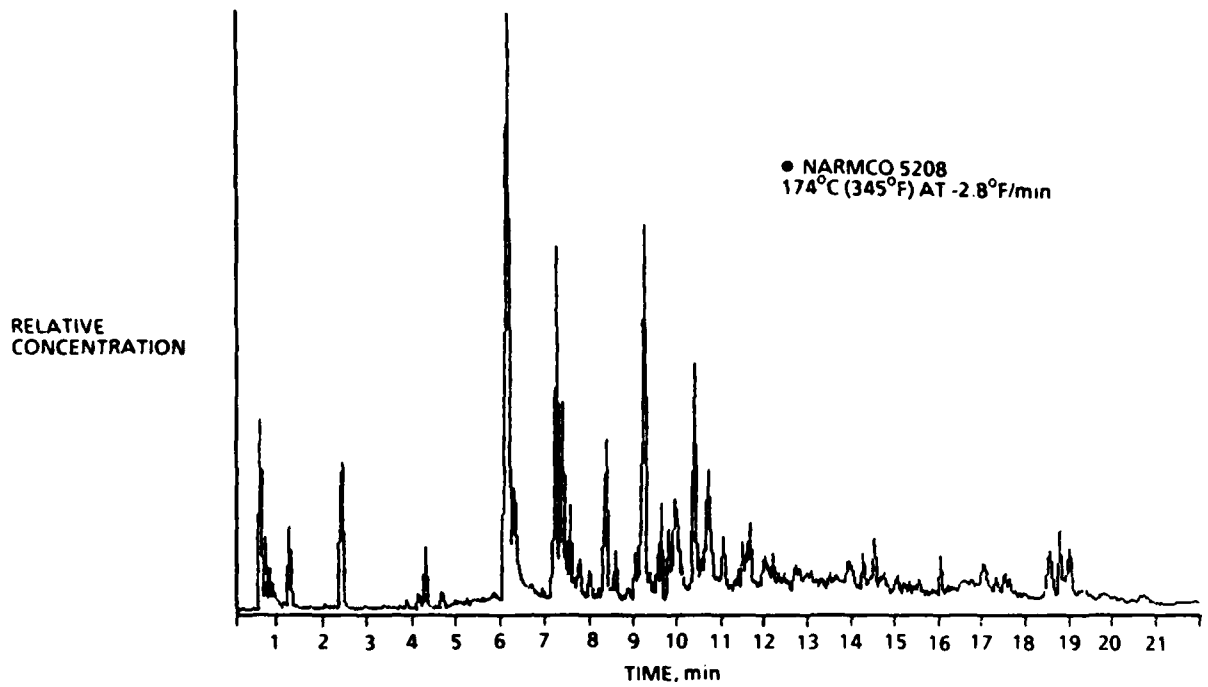


Figure S-11. Pyrolysis Gas Chromatography (PGC) of Two Different Resin Systems

record of the events involved in failure. The study of these fracture surfaces is called fractography, a process that attempts to reconstruct the failure sequence through detailed microscopic analysis. In fractographic analyses, primary emphasis is placed on:

- o Locating the origin of the failure
- o Establishing the direction of fracture
- o Identifying the load state and modes of crack growth
- o Determining if environmental conditions or defects contributed to reduced material strength or premature fracture.

The use of fractography for the analysis of metals dates back to the early 1900s, and well-established procedures exist for its application. Under Task 1, these traditional guidelines were reviewed and modified to yield the detailed fractography FALN illustrated in Figure 5-12. The chart diagrams three distinct operations: classification of failure types, crack mapping, and fracture surface chemical examinations.

A failure classification breaks down the relatively complex nature of composite fractures into two distinct types: interlaminar or translaminar. This classification is useful because different analytical methods are best suited for each fracture type. Interlaminar fractures are best analyzed for crack direction using optical microscopy, whereas trans-laminar fractures are best analyzed by scanning electron microscopy.

Determining the direction of crack propagation is one of the most significant concerns in fractography. The recommended technique for crack mapping uses the lowest magnification capable of performing the job. This recommendation is made because one of the fundamental problems in detailed microscopy of large fractures is that there is an extremely limited perspective on how the area being examined relates to the part as a whole. The situation is similar to the old adage, "one can't see the forest for the trees." With a limited perspective, it is often possible to improperly characterize the direction, mode, or load state at fracture. By emphasizing the use of lower magnification for early investigations, the FALN imposes a sense of perspective on later, high-magnification inspections.

The chemical analysis of fracture surface features (shown in Figure 5-12) may be required to determine the sequence of fracture events. By carrying out these examinations after identifying the fracture origin, emphasis can be placed on any anomalies encountered.

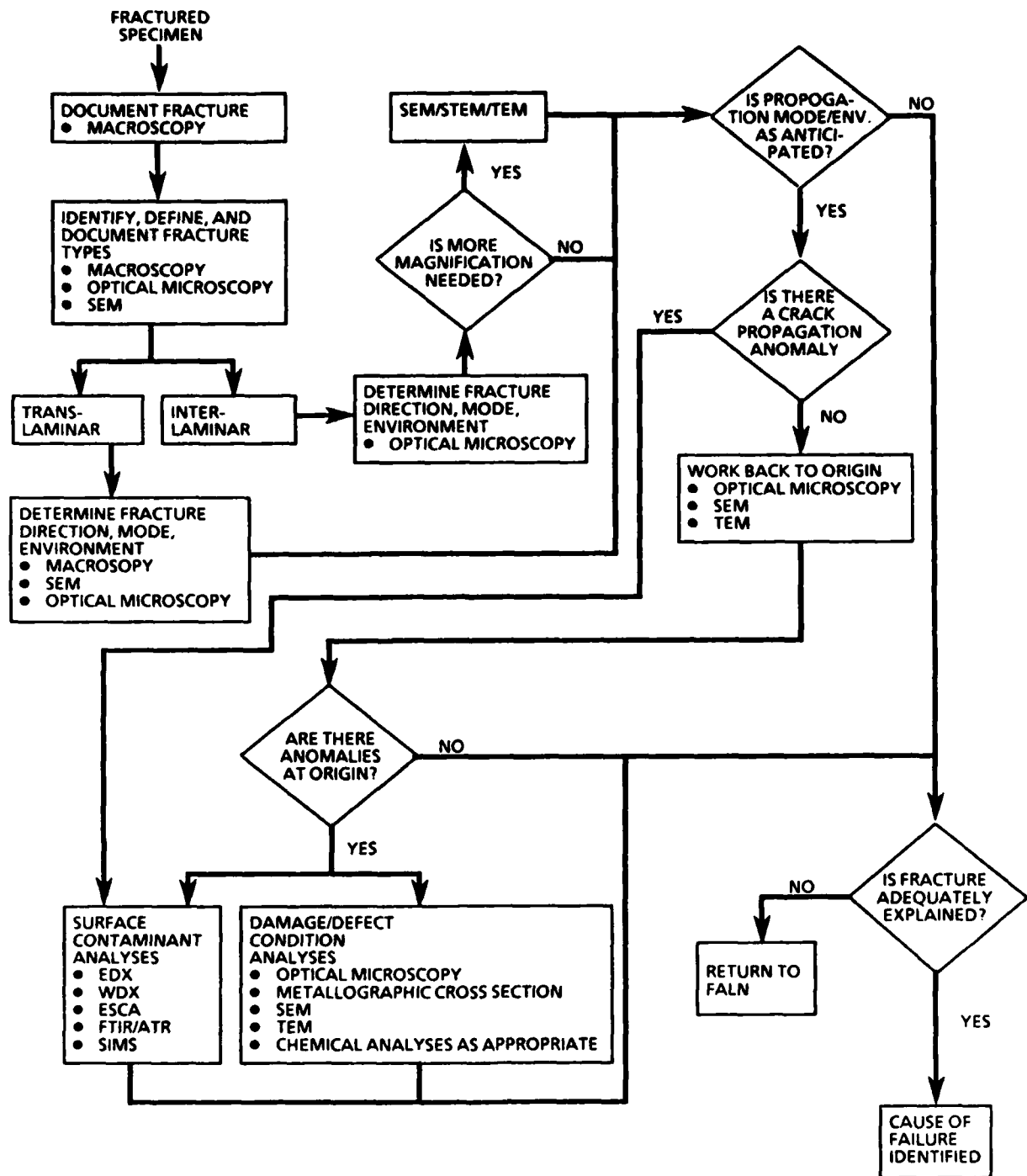


Figure 5-12. Fractography FALN

The examination of features for their chemical nature requires a different set of analytic techniques than noted in Section 5-4. Since novice investigators may not be well versed in the techniques of the detailed fractography FALN, Figures 5-13 and 5-14 review valuable methods, their description, and use.

TECHNIQUE	DESCRIPTION	USE	VALUE
Optical macroscopy	Optical examination at magnification generally at or below 10X	Plan-view examination and identification of fracture surface features, damage, and defects	<ul style="list-style-type: none"> • Documentation of fracture • Identification of fracture types (translaminar vs. interlaminar) • Determination of translaminar fracture modes
Optical microscopy	Optical examination at magnifications above 10X	Plan view examination and identification of fracture surface features, damage, and defects	<ul style="list-style-type: none"> • Identification of fracture types (translaminar vs. interlaminar) • Determination of interlaminar fracture direction, mode, and environment • Determination of origin • Identification and characterization of defect and damage conditions
Optical cross section	Metallographic optical examination at magnifications above 10X	Cross-sectional examination of laminate, defect, and damage conditions	<ul style="list-style-type: none"> • Identification of fracture locations • Determination of laminate orientation and drawing compliance • Identification and characterization of defect conditions
Scanning electron microscopy (SEM)	Microscopy performed by mapping; secondary electrons from the sample generated by a primary electron beam raster	High-magnification examination of fracture surfaces and defects with excellent depth of field	<ul style="list-style-type: none"> • Documentation of fracture surface • Identification of interlaminar fracture mode, direction, and environment • Identification of translaminar fracture mode, direction, and environment • Determination of origin • Identification and characterization of defect conditions
Transmission electron microscopy (TEM)	Microscopy performed by examining the focused pattern of electrons attenuated by a thin fracture surface replica	High-magnification examination of replicated fracture surfaces with better depth of field than in optical microscopy	<ul style="list-style-type: none"> • Limited to delamination fractures • Documentation of fracture surface • Identification of interlaminar fracture mode, direction, and environment • Determination of origin • Identification and characterization of select conditions
Back-scatter electron microscopy	Microscopy performed by imaging back-reflected primary beam electrons generated by a rastered electron beam	Intermediate magnification of fracture surface and defects. Back-reflected electrons are sensitive to atomic number and can be used to distinguish surface details as a function of atomic number.	<ul style="list-style-type: none"> • Documentation as a function of atomic number • Identification and characterization of defect conditions

Figure 5-13. Failure Analysis Techniques – Fractography

5.6 STRESS ANALYSIS FALN

Defining the cause of a component failure requires the accurate understanding of the loads and stresses involved as a part functions. In metals, this understanding is commonplace. Fracture mechanics calculations are usually carried out during initial design stages as well as after component failure. Stress analyses are run after failure to review initial design stresses in more detail, to evaluate configurational and material errors, and to determine if damage (cracking) was incurred in service or during

TECHNIQUE	DESCRIPTION	USE	VALUE
SEM/microprobe energy dispersive X-ray analysis (EDX)	Quantitative microchemical analysis, photographic mapping of X-ray energies created by primary electron beam raster	Determines microchemical elemental composition of micro-inhomogeneities and particles	<ul style="list-style-type: none"> ● Identification of contaminants ● Particle size analyses
SEM/microprobe wavelength dispersive X-ray analysis (WDX)	Quantitative microchemical analysis, photographic mapping of X-ray wavelengths created by primary electron beam raster	Determines microchemical elemental composition of micro-inhomogeneities and particles	<ul style="list-style-type: none"> ● Identification of contaminants ● Particle size analyses
Auger electron spectroscopy (AES)	Quantitative surface chemical analysis (top 5 nm) of Auger electrons ejected due to primary electron beam	Determines elemental chemistry of upper 5 nm of surface (requires conductive surfaces)	<ul style="list-style-type: none"> ● Identification of contaminant monolayers ● Identification of adhesive failure interfaces
X-ray photoelectron spectroscopy (XPS)	Quantitative surface chemical analysis (top 5 nm) of photoelectrons ejected due to primary X-ray beam	Determines elemental chemistry and chemical state of upper 5 nm of surface (does not require surface conductivity)	<ul style="list-style-type: none"> ● Identification of contaminant monolayers ● Identification of adhesive failure interfaces
Secondary ion mass spectroscopy (SIMS)	Qualitative surface chemical analysis of surface monolayer atoms removed by ion sputtering	Determines elemental and chemical state of surface monolayers; repeated operation allows elements to be profiled versus depth	<ul style="list-style-type: none"> ● Identification of contaminant monolayers

Figure 5-14. Failure Analysis Techniques – Fracture Surface Material and Chemical Characterization for Fractography

maintenance. The logical investigative sequence for metals and composites is similar. Figure 5-15 illustrates the detailed stress analysis FALN developed under Task 1 based on existing metals procedures and inputs from experts in the area of composite materials stress analysis.

Stress analysis is carried out at three different stages: initial design review, a structural level, and a microstructural level.

At the initial design review, the analyst's objective is to verify initial design assumptions and calculations with respect to the available service history and the location of fracture. This review establishes what analyses were performed and their adequacy.

The next level of investigation encompasses the most critical analysis. At the structural level, inputs from the main FALN are incorporated, and detailed strains and stability at fracture origin area are defined. Since most components are designed to gross average strain and stability criteria, the information from this analysis usually provides adequate detail to understand the cause of failure. For the analyst, investigations at this level may involve detailed finite-element modeling—depending on the level of initial analyses.

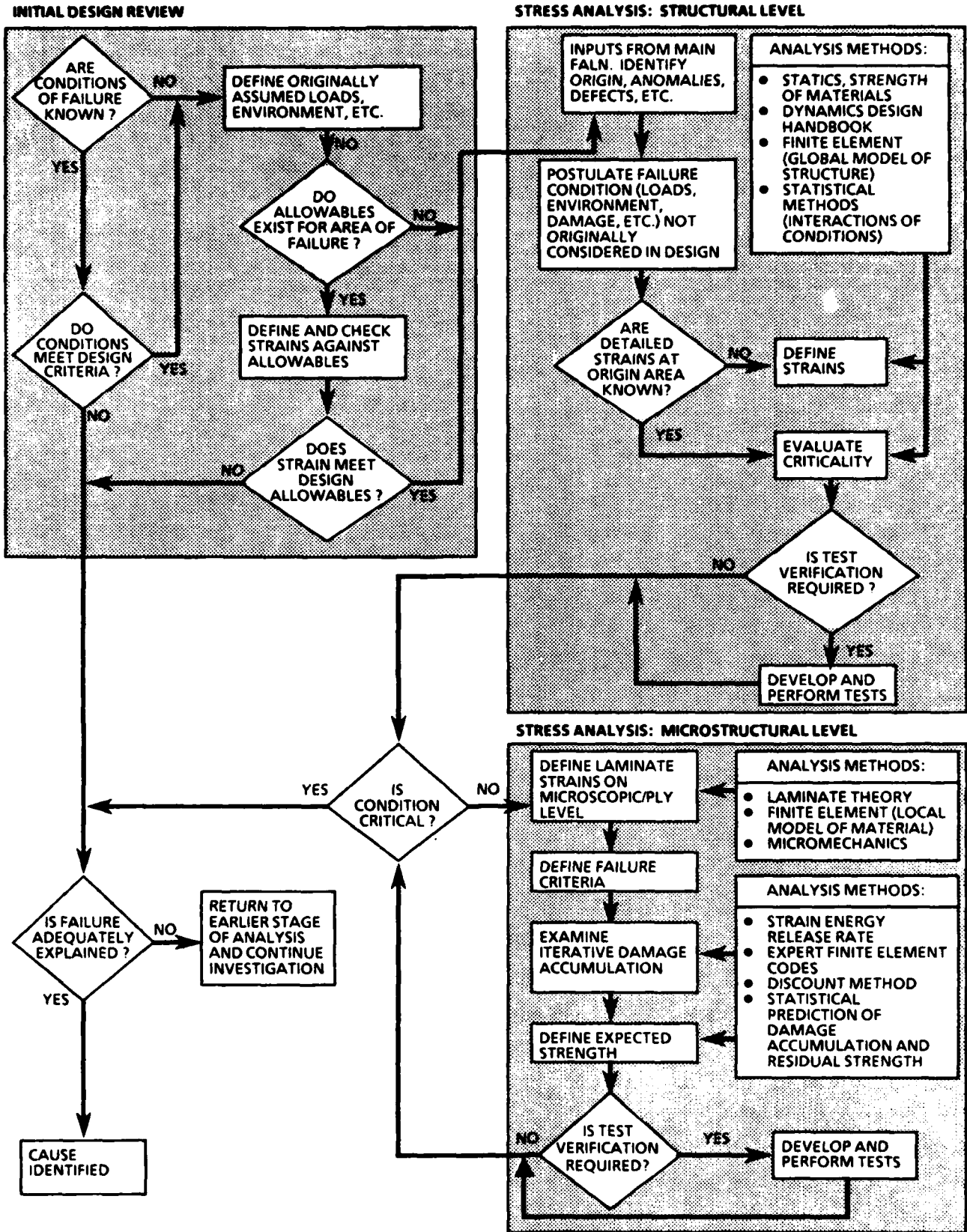


Figure 5-15. Stress Analysis FALN

Investigation of stress at a finer microstructural level is unique to composite materials. Because of the highly anisotropic nature of laminated composites, internal stresses can exist on a ply-by-ply level, and individual ply stresses and failure predictions can be handled with various degrees of detail. As discussed in the literature review (Section 4.4), the simplest level of investigation employs laminate theory combined with relatively simple failure criteria. However, since individual ply failure does not usually constitute catastrophic fracture, additional iterative analyses are required. These analyses can be performed with a variety of computer programs (Figure 5-16); however, using such programs requires a detailed understanding of the methods used and their accuracy.

NAME	FEATURES	USER MANUAL	COMPUTER	APPLICATION
AC-50	Inplane laminate allowable stress	Rockwell TFD-75-1180 Nov. 1975	CDC 6600	Advanced composite analysis
NASTRAN	<ul style="list-style-type: none"> • Finite element analysis • Resize for minimum weight 	NASA SP-222 (01) 1972		Analysis and resizing of complex structures
BOP (Buckling of panels)	Combined compression and shear of stiffened, variable-thickness flat rectangular orthotropic panels on discrete springs	NASA TND-7996 Oct. 1975	CDC 6600	Graphite-epoxy composite panels
SO 5	Point stress analysis of laminated composites for: <ul style="list-style-type: none"> • Inplane loads • Moments • Temperature • Transverse shear 	AFFDL tech memo FBC-74-107 July 1974	CDC 6600	Advanced composite analysis
STAGS	Stress analysis and panel stability evaluations	Lockheed document, Structural Analysis of General Shells, Volume 3, Dec. 1975	CDC 6600	Plotting of buckling mode shapes
VIPASA (Vibration and instability of plate assemblies including shear and anisotropy)	Natural frequencies of loaded structures <ul style="list-style-type: none"> • Critical buckling loads • Thin, flat rectangular plates • Thermal stress 	COSMIC file ISCL Doc. ID 00 17437 Jan. 1973 NASA TMX-73914 May 1976	CDC 6600	Compression loaded stiffened graphite-epoxy panels

Figure 5-16. Computer Analysis Programs

6.0 TASK 2: SPECIMEN FABRICATION AND TESTING

6.1 OBJECTIVE AND STATUS

The objective of Task 2 was to design, fabricate, and test specimens to failure under singular and multiple causative conditions, producing both simple and complex fractures. This task has been divided into two subtasks that reflect the division of specimen types. Under subtask 2A, specimens were designed, fabricated, and tested to create fractures under controlled conditions of crack propagation, direction, mode, origin, and environment. In Task 2B, complex failure specimens were designed, fabricated, and are currently being tested to study the effects of:

- o Contaminants
- o Voids and porosity
- o Mechanical damage
- o In-service damage
- o Structure-specific geometric configuration
- o Multiple load conditions.

During the period covered by this report, all of the testing for subtask 2A has been completed. Specimens for subtask 2B have been fabricated and are currently under test. The following discussion reviews the pedigree of the materials used, specimen fabrication for Tasks 2A and 2B, and the test history of subtask 2A specimens.

6.2 GENERAL APPROACH TO TASK 2

For Task 2, there were two sets of specimens: those failed by a singular cause (subtask 2A) and those failed under multiple conditions (subtask 2B). Figure 6-1 summarizes the test matrix and test geometries used in these subtasks. Subtask 2A singular-failure-mode specimens were designed to create the mode 1 and mode 2 failure circumstances illustrated in Figure 6-2. The specimens fabricated for subtask 2A differ from the typical ultimate-strength test specimens used in some failure analysis investigations in that they are specifically designed to generate well-characterized sites of failure initiation, crack propagation, and failure mode. The effect of varying fiber orientations on failure characteristics was assessed by testing a variety of layups and interfacial ply orientations. For all specimens in this program, the 0-degree plies were oriented along the longitudinal axis. In the case of interfacial failures, five interfacial orientations were examined: 0/0,

SPECIMEN*	PLY LAYUPS, NUMBER OF PLYS, deg				COMMENTS	NUMBER OF SPECIMENS	SPECIMEN CONFIGURATION, cm (in.)
	24/0	24/±45	24/0,45*	24/0,90*			
TASK 2A: SINGULAR-FAILURE-CONDITION SPECIMENS INTERLAMINAR	24/0	24/±45	24/0,45*	24/0,90*	24/90 ^b	5 each	
	24/0	24/±45	24/0,45*	24/0,90*	b	5 each	
	-	32/±45	32/quasi	32/0,90	-	5 each	
TRANSLAMINAR	32/0	32/±45	32/quasi	32/0,90	-	5 each	
	-	-	32/quasi	32/0,90	-	5 each	
	-	-	32/quasi	32/0,90	-	5 each	
HOTWET - 54°C (-65°F) ENVIRON.	24/0	24/±45	24/0,45	24/0,90	24/90	5 each	Same as Task 2A specimens above
	24/0	24/±45	24/0,45	24/0,90	-		
	32/0	32/±45	32/quasi	32/0,90	-		
	32/0	32/±45	32/quasi	32/0,90	-		
	32/0	32/±45	32/quasi	32/0,90	-		
	32/0	32/±45	32/quasi	32/0,90	-		

*DCB: double cantilever beam; ENF: end-notched flexure; MMF: mixed-mode flexure; CLS: cracked lap shear
 Figure 6-1. Singular- and Multiple-Failure-Condition Test Specimen Matrix (Page 1 of 3)

SPECIMEN*	PLY LAYUPS, NUMBER OF PLYS, deg				COMMENTS	NUMBER OF SPECIMENS	SPECIMEN CONFIGURATION, cm (in.)
STRUCTURAL CONDITIONS	TASK 2A: SINGULAR-FAILURE-CONDITION SPECIMENS						
	INTERLAMINAR					5 each	
	• Mode I, II, MMF						
	• Fatigue						
	• Mode I, DCB					10 each	See Task 2A for specimen matrix; Mode I DCBs will be bonded to height-tapered beams
	• Mode II, CLS					10 each	
	TRANSLAMINAR						
	• Laminate flexure					5 each	
	• Fastener					5 each	
	• Filled-hole compression					5 each	
• Filled-hole tension					5 each		
• Buckling studies, FEP insert					5 each		
TASK 2B: MULTIPLE-FAILURE-CONDITION SPECIMENS							
INTERLAMINAR					5 each		
• Drill breakout							
• Frekote							
• Mode I, DCB					5 each	See Task 2A for specimen matrix	
• Mode II, ENF					5 each		
DEFECTS							

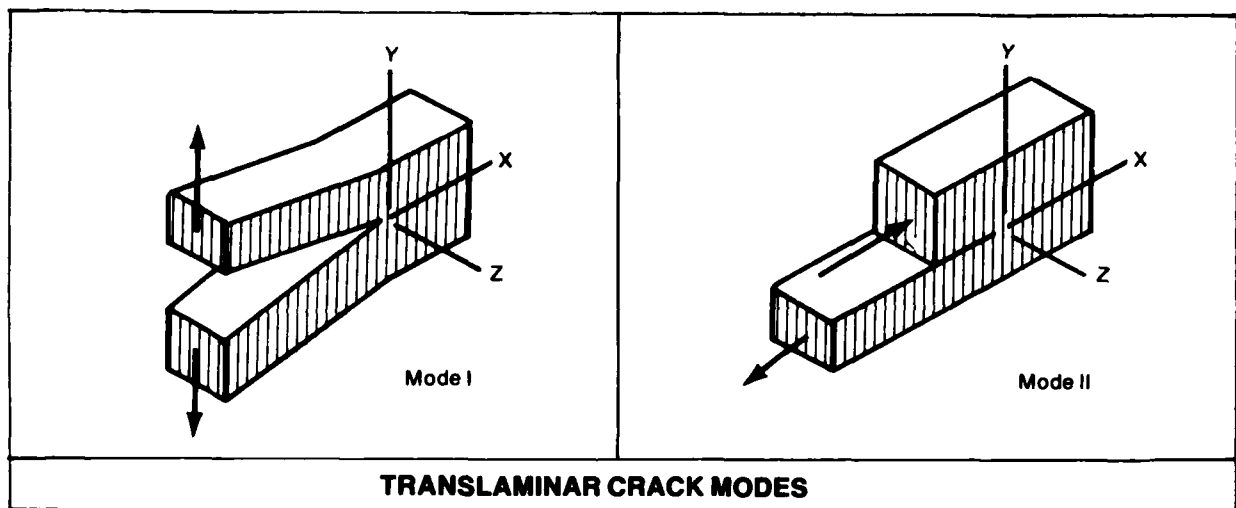
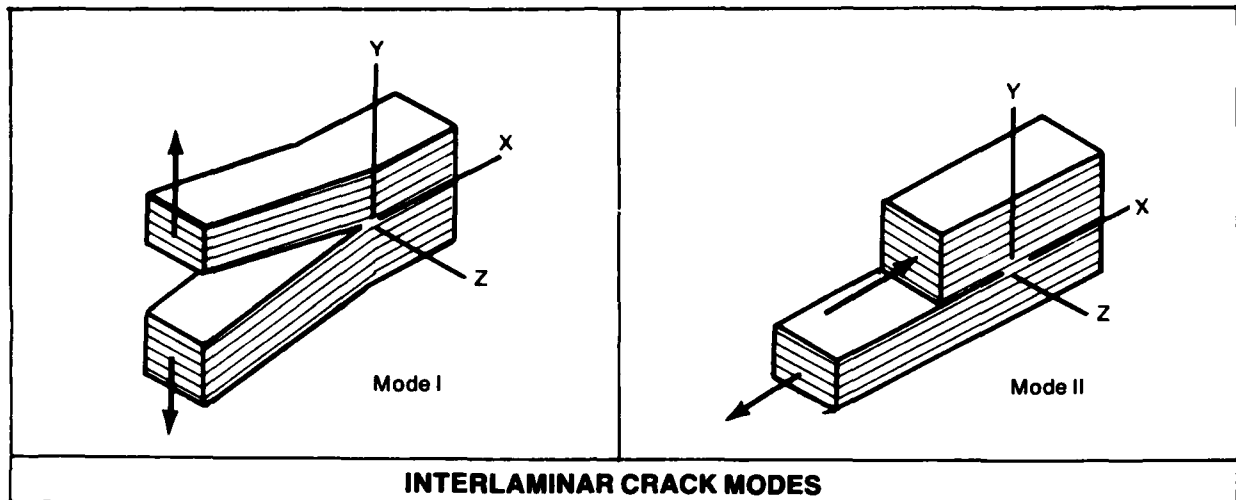
*DCB: double cantilever beam; ENF: end-notched flexure; MMF: mixed-mode flexure; CLS: cracked lap shear

Figure 6-1. Singular- and Multiple-Failure-Condition Test Specimen Matrix (Page 2 of 3)

SPECIMEN*	PLY LAYUPS, NUMBER OF PLYS, deg				COMMENTS	NUMBER OF SPECIMENS	SPECIMEN CONFIGURATION, cm (in.)
TASK 2B: MULTIPLE-FAILURE-CONDITION SPECIMENS <ul style="list-style-type: none"> • Teflon squeegee • Mode I, DCB • Mode II, ENF • Voids • Mode I, DCB • Mode II, CLS • Impact • Compression after impact 	24/0	24/±45	24/0,45	24/0,90	-	5 each	See Task 2A for specimen matrix
	24/0	24/±45	24/0,45	24/0,90	-	5 each	
	24/0	24/±45	24/0,45	24/0,90	-	5 each	
	24/0	24/±45	24/0,45	24/0,90	-	5 each	
	32/quasi	-	-	-	-	5 each	

*DCB: double cantilever beam; ENF: end-notched flexure; MMF: mixed-mode flexure; CLS: cracked lap shear

Figure 6-1. Singular and Multiple-Failure-Condition Test Specimen Matrix (Page 3 of 3)



 Denotes ply orientation

- Mode I Opening or tensile mode, where the crack surfaces move directly apart.
- Mode II Sliding or in-place shear mode, where the crack surfaces slide over one another in a direction perpendicular to the leading edge of the crack.

Figure 6-2. Basic Modes of Loading Involving Different Crack Types and Surface Displacements (Interlaminar and Translaminar)

0/90, 0/45, +45/-45, and 90/90 degrees—indicating the angular orientation between which delamination was produced. For example, 90/90 indicates a condition where interlaminar fracture was produced between two adjacent 90-degree plies. In the latter part of subtask 2A, the effect of environmental conditions on fracture characteristics was assessed by testing at a variety of temperatures, both with and without absorbed moisture.

Testing of subtask 2B specimens is currently underway. These specimens were designed to produce multiple failures while maintaining as much control as possible over the variables being analyzed. Two basic kinds of specimens are being tested: specimens that use the singular-failure-condition configurations employed in subtask 2A, with the addition of fatigue and defect conditions, and specimens designed to create mixed loading and structural detail simulations that are complex in load state and application. By using these types of specimens, a set of failure types and modes will be generated that, when analyzed in Task 3, will provide basic information concerning the effect of these multiple conditions and will aid in verifying and evaluating the diagnostic techniques developed in subtask 3A.

6.3 MATERIAL PEDIGREE

Currently, a fairly wide variety of resin systems and fiber combinations exist for use in graphite-epoxy composite materials. However, due to the high performance demands of military and commercial aircraft structures, the number of available materials is limited to those systems that exhibit good environmental behavior, toughness, and high ultimate strength. These systems are typically 176°C- (350°F-) cured graphite-epoxy systems based on tetraglycidyl diaminodiphenyl methane-diaminodiphenyl sulfone (TGDDM-DDS) epoxy matrices, with or without BF₃-amine catalysis additions. For this program, Hercules 3501-6/AS-4 carbon epoxy tape was selected.

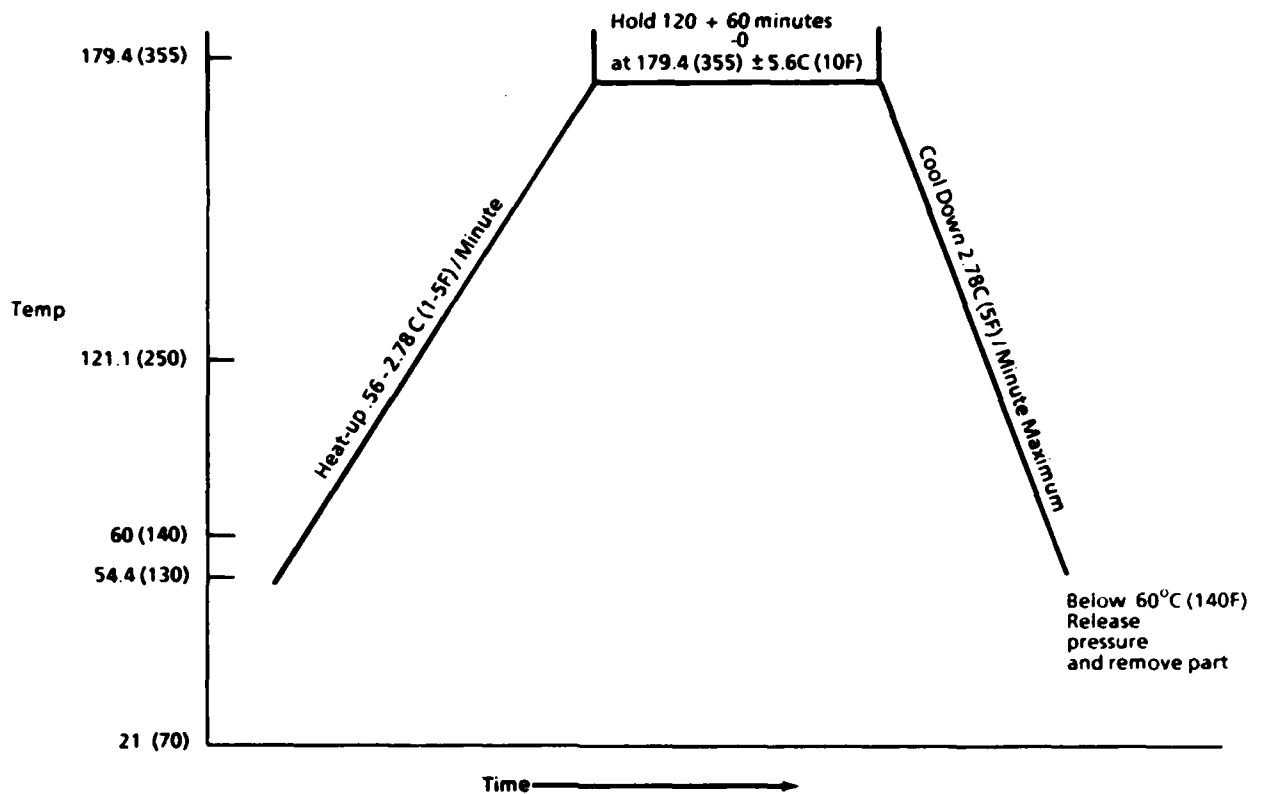
To guarantee the pedigree of the material, the prepreg tape was purchased in accordance with XBMS 8-294, Type 1, Form I, Class 1, Grade 145. The pedigrees of the materials were assessed by the vendor; Figure 6-3 illustrates the vendor-supplied certification records for the material.

6.4 SPECIMEN FABRICATION

Specimens for subtask 2A and 2B were fabricated per Boeing process specification BAC 5562 using the layups illustrated in Figure 6-5. In accordance with this specification, panels were cured at 586 Pa (85 psi) and 179°C (355°F) for 120-180 minutes, using a no-bleed vacuum bag system. The cure cycle used is illustrated in Figure 6-4. Following cure, some interlaminar fracture panels were rejected due to warpage and splitting adjacent to the fluorinated ethylene propylene (FEP) crack starter insert. Problems with these panels were corrected and replacement panels fabricated. Analysis of these panels

FIBER AND RESIN PROPERTIES		BMS 9-8 SPEC REQUIRED		LOT AVERAGE		
Filament tensile strength, GPa* (ksi) Filament tensile modulus, GPa* (ksi) Filament elongation, % Fiber yield, m/kg (yd/lb) Fiber density, g/cm ³ (lb/in. ³) Fiber twists, twists/cm(in) Resin density, kg/cm ³ (lb/in. ³)		2 654 (385) minimum 270.6 (32) to 241.3 (35) 1.1 minimum 11.53 (550) to 12.79 (610) 1.73 (0.062) to 1.81 (0.0653) 2.03 (0.8) maximum Report		3 634 (527) 227.5 (33) 1.5 12.01 (573) 1.78 0.0508 (0.02) 0.1456 (0.0457)		
*Data normalized to 100% fiber volume						
LAMINATE MECHANICAL PROPERTIES		SPEC REQUIRED (MIN. AVERAGE)	PANEL NO.	AVERAGE	INDIVIDUAL	
0-deg tensile strength, 21°C (70°F), GPa** (ksi)		2 654 (185)	29942	2 031 (292)	2 07 (301), 1.70 (246), 2.13 (309), 2.02 (293), 2.03 (295)	
0-deg tensile modulus, 21°C (70°F), GPa** (msi)		124.11 (18.0)	29942	126.18 (18.3)	126.87 (18.4), 126.87 (18.4), 126.18 (18.3), 123.42 (17.9), 126.18 (18.3)	
0-deg elongation, %		0.95	29942	1.5	1.5, 1.4, 1.6, 1.6, 1.5	
0-deg compression interlaminar shear, 21°C (70°F), GPa** (ksi)		Report	29943	0.89 (12.9)	0.91 (13.2), 0.883 (12.8), 0.91 (13.2), 0.89 (12.9), 0.84 (12.2)	
0-deg compression interlaminar shear, 82°C (180°F), GPa** (ksi)		Report	29943	0.80 (11.6)	0.82 (11.9), 0.80 (11.6), 0.81 (11.8), 0.80 (11.6), 0.76 (11.1)	
0-deg compression strength, 21°C (70°F), GPa** (ksi)		Report	29942	1.59 (230)	1.57 (228), 1.59 (230), 1.52 (221), 1.61 (233), 1.65 (240)	
0-deg compression strength, 93°C (200°F), GPa** (ksi)		1 069 (155)	29942	1.62 (235)	1.73 (251), 1.61 (234), 1.52 (220), 1.61 (234), 1.63 (236)	
** Data normalized to 0.01435 cm (0.00565 in.) ply thickness						
PANEL PHYSICAL PROPERTIES		SPEC REQUIRED	AVERAGE		INDIVIDUAL	
Spool no. 3, panel no. 29942		Report	1.56 (0.0563)		1.57 (0.0567), 1.56 (0.0563), 1.56 (0.0563), 1.57 (0.0567)	
Density, g/cm ³ (lb/in. ³)		Report	58		58, 58, 58, 58, 58	
Fiber volume, %		0.0132 (0.0052) to 0.0155 (0.0061)	0.0147 (0.0057)		N/A	
Ply thickness, cm (inch)		Report	1.56 (0.0563)		1.55 (0.056), 1.56 (0.0563), 1.55 (0.056), 1.56 (0.0563), 1.56 (0.0563)	
Spool no. 3, panel no. 29943		Report	57		57, 57, 57, 57, 57	
Density, g/cm ³ (lb/in. ³)		Report	0.0147 (0.0058)		N/A	
Fiber volume, %		0.0132 (0.0052) to 0.0155 (0.0061)				
Ply thickness, cm (inch)						
INDIVIDUAL SPOOL PHYSICAL PROPERTIES						
VOLATILES CONTENT, %		RESIN CONTENT, %		FIBER AREAL WEIGHT, g/m ² (lb/yd ²)		
SPOOL NO.	SPEC REQUIREMENT		ACTUALS		ACTUALS	
	AVG.	INDIV.	AVG.	INDIV.	AVERAGE	INDIVIDUAL
1	1.0 max	2.0 max	0.9	1.0, 1.0, 0.6	140 (0.258) to 150 (0.276)	144 (0.263), 145 (0.267), 144 (0.265), 144 (0.265), 146 (0.269), 144 (0.265)
2			0.8	0.8, 0.9, 0.8	Report	144 (0.265), 145 (0.267), 144 (0.265), 144 (0.265), 146 (0.269), 144 (0.265)

Figure 6-3. Vendor Certification Records



Apply 55.88 cm (22 inches) Hg vacuum minimum to vacuum bag.

Apply $0.586 \begin{smallmatrix} +0.103 \\ -0 \end{smallmatrix}$ MPa ($85 \begin{smallmatrix} +15 \\ -0 \end{smallmatrix}$ psig) pressure.

Pressure under vacuum bag is not to exceed $0 \begin{smallmatrix} +.035 \\ -.007 \end{smallmatrix}$ MPa ($0 \begin{smallmatrix} +.5 \\ -.1 \end{smallmatrix}$ psig).

- 1/ Time in cure is based on lagging thermocouple.
- 2/ Vent vacuum bag to atmosphere when pressure reaches 0.134 MPa (20 psig). Keep vented until end of cure.
- 3/ Heat-up and cool-down rates for all part thermocouples shall be in specified range when measured in any 15 minute interval. Heat-up rate requirements apply only from 54.4C (130F) to 173.9C (345F).
- 4/ From 165.6C (330F) to 173.9C (345F), the minimum heat-up rate is 0.167C (0.3F)

Figure 6-4. Laminate/Sandwich Cure cycle

revealed that the original layup configurations were asymmetric on either side of the FEP insert and intended fracture plane. As a result, panel edge warpage occurred over the FEP insert areas and produced delamination growth into the panel and localized transverse splitting (Figure 6-6). By refabricating new panels with a more symmetric layup—balanced on both sides of centerline as well as within each half—the undesirable features were eliminated. More specific details regarding the changes for each panel are illustrated in Figure 6-5.

ORIGINAL LAYUP SEQUENCE, deg	MODIFIED LAYUP SEQUENCE, deg	INTENDED FRACTURE PLANE, deg	COMMENTS
(0) ₁₂ FEP insert (0) ₁₂	Not modified	Interlaminar between 0 plies	<ul style="list-style-type: none"> Original layup balanced on both sides of FEP insert
(+45/-45) ₆ FEP insert (+45/-45) ₆	Not modified	Interlaminar between +45 and -45 plies	<ul style="list-style-type: none"> Original layup balanced on both sides of FEP insert
(0) ₁₁ (+45/-45) FEP insert (0) ₁₁	(-45/0/+45) (0/90/0) ₂ (+45/0/-45) FEP insert (0) (-45/0/+45) (0/90/0) ₂ (+45/0/-45)	Interlaminar between 0 and 45 plies	<ul style="list-style-type: none"> Added 45-deg plies to top and bottom surfaces to balance 45-deg plies at the center of panel Increased number of 45/0-deg sets at center of panel to assure maintenance of 45/0-deg fracture plane during crack propagation Added 90-deg plies to achieve a more isotropic layup
(0) ₁₁ (90) ₂ FEP insert (0) ₁₁	(0/90) ₆ FEP insert (0) (90/0) ₆	Interlaminar between 0 and 90 plies	<ul style="list-style-type: none"> Added 90-deg plies to top and bottom surfaces to balance 90-deg plies at the center of panel Created a totally 0/90-deg layup to maintain a 0/90-deg fracture plane during crack propagation
(0) ₁₁ (90) FEP insert (90) (0) ₁₁	(90/0) ₆ (90) FEP insert (90) (0/90) ₆	Interlaminar between 0 and 90 plies	<ul style="list-style-type: none"> Added 90-deg plies to top and bottom surfaces to balance 90-deg plies at the center of panel
(-45/0/+45/90) ₈	Not modified	Translaminar and combinations	<ul style="list-style-type: none"> Balanced layup
(0) ₃₂	Not modified	Translaminar and combinations	<ul style="list-style-type: none"> Balanced layup
(+45/-45)	Not modified	Translaminar and combinations	<ul style="list-style-type: none"> Balanced layup
(0/90) _{8s}	Not modified	Translaminar and combinations	<ul style="list-style-type: none"> Balanced layup

Figure 6-5. Panel Layup Stacking Order

Through-transmission ultrasonic (TTU) techniques were used to inspect each specimen for defects resulting from panel fabrication or subsequent machining. Those specimens with areas greater than approximately 0.322 square cm (0.05 square inch) that exhibited ultrasonic indications 3 levels higher (18 dB) than the baseline were rejected and scrapped. Over 97% of the fabricated specimens were found to be acceptable. Figure 6-7 illustrates a typical TTU scan and reject-specimen condition.

6.5 ENVIRONMENTAL MOISTURE PRECONDITIONING

Moisture preconditioning of subtask 2A specimens consisted of a 71°C (160°F), 100% relative humidity environment with a goal of 1.0% maximum moisture content by weight.



Figure 6-6. Panel Warpage, Splitting, and Delamination Over FEP Insert Areas; Panel #3, Original Layup Sequence



This specimen was rejected and cross-sectioned at location A-A (Figure 3.2.1-4) for evaluation of defect condition. The specimen baseline output symbol is 1. For this program, specimens having areas greater than 322 cm² (0.05 inch²), and exhibiting ultrasonic attenuation indications three levels higher than specimen baseline were rejected. One numerical level change is equal to a six dB change in sound transmittance.

Figure 6-7. Typical TTU Plan View of Specimen No. 7-2

In addition to ultrasonic inspection, representative samples from each of the panels were optically examined in cross-section, and subjected to thermomechanical analysis (TMA). Optical microscopy of representative cross-sections confirmed that the ply stacking sequence for all but one of the panels was correct. For this one panel, a +45-degree ply was inadvertently laid up with a -45-degree orientation. However, this error was considered inconsequential given the strictly fractographic aims of Task 3. Additional microscopy evaluated defect conditions identified by TTU on rejected specimens. The TTU-identified defects corresponded with matrix voids, as shown in Figure 6-8. The degree of panel cure was evaluated by determining the glass transition temperature of each panel by thermomechanical analysis (TMA) in the flexure mode; Figure 6-9 documents the glass transition temperature values measured for each panel. All measured values were found to be typical of full cure and were judged acceptable.

This maximum moisture content was selected as representative of typical values that can be anticipated for long term in-service exposure. Figure 6-10 illustrates moisture gain data gathered by NASA on ground-rack-exposed samples at various locations around the world, indicating a stable equilibrium value of about 1% for 3501 epoxy systems.

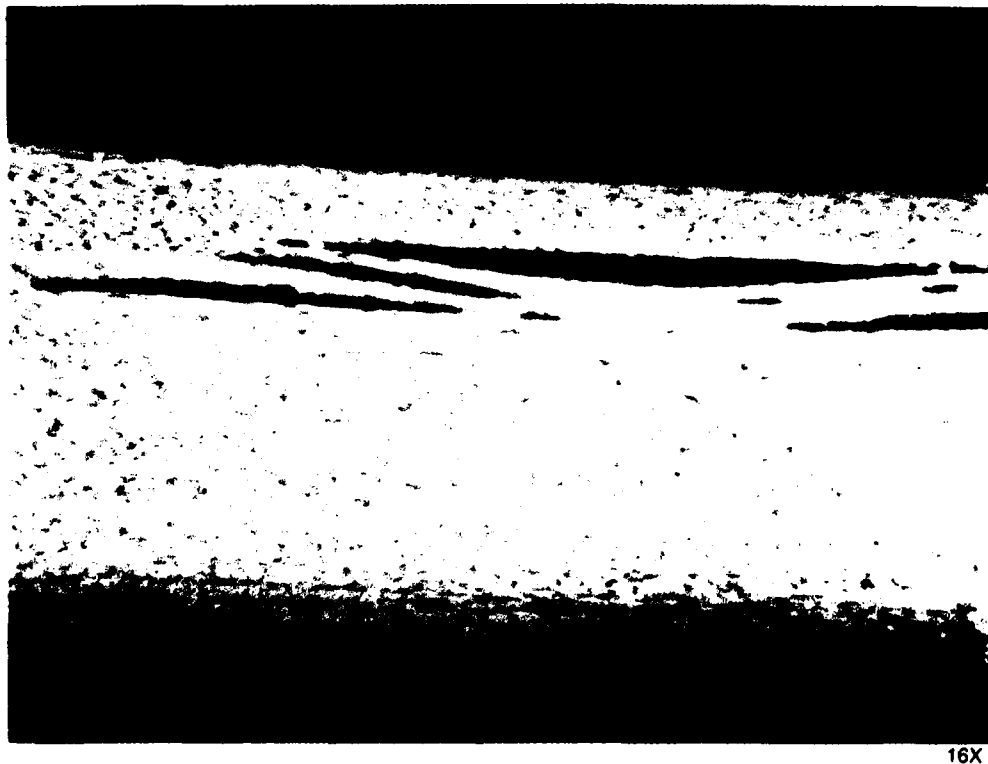


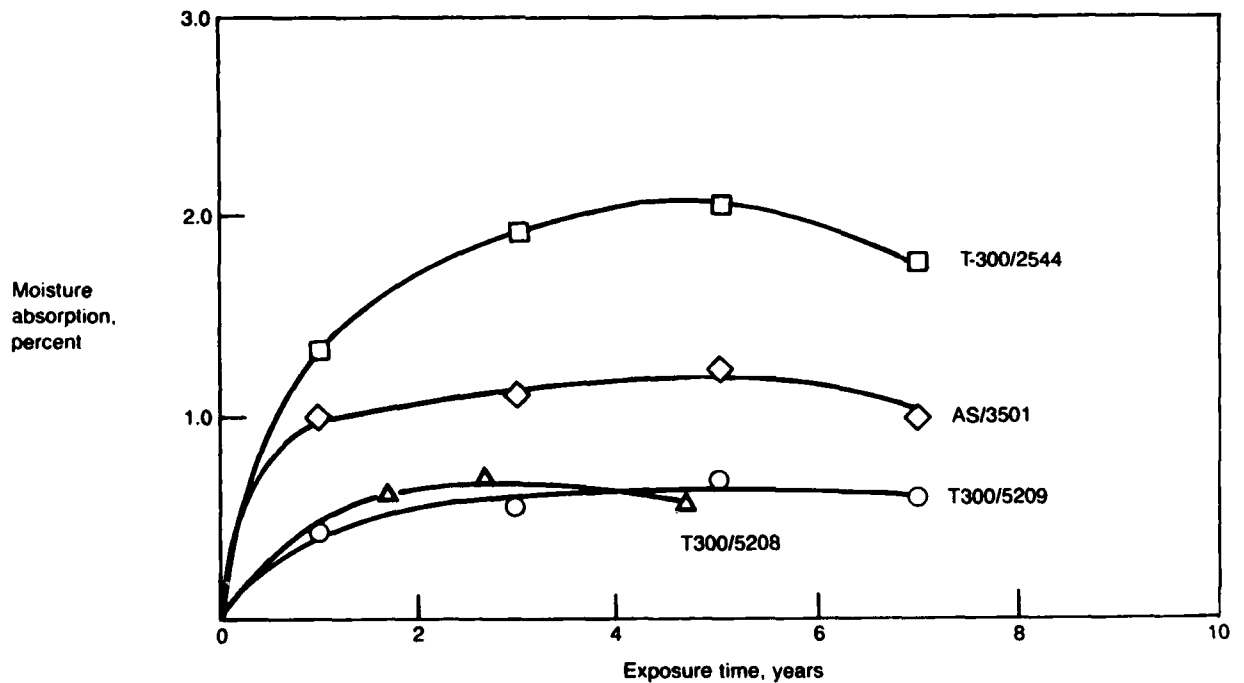
Figure 6-8. Cross section A-A (Figure 6-7) of TTU Identified Defect, Showing Localized Voids in Laminate

PANEL NUMBER	T _g , °C (°F)	AVG T _g , °C (°F)	PANEL NUMBER	T _g , °C (°F)	AVG T _g , °C (°F)
1	196 (384.8)	197.7 (387.9)	6	198 (388.4)	199.0 (390.2)
	197 (386.6)			198 (388.4)	
	200 (392)			201 (393.8)	
2	195 (383)	195.7 (384.3)	7	196 (384.8)	197.3 (387.1)
	193 (379.4)			197 (386.6)	
	199 (390.2)			199 (390.2)	
3	198 (388.4)	196.3 (385.3)	8	202 (395.6)	200.3 (392.5)
	194 (381.2)			202 (395.6)	
	197 (386.6)			197 (386.6)	
4	184 (363.2)	191.7 (377.1)	9	197 (386.6)	198.6 (389.5)
	194 (381.2)			202 (395.6)	
	197 (386.6)			197 (386.6)	
5	193 (379.4)	194.0 (381.2)			
	195 (383)				
	194 (381.2)				

• Test equipment: Perkin-Elmer model TMS1

• Test parameters: Flexure probe; 10 gram (0.22 lb) weight; heat-up rate 20°C (68°F)/min

Figure 6-9. Glass Transition Temperature Values, Thermomechanical Analysis-Flexure Mode



Note: Data from NASA document No. CP 2321.

Figure 6-10. NASA Moisture Absorption Data of Composite Materials Following Worldwide Outdoor Exposure

Exposure at 71°C (160°F), 100% relative humidity, was selected to provide an accelerated rate of moisture gain without imposing large moisture gradients within the sample. Figure 6-11 presents typical moisture weight gain measured on subtask 2A specimens.

6.6 INTERLAMINAR MODE I (TENSION) TESTING

Mode I interlaminar tension fractures were produced using a double cantilever beam specimen configuration. This specimen geometry has been extensively used to assess the mode I interlaminar tension fracture toughness of composite materials. In this test, interlaminar tension conditions are generated at the specimen mid-plane by deflecting two beam halves, formed at one end of the specimen by an FEP insert, in opposite directions. Special fixtures were developed for this specimen to allow free-pin rotation at the beam end and mechanical grip attachment. Bonded grips, which are normally used, were rejected because of inadequate strength in elevated temperatures. The specimen grip fixtures, which were of a clamp-type configuration, were wedged into the crack tip formed by the FEP insert. Each clamp thickness was 0.127cm (0.05 in.), resulting in a total 0.254-cm (0.10-inch) mouth opening displacement at the beam end prior to

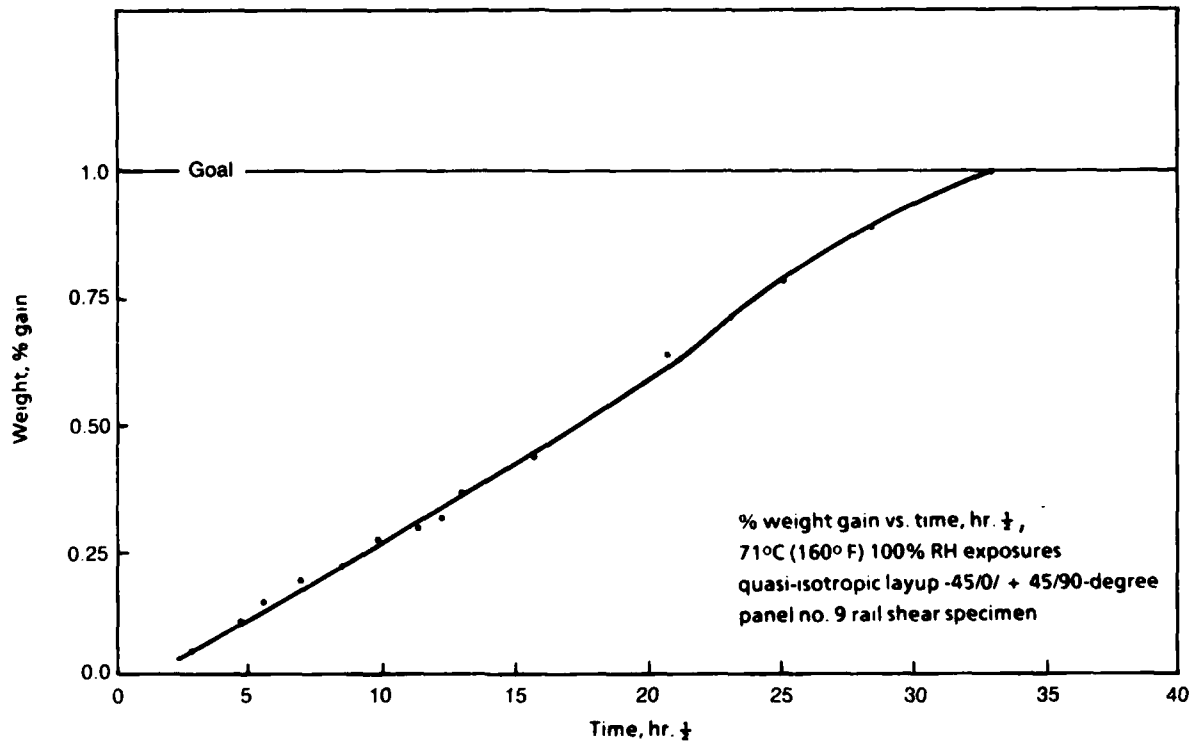


Figure 6-11. Environmental Conditioning

mechanical test. Any precrack observed during clamping was marked on the specimen edge. Specimens were loaded under deflection control on an MTS servo-hydraulic load frame with the rate of cross-head deflection adjusted during the test to produce a relatively constant rate of crack extension. In general, crack extension occurred in a progressive manner, with observed crack growth rates of about 1.27 to 2.54 cm (0.5 to 1.0 in.)/minute. Cross-head deflection rates ranged from 0.25 to 0.51 cm (0.1 to 0.2 in.)/minute. Figure 6-12 illustrates a specimen during test.

Generating singular failure mode I fractures between various cross-ply orientations was successfully completed using the double cantilever beam specimen geometry. Crack progression occurred in a gradual manner, as indicated above, allowing visual inspection of the direction of crack growth and verification of specimen behavior. In some instances, out-of-plane crack divergence was noted during both the test and subsequent subtask 3A analyses. In some cases, this crack divergence resulted in local regions of fracture other than along the intended fracture interface. This behavior is most likely attributed to the lower interfacial and intra-ply fracture toughness of lamina adjacent to the intended fracture plane. Such divergence was generally accompanied by instantaneous crack

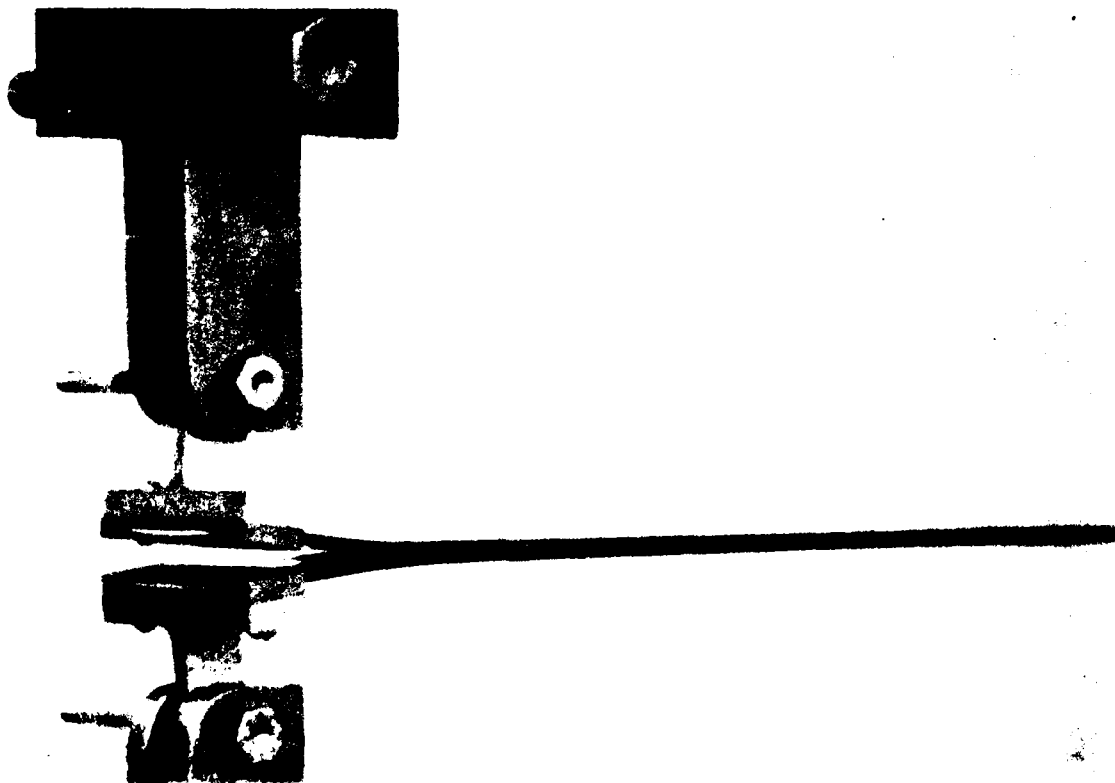


Figure 6-12. DCB Test Fixture During Trial Testing

extension and a sharp drop in applied load. Extensive divergence occurred for the 0/90-degree interface condition at 82°C (180°F) dry and 132°C (270°F) dry.

For these two conditions, such divergence precluded Task 3 examinations because the desired fracture plane was not produced. Divergence for all other samples, however, was limited to extremely localized zones such that a significant portion of fracture occurred between the interfaces desired.

6.7 INTERLAMINAR MODE 2 (SHEAR) TESTING

Conditions of interlaminar mode 2 shear were produced using a modified end-notch flexural specimen geometry. Trial tests of the three-point load geometry that was initially proposed proved unsuccessful; these attempts revealed that the compliance of the 24-ply specimens was too great, allowing extensive flexure with tensile fracture of the lower surface fibers occurring prior to any midplane delamination. Different span lengths were evaluated and found to be unacceptable. Tests were subsequently carried out using a cantilever geometry fixture available at Boeing. As schematically illustrated in Figure 6-13, conditions of mode 2 shear are created in this specimen by deflecting the cracked end of a cantilevered beam. The uncracked end cannot rotate or move vertically, but may move horizontally. Such movement prevents the introduction of extraneous (vertical)

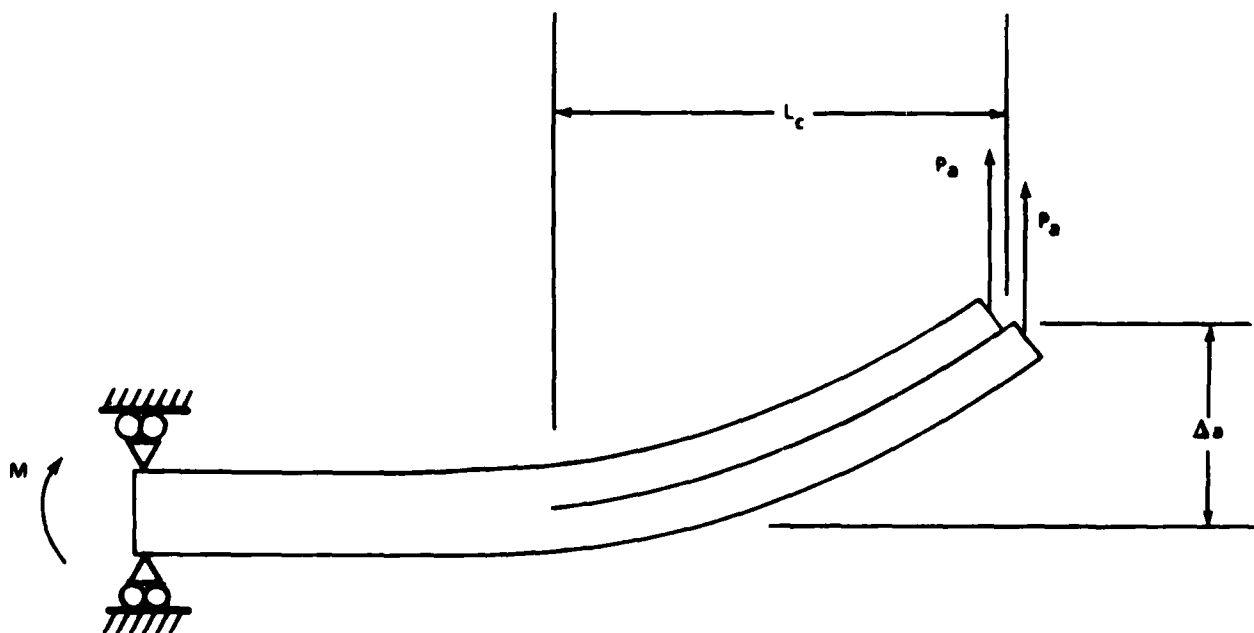
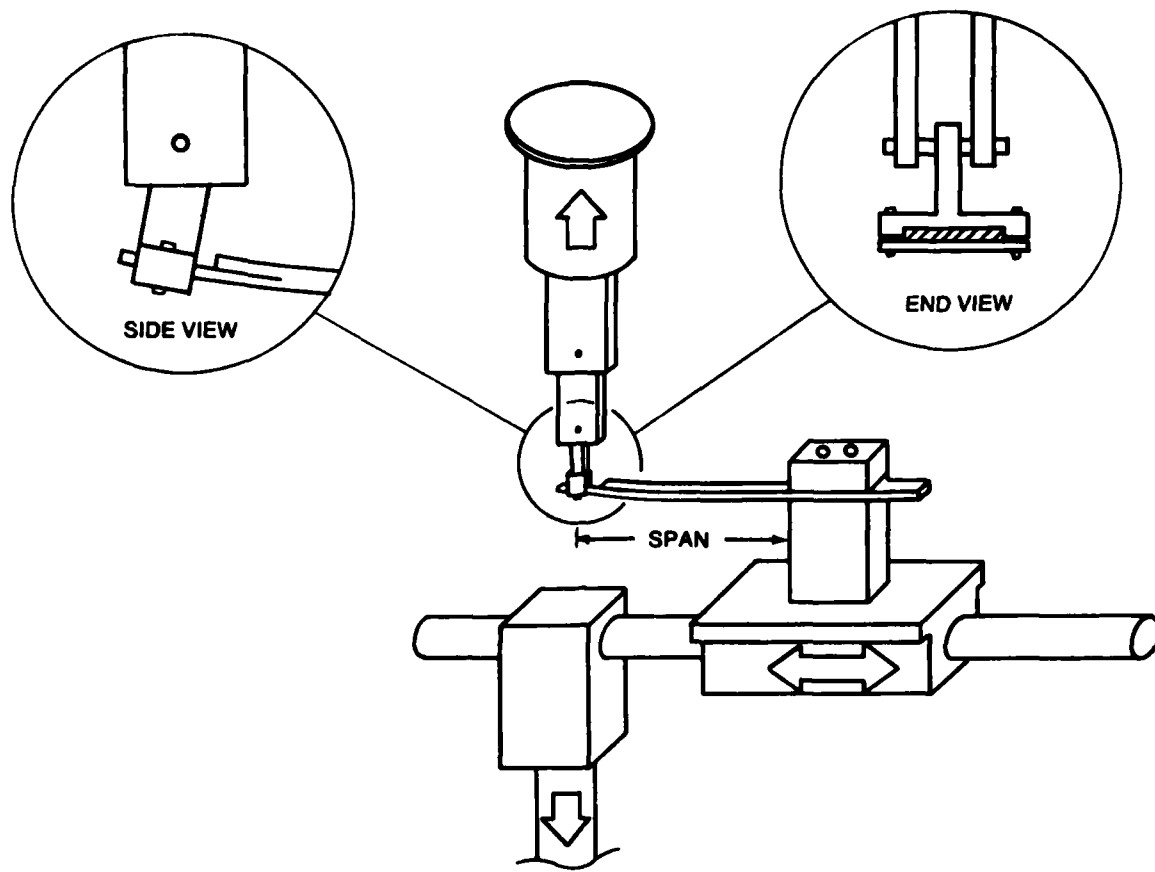


Figure 6-13. 100% Mode 2 Interlaminar Shear - Asymmetric Cantilever Beam Geometry

loads as the beam shortens under deflection. With this geometry the top crack surface is loaded in pure tension, while the bottom surface is in pure compression resulting in pure shear at the crack tip. This fixture originally used a knife edge to apply cantilever loads to the specimen, but the knife edge allowed specimen slippage when tested in combination with the more compliant specimen layups. Slippage was eliminated by utilizing the DCB-developed attachment grip in combination with reduced span lengths.

In the end-notch flexure geometry used, two beam halves were formed at one end of the specimen by an implanted FEP insert. In this case, conditions of interlaminar shear were imposed at the specimen midplane by cantilever deflection of both beam halves in the same direction. Figure 6-14 schematically illustrates the test configuration as modified for the current program. This test configuration was previously used for assessing interlaminar shear (mode 2) fracture toughness in composite materials. The magnitude of the shear produced at the notch (or crack tip) depended on both the extent of deflection imposed and the percentage of the span length penetrated by the notch (crack length). During trial tests, it was discovered that at least a two-to-one span-length-to-crack-length ratio was required to initiate crack extension without excessive beam bending. As a result, each specimen was tested using step-increased span lengths of 5.1, 10.2, and 15.2 cm (2, 4, and 6 in.). An additional step at 7.6 cm (3 in.) was included for the +45/-45-degree layup configuration to further minimize excessive beam deflection for this more compliant layup. Testing was performed using deflection-controlled loading with the rate of cross-head travel modified between 1.0 and 2.0 cm (0.4 and 0.8 in.)/minute to produce an overall test time of approximately 15 minutes per specimen. Figure 6-15 illustrates the modified fixture during trial testing.

Crack propagation during testing typically occurred by rapid extension of the crack along the specimen midplane. In general, such rapid growth extended over 60% of the test span during the first crack extension, and then was followed by several increments of slower, more observable growth--particularly at longer span lengths. Rapid crack growth precluded the full monitoring of the direction of cracking. However, during those periods of slow, stable growth, crack extension was observed in a direction away from the FEP crack starter region, and toward the cantilever beam support fixture, as expected. Fracture occurred between the intended fracture interfaces with crack divergence observed (to a limited extent) for some samples.



ENF TEST SPANS				
LAYUP, deg	SPAN LENGTHS, cm (In)			
0,0	5.08 (2)	10.16 (4)	15.24 (6)	
+45,-45	5.08 (2)	7.62 (3)	10.16 (4)	15.24 (6)
0,45	5.08 (2)	10.16 (4)	15.24 (6)	
0,90	5.08 (2)	10.16 (4)	15.24 (6)	
90,90	5.08 (2)	10.16 (4)	15.24 (6)	

Figure 6-14. Interlaminar Mode 2 (Shear) Test Configuration

Following test, permanent post-fracture deformation was evident for the +45/-45-degree specimens tested at 132°C (270°F) dry and wet. Most of this deformation consisted of permanent beam deflection along the 0-degree axis. Coincident with the deflection, some localized deformation was also evident along the specimen edges. This deformation consisted of short-transverse warpage of each beam halfway from the plane of fracture. This warpage probably constitutes a source of mixed-mode loading along the specimen

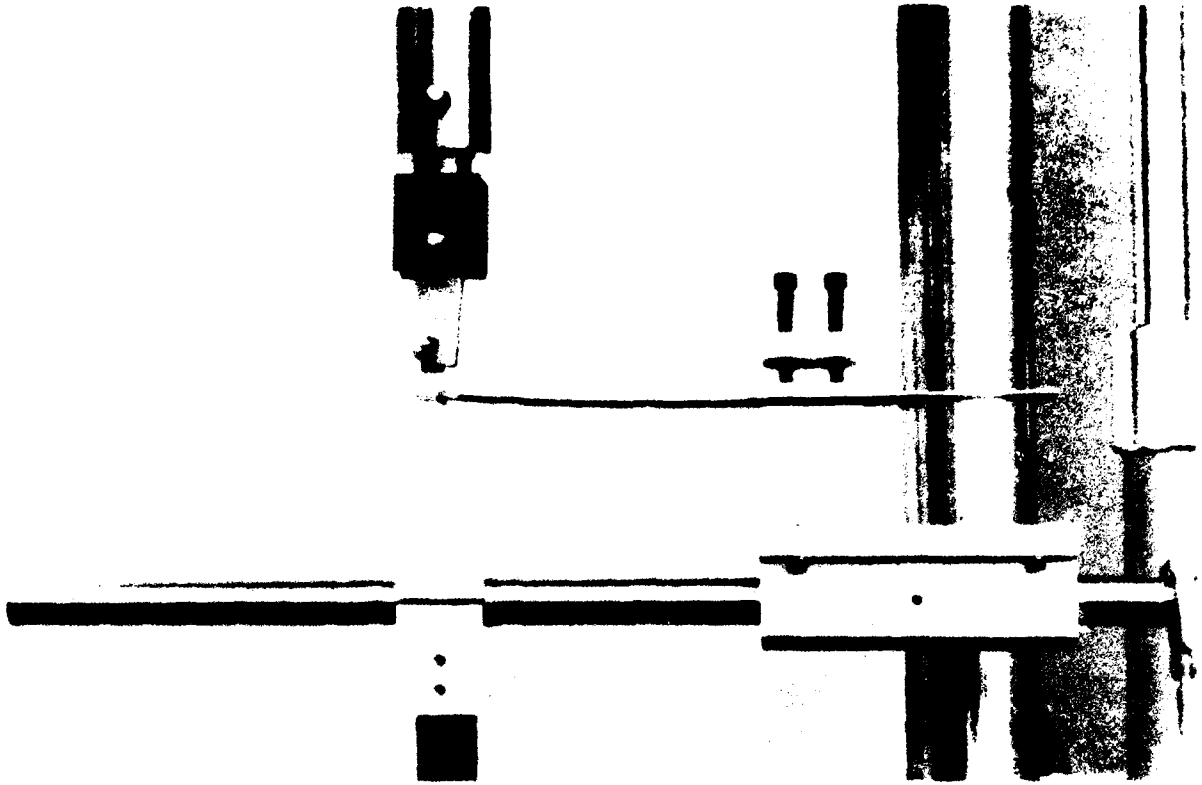


Figure 6-15. ENF Test Fixture During Trial Testing

edges. It represents an undesirable condition for generating fractures with known singular-failure conditions. As a result, analyses of these specimens were confined to the specimen center, and interpreted with some caution.

6.8 MODE I TRANSLAMINAR TENSION AND COMPRESSION TESTING

As noted in Figure 6-1, conditions of controlled translaminar tension and compression were generated using a simple, notched-bend-bar specimen geometry. The configuration of these samples is relatively similar to metals fracture toughness bend-bar specimens such as the Charpy impact specimen. Similar to the interlaminar specimens discussed earlier, the chief advantage of this type of specimen configuration is that it provides controlled crack initiation and growth.

With respect to the originally proposed test configurations, some modifications were found necessary to provide optimal specimen control. Initial testing of the originally proposed 2.54- by 12.70-cm (1- by 5-in.) specimen with reinforced side plates revealed poor control over crack initiation and the direction of growth for all but the 0/90 degree

ply orientations. Subsequent trial tests of modified samples revealed that a 1.27- by 6.35-cm (0.5- by 2.5-in.) specimen notched to about 60% to 75% of the specimen depth worked well for both tension and compression testing. Figure 6-16 illustrates the tensile test configuration developed. In this configuration, conditions of translamellar tension were produced by four-point beam loading a chevron-notched specimen with the notch located transverse to the beam's lower tensile surface. Conditions of translamellar compression were generated using the same basic specimen geometry employed for tension testing, with the central notch located transverse to the beam's upper compressive surface. To prevent contact of the notch surfaces under compression, an additional V-notch (as illustrated in Figure 6-17) was necessary. These specimens were tested on a Tinius Olsen screw drive instrument under displacement driven control.

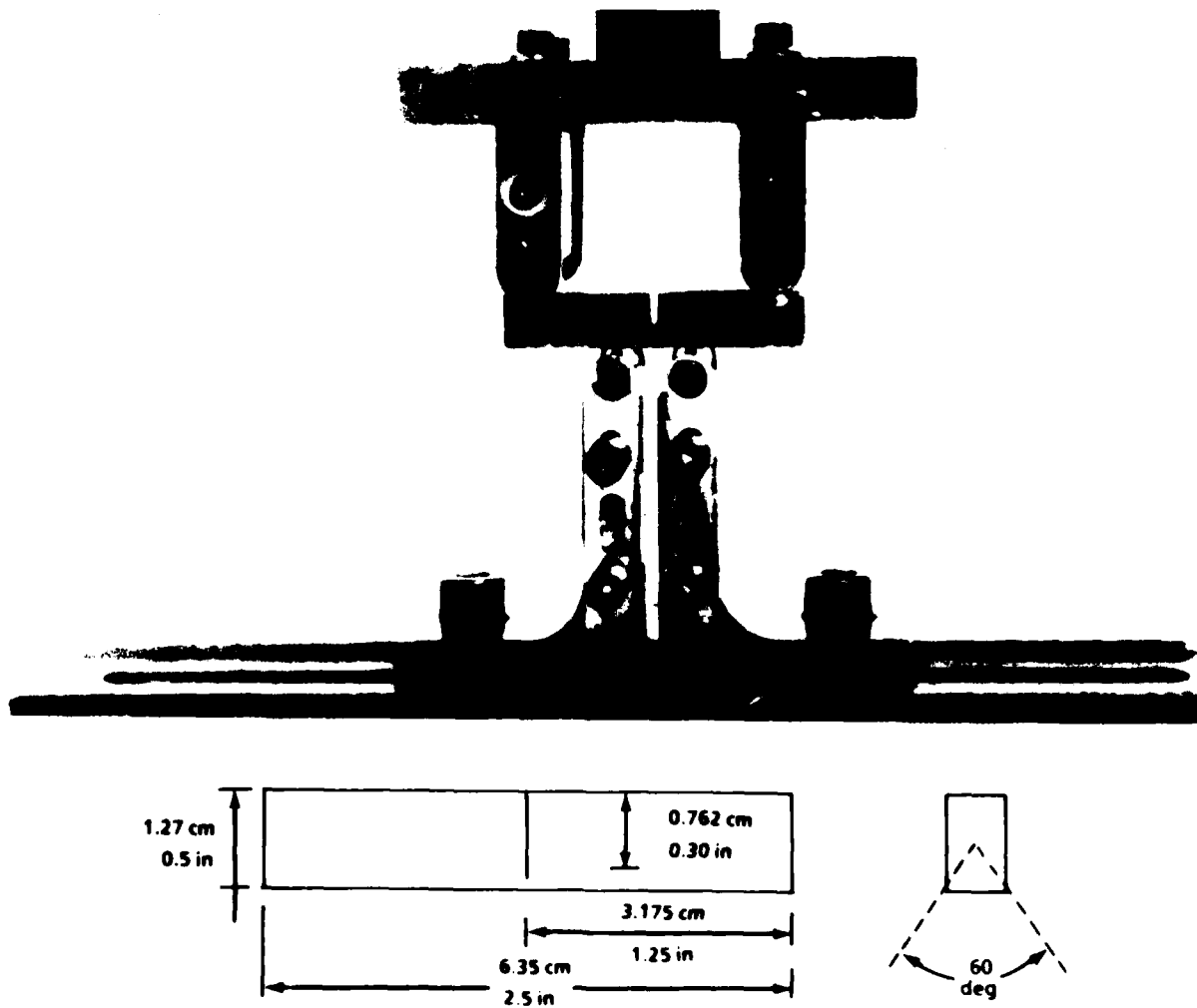


Figure 6-16. Translamellar Tension Specimen in Test

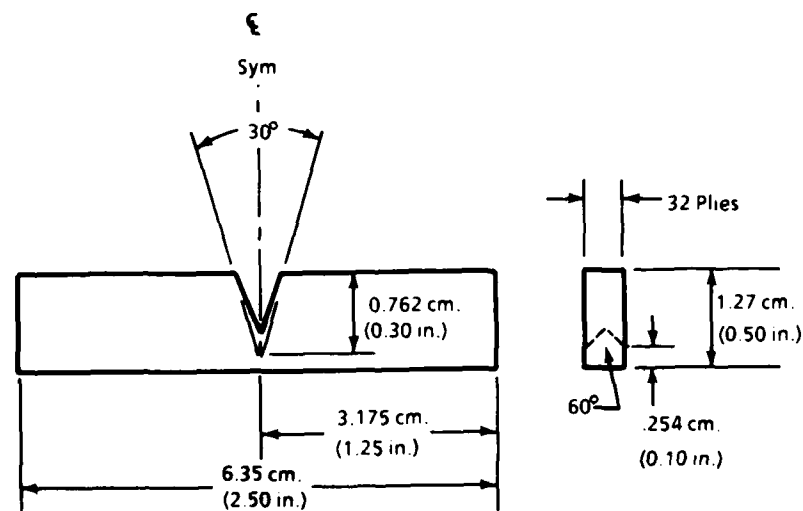
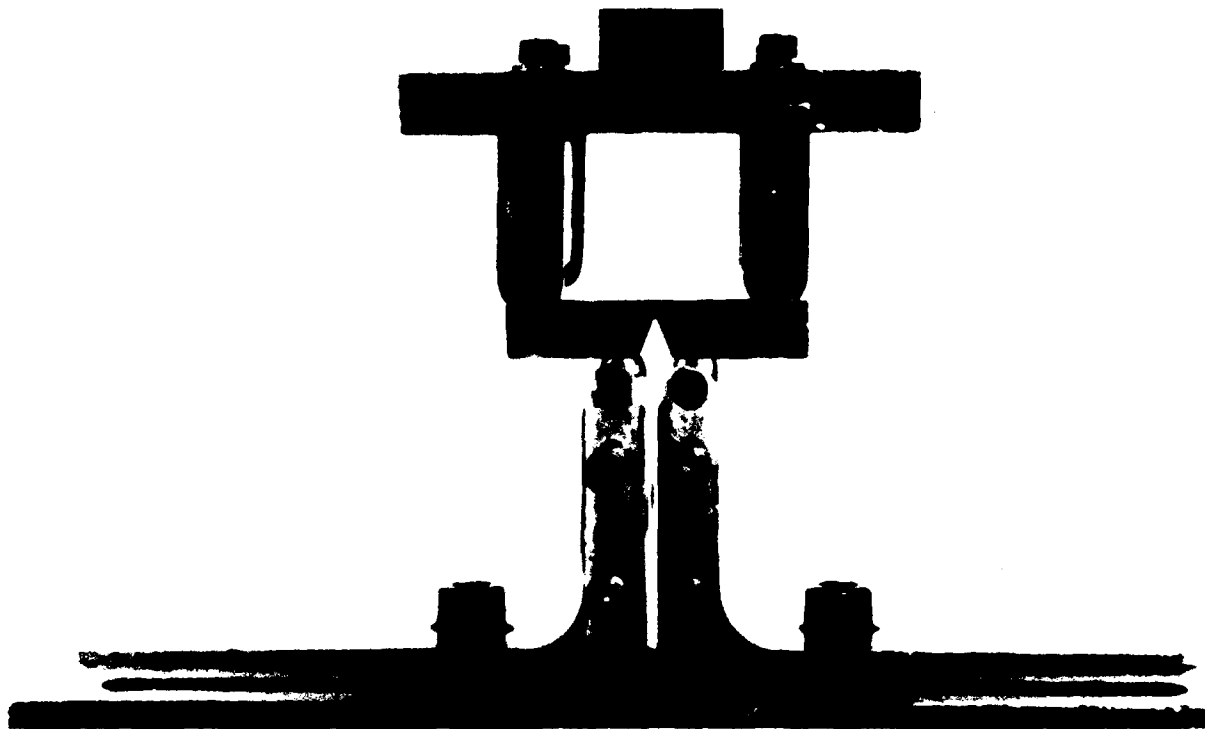


Figure 6-17. Translaminar Compression Specimen in Test

While testing worked well for most layup orientations, some problems were encountered with tensile loading of all unidirectional layups. Unidirectional layups produced crack initiation on multiple planes throughout the specimen, resulting in numerous longitudinal splits or delaminations. Further testing of alternate configurations failed to produce a configuration capable of generating a consistent through-translaminar tension fracture for this layup. Fracture of the 0/90-degree layup, however, was judged to provide the same basic information regarding the fracture characteristics of 0-degree plies. As a result, tension tests of all 0-degree ply layups were discontinued. For the remaining layups,

crack initiation and growth was visually observed to begin at the chevron notch and proceed through the specimen depth, resulting in the fracture conditions desired. Within the time frame covered by this report, testing has been completed for each layup, at the environmental and absorbed-moisture conditions indicated in Figure 6-1.

6.9 MODE 2 TRANSLAMINAR SHEAR TESTING

Translaminar shear was produced using a modified rail-shear specimen (Figure 6-18). As with the other subtask 2A specimens, the configuration used was developed to provide controlled conditions of crack initiation and growth. Tests of the initially proposed rail-shear specimen revealed inadequate control over the location of specimen crack initiation and the direction of crack growth; this condition was attributed to the existence of shear-stress concentrations at both ends of the rail-shear specimen. In the modified configuration (Figure 6-18) a shear-stress gradient (rather than uniform shear) was generated by loading both halves of the shear rail at the end opposite the crack tip, and only one half at the other end.

Testing of the modified specimen revealed it to be a significant improvement over that originally proposed; however, several layup problems were encountered during testing. These problems were limited to two specific ply layups, 90/90- and +45/-45-degree. For both of these orientations, extensive delamination—as opposed to the intended fiber fracture—tended to occur parallel to the principal fiber orientations. As a result, testing of these layups was discontinued. Testing of both the quasi-isotropic and 0/90-degree layups produced fairly well-controlled conditions of translaminar fiber fracture.

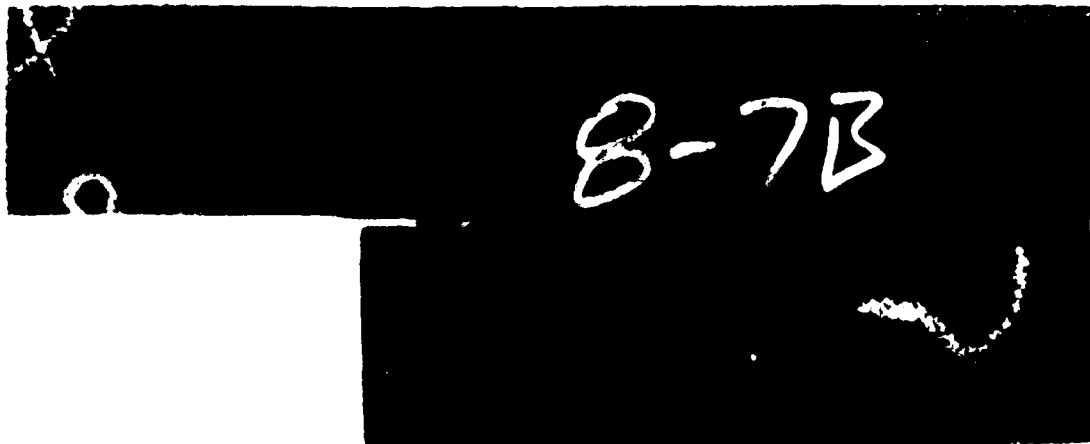


Figure 6-18. Translaminar Shear Specimen After Test

7.0 TASK 3: DIAGNOSTIC TECHNIQUE EVALUATION

7.1 OBJECTIVES

Activities in Task 3 were aimed at developing a detailed understanding of the fracture surface characteristics of composite materials. The literature search (Section 4.3) revealed that a number of investigations have been carried out to this end. However, since the overall objective of this program is the failure analysis of composite structures, effort was specifically devoted to understanding how fracture features relate to the direction of crack propagation, the load state at failure, and contributory factors such as environment, defects, and structural details. By understanding these relationships, physical evidence such as fracture features can be used to reconstruct the order of events involved in component failure.

7.2 APPROACH

Task 3 undertakes to understand the basic relationship of fracture features to crack direction, load state, and environment by examining relatively simple specimens with well-controlled failure conditions. Using this approach, direct comparisons can be made between fracture features and simple failure conditions, thereby eliminating much of the complexity associated with most fractographic studies. After simple failure specimens are thoroughly characterized, a well-developed data base should exist, in which subtle changes in fracture features likely to occur under more complex failure conditions will be readily distinguishable. To understand these changes and to determine how the developed data base can be applied to real structures, the later stages of Task 3 will examine specimens with relatively complex modes of failure.

Task 3 has two subtasks, 3A and 3B. In subtask 3A, specimens with relatively simple modes of failure were examined with respect to crack direction, load state, and environment. During the current report period nearly all of the specimens in this subtask were examined, and are reviewed in the latter part of Section 7.0. In subtask 3B, specimens were tested under relatively complex modes of failure; analyses of these specimens are currently underway.

In examining the fracture surfaces of specimens failed during this program, a number of techniques were used involving examination at successively higher magnifications. Initial

low-magnification inspection was carried out from 8X to 40X on a Bausch & Lomb stereo-zoom widefield microscope. Higher magnification inspections were performed on the majority of fractures at magnifications ranging from 50X to 400X using a Nikon Optiphot microscope fitted with long-working-distance objectives that give greater depth of field than other systems at equivalent magnifications. The finest fracture details were examined using an AmRay 1400 scanning electron microscope (SEM) at magnifications ranging from 20X to 20,000X.

Optical characterization of Task 2A fractures contributed to a critical Task 3 step in the development of a comprehensive failure analysis capability. Optical examinations of the characteristics of fracture identified specific features and morphologies that are valuable in performing failure analyses. Low-magnification examinations verified the plane of intended interlaminar fracture, the location of visible macroscopic beach marks, and identified the local direction of crack propagation. More detailed examination using the Nikon Optiphot characterized specific fracture features with respect to their appearance, consistency over the fracture surface, and relationship with the imposed mode and direction of fracture. Correlation of these features with the crack direction and mode under which failure occurred is directed toward development of an optical fractography data base. In general, optical fractography is performed in metals fracture analysis as a means of rapidly identifying fracture origins and areas of further interest; similar benefits will be realized by the development of a methodology in which optical analysis is used to increase the time and cost effectiveness of analyzing failed composite material structures.

Each fracture surface was characterized and inspected using an Am Ray 1400 SEM with a beam acceleration voltage of 20 keV. This voltage was selected to enhance the resolution of shallow surface details such as resin microflow. Prior to examination, approximately 20 nm (7.9×10^{-7} in.) of gold-palladium was applied to the specimens in a Hummer V sputter coater. The coating was applied using the DC-pulsed mode for 5 minutes after backfilling the vacuum chamber to 4.0-6.6 Pa (30 to 50 millitorr) with argon. To provide a controlled point of reference, SEM examinations were performed at two standard tilt angles: 15 and 60 degrees. The 15-degree tilt was chosen to give a relatively flat perspective similar to that characteristic of optical microscope examinations. Sixty-degree examinations revealed more of the dimension and height of specific features. In a manner similar to earlier optical examinations, photomicrographs with

successively higher magnifications were taken to document the fracture topography and guarantee analysis of an area typical of the overall surface.

7.3 INTERLAMINAR FRACTURES

This portion of the report is divided into three parts: the first section presents fractures generated under mode 1 (tension), the second section presents mode 2 (shear) fractures, and the last section covers the effects of environmental exposure on interlaminar fracture surface characteristics. In each section, the results of fractographic analysis are arranged in sequence based on the five different ply orientations in which fractures were generated.

7.3.1 INTERLAMINAR MODE 1, TENSION, 21°C (70°F)

Fractographic analysis of delaminated surfaces produced under interlaminar tension typically identified a mixture of fiber/matrix separation and cohesive resin fracture. The extent to which either of these features occurred depended on the percentage (by volume) of reinforcing fibers and the proximity of the fracture plane to the fibers. In general, areas of *fiber/matrix separation were relatively smooth and featureless*. Cohesive resin fractures dominated the overall surface topography. Such areas typically appeared flat, and exhibited pronounced river markings and resin microflow. The combination of these features appeared unique to interlaminar tension and provided a means for identifying the direction of fracture.

o MODE 1, 0/0-DEGREE INTERFACE FRACTURE SURFACE

The surface characteristics of interlaminar tension fractures generated between adjacent 0-degree plies is illustrated in Figure 7-1. Macroscopic examination of the surface reveals that interlaminar fracture occurred as intended between the 0-degree plies, with no out-of-plane crack wandering. Although not visible in the 0.6X macrograph, several arced bands were found running transverse to the specimen length. These bands are similar in appearance to beach markings found in metals and unreinforced polymer fractures. Such markings are indicative of the crack-front geometry and are formed in response to pronounced changes in crack velocity. Internal Boeing studies performed on similar beach markings revealed that they consist of a distinct morphological change in fracture surface roughness and microplane. This observation supports the concept of a

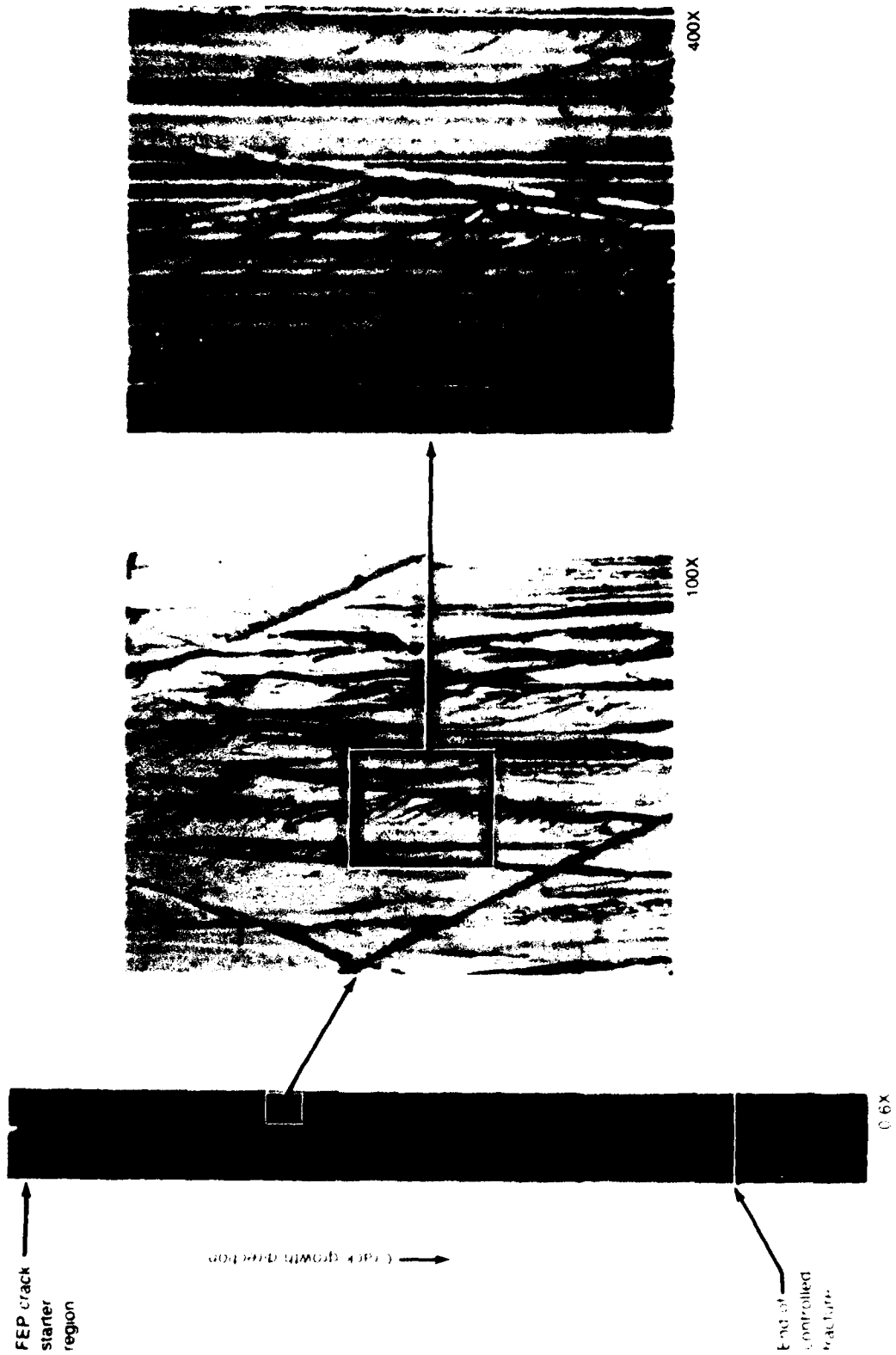
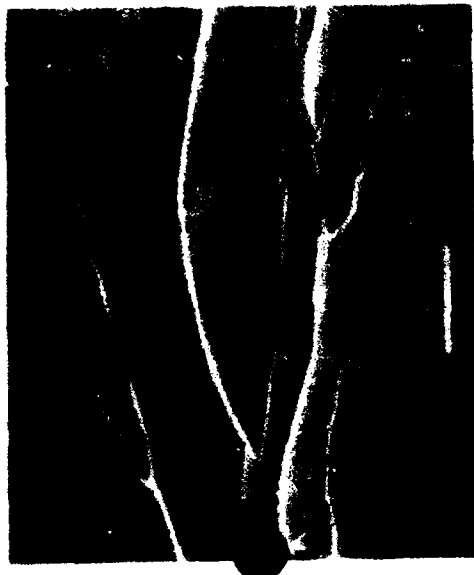


Figure 7-1. Optical Photomicrographs of Intended Fracture Plane Between 0/0-Degree Plies, DCB 210C (70°F) Specimen

distinct change in crack-front propagation rate. Numerous investigators have demonstrated that in neat polymeric materials, low crack velocities resulted in mirror-smooth fracture surfaces, and high crack velocities result in roughened, less reflective fracture topographies. The overall shape and curvature of the beach marks indicate that crack propagation occurred away from the implanted FEP crack starter, and toward the opposite end of the specimen. The arced shape, however, suggests that some crack growth retardation occurs at, or adjacent to, the specimen edges. This retardation corresponds with a localized shift in the direction of crack propagation off the center axis, toward the specimen edge. It is significant to note that this behavior occurs in unreinforced polymers as well as metals. Its appearance is typically associated with the tendency of a propagating crack front to run toward a free surface. This observation led to further high-magnification examinations concentrating on those areas in which crack progression occurred directly along the specimen length.

High-magnification optical inspection of the fracture surface reveals a reflective appearance with flat areas of resin fracture. These areas of resin fracture are separated by intermittent lines corresponding to fiber-matrix separation. Inspection at 400X reveals a distinct branched structure (river markings) in these flat resin fracture areas, along with more subtle evidence of resin microflow; the direction of river mark coalescence corresponds with the direction of induced crack progression. At higher magnification, the direction of river mark coalescence is often biased at an angle to the induced direction of crack propagation. However, at lower magnification (200X) the direction of coalescence appears to correspond well with the direction of induced fracture. These observations suggest that the direction of coalescence does coincide with the overall crack direction as long as local variations are averaged either by supplemental examination at lower magnifications or by additional high-magnification examinations of adjacent areas.

Following optical microscopy, scanning electron microscope (SEM) examinations were performed. Typical fracture surface characteristics identified by SEM analysis are illustrated in Figures 7-2 and 7-3. One of the most distinctive features of the fracture in Figure 7-2 is its relatively smooth, planar topography. At 400X, the overall fracture surface is composed of microstructural areas of cohesive resin fracture, fiber/matrix separation, and partially buried fibers. Of these three, regions of cohesive resin fracture constitute the predominant features in terms of exposed area. The areas are divided into roughly longitudinal segments by regions of fiber/matrix separation and partially buried fibers. At higher magnification, partially buried fibers occur when the fracture plane



←
Mechanically induced crack direction

- Legend:
- M Matrix fracture
 - F Fiber matrix separation
 - R River markings

Figure 7-2. SEM Fractographs of Mode I Delamination Between 0/0-Degree Plies

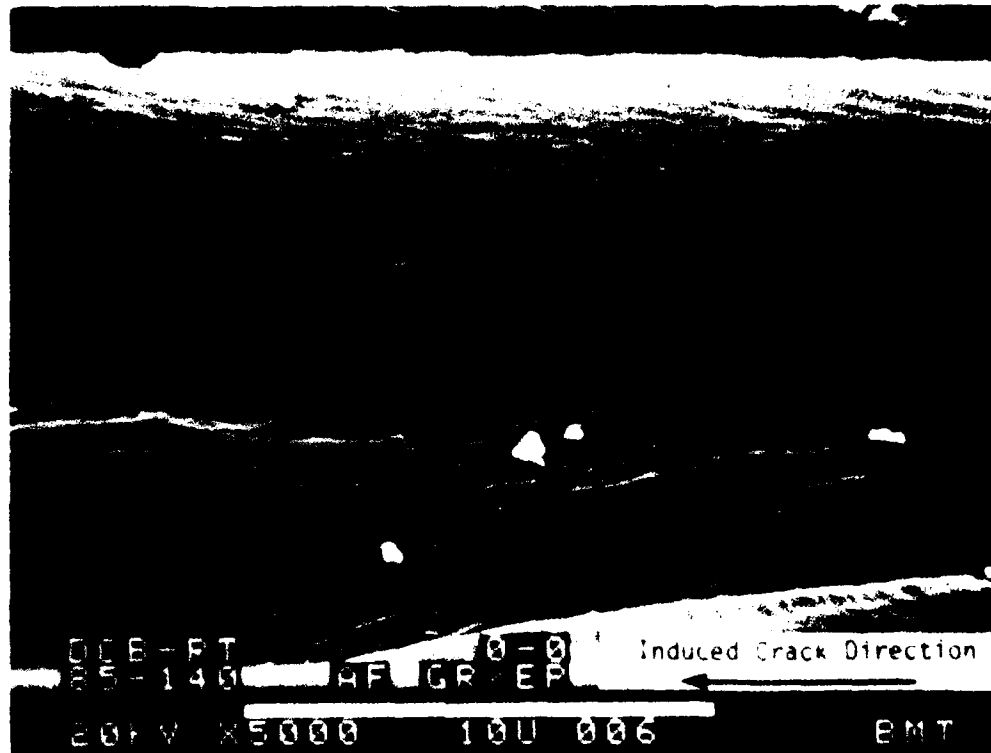


Figure 7-3. Photomicrograph Illustrating Adhesive Areas of Fiber/Matrix (F) Separation and Textured Microflow (T)

intersects underlying fibers at a shallow angle. In such cases, a general progression from cohesive matrix fracture to interfacial fiber/matrix separation occurs. In this transitional region, residual resin can be seen adhering to the fiber surface. However, once the fiber intersects the surface, the cleanly replicated impression of the AS-4 fiber becomes apparent, as illustrated in Figure 7-3. This condition indicates that fiber separation under interlaminar tension occurs adhesively, except where the fiber just intersects the fracture surface. Because of the adhesive type separation, areas of fiber/matrix separation are generally devoid of any morphological features related to the direction of crack propagation.

Areas of flat resin fracture represent some of the more dominant features of mode I (tension) delaminations. Detailed inspection of these cohesive matrix fracture regions reveals several distinctive morphological features. The most easily distinguished of these is a series of longitudinal branching lines which form a riverlike pattern (Figure 7-2: 400X and 2000X). These river markings are analogous to the cleavage fracture features commonly recognized in brittle metals, ceramics, and polymeric materials. It has been determined that in these materials such features result from progressive joining of

adjacent microscopic fracture planes during crack growth. More specifically, each line segment represents a local step formed when the thin ligament separating displaced planes is fractured during crack growth. As presented by Griffith, the amount of strain energy involved in fracture is proportional to the area of fracture surface created and amount of material plastic deformation. As a result, a large number of locally displaced fracture planes represents a higher energy condition than a single continuous fracture surface. Since crack propagation tends to occur along the path requiring the least energy, there is a tendency for the planes to coalesce. In metals and other material systems, it has been recognized that the joining of these planes generally produces coalescence of the ligaments, resulting in a riverlike pattern. The direction in which the ligaments coalesce indicates the local direction of crack growth. This argument appears valid for the river markings visible in Figure 7-2, since the general direction of macroscopic cracking correlates well with the average direction of river mark coalescence.

The second distinctive feature in areas of cohesive matrix fracture is microflow lines that are visible at high magnifications as a fine-grained structure or texture on the fractured resin surface (Figure 7-3). Detailed inspection of the overall flow of this grained structure reveals a herringbone or chevron pattern oriented with its wide end in the direction of crack growth. These features are commonly encountered in the fracture of metallic structures. The appearance of chevrons in metals is associated with microscopic deformation in the direction of local crack propagation. The herringbone pattern results from the inherent tendency of a propagating crack to take the shortest path to a free surface. Chevrons tend to rotate from the direction of overall crack growth toward adjacent cracks of free surfaces. Based on this interpretation, the localized direction of crack propagation can be determined by examining the direction and orientation of herringbone-shaped patterns. As illustrated in Figure 7-3, the induced crack propagation direction coincides with the direction of expanding and radiating microflow texture.

o **Mode I, 0/90-Degree Interface**

Interlaminar tension fracture characteristics produced between 0-degree and 90-degree ply orientations are illustrated in Figure 7-4. The macrograph shows that crack propagation generally occurs along the desired 0- to 90-degree interface. However, occasional intraply fracture into the 90-degree ply is evident adjacent to the FEP crack starter insert. A detailed inspection of this macrograph reveals numerous beach marks in the 0/90-degree interface area. The orientation of the beach marks indicate that crack

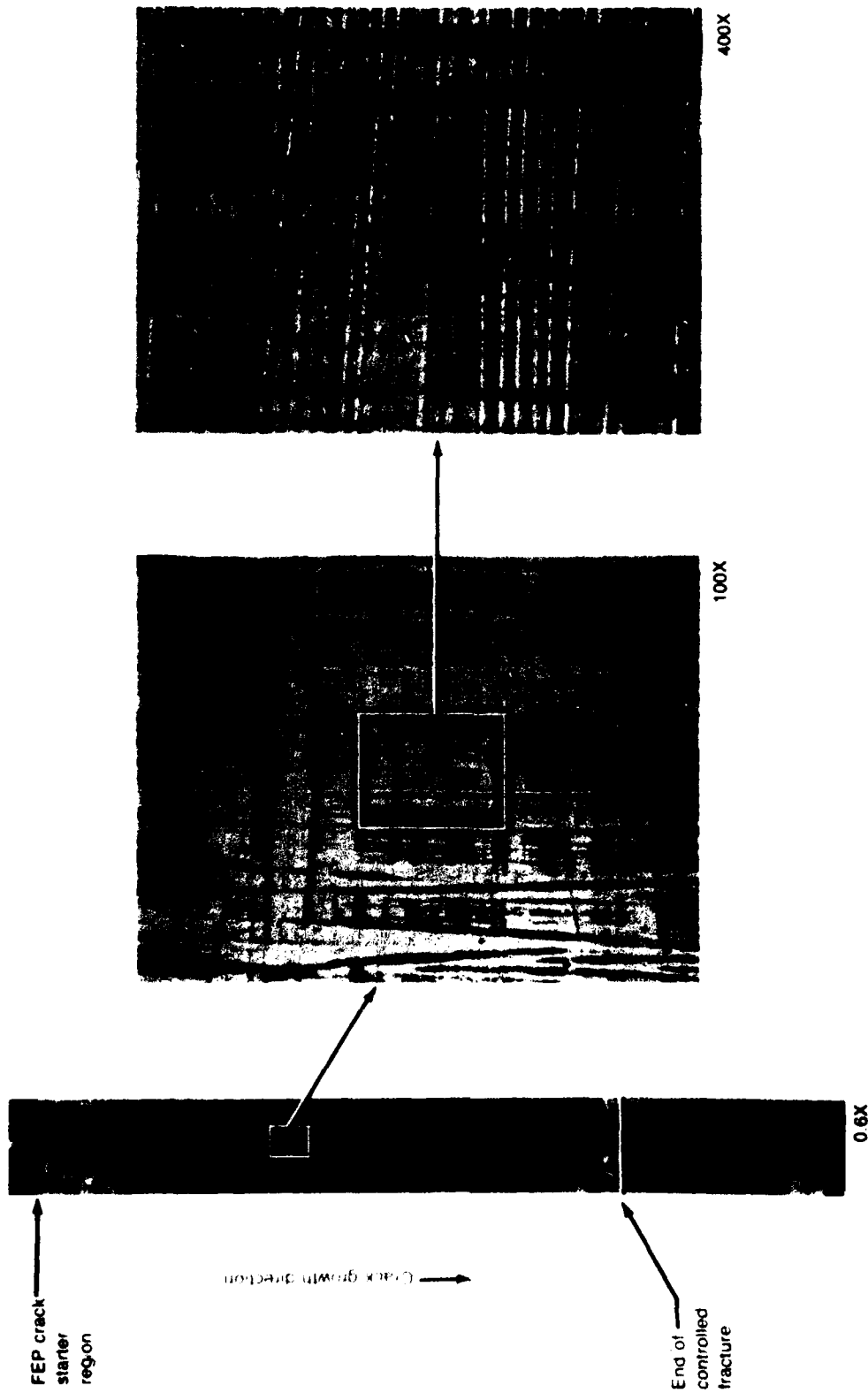


Figure 7-4. Optical Photomicrographs of Intended Fracture Plane Between 0/90-Degree Plies, DCB 2 10C (70°F) Specimen

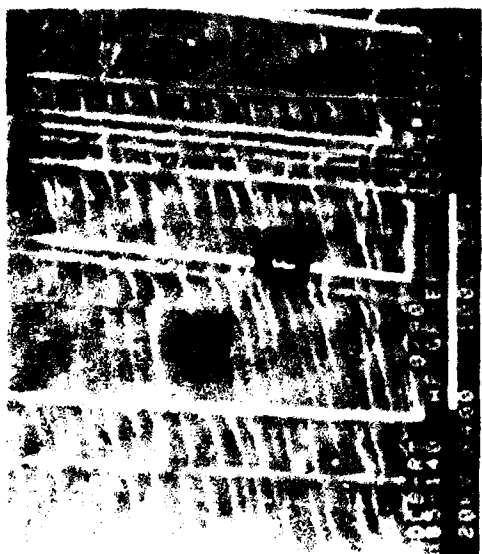
progression occurred from the implanted FEP insert toward the opposite end of the specimen. The general contour of these marks is relatively straight, indicating less variation in the local crack direction over the full specimen width as compared to the 0/0-degree specimens.

Detailed optical microscope inspection of the surface reveals a relatively flat fracture topography with a limited amount of fiber/matrix interfacial separation. The 90-degree oriented fibers act as sites of localized microcrack/microplane initiation, with subsequent microplane coalescence (or river markings) in the adjacent resin-rich areas. As with the 0/0-degree fracture, the direction of river mark coalescence coincides with the direction of induced crack propagation.

Results of scanning electron microscope examinations are presented in Figure 7-5. Observed at 400X, locations of 0- and 90-degree fiber/matrix separation tended to divide the surface into roughly rectangular areas of matrix fracture. Examining these areas reveals both distinct river markings and subtle conditions of resin microflow. It is particularly interesting to note that in this fracture, river mark branching appears to be associated with areas of partially buried or exposed fibers, suggesting that local disruption of the fracture plane results in crack-plane divergence and initiation of multiple-crack microplanes. Viewed at high magnification, the direction of coalescence of these microplanes and the general texture of microflow coincides with the direction of crack propagation. These findings indicate that such features can be used to identify the direction of crack propagation fractographically.

o **Mode I, +45/-45-Degree Interface**

The appearance of fracture surfaces produced by interlaminar tension between +45 and -45-degree ply interfaces are illustrated in Figure 7-6 (optical) and 7-7 (SEM). In Figure 7-6, the fracture occurred between the intended interfaces, with limited amounts of intraply wandering into either of the 45-degree plies. Further visual examination revealed numerous beach mark features similar to those noted previously for other fracture interface conditions. The general shape of these beach marks indicates that fracture began at the FEP insert and progressed towards the opposite end of the specimen as intended. The particularly curved contours of the beach marks indicates that significant crack deflection occurred adjacent to the specimen edge, altering the local direction of propagation by as much as 60-degrees (Figure 7-8). As noted earlier, such divergent



Mechanically induced crack direction

Legend:

- M Matrix fracture
- F Fiber matrix separation
- R River markings
- T Textured microflow

Figure 7-5. SEM Photomicrographs of Mode I Delamination Between 0/90-Degree Plies

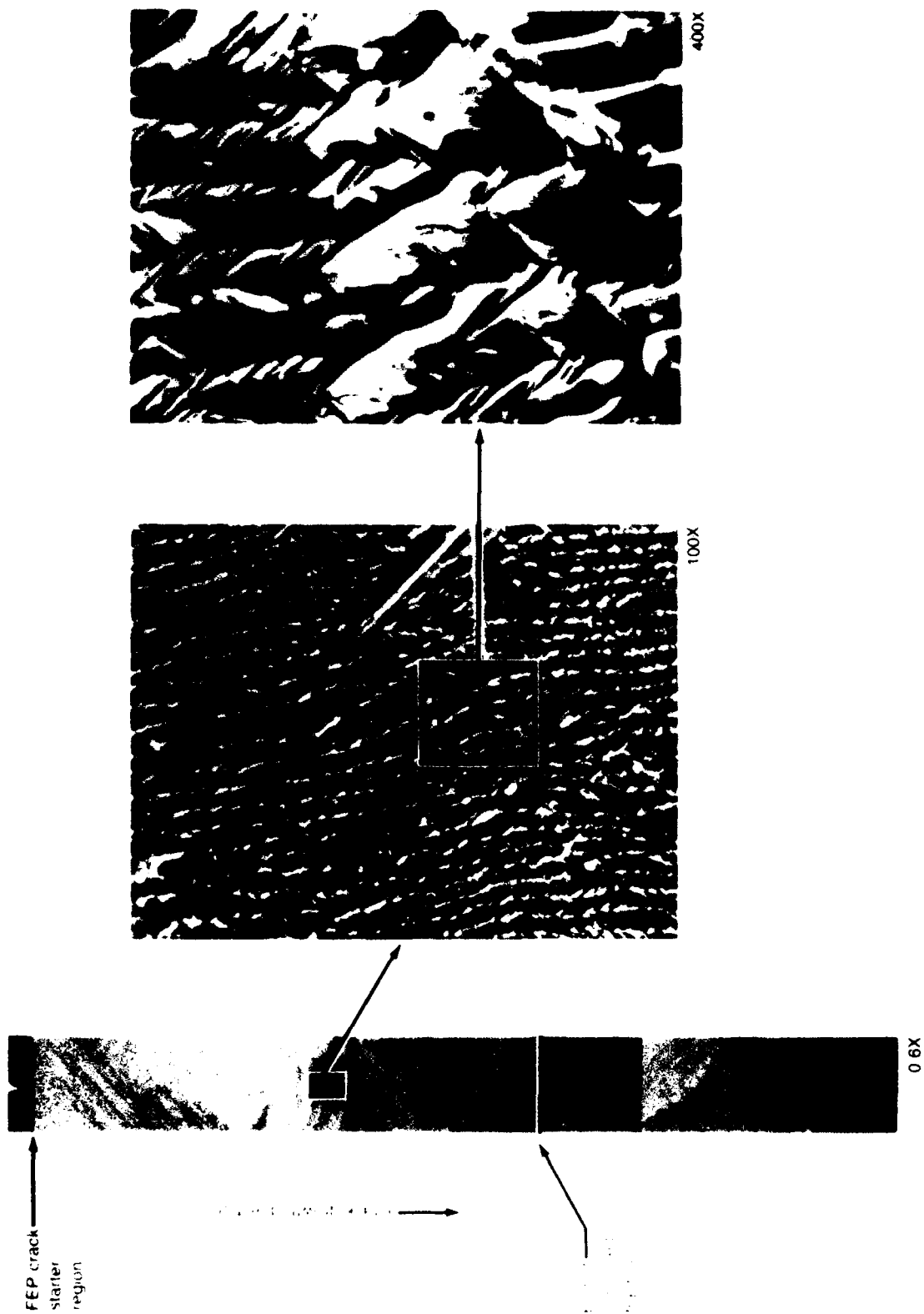


Figure 7-6. Optical Photomicrographs of Intended Fracture Plane Between +45 5-Degree Plies, DCB 21°C (70°F) Specimen



Mechanically induced crack direction

Legend

- M Matrix fracture
- F Fiber matrix separation
- R River markings
- T Textured microflow



Figure 7-7. SEM Fractographs of Mode 1 Delamination Between +45/-45-Degree Plies



20X

This closeup of the fracture surface presents the locally variable crack front position relative to the imposed macroscopic crack growth direction (shown by large arrow). Small arrows represent localized front propagation directions. This is a ± 45 cross-ply DCB 21°C (70°F) specimen

Figure 7-8. Fracture Surface

conditions also occur in metals near free edges and are generally ignored or averaged out in determining the direction of macroscopic crack growth. To avoid these areas of crack deflection, subsequent optical and SEM inspections were carried out in the central areas of the specimen.

Inspecting the fracture surface at increasing magnifications revealed a relatively rough topography consisting of numerous longitudinal rows of fan-shaped resin fracture zones intersected by the underlying 45-degree oriented fibers. For the optical photomicrograph (Figure 7-6), the strong light/dark contrast of the fracture surface is due to the tilt of fan-shaped zones with respect to the incident coaxial light source. Relatively reflective areas have shallow tilt angles, whereas darker, less reflective regions have relatively large tilt angles. Further SEM examination of the fan-shaped resin fracture areas revealed river markings associated with zones of fiber/matrix separation, and subtle conditions of textured resin microflow (Figure 7-7). The direction of river mark coalescence and microflow progression often deviate from the direction of induced crack propagation; this condition can be attributed to local rotation of the direction of crack propagation toward adjacent microscopic fracture zones. For this layup, deviations in the direction of crack propagation tended to be the most pronounced in small areas of resin fractures. However, these local variations average together, so that the overall direction of river mark branching and resin microflow correspond well with the direction of induced fracture. This finding indicates that the direction of crack propagation may be determined by examining the larger areas of resin fracture or by averaging the detailed crack directions of both large and small areas of resin fracture. The first of these two methods appears attractive in that it requires less effort and produces less data scatter; however, this approach ignores a portion of the actual fracture behavior and may be more susceptible to errors caused by spurious or secondary crack growth. The method choice should be predicated upon both the degree of accuracy desired and the time available for analysis.

o Mode I, 0/45-Degree Interface

The interlaminar tension fractures produced between 0- and 45-degree-oriented plies are illustrated in Figure 7-9 (optical) and 7-10 (SEM). The overall optical macrograph (Figure 7-9), shows that fracture occurred between the desired ply orientations with some limited intraply fracture of the 45-degree ply. As with other orientations described previously, arced bands were apparent running transverse to the specimen length. The contour of

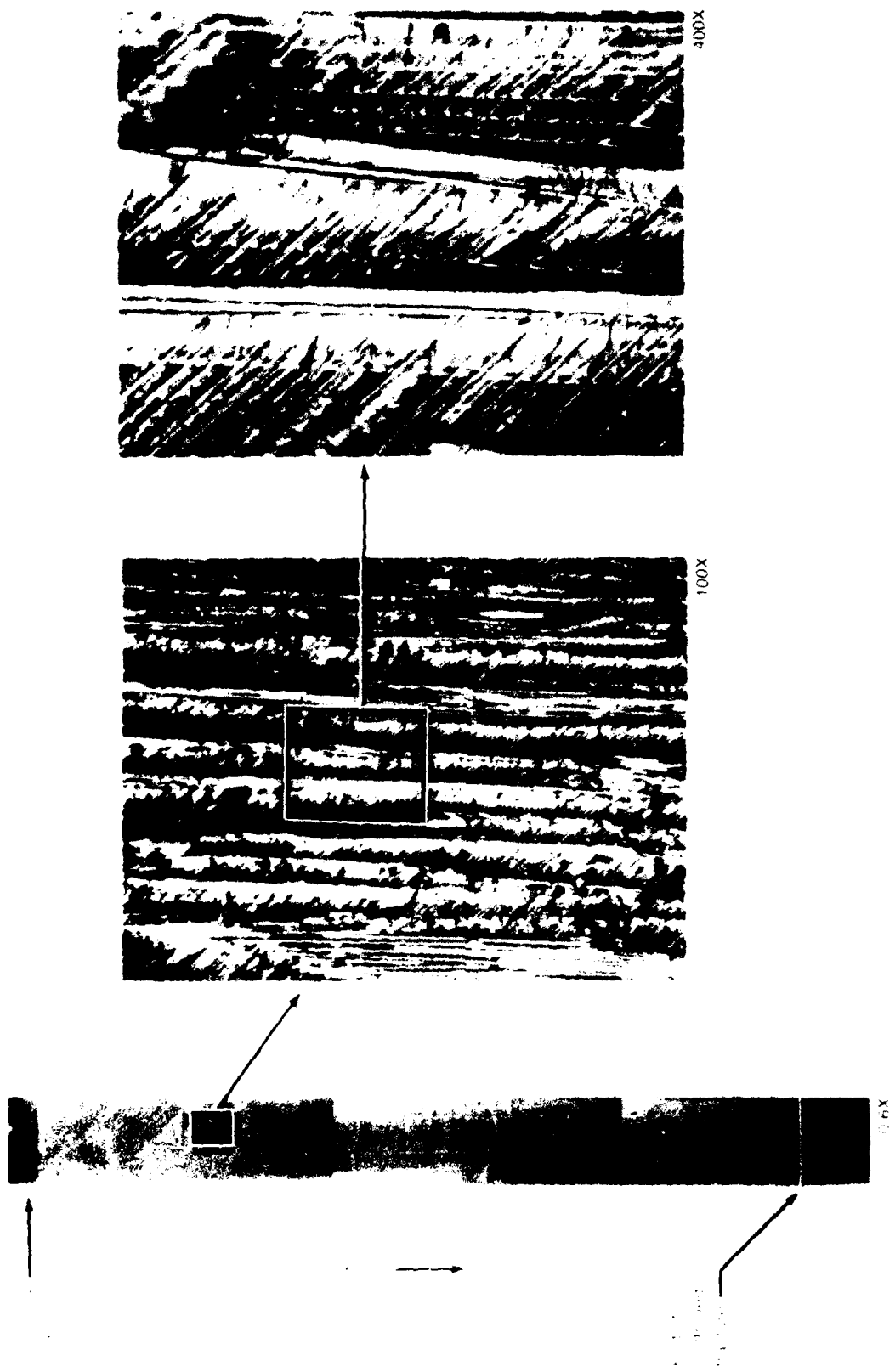


Figure 7-9. Optical Photomicrographs of Intended Fracture Plane Between 0/45-Degree Plies, DCB 21°C (70°F)



Mechanically induced crack direction

Legend

- M Matrix fracture
- F Fiber matrix separation
- R River markings
- T Textured microflow



Figure 7-10. SEM Photomicrographs of Mode I Delamination Between 0/+45-Degree Plies

these bands indicate that crack propagation occurred along the specimen length and away from the FEP insert as intended. Additionally, some rotation of the crack direction toward the specimen edge is apparent. Further analyses concentrated on those central fracture regions where the contour of beach markings indicated that the direction of crack propagation coincides with the specimen's longitudinal axis.

Detailed optical and SEM inspection of the surface revealed an overall topography of matrix fracture zones that exhibits extensive evidence of fiber/matrix separation in the 45-degree fibers. These zones are roughly divided into longitudinal segments by intermittent penetration of the underlying 0-degree fibers into the fracture surface. The underlying 0-degree fibers are visible as longitudinally oriented, diffused reflections. As

with the +45/-45-degree interface, most of these resin fracture areas appear inclined at acute angles to the fracture surface. SEM examinations of resin fracture areas exhibited the river marking and resin microflow morphology discussed previously. As evident in the SEM photomicrograph at 2000X, significant variations in the direction of these features can occur. With respect to the direction of induced crack propagation, these variations appear to extend up to 90 degrees from the macroscopic crack direction. However (as with the +45/-45-degree interface) the averaged direction of river marks and resin microflow gives a much better correlation with the macroscopic direction of crack propagation. The averaged direction of these features varied by as much as 30 to 45 degrees from the direction of induced failure. This finding indicates that while the approximate direction of fracture may be determined by examining river markings, precise determination may not be possible for all failure conditions.

o Mode I, Adjacent 90-Degree Interfaces

Fracture surfaces produced under interlaminar tension between adjacent 90-degree plies are illustrated in Figure 7-11 (optical) and 7-12 (SEM). As seen in the optical macrograph, a majority of the fracture diverged from the intended 90/90-degree interface either into the 0/90-degree interface or within a 0-degree ply. Between 15% and 20% of the fracture occurred within a 90-degree ply. While fracture did not occur at the intended interface, separation inside the 90-degree ply does constitute a 90/90-degree fracture condition. Detailed microscopic examinations revealed a distinctly dissimilar morphology than that of the four other ply orientations examined. Fracture along the 90-degree interface produced considerably more exposed fiber/matrix separation combined with relatively small areas of cohesive resin fracture. At low magnifications this topography appears noticeably rough, accounting for the difficulty encountered in optically examining and understanding the morphology of this fracture surface.

SEM analysis at 2000X indicated the presence of two types of cohesive resin fracture morphology. In one type, areas of resin fracture appear relatively flat, similar to those noted in the mode I fracture interface conditions. In the other type, several rougher areas of resin fracture exist that appear to be made up of numerous platelets of fractured epoxy inclined at a shallow angle to the plane of fracture. Both the tilted platelets and flat areas of resin fracture exhibit branched river markings adjacent to areas of fiber/matrix separation. In contrast to the other ply orientation fractures, the direction of river mark coalescence was both coincident with, and opposite to, the direction of

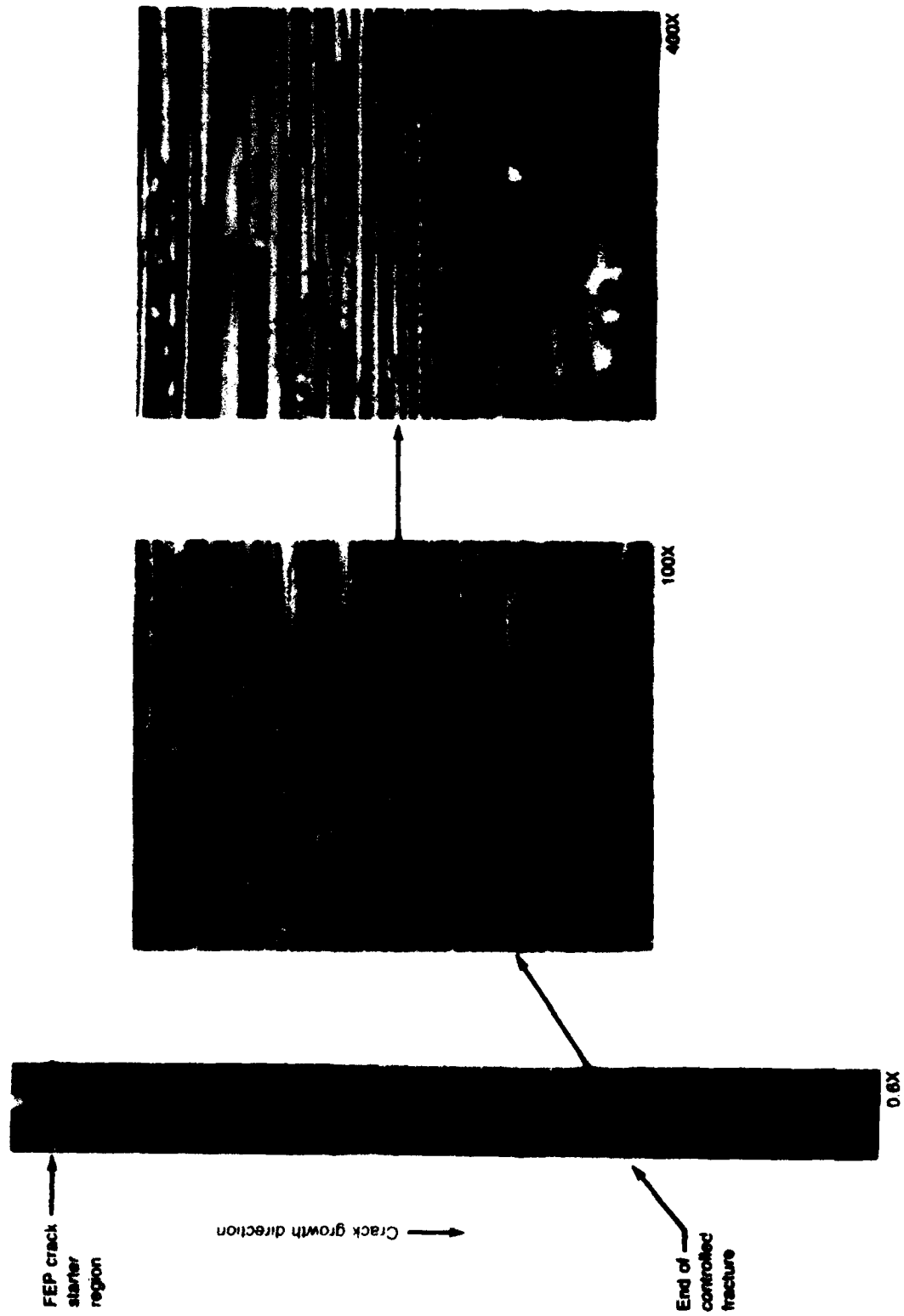
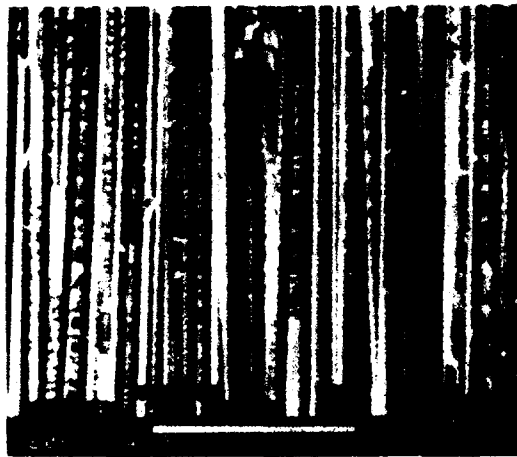


Figure 7-11. Optical Photomicrographs of Intended Fracture Plane Between 90/90-Degree Plies, DCB 21°C (70°F) Specimen



Mechanically induced crack direction

Legend

- M Matrix fracture
- F Fiber matrix separation
- R River markings
- T Textured microflow



Figure 7-12. SEM Fractographs Illustrating the Fracture Topography of Mode 1 Delamination Between Adjacent 90-Degree Plies

crack propagation. This finding is of particular concern, since for the other interfacial fracture conditions, the direction of river mark coalescence appeared to be a reliable indicator of the overall direction of crack propagation.

In an attempt to understand this condition, the fracture surface illustrated in Figure 7-12 was examined in detail at several tilt orientations. Figure 7-13 shows that increasing the tilt of this fracture surface to approximately 66 degrees revealed:

- o Areas of resin fracture are inclined at a wide variety of angles with respect to the plane of fracture



TILT = 15 deg



TILT = 66 deg



TILT = 66 deg

Figure 7-13. SEM Fractographs of Mode I Delamination Between Adjacent 90-Degree Plies Illustrating the Effect of Tilt Angle

- o Areas exhibiting river mark coalescence opposite to the direction of induced crack propagation are generally oriented at steep vertical angles to the plane of fracture
- o Resin fracture areas lying roughly in the plane of fracture tend to exhibit river pattern coalescence coincident with the direction of induced crack growth
- o Examinations at higher angles of tilt tend to increase the serrated appearance of all resin fracture areas, both flat and serrated.

These observations suggest that the direction of crack growth may be determined by considering both the direction of river mark coalescence and the relative plane of resin fracture. A relatively good correlation appears to exist between the direction of river mark coalescence and induced crack growth as long as examinations are limited to those areas lying roughly in the plane of fracture. Areas inclined out of the plane of delamination may not exhibit this correlation for several reasons. First, areas of vertical fracture may arise from bridged fibers being pulled out from behind the main crack tip. Alternatively, steep fracture areas may occur through the secondary joining of displaced fracture planes. In either case, the generation of inclined areas occurs as a secondary event after propagation of the main crack front. Because of their secondary nature, both fiber pullout and fracture plane coalescence may give rise to locally spurious crack propagation directions.

Figure 7-13 shows that increasing the tilt of the fracture surface significantly altered the appearance of both specific surface features and the overall morphology. This finding emphasizes the importance of having investigators document the viewing angle, examine features at several angles to understand their actual morphology, and use photographic stereo pairs where possible. The actual fracture morphology in Figure 7-13 is best described by examining both tilt angles. The relatively flat area of fracture on the left actually consists of several localized fracture planes inclined at about 5 to 10 degrees. In many cases, the edges of these planes sweep upward giving them a steeper appearance. The heavily serrated areas on the right consist of fracture planes inclined at between 20 and 30 degrees. In contrast to the area on the left, the overlapping fracture planes on the right tend to be thicker and more undercut. These resin fracture areas exhibit both thicker fracture plates and significant undercutting of adjacent fracture areas. The appearance of this plate structure and its formation is not well understood at present.

However, the experience of Boeing and other investigators observing these platelets suggests failure under mixed-mode load conditions.

7.3.2 Interlaminar Mode 2, Shear, 21°C (70°F)

Interlaminar fractures produced under mode 2 (shear) appeared distinctly different from delaminations under mode 1 (tension). In both cases, two principal zones of fracture were observed: areas of resin matrix fracture, and regions of fiber/matrix separation. However, fractures produced under interlaminar shear exhibited larger amounts of fiber/matrix separation and smaller, finely spaced areas of cohesive matrix fracture. In contrast to mode 1 delaminations, these finely spaced areas of matrix fracture exhibited a relatively rough topography. Detailed inspection revealed numerous inclined platelets (hackles) of fractured epoxy, oriented normal to the direction of resolved tension. Under certain circumstances, the orientation of these hackles correlated positively with the direction of induced cracking. Secondary cracking was also evident, aligned in the direction of fiber orientation of adjacent plies. These secondary cracks were not found to be significant for determination of crack direction.

o Mode 2, 0/0-Degree Interface

The fracture surface characteristics of mode 2 (shear) delaminations generated between adjacent 0-degree plies is illustrated in Figures 7-14 (optical) and 7-15 (SEM). Macroscopic examination of the fracture surface revealed that fracture occurred between the intended 0-degree plies with no out-of-plane crack divergence. The transversely arced bands (beach marks) typically found in interlaminar tension fractures were absent. Although there were no macroscopic details that suggested any variations or shifts in the direction of crack propagation across the specimen width, further optical and SEM examinations concentrated on the central region of each specimen.

When compared to interlaminar tension fractures, high-magnification inspection of the shear fracture surface revealed a much rougher topography with more fiber/matrix separation. Inspection of narrow resin-fracture zones between fibers at 400X showed a series of small, parallel resin particles. Optical microscopy disclosed that the particles are translucent and stand normal to the fracture surface. The long axes of the particles are aligned normal to the direction of imposed crack propagation. The large, flat zones and river mark branch structure typical of matrix resin areas in mode 1 delaminations are

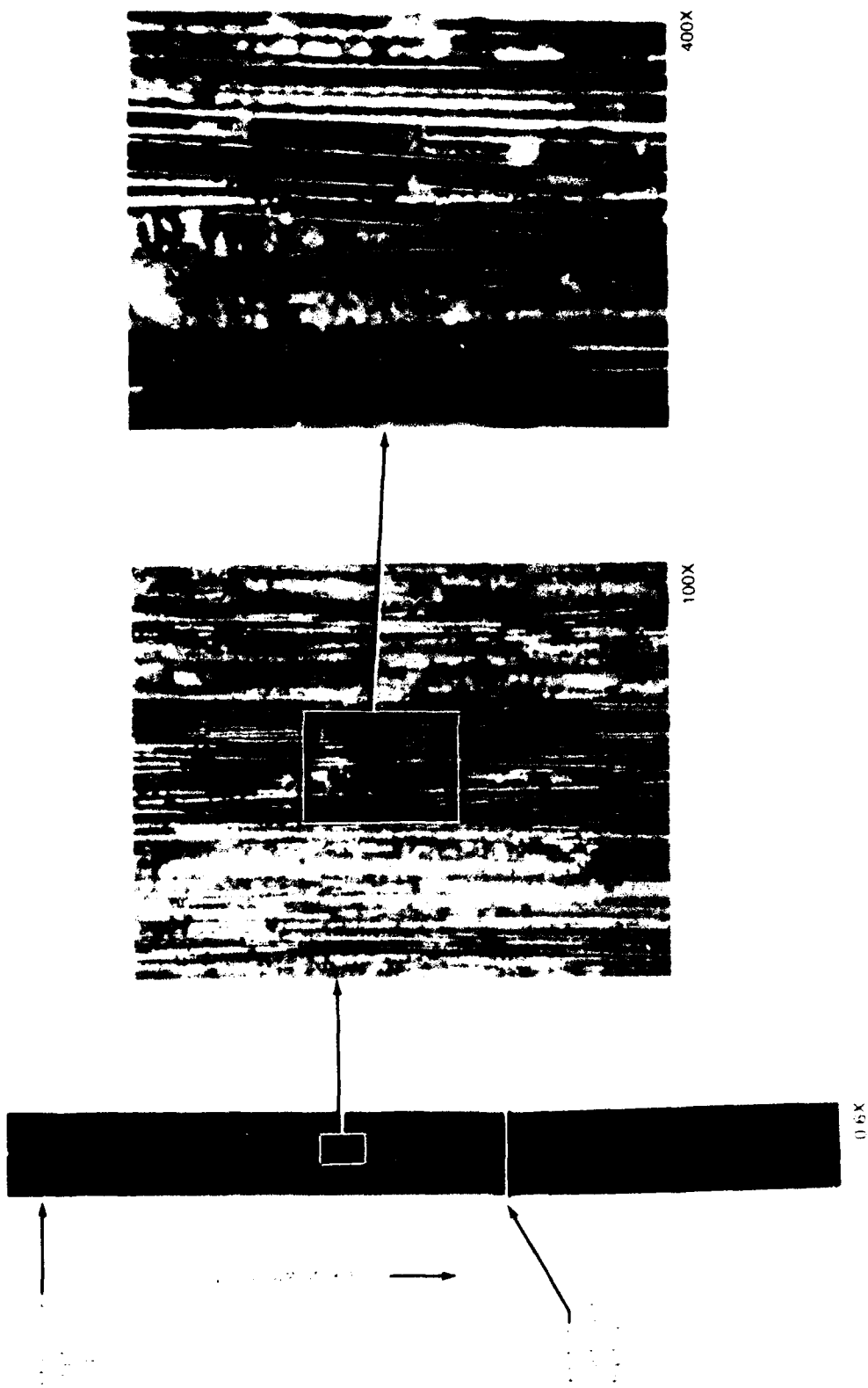


Figure 7-14. Optical Photomicrographs of Intended Fracture Plane Between 0/0-Degree Plies, ENF 21°C (70°F) Specimen



Mechanically induced crack direction

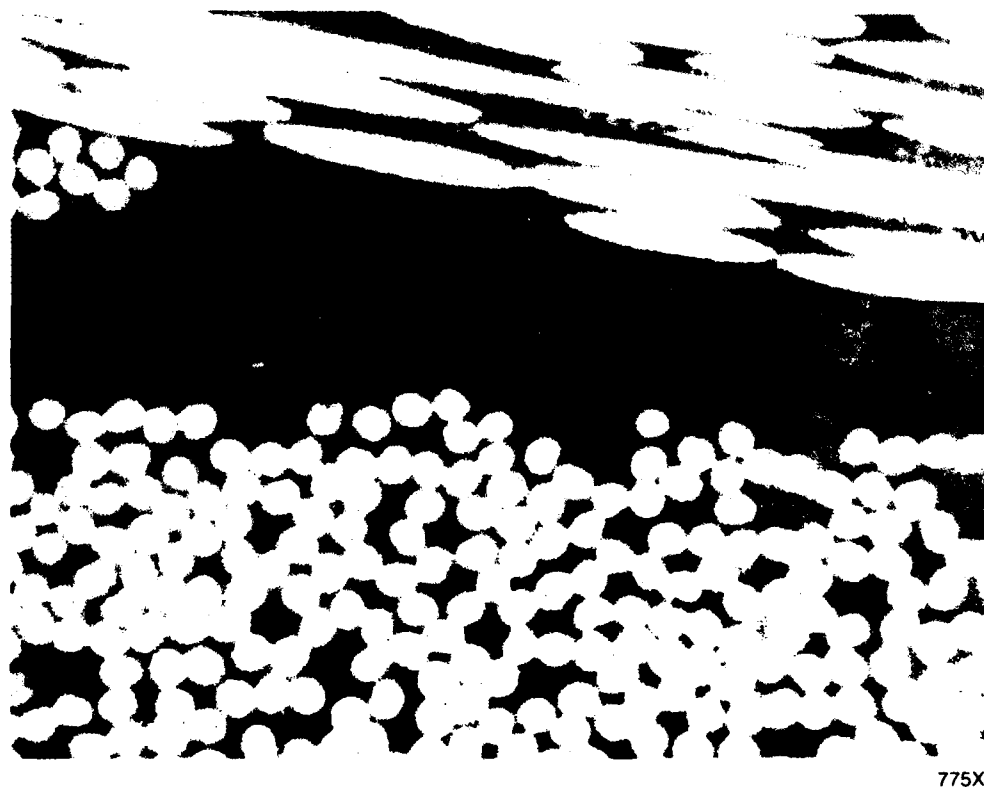
Legend

- F Fiber matrix separation
- H Hackles
- R River markings
- T Textured microflow

Figure 7-15. SEM Photomicrographs of Mode 2 Delamination Between 0/0-Degree Plies

not present. These distinct differences between observed features for each load state permit the use of optical analysis to rapidly differentiate between pure mode 1 and pure mode 2 delaminations.

Under detailed SEM examination, the narrow rows of cohesive resin fracture between areas of fiber separation exhibited numerous inclined platelets oriented crosswise to the 0-degree fiber orientation. Some investigators (see Section 4.3) refer to these platelets as hackles, and suggest that they result from flexural loading associated with local bending of the fracture surface just behind the crack tip. However, the presence of hackles only under conditions of mode 2 (rather than mode 1), suggests interlaminar shear as the primary load source for their formation. The appearance of hackles suggests that their formation occurs from coalescence of numerous microcracks inclined at an angle to the plane of applied shear. This is supported by the observation of S-shaped cracks at the midplane of short beam shear specimens (highest shear loading) in previous Boeing studies (Figure 7-16). In general, the hackle structures visible in Figure 7-15, and microcracks visible in Figure 7-16, are oriented at angles of 40 to 60 degrees to the plane of applied



(Ref 1 Copyright © ASTM reprinted with permission)

Figure 7-16. Microstructure of Cracks Found in Short Beam Shear Specimen Tested at 132°C (270°F)

shear and approximately normal to the resolved tension component of applied shear. This finding suggests that hackle and microcrack formations occur under locally resolved tension conditions. Based on these observations, the orientation of applied interlaminar shear (clockwise or counterclockwise) can be determined by examining the tilt of hackles with respect to the plane of fracture.

Further inspection of the surface revealed areas of scalloped or concave resin fracture (Figure 7-17). Detailed examination of these features suggests that they are formed as hackles separate from the fracture surface. This conclusion is substantiated by the existence of nearly separated hackles and the formation of underlying scalloped areas as shown in Figure 7-17. Separation of hackles can produce two possible relationships (mechanisms A and B) between hackle tilt and the direction of crack propagation, depending on which side of the shear plane retains the hackles (Figure 7-18). In mechanism A, separation occurs such that hackles are retained on the side in which the direction of crack propagation coincides with the direction of the local shear component. This condition produces hackles tilted in the direction of crack propagation, and normal to the direction of resolved tension. Conversely, in mechanism B, separation occurs such that hackles are retained on the side in which the direction of crack propagation opposes the direction of the local shear component. In this condition, the tilt of hackles oppose the direction of crack propagation.

To identify the dominant mechanism of hackle separation, both sides of each fracture surface were examined. As shown in Figure 7-19, both sides of fracture between adjacent 0-degree plies exhibit pronounced hackle formations. The existence of hackles on both surfaces indicates that hackle separation occurred by both mechanisms A and B. This finding indicates that hackle tilt is not a useful means of fractographically determining the direction of crack propagation for shear fractures between adjacent 0-degree plies. However, it appears that the direction of crack propagation can be generally identified as parallel to the direction of hackle tilt.

While the above discussion has been concerned with the overall structure of hackles, several finer morphological features are apparent on both hackled and scalloped areas. As illustrated in Figures 7-15 and 7-16, these areas exhibit textured resin microflow and branched river markings analogous to those identified under mode I. Additionally, secondary hackles—or rather, smaller platelet structures found on the sides of the large hackles—also align in the direction of overall hackle tilting. The presence of these small

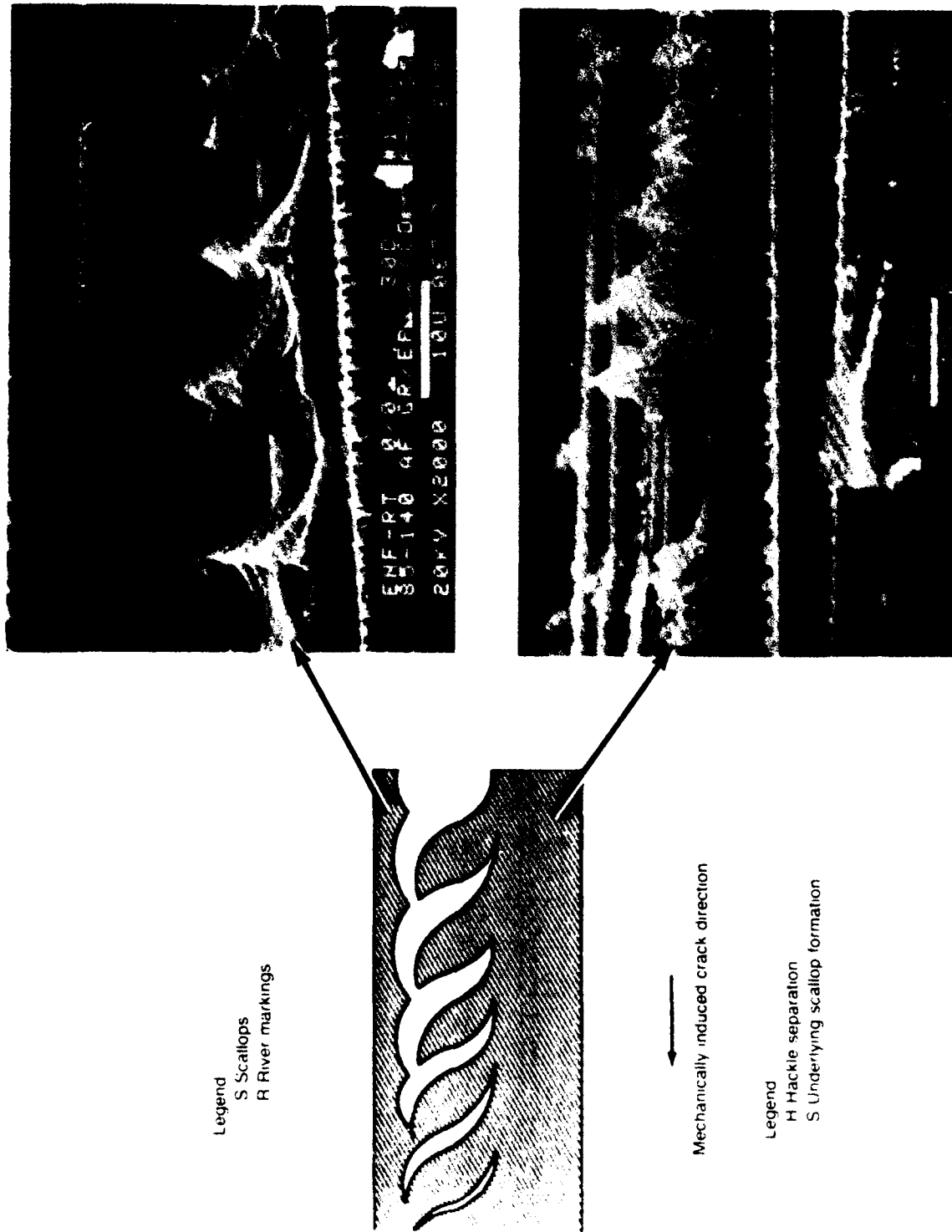


Figure 7-17. Scalloped Resin Fracture Areas and Their Development

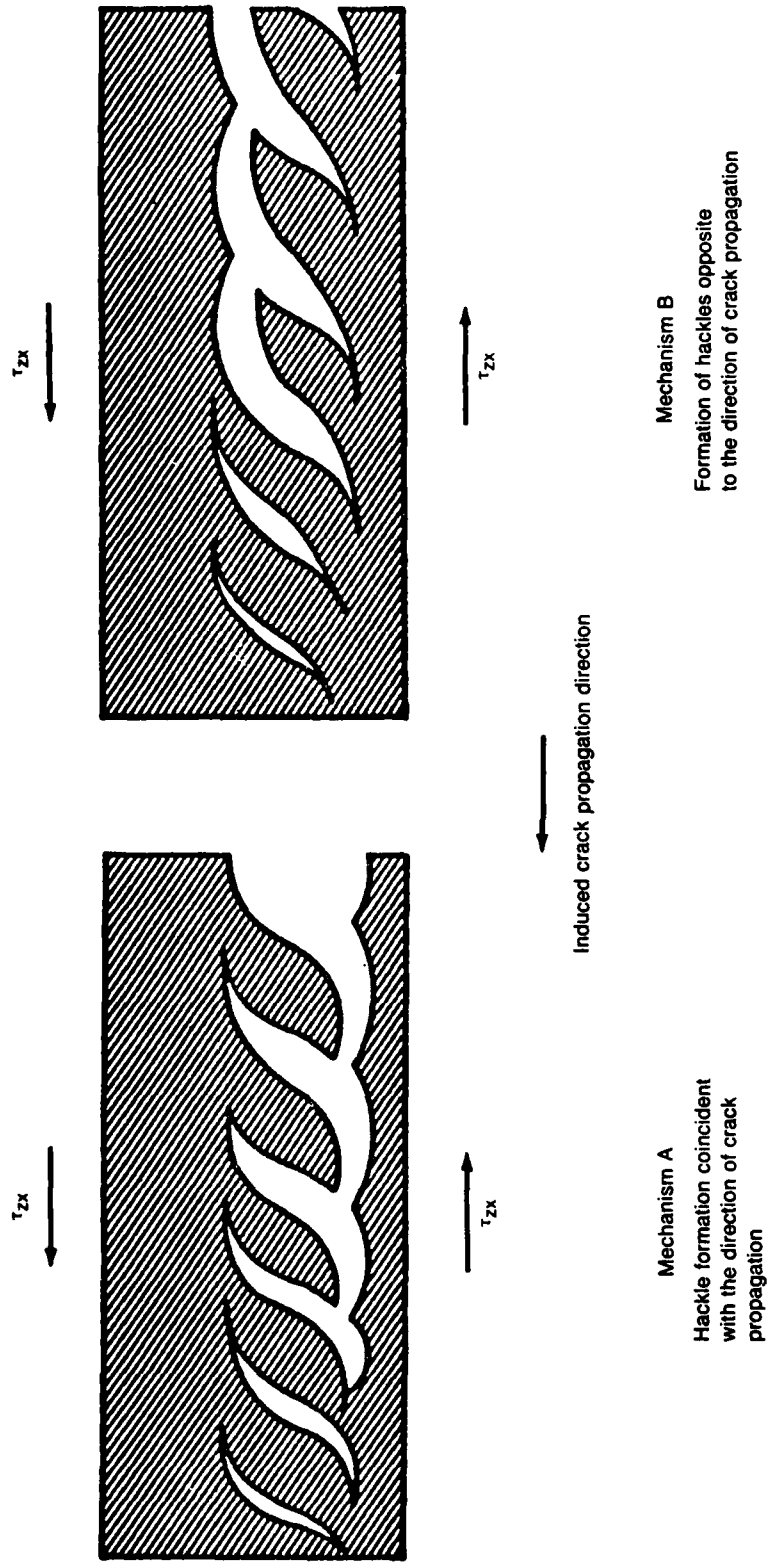


Figure 7-18. Possible Hackle Separation Mechanisms



Figure 7-19. Opposing Hackle (H) Tilts on Mating Sides of Mode 2 Delamination Between Adjacent 0-Degree Plies

hackles indicates that, although several microcracks form near or at the fiber/matrix interface, continued growth favors the larger centrally located microcracks. The microflow and river marks of these primary and secondary hackles appear to emanate from areas of fiber/matrix separation and rotate to align with the direction of hackle tilting. They are either coincident with, or opposite to, the direction of imposed crack propagation (mechanism A or B). Examining these features at a microscale indicates the local direction of crack propagation involved in hackle formation and separation. The fact that these features emanate from areas of fiber/matrix separation suggests that hackle formation initiates along the fiber interface and progresses either coincident with, or opposite to, the direction of overall propagation.

o **Mode 2, 0/90-Degree Interface**

Typical fracture surface features characteristic of mode 2 delaminations for the 0/90-degree cross-ply interface are presented in Figures 7-20 (optical) and 7-21 (SEM). No out-of-plane crack divergence was observed in these specimens. Similar to the interlaminar shear 0/0-degree interfacial fractures, the mode 2 topographies are much rougher and exhibit more fiber/matrix separation than those observed in mode 1 fractures. High-magnification optical inspection of the resin fracture zones between fibers reveals translucent, parallel resin particles whose long axes are aligned normal to the direction of imposed crack propagation. No river mark branching is present. It was concluded that optical microscopy can be used to accurately identify mode 2 fractures and differentiate this load condition from mode 1 delaminations of cross-ply interfacial orientations.

Hackles are tilted normal to the local direction of resolved tension and occur almost exclusively on one side of the fracture surface, with scallops on the opposite side (Figure 7-22). In Figure 7-18, the hackles are tilted coincident with the direction of crack propagation, indicating separation by mechanism A. In contrast to the 0/0-degree ply condition, this observation indicates a positive correlation between hackle tilt and the direction of crack propagation for the 0/90-degree cross-ply condition. However, further studies should determine if the mechanism of hackle separation depends on conditions such as specimen geometry, layup, or degree of mixed-mode loading.

In addition to the gross topography discussed above, further inspection of hackled and scalloped fracture areas revealed several finer morphological features. As illustrated in Figure 7-21 at 5000X, detailed examination reveals textured resin microflow and branched

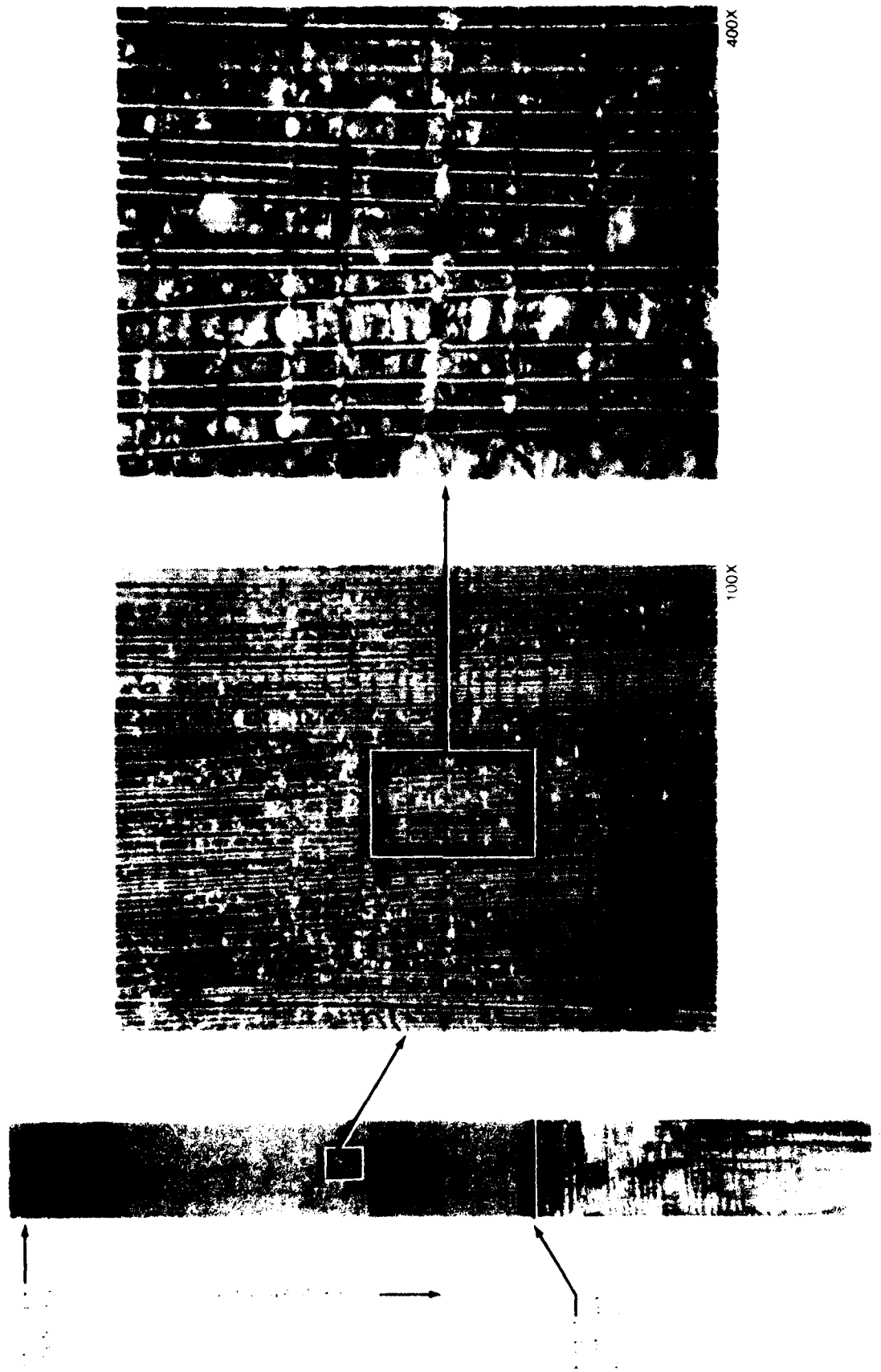
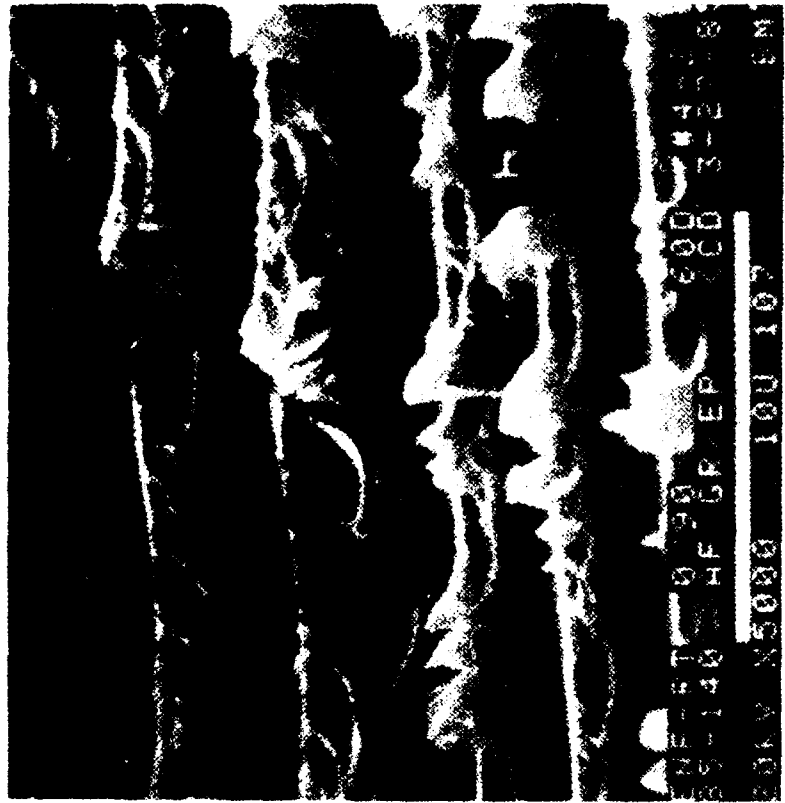


Figure 7-20. Optical Photomicrographs of Intended Fracture Plane Between 0/90-Degree Plies, ENF 21°C (70°F) Specimen



←
Mechanically induced crack direction

Figure 7-21. SEM Photomicrographs of Mode 2 Delamination Between Adjacent 0/90-Degree Plies Illustrating Areas of Fiber/Matrix Separation (F) and Hackles (H)

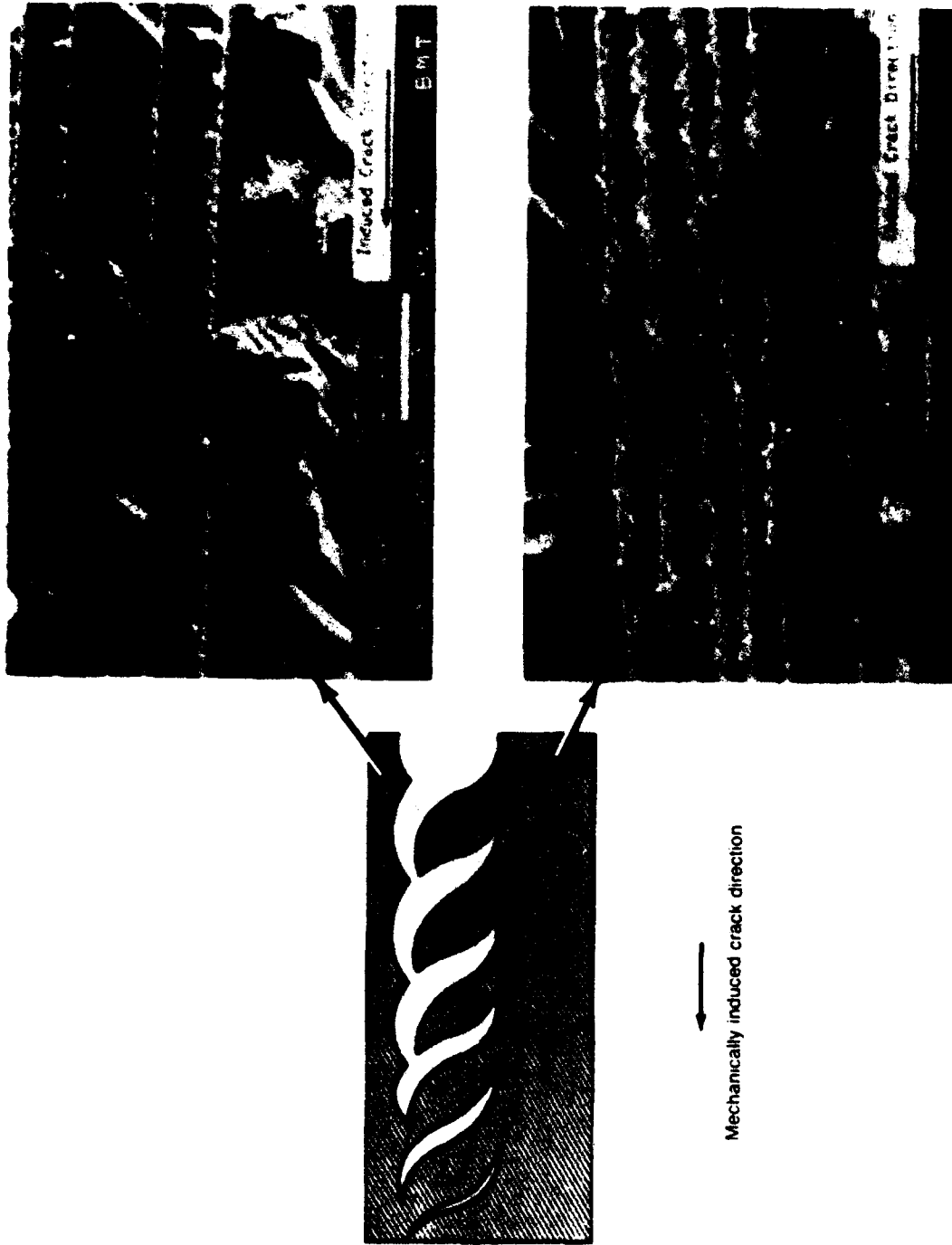


Figure 7-22. Topography of Mating Fracture Surfaces Produced Under Mode 2 Between 0- and 90-Degree Ply Orientations. Hackle (H) Separation Occurs by Mechanism A With Hackles Tilted in the Direction of Crack Propagation

river mark features. Both of these features appear to emanate from regions of fiber/matrix separation. In contrast to delamination between adjacent 0-degree plies where features progress both toward and away from the macroscopic direction of crack propagation, microflow and river markings for the 0/90-degree orientation progress only in the direction of crack propagation. Because of their nature, these features reflect the microscopic direction of cracking. Therefore, it can be inferred that hackle formation occurs from the initiation and growth of S-shaped microcracks in the direction of macroscopic crack growth; this condition supports the interpretation of hackle separation by mechanism A.

o **Mode 2, +45/-45-Degree Interface**

Typical fracture surface features characteristic of mode 2 delaminations for the +45/-45-degree cross-ply interface are presented in Figures 7-23 (optical) and 7-24 (SEM). No out-of-plane crack divergence was observed in these specimens. Similar to the interlaminar shear 0/0-degree interfacial fractures, the mode 2 topographies are much rougher and exhibit more fiber/matrix separation than those observed in mode 1 fractures. High-magnification optical inspection of the resin fracture zones between fibers reveals translucent, parallel resin particles whose long axes are aligned normal to the direction of imposed crack propagation. No river mark branching is present. It was concluded that optical microscopy can be used to accurately identify mode 2 fractures and differentiate this load condition from mode 1 delaminations of these cross-ply interfacial orientations.

Consistent with the above findings, mode 2 delaminations exhibit more fiber/matrix separation and smaller, narrower rows of cohesive resin fracture than mode 1 delaminations. In comparison to the 0/0-degree mode 2 fracture, a distinct alteration in the size and shape of hackles was evident. As shown in Figure 7-24, the overall fracture surface exhibits a large amount of cohesive resin fracture, as well as larger, triangular-shaped hackles. Hackles are tilted normal to the direction of resolved tension and occur almost exclusively on one side of the fracture surface, with scallops on the mating fracture surface (Figure 7-25). In Figure 7-18, these hackles are tilted coincident with the direction of crack propagation, indicating separation by mechanism A. Closer inspection of the hackled and scalloped features reveals resin microflow and branched river marks. These finer morphological features appear to emanate from regions of fiber/matrix separation and progress only in the direction of induced crack propagation, reflecting the microscopic direction of cracking. Similar to other ply orientations discussed previously,

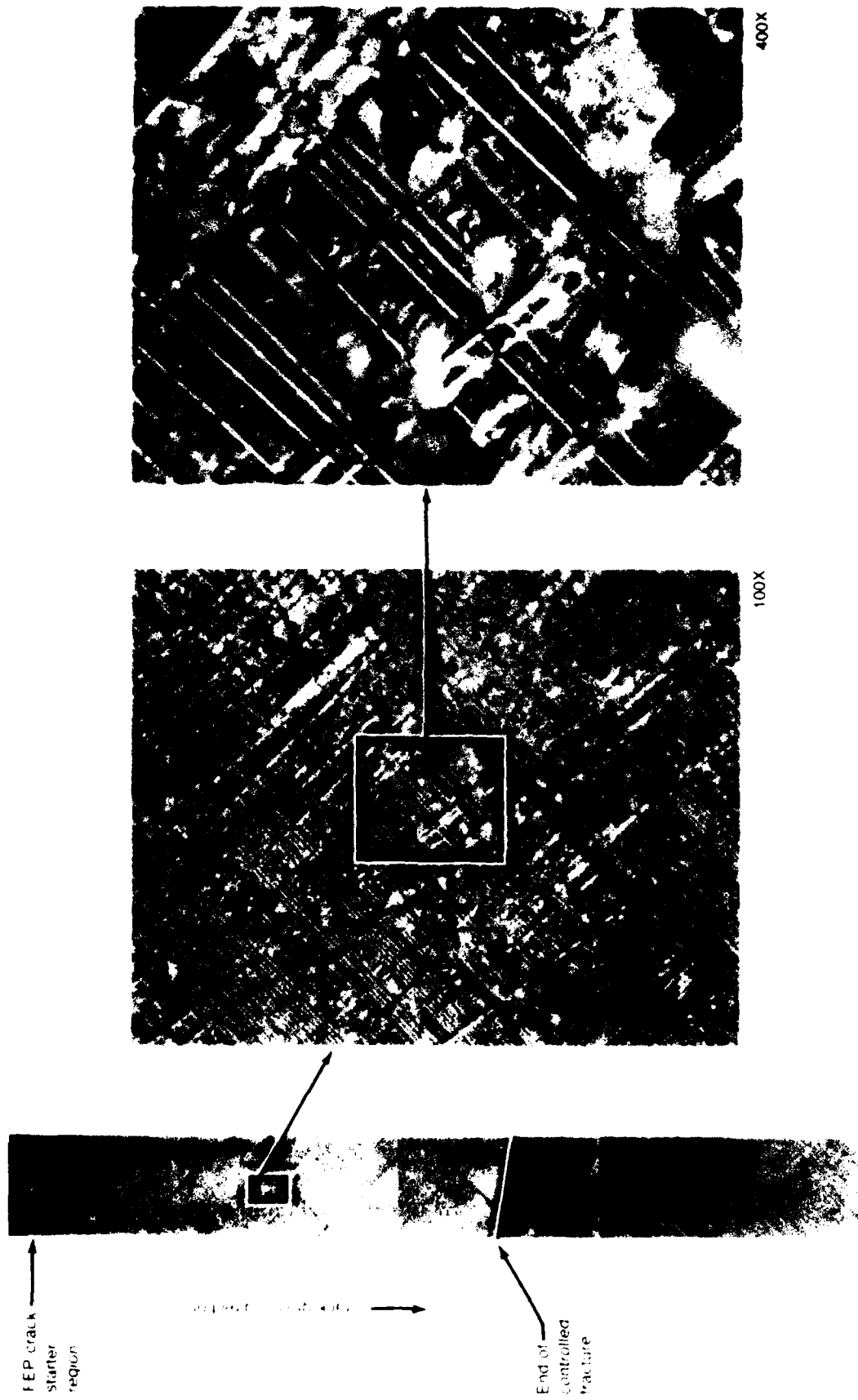
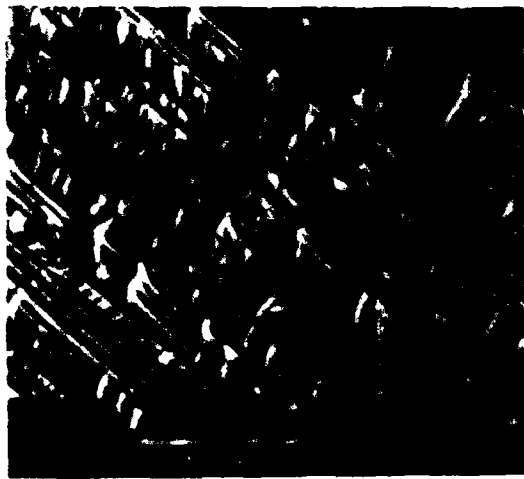


Figure 7-23. Optical Photomicrographs of Intended Fracture Plane Between +45/-45-Degree Plies, ENF 21°C (70°F) Specimen



Mechanically induced crack direction

- Legend
- F Fiber matrix separation
 - H Hackles
 - R River markings

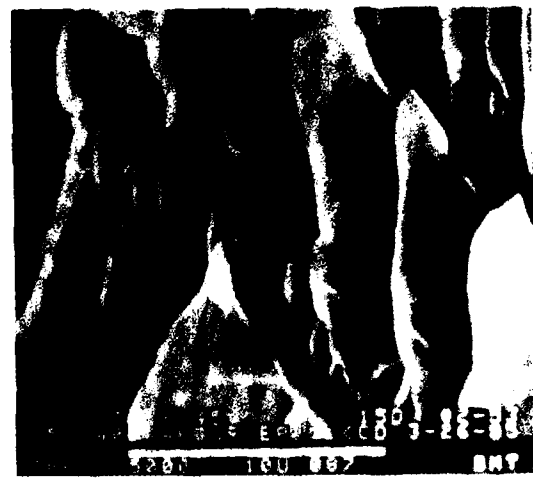
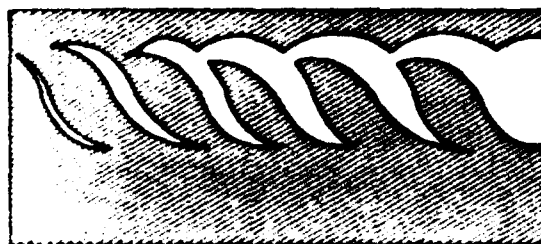


Figure 7-24. SEM Fractographs of Mode 2 (Shear) Delamination Between +45/-45-Degree Plies

hackle formation appears to occur from the initiation and growth of S-shaped microcracks in the direction of macroscopic crack growth. This condition supports the interpretation of hackle separation by mechanism A.

o Mode 2, 0/+45-Degree Interface

Typical fracture surface features characteristic of mode 2 delaminations for the 0/+45-degree cross-ply interface are presented in Figures 7-26 (optical) and 7-27 (SEM). No out-of-plane crack divergence was observed in these specimens. Similar to the interlaminar shear 0/0-degree interfacial fractures, the mode 2 topographies are much rougher and exhibit more fiber/matrix separation than those observed for mode 1 fractures. High-



←
Mechanically induced crack direction



Figure 7-25. Fractographs of Mating Fracture Surfaces Produced Under Mode 2 Between +45/-45-Degree Plies. (Hackle Separation Occurs by Mechanism A, in Which Hackles (H) Are Retained on One Side, Tilted Coincident With the Direction of Crack Growth)

magnification optical inspection of the resin fracture zones between fibers reveals translucent, parallel resin particles, whose axes are aligned normal to the direction of imposed crack propagation. No river mark branching is present. It was concluded that optical microscopy can be used to accurately identify mode 2 fractures and differentiate this load condition from mode 1 delaminations of these cross-ply interfacial orientations.

As illustrated in Figure 7-27, the fracture morphology produced between 0- and 45-degree plies is consistent with the mode 2 morphology discussed above. Similarly, this hackled

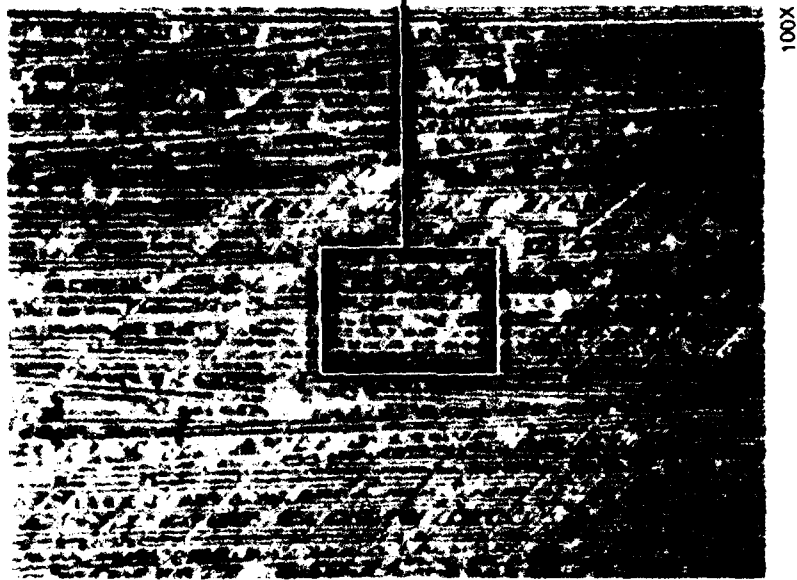
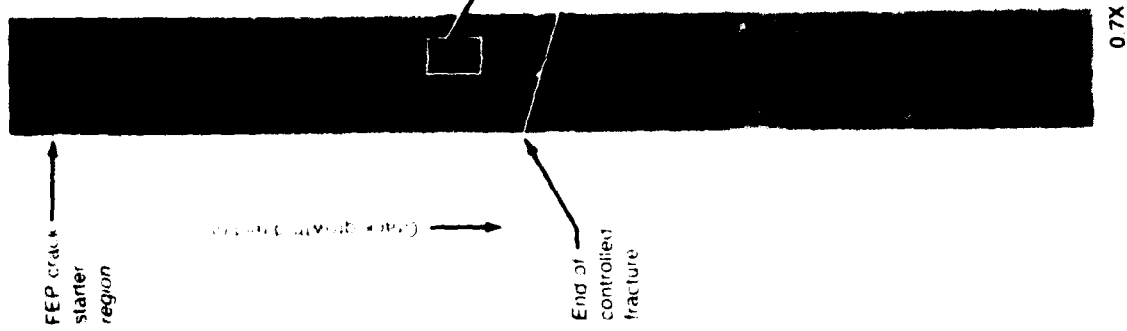
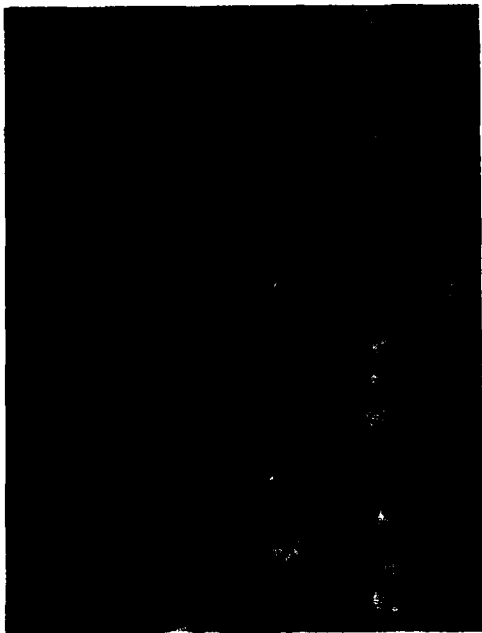


Figure 7-26. Optical Photomicrographs of Intended Fracture Plane Between 0/45-Degree Plies, ENF 210C (700F) Specimen



Mechanically induced crack direction

Legend

- F Fiber matrix separation
- H Hackles
- R River markings
- T Textured microflow

Figure 7-27. SEM Fractographs Illustrating Delamination Produced Between 0/+45-Degree Plies Under Mode 2 Loading

morphology exhibits intermittent areas of scalloped matrix fracture. The mating side to this fracture surface has not been examined; however, consistent with previous findings, the hackles visible in Figure 7-27 are tilted normal to the direction of locally resolved tension, and coincident with the direction of mechanically induced crack growth.

The overall morphology of hackled and scalloped areas for this ply orientation appears similar to that noted for the +45/-45-degree fracture interface (Figure 7-24). As shown in Figure 7-27, there is a general tendency for the hackles to be somewhat elongated into a roughly triangular shape and exhibit river mark branching along only one side, at the fiber/matrix junction. It is likely that this triangular appearance is a result of single-sided crack initiation, since this single initiation point forms a distinct apex and crack front expansion occurs during propagation. Reflecting this morphology, scalloped areas—particularly those visible in the upper left at 5000X—also tend to exhibit single-sided river branching and elongation into a roughly triangular shape. In general, areas with hackles exhibit an average direction of river-mark coalescence and microflow coinciding with the direction of mechanically induced crack growth. While not examined, areas of scallop formation on the mating fracture surface would be expected, coinciding with crack propagation direction.

Occasionally some scalloped areas on the hackled surface were found to have river marks microflow, which was examined. Consistent with the hackle separation mechanisms, the direction of river marks and microflow in these occasional regions opposed the direction of induced crack propagation. The behavior is indicative of overall separation by mechanism A, with some localized areas of separation by mechanism B (as verified by the presence of a few scallops on the side that was examined). Further examinations of the mating fracture half will be conducted to verify these observations and establish the ability to identify clearly the direction of crack propagation by using the features discussed above. It should be noted that the extent of either A or B hackle separation mechanisms will directly control the value of using river marks and microflow for the determination of crack propagation directions; i.e., the further from either pure A or B mechanisms, the less value and confidence an investigator can place on data gained from river marks and microflow.

o **Mode 2, 90/90-Degree Interfacial Fractures**

Macroscopic and microscopic examination of these specimens revealed that fracture did not occur on the intended interface between the 90/90-degree plies. Rather, the crack

diverged into the adjacent 0/90-degree interface and remained in this plane throughout the entire specimen length. The typical fracture surface features are presented in Figures 7-28 (optical) and 7-29 (SEM), and are identical to those found in the 0/90-degree specimens.

7.3.3 Environmental Effects on Interlaminar Mode 1 and 2 Fracture Features

Environmental effects on interlaminar mode 1 and 2 fractures did not significantly alter characteristics observed in resin fracture morphology. However, some distinct changes were observed in the degree of fiber/matrix adhesion under certain environmental conditions.

Nonetheless, for mode 1 delaminations, examination of river mark branching and resin microflow is a reliable means for determining the load state and crack propagation direction for all environmental conditions. Similarly, mode 2 delaminations exhibit hackles and scallops that are indicative of this fracture mode for all environmental conditions evaluated.

One significant effect is the pronounced increase in fiber/matrix separation at elevated temperature and moisture conditions, for both mode 1 (tension) and mode 2 (shear) fractures. Typically, lower temperature fractures (such as -54°C (-65°F) dry and 21°C (70°F) dry/wet) appear very similar to one another for each fracture mode and cross-ply type. These lower temperature fractures tend to occur within the resin-rich zones between laminae. Conversely, the higher temperature fractures (82°C (180°F) and 132°C (270°F) dry/wet) appear similar to one another for each fracture mode and cross-ply type. Fractures at these elevated temperatures tend to occur within, or adjacent to, densely packed fiber regions within the laminae, resulting in a fiber-dominated fracture appearance, with small, localized regions of resin fracture.

o Interlaminar Tension Fracture Features

Interlaminar fractures typically exhibit a mixture of flat, cohesive resin fracture and zones of fiber/matrix separation. Environmental effects markedly increase the level of fiber/matrix separation with increasing temperature and absorbed water content. This

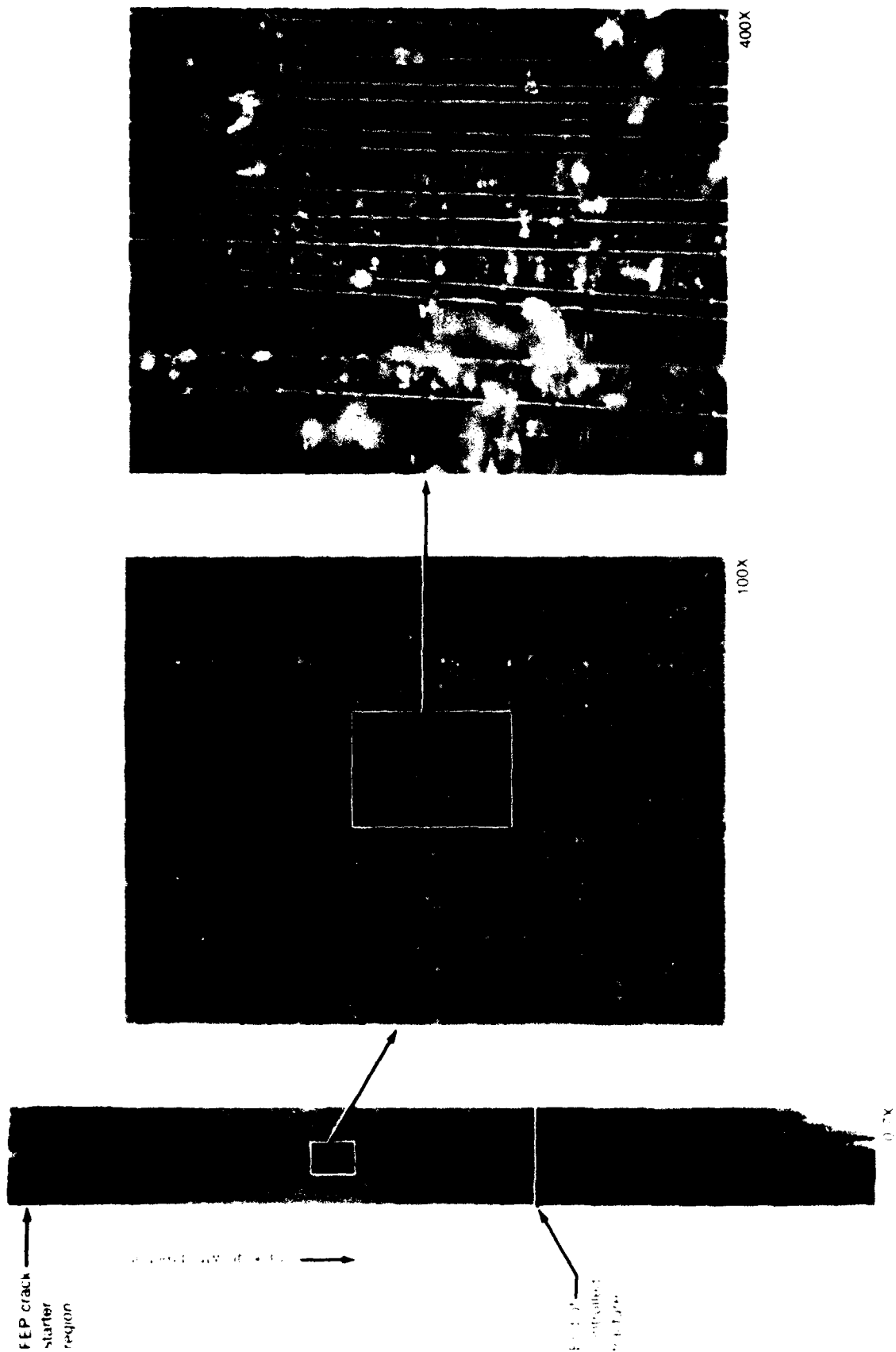
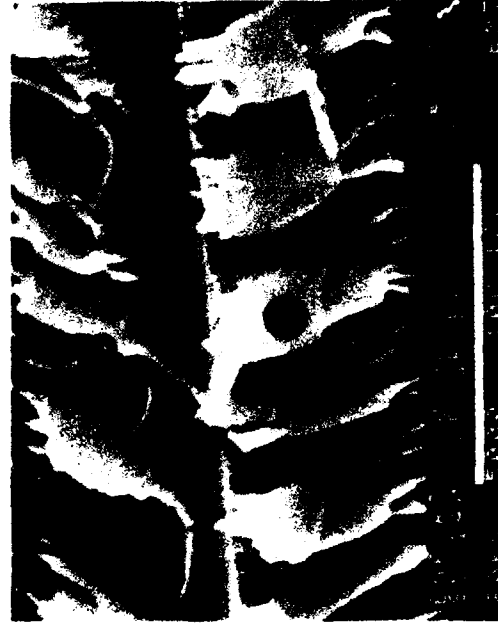
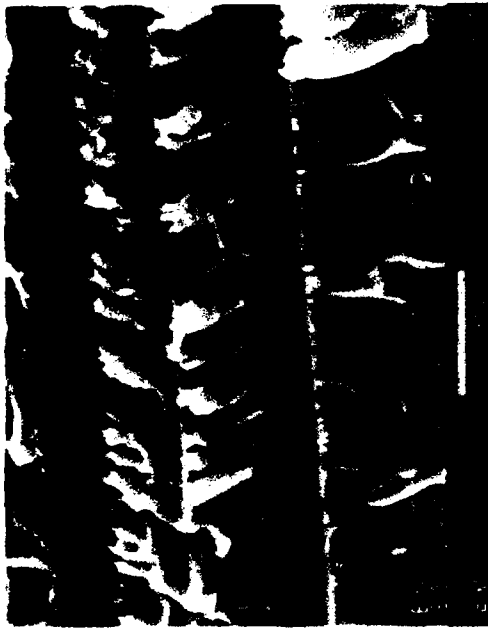


Figure 7-28. Optical Photomicrographs of Intended Fracture Plane Between 0/90-Degree Plies, ENF 210C (700F) Specimen



Mechanically induced crack direction



- Legend
- F Fiber matrix separation
 - H Hacksles
 - R River markings

Figure 7-29. SEM Fractographs of Mode 2 Delamination Produced for 90/90-Degree Specimen (Separation Occurred Along Either the Adjacent 0- and 90-Degree Interface or Within the 0-Degree Ply.)

trend is illustrated in Figures 7-30 and 7-31, in which the effects of environment are listed for fractures produced between adjacent 0-degree plies. The fracture topographies characteristic of -54°C (-65°F) dry and 21°C (70°F) wet appear similar to one another and similar to the 21°C (70°F) dry results presented in Section 7.3.1. All exhibit large amounts of flat resin fracture divided into relatively large longitudinal areas by zones of fiber/matrix separation. The 82°C (180°F) dry/wet specimens are also similar to the lower temperature specimens, with a slightly greater amount of exposed fibers. Microscopic examinations of 132°C (270°F) dry and wet specimens indicated that these elevated temperature fractures are similar to one another, although quite different from the -54°C (-65°F) dry and 21°C (70°F) fractures. All 132°C (270°F) fracture topographies are characterized by significantly larger amounts of exposed fiber/matrix separation. Consequently, a corresponding decrease in the size and amount of flat-resin matrix-fracture zones is evident. Fractures at 132°C (270°F), dry and wet, result in large amounts of randomly oriented fibers, apparently pulled out from the surrounding matrix, scattered over the fracture surface. Macroscopically, the 132°C (270°F) fracture surfaces appear distinctly different than those generated at -54°C (-65°F) and 21°C (70°F) because of these easily visible pulled-out fibers.

Similar to the 0/0-degree interfaces, interlaminar fractures exhibit increasing amounts of fiber/matrix separation with increasing temperature and absorbed water content. As illustrated in Figures 7-32 through 7-37, the -54°C (-65°F) dry, 21°C (70°F) wet, and 82°C (180°F) dry/wet fracture conditions appear similar. In general, for these lower temperature conditions, regions of cohesive resin fracture appear somewhat smaller than those noted for adjacent 0-degree fractures, and are divided into discrete regions by areas of exposed cross-ply fiber/matrix separation. The fracture surfaces generated at 132°C (270°F) dry and wet conditions for each cross-ply configuration appear distinctly different than those generated at lower temperatures. These figures show that the overall fracture surface topography is dominated by large amounts of fiber/matrix interfacial fracture, with occasional regions of cohesive matrix fracture; randomly pulled-out fibers (similar to the 0/0-degree interface fractures noted above) are visible without magnification.

For all cross-ply interface orientations, increasing amounts of fiber/matrix separation is manifested by crack propagation in, or immediately adjacent to, densely packed areas of fibers within the laminate ply. However, at lower temperatures, the fracture plane occurs within the thin, resin-rich zones between plies. In general, the phenomenon of increasing fiber/matrix separation is consistent with behavior observed for graphite/epoxy



82 C (180 F) Dry



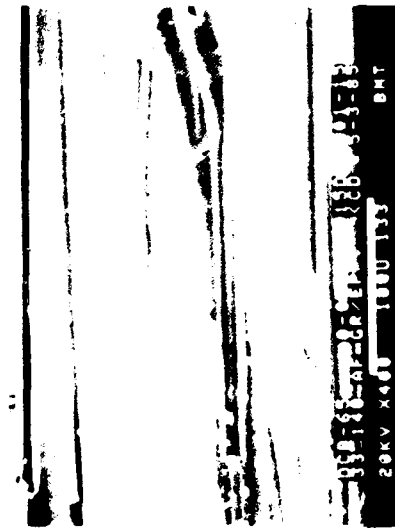
132 C (270 F) Wet



21 C (70 F) Wet



132 C (270 F) Dry



54 C (125 F) Dry



92 C (198 F) Wet

←
Mechanically induced crack direction

Figure 7-30. Low Magnification Series of Characteristic 0/0-Degree Interface Mode I Fractures at Each Environmental Condition



82°C(180°F) Dry



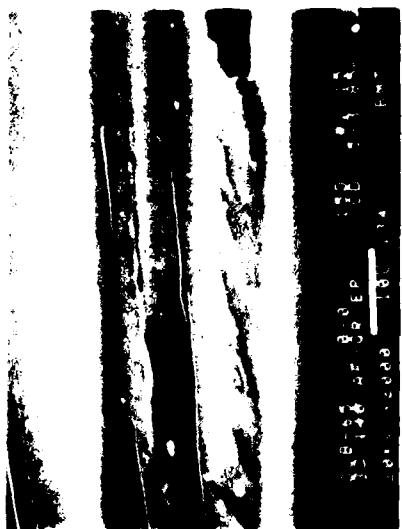
132°C(270°F) Wet



21°C(70°F) Wet



132°C(270°F) Dry



50°C(115°F) Dry



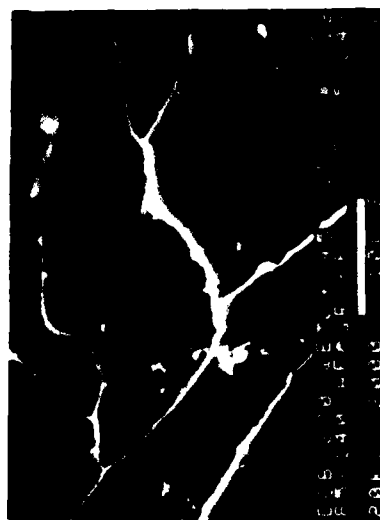
82°C(180°F) Wet

← Mechanically induced crack direction

Figure 7-31. Higher Magnification Series of 0/0-Degree Interface Mode 1 Fractures Presented in Figure 7-30 Showing Features of Fiber/Matrix (F) Separation and River Markings (R)



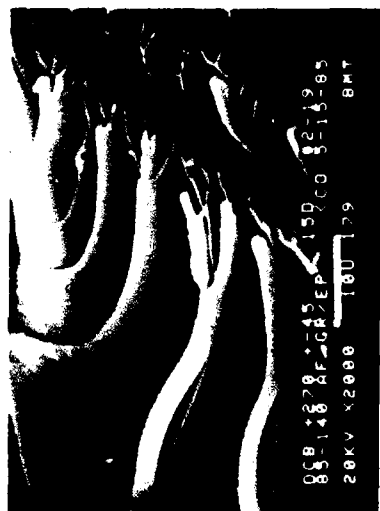
82°C(180°F) Dry



132°C(270°F) Wet



21°C(70°F) Wet



132°C(270°F) Dry

←
Mechanically induced crack direction

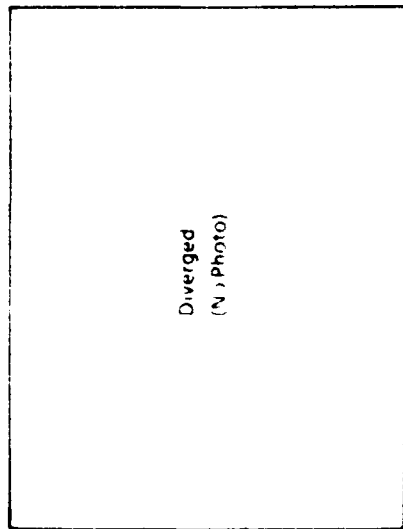


-54°C(-65°F) Dry



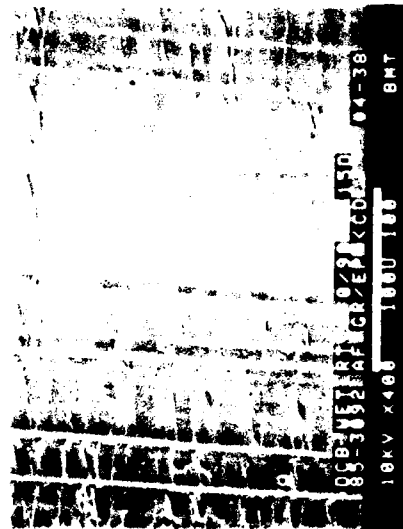
82°C(180°F) Wet

Figure 7-33. Higher Magnification Series of +45/-45-Degree Interface Mode I Fractures Presented in Figure 7-32 Showing Features of Fiber/Matrix (F) Separation and River Markings (R)



Diverged
(No Photo)

82°C (180°F) Dry



Diverged
(No Photo)

21°C (70°F) Wet

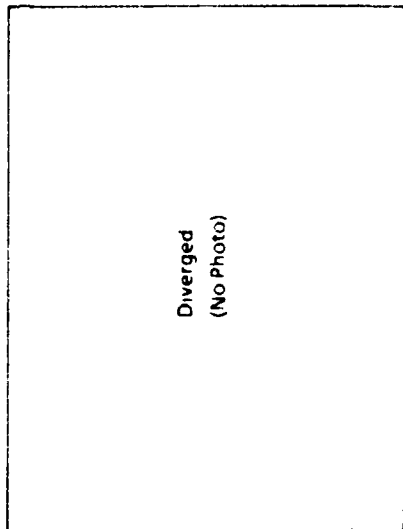


Diverged
(No Photo)

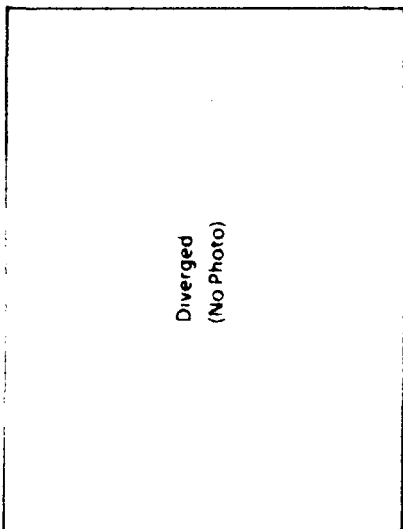
54°C (125°F) Dry



132°C (270°F) Wet



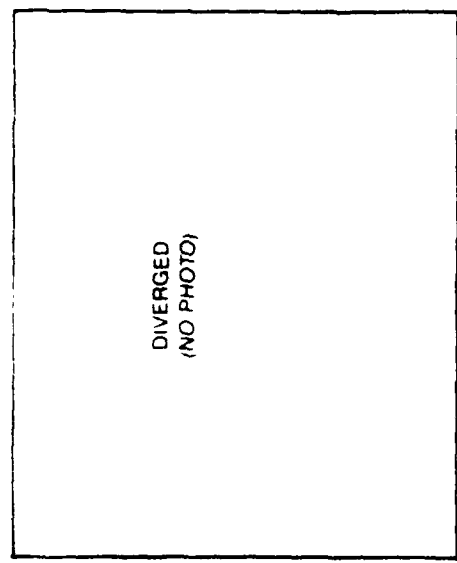
132°C (270°F) Dry



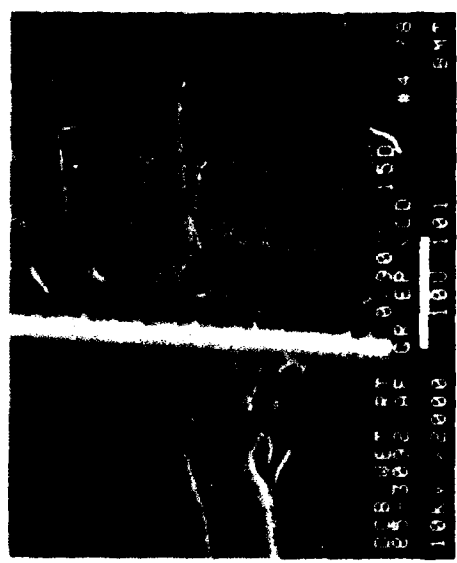
82°C (180°F) Wet

←
Mechanically induced crack direction

Figure 7-34. Low Magnification SEM Series of Characteristic 0/90-Degree Mode 1 (Tension) Fractures at E_2 -h Environmental Condition



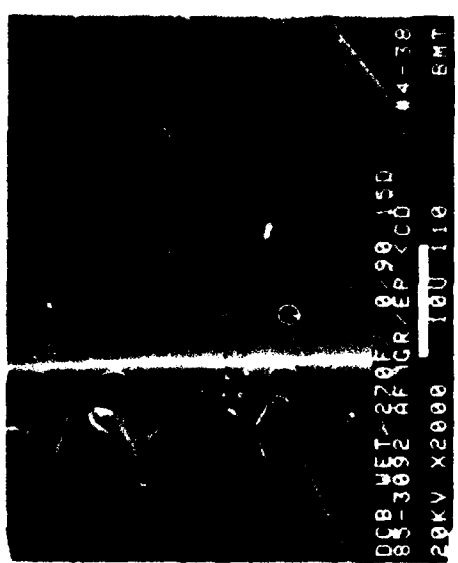
82°C(180°F) Dry



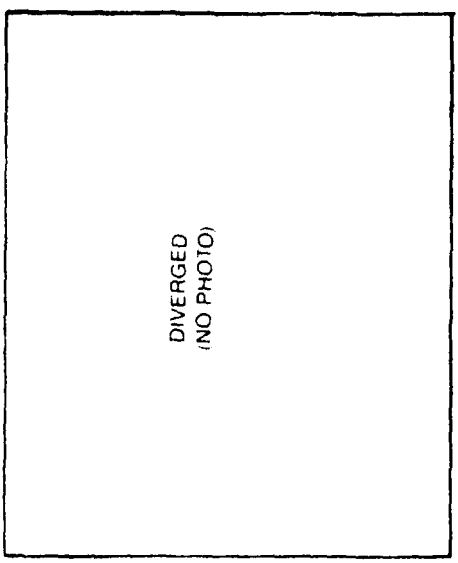
21°C(70°F) Wet



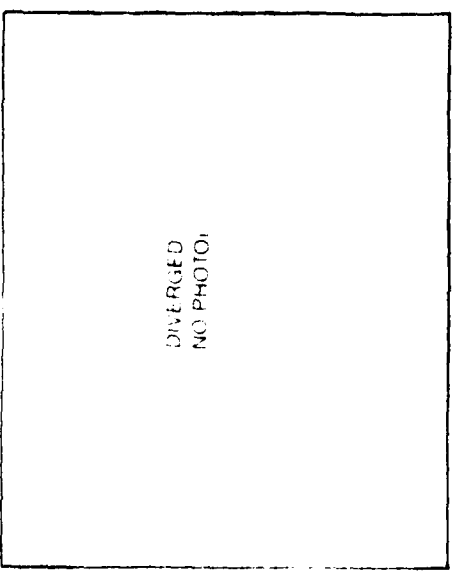
-54°C(65°F) Dry



132°C(270°F) Wet



132°C(270°F) Dry



82°C(180°F) Wet

Mechanically induced crack direction

Figure 7-35. Higher Magnification Series of 0/90-Degree Interface Mode 1 (Tension) Fractures Presented in Figure 7-34 Showing Features of Fiber/Matrix (F) Separation and River Markings (R)

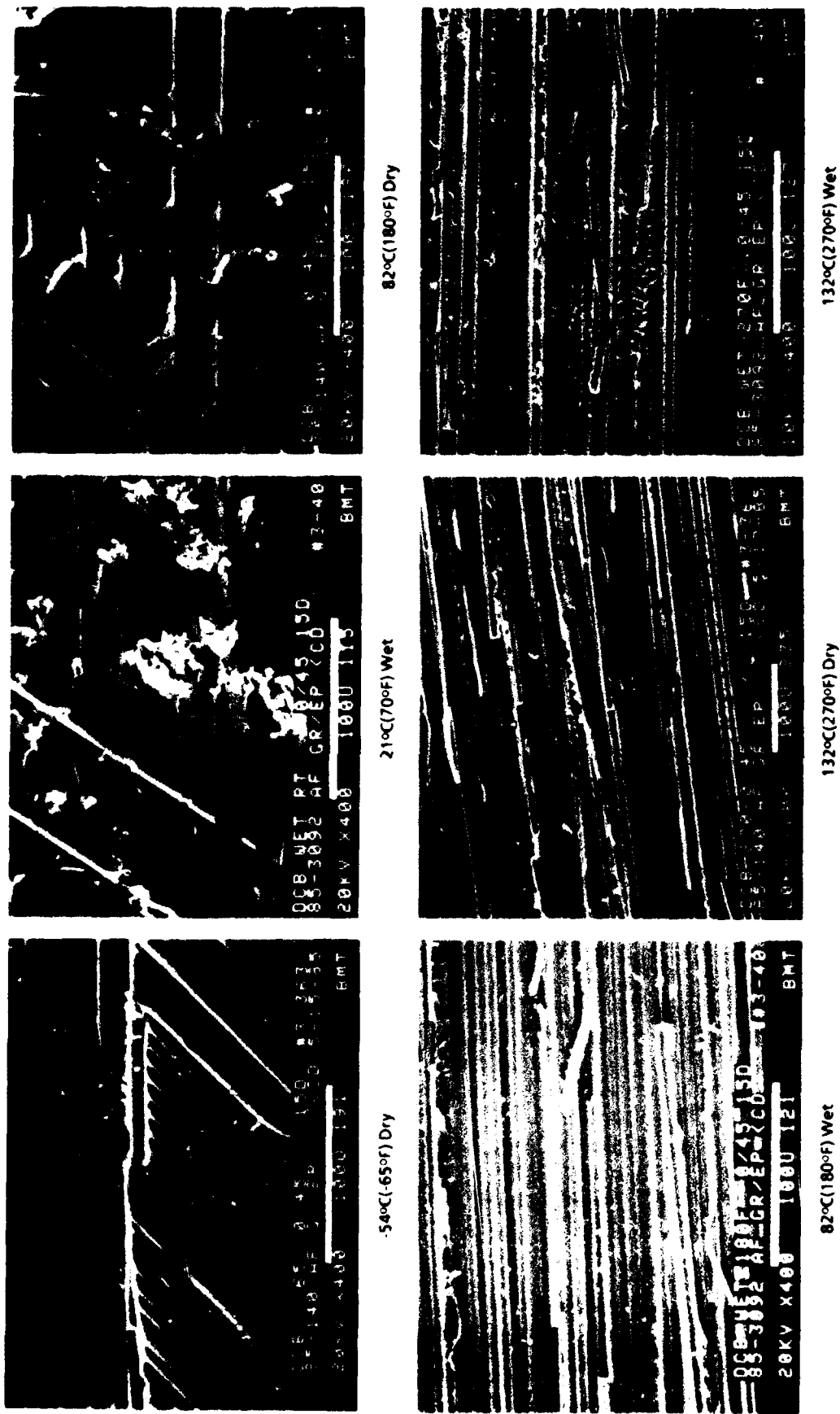
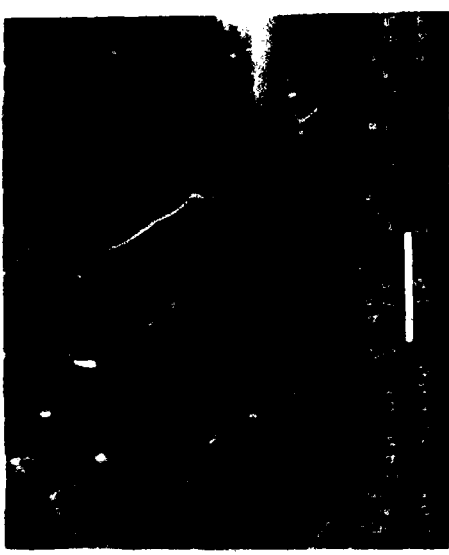
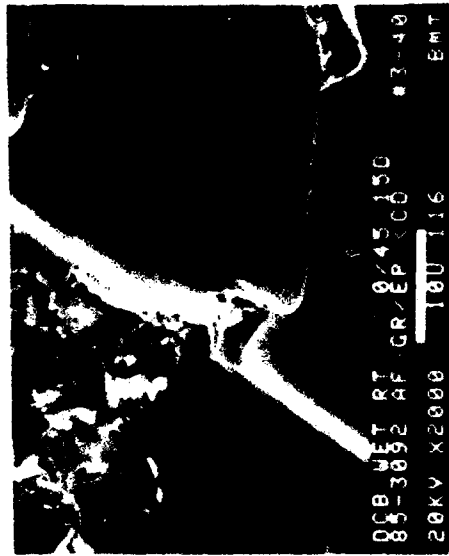


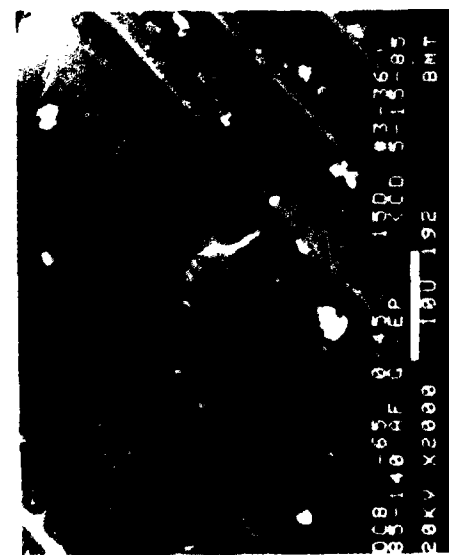
Figure 7-36. Low Magnification SEM Series of Characteristic 0/45-Degree Interface Mode I Fractures at Each Environmental Condition



82°C(180°F) Dry



21°C(70°F) Wet



54°C(125°F) Dry



132°C(270°F) Wet



132°C(270°F) Dry



82°C(180°F) Wet

←
Mechanically induced crack direction

Figure 7-37. Higher Magnification SEM Series of 0/45-Degree Interface Mode 1 Fractures Presented in Figure 7-36 Showing Features of Fiber/Matrix (F) Separation and River Markings (R)

translaminar tension fractures. In the investigation by Miller and Wingert, increasing amounts of fiber pullout and fiber/matrix interfacial fracture were observed with increasing temperature and absorbed moisture (see Figure 4-2 in the literature survey section on fractography). This behavior, observed for both interlaminar and translaminar tension fractures, suggests that a decrease in fiber/matrix interfacial strength occurs with increasing temperatures and moisture content. However, an alternate explanation may be that increased matrix resin toughness and ductility results in an increased resistance to crack propagation within the resin rich zones. Most likely, a combination of these two material properties influence the crack divergence into the fiber-dominated laminate. However, further studies must determine the dominant causative factor for this phenomena.

As noted in Section 7.3.1 regarding 21°C (70°F) dry fractures, river markings and resin microflow appear to be characteristics of flat, cohesive-matrix fracture zones. At 21°C (70°F) dry, these features provide a means of determining the direction of local crack propagation for interlaminar tension fractures. Examination of these dry fractures revealed that river mark branch coalescence and microflow progression coincide with the direction of induced crack propagation. Also, environmental conditions do not significantly alter these characteristics, even at extremes of -54°C (-65°F) dry or 132°C (270°F) wet, for all cross-ply orientations. Therefore, it can be concluded that examination of river markings and resin microflow provides an accurate means for determining the direction of crack propagation for all cross-ply orientations and for every environmental condition evaluated in this study.

Although significant alterations in the direction of crack propagation do not occur, there is some variation in local regions. Local variation is evident at 132°C (270°F) dry/wet for all ply orientations. For elevated temperature delaminations, local zones exhibit significant alterations in the direction of river mark branching with respect to the known direction of induced crack propagation. In some cases, there is as much as a 95-degree variation in the localized crack propagation direction, probably attributable to local rotation of the crack front toward the nearest free surface (usually the immediately adjacent fiber/matrix interface). However, by averaging these local variations, or by examining only large areas of resin fracture (see Section 7.3-1, Interlaminar Mode 1, Tension, 21°C (70°F) Mode 1, +45/-45-degree interface) the direction of river mark branching and resin microflow corresponds to the macroscopic direction of induced fracture.

o Interlaminar Shear Fracture Features

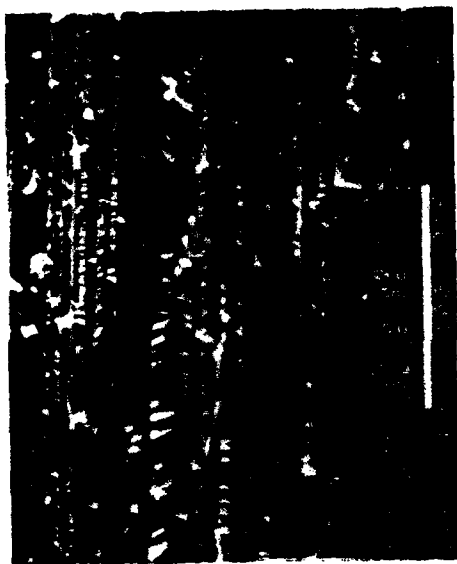
Similar to mode 1 (tension), fractures produced under mode 2 (shear) conditions typically exhibit a mixture of fiber/matrix separation and cohesive resin fracture. However, in contrast to the nearly flat matrix topography representative of mode 1, mode 2 cohesive matrix fractures exhibit characteristic hackles. These hackles provide a means to positively differentiate mode 2 from mode 1 fractures for all environmental conditions tested. In general, the effect of high temperature on mode 2 fractures is a pronounced increase in the amount of fiber/matrix separation, similar to that found for mode 1 (tension) fractures. However, such areas were not documented in the interest of recording the appearance of resin-dominated fracture features. The appearance of resin fracture features is illustrated in Figures 7-38 through 7-45, in which controlled fractures were produced between 0/0-, 0/90-, +45/-45-, and 0/45-degree interfaces at -54°C (-65°F) dry, 21°C (70°F) wet, 82°C (180°F) dry/wet and 132°C (270°F) dry/wet. The topographies characteristic of -54°C (-65°F), 21°C (70°F), and 82°C (180°F) fractures appear very similar. These lower temperature delaminations exhibit large amounts of fractured resin, in which long rows of inclined hackles are bounded by zones of fiber/matrix separation. In contrast, fractures produced under 132°C (270°F) dry and wet conditions are characterized by a significantly larger amount of fiber/matrix separation, and a corresponding decrease in the size and amount of resin-hackle features. The hackles are sometimes twisted and deformed, indicative of an increase in matrix ductility at elevated temperatures. As found for interlaminar tension, the 132°C (270°F) conditions result in pulled-out fibers scattered over the fracture surface; while not shown in the figures illustrated, these fibers could be seen at both a macroscopic and microscopic level. For each cross-ply orientation, delamination surfaces exhibit increasing amounts of fiber/matrix separation with increasing temperature and absorbed water content. This phenomenon is particularly evident in the lower magnification photomicrographs in which an overview of the fracture surface morphology can be seen.

7.4 TRANSLAMINAR FRACTURES

This section describes the surface features characteristic of translaminar fractures generated at room temperature (21°C (70°F)) under mode 1 tension and mode 1 compression loading conditions. For each loading type, the results of fractographic analysis are arranged in sequence based on the ply orientations studied in this program.



82°C(180°F) Dry



21°C(70°F) Wet



-54°C(-65°F) Dry



132°C(270°F) Wet



132°C(270°F) Dry



82°C(180°F) Wet

← Mechanically induced crack direction

Figure 7-38. Low Magnification SEM Series of Characteristic 0/0-Degree Interface Mode 2 (Shear) Fractures at Each Environmental Condition



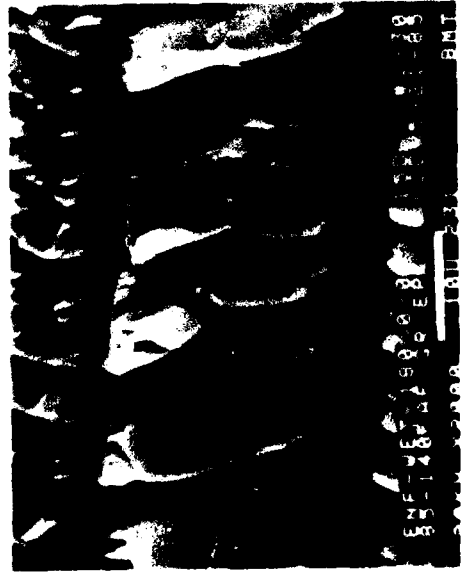
54°C (65°F) Dry



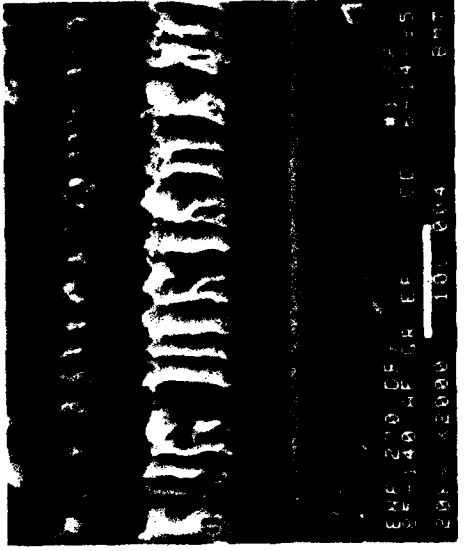
21°C (70°F) Wet



82°C (180°F) Dry



82°C (180°F) Wet



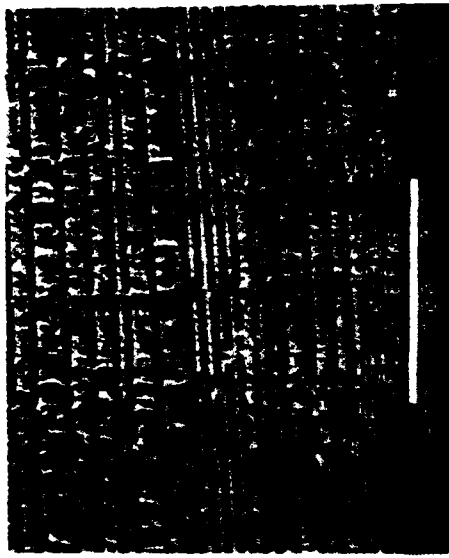
132°C (270°F) Dry



132°C (270°F) Wet

← Mechanically induced crack direction

Figure 7-39. High Magnification SEM Series of 0/0-Degree Interface Mode 2 (Shear) Fractures Presented in Figure 7-38 Showing Features of Fiber/Matrix (F) Separation and Hackles (H)



82°C(180°F) Dry



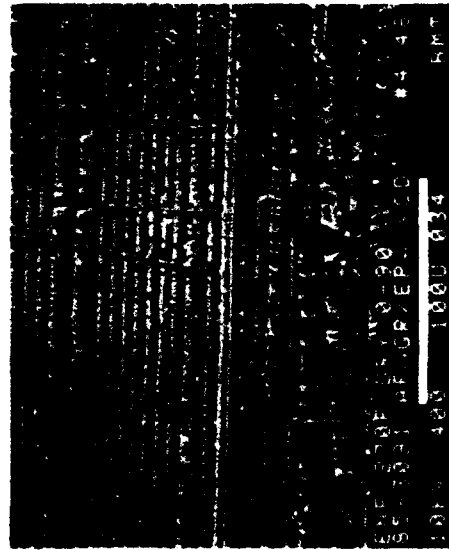
21°C(70°F) Wet



-54°C(-65°F) Dry



132°C(270°F) Wet



132°C(270°F) Dry



82°C(180°F) Wet

← Mechanically induced crack direction

Figure 7-40. Low Magnification SEM Series of Characteristic 0/90-Degree Interface Mode 2 Fractures at Each Environmental Condition

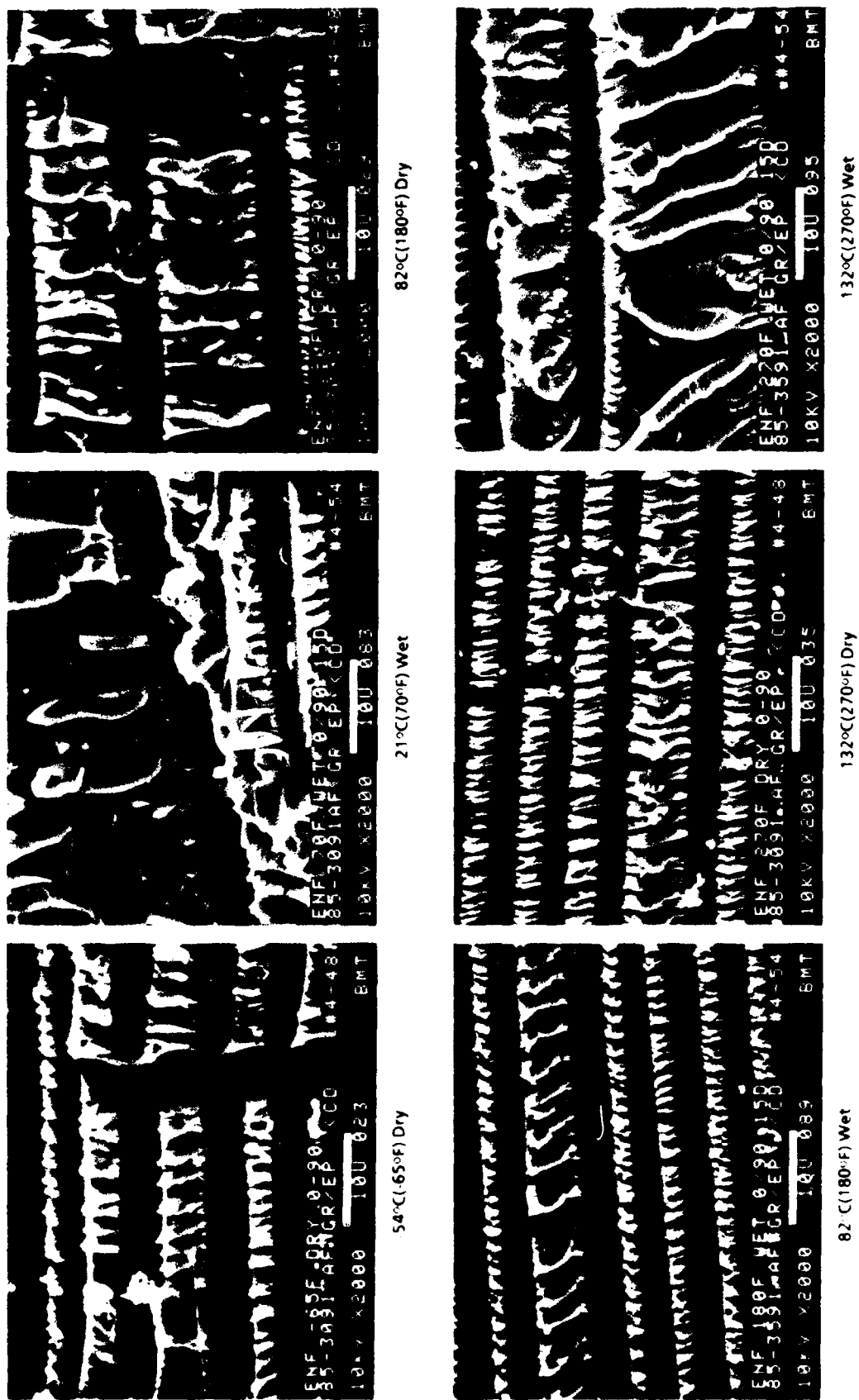


Figure 7-41. Higher Magnification SEM Series of 0/90-Degree Interface Mode 2 (Shear) Fractures Presented in Figure 7-40 Showing Features of Fiber/Matrix (F) Separation and Hackles (H)

AD-A172 236

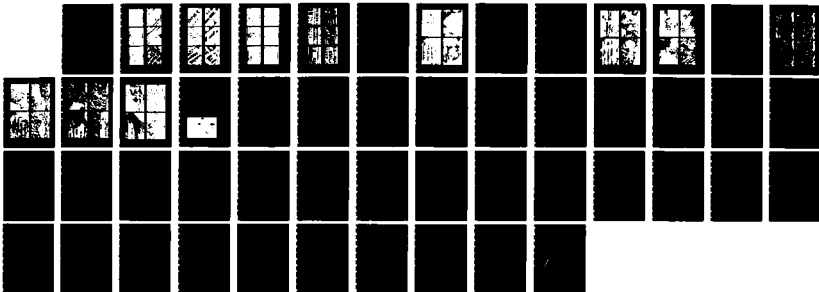
FAILURE ANALYSIS OF COMPOSITE STRUCTURE MATERIALS(U)
BOEING MILITARY AIRPLANE CO SEATTLE WA B SMITH ET AL.
MAY 86 AFMAL-TR-86-4033 F33615-84-C-5010

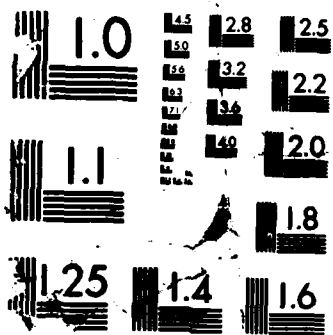
3/3

UNCLASSIFIED

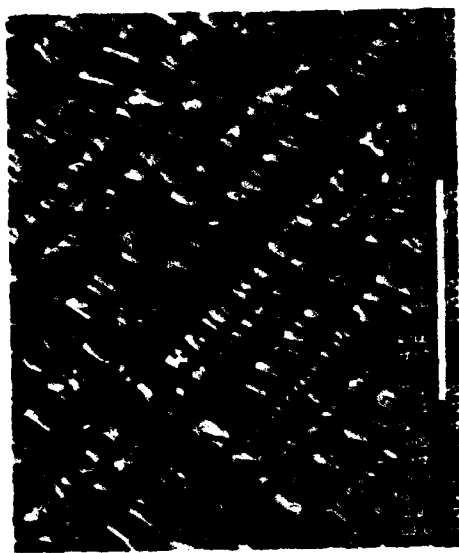
F/G 11/4

NL

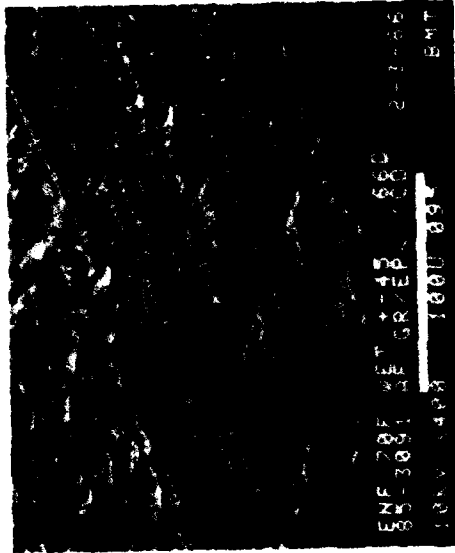




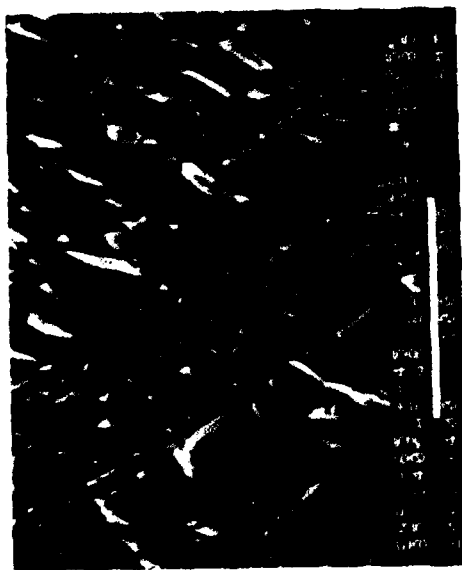
MICROCOPY RESOLUTION TEST CHART
NATIONAL BUREAU OF STANDARDS-1963-A



82°C(180°F) Dry



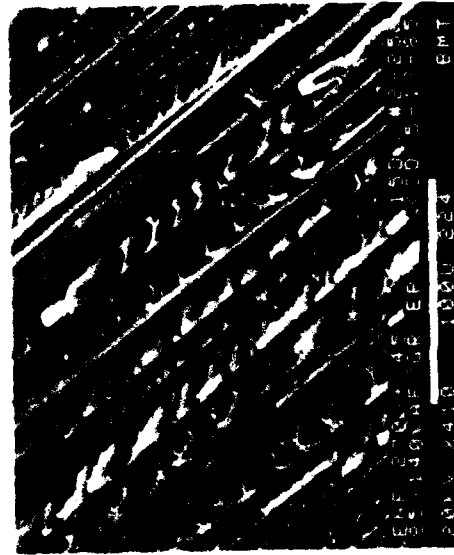
21°C(70°F) Wet



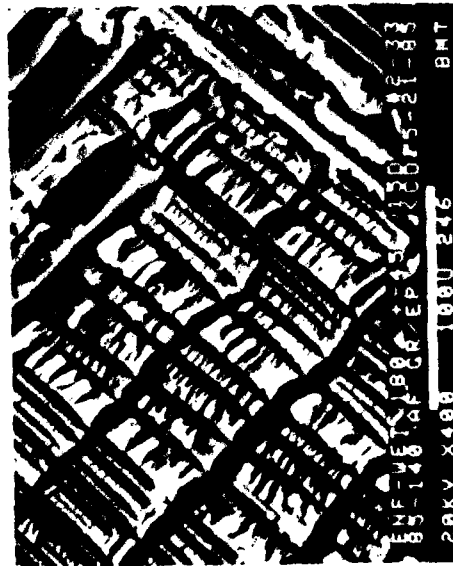
-54°C(-65°F) Dry



132°C(270°F) Wet



132°C(270°F) Dry



82°C(180°F) Wet

←
Mechanically induced crack direction

Figure 7-42. Low Magnification SEM Series of Characteristic +45/-45-Degree Interface Mode 2 Fractures at Each Environmental Condition



-54°C(65°F) Dry



21°C(70°F) Wet



82°C(180°F) Dry



82°C(180°F) Wet



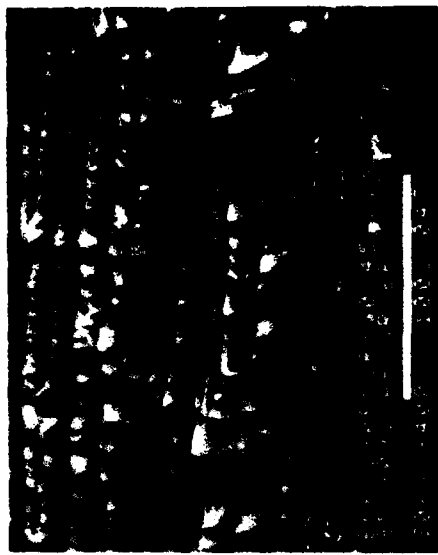
132°C(270°F) Dry



132°C(270°F) Wet

←
Mechanically induced crack direction

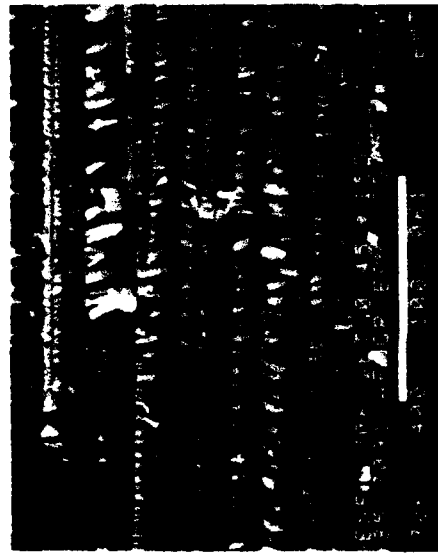
Figure 7-43. Higher Magnification SEM Series of +45/-45-Degree Interface Mode 2 (Shear) Fractures Presented in Figure 7-42 Showing Features of Fiber/Matrix (F) Separation and Hackles (H)



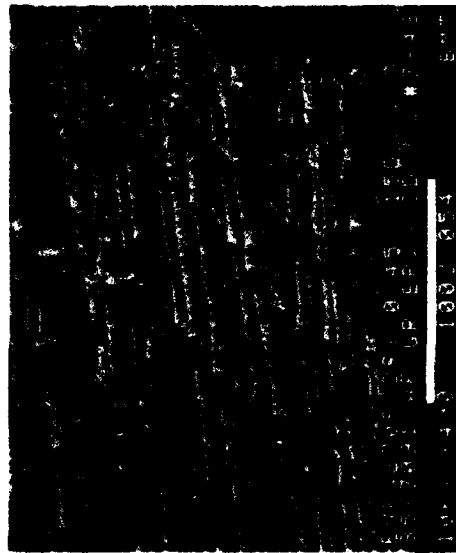
82°C(180°F) Dry



132°C(270°F) Wet



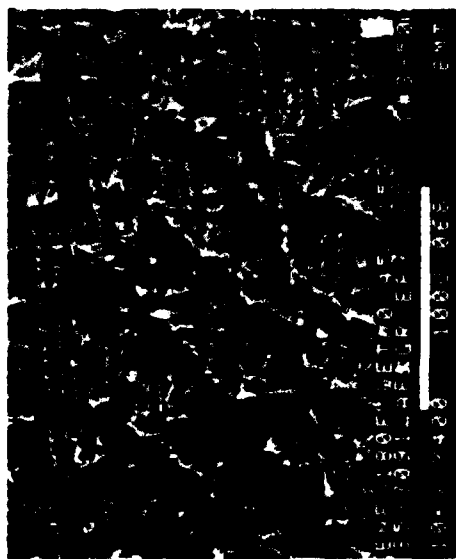
21°C(70°F) Wet



132°C(270°F) Dry



-54°C(-65°F) Dry



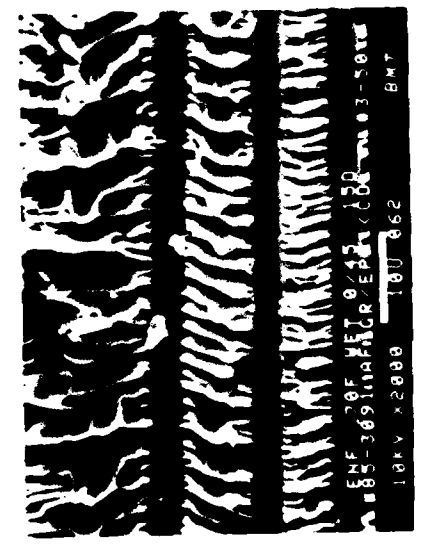
82°C(180°F) Wet

← Mechanically induced crack direction

Figure 7-44. Low Magnification SEM Series of Characteristic 0/45-Degree Mode 2 (Shear) Fractures at Each Environmental Condition



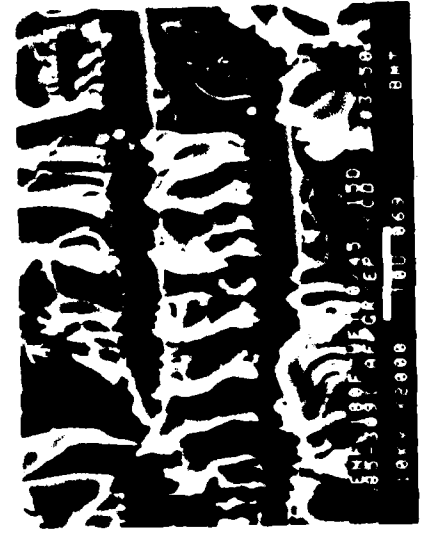
54°C(130°F) Dry



21°C(70°F) Wet



82°C(180°F) Dry



82°C(180°F) Wet



132°C(270°F) Dry



132°C(270°F) Wet

←
Mechanically induced crack direction

Figure 7-45. Higher Magnification SEM Series of 0/-45-Degree Mode 2 (Shear) Fractures Presented in Figure 7-44 Showing Features of Fiber/Matrix (F) Separation and River Markings (R)

7.4.1 Translaminar Mode I Tension—21°C(70°F)

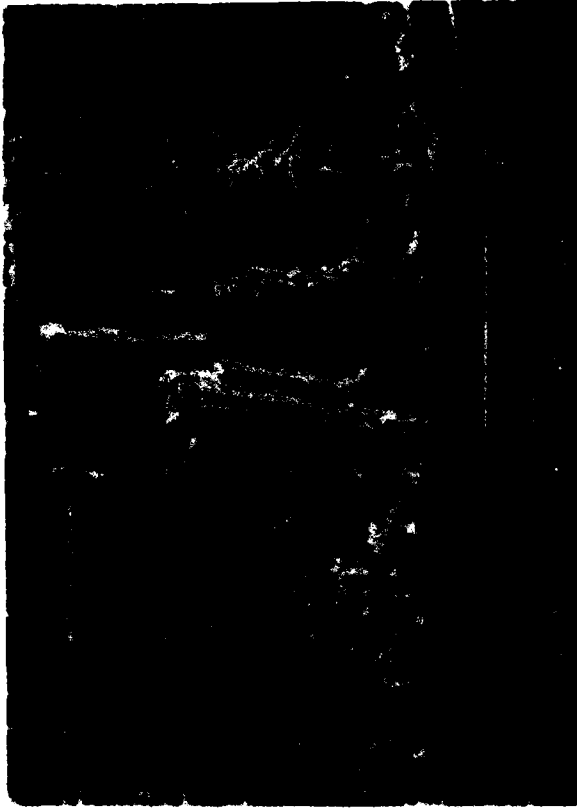
These transverse fiber fracture laminates, which have very high toughness properties, exhibited a considerable amount of gross postfracture damage. Microscopic inspection identified a combination of fiber fracture, fiber pullout, and matrix-resin fracture. The extent to which these features occurred depended greatly on the cross-ply orientation and the localized plane of fracture. The most striking aspect of the failures was the existence of broken and pulled out fibers which were much rougher than mode I. Typically, the surface exhibited a fiber-fracture dominated appearance, and was much rougher than mode I compression fractures (discussed in the following section). The combination of observed features for both resin and fiber fracture was found to be unique to translaminar tension, and provided a means for identifying both the localized and overall direction of fracture.

o Mode I, 0/90-Degree Cross-ply Laminate

The typical surface characteristics of translaminar tension fractures generated across the 0/90-degree specimen is illustrated in Figure 7-46. Macroscopic examination of the overall surface revealed that fracture occurred at the intended plane: parallel to the 90-degree fiber orientation. Visual observation during testing revealed that cracking initiated at the specimen notch tip and progressed toward the specimen's opposite side.

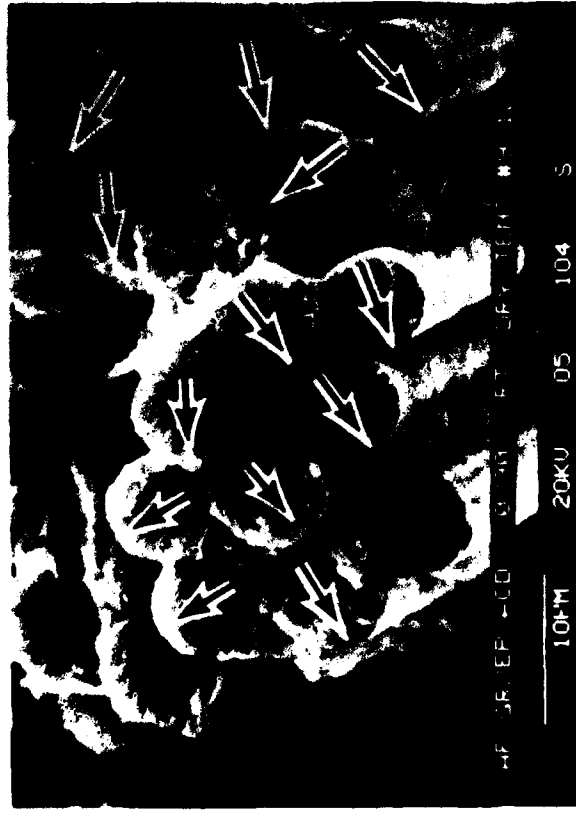
High-magnification optical and SEM analysis concentrated on the area adjacent to the initiation zone in an effort to stay as far away as possible from the compression side of this 4-point-loaded specimen.

High-magnification optical inspection included the areas of intralaminar matrix fracture within the 90-degree plies. Such areas typically appeared flat and exhibited pronounced river markings and resin microflow, similar to features found for the mode I 0/0-degree delamination specimens. For these fractures, river marks were observed running in the direction of induced cracking in the central portion of each 90-degree ply. However, at the 90-degree plies junction with 0-degree ply these river marks typically turned perpendicular to the direction of induced fracture, running toward the 0-degree bundles. This behavior suggests that 90-degree ply cracking occurs prior to 0-degree ply separation. This type of behavior has been fairly well documented in literature. In general, failure of these 90-degree plies exhibited a higher level of fiber/matrix separation and fiber breakage than that characteristic of interlaminar fractures. This condition probably occurs due to misalignment of the crack plane with the 90-degree fiber orientation (bridging).



50X

← Mechanically induced crack direction →



2000X

5000X

Figure 7-46. Translamellar Tension Fractures; 0/90-Degree Laminate

SEM examinations were principally focused on the fracture regions in which fiber bundles, pullout, and end-fracture features were evident (see Figure 7-46). 0-degree fibers tend to fracture in bundles or tiers, with each bundle having a relatively flat, common fracture zone. Fibers within the bundles, as well as individual pulled-out fibers, were found to have significant amounts of adhering matrix resin, indicative of good fiber/matrix adhesion and adhesive fracture. Detailed inspection of this adhering matrix resin revealed the presence of hackles, associated with mode 2 shear fracture. Examinations of the fractured end of each fiber revealed a radial morphology—axially diverging lines emanating from a single point. The radial morphology is analogous to the chevron patterns commonly recognized in brittle metals—particularly for fractured bar or rod forms. The appearance of chevrons in metals is associated with microscopic variations in the plane of fracture, aligned in the direction of local crack propagation, and diverging from the point of initiation. Based on this interpretation, the localized direction of crack propagation for each individual fiber fracture can be determined by examining the radial morphology. The initiation points—origins—were primarily located at flaws or notches in the crenulated fiber surfaces, although isolated origins were found at internal flaws such as voids. Crack propagation along the fiber ends did not progress by the development and motion of a well-defined crack front. This was evidenced by the variety of directions of radials within a given bundle, even to the point of opposite directions for adjacent fibers. However, through overall mapping of the fracture growth direction for the individual 0-degree fiber ends, it was determined that the direction of radial features coincided with the direction of induced fracture. As illustrated in the lower photomicrographs of Figure 7-46, the induced crack direction coincides with the general direction of fiber-end fracture (note arrows on fiber ends indicating individual fracture direction).

The above findings for this 0/90-degree ply orientation specimen indicate that SEM or optical analysis can be used to identify crack growth directions for matrix resin fracture within 90-degree plies. Similarly, SEM analysis can be used to determine localized crack growth directions of 0-degree fiber ends. By interpreting river marks and radial features, the general fracture direction can be determined for 0/90-degree translamellar fractures. It should be noted that extreme caution must be exercised in the extrapolation of isolated microstructural details to the overall process; therefore, a coherent approach and extensive analysis are required to ensure accurate crack mapping.

Mode I, +45/-45-Degree Cross-ply Laminate

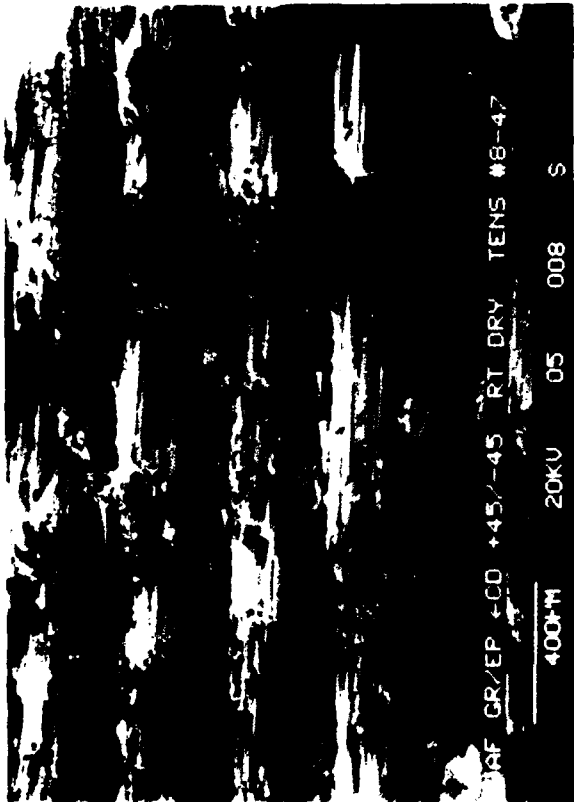
The typical surface characteristics of translaminar tension fractures generated in +45/-45-degree specimens are illustrated in Figure 7-47. Macroscopic examination of the overall surface indicated that fracture occurs at the intended plane, parallel to the 90-degree orientation. High-magnification optical and SEM analysis concentrated on the tensile-dominated initiation zone.

High-magnification optical analysis involved the areas of matrix resin fracture found on the sides of large bundles of +45- and -45-degree fibers. Such areas typically appear flat, and exhibit both river marks and hackles--with the latter feature in much greater abundance. This observation indicates that these intralaminar fractures separate in a mixed-mode-loading condition, not surprising considering the 45-degree angle-of-fracture with respect to the overall loading condition. The direction of coalescence of the river marks was found not to be oriented in any particular manner, and thus did not provide information of value in determining the direction of crack propagation.

The SEM photographs in Figure 7-47 show that the fracture surface consists primarily of large bundles of fibers which have a common, rather flat fracture plane. Each bundle of the +45/-45-degree laminates contained between 10 and 100 fibers, more fibers than were found in the 0/90-degree laminate. However, the fracture surface exhibited fewer single, standalone, pulled-out fibers than the 0/90-degree laminate. Most fibers had a significant amount of matrix resin adhering to them, indicating a good fiber/matrix adhesion and cohesive resin fracture. Examination of the fractured end of each fiber (for both the +45- and -45-degree bundles) revealed a radial morphology, and the average individual crack direction coincided with the direction of induced fracture (see bottom photomicrographs in Figure 7-47).

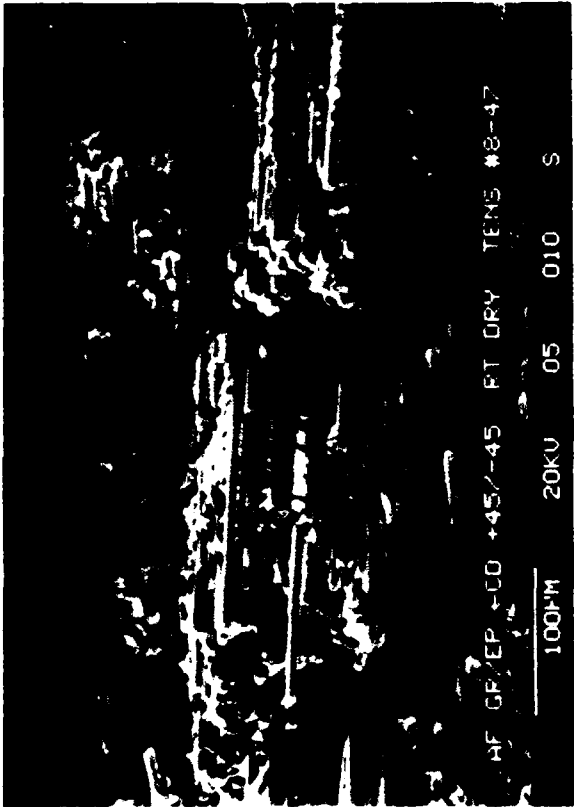
o Mode I, Quasi-Isotropic Laminate

The typical fracture surface characteristics of translaminar tension fractures generated in the quasi-isotropic specimens are illustrated in Figure 7-48. Similar to the other two laminates discussed previously, macroscopic examination verified that cracking occurs parallel to the 90-degree plies.



50X

→ Mechanically induced crack direction



200X



2000X

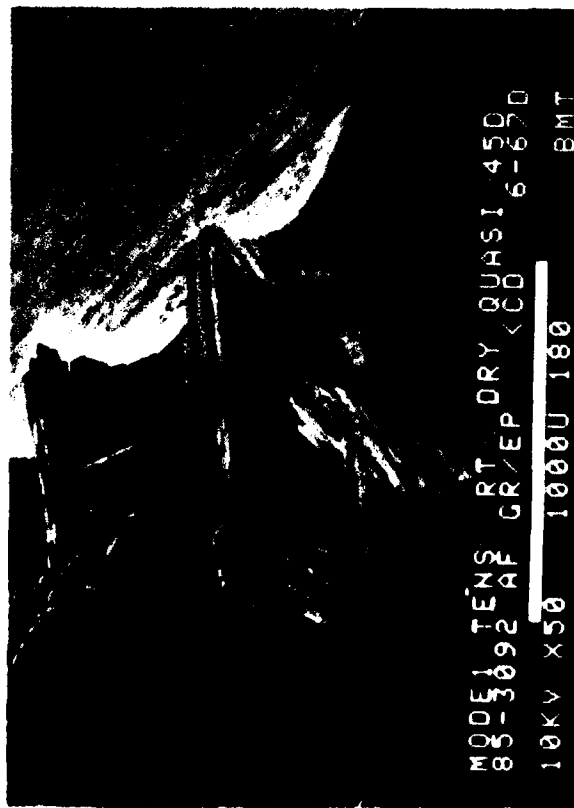
-45-Degree plies



2000X

+45-Degree plies

Figure 7-47. Translaminar Tension Fractures; +45/-45-Degree Laminate

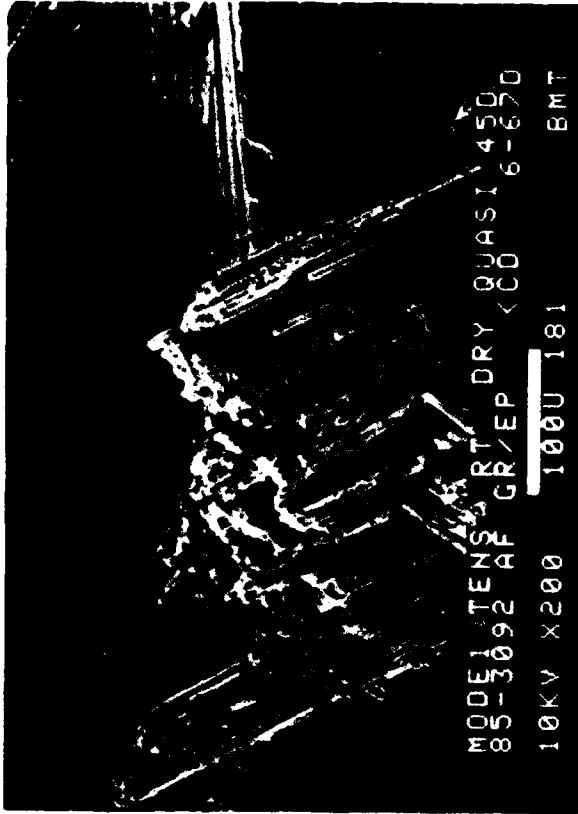


50X

← Mechanically induced crack direction →



200X



200X



500X

Figure 7-48. Translamellar Tension Fractures: Quasi-Isotropic Laminate

High-magnification optical inspection of the fracture surface involved the areas of intralaminar matrix fracture within the 90-degree plies. Such areas typically appear flat, and exhibit river marks and resin microflow—similar to features found for the 90-degree plies of the 0/90-degree laminate. The coalescence of river markings coincides with the direction of induced cracking.

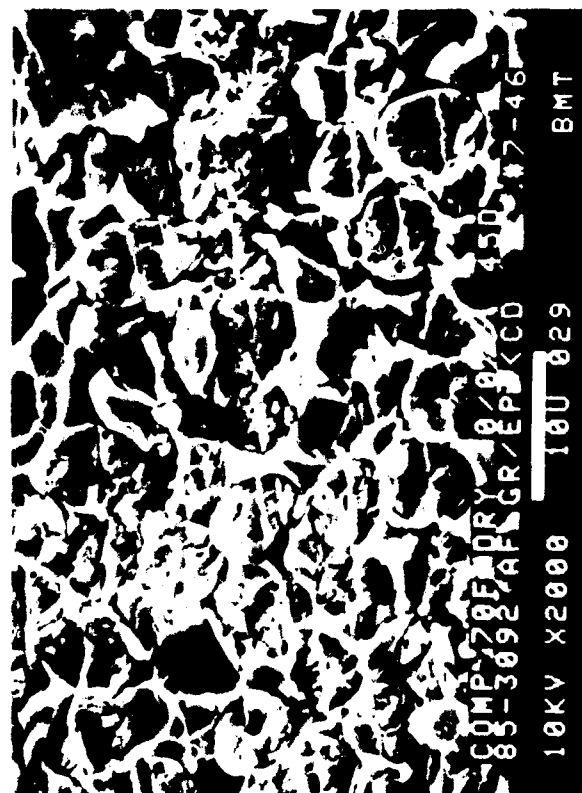
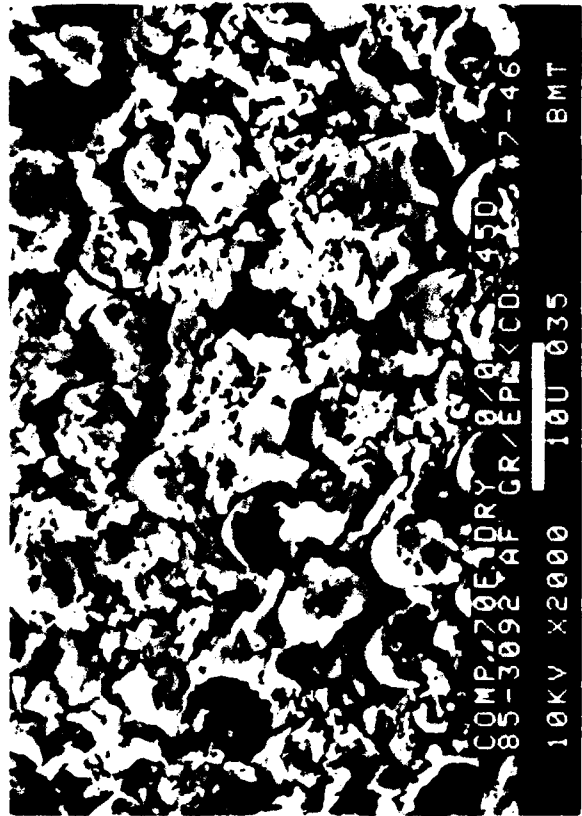
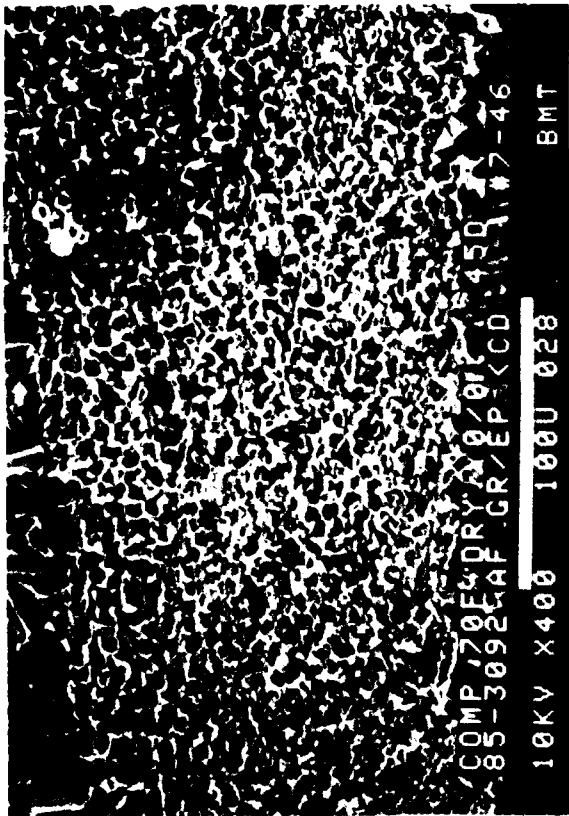
SEM examinations of the fracture regions revealed fiber bundles, pullout, and end fractures in the +45-, -45-, and 0-degree plies. These fiber fractures are very similar in appearance to the 0/90- and +45/-45-degree laminates, in that the fiber sides tend to have a fair amount of adhering matrix resin. The resin on the sides of the +45- and -45-degree bundles exhibited both river marks and hackles, indicating mixed mode fracture, whereas the 0-degree bundles exhibited resin hackles associated predominantly with shear fracture conditions.

Examination of the fiber ends for both 0- and 45-degree oriented fibers revealed a radial fracture morphology, as shown in the lower photomicrographs in Figure 7-48. In these photos, the fiber ends of a 45-degree bundle are illustrated. After thorough analysis of the fiber-end fractures, it was concluded that the average of the individual crack directions coincided with the direction of induced fracture. The findings presented above indicate that optical and/or SEM analysis can be used to identify river marks and radial features which define the overall direction of crack growth for quasi-isotropic translaminar fractures.

7.4.2 Translaminar Mode I, Compression, 21°C (70°F)

Fractographic analysis was performed on 4 different laminate types; each was subjected to mode I, 4-point loading. The laminates evaluated were: 0-degree (unidirectional), +45/-45-degree, 0/90-degree, and quasi-isotropic. The features characteristic of translaminar mode I fracture surfaces are presented for each laminate type in Figures 7-49 through 7-52.

Macroscopic and optical microscopic examinations revealed a distinct, flat fracture that occurred on the intended plane. The surface was much flatter than those of translaminar tension fractures, and was virtually devoid of pulled-out fibers. This flat fracture morphology can be seen in the upper left photomicrographs of Figures 7-49 through 7-52, and is most visible in Figure 7-49 of the unidirectional laminate. SEM examination



← Mechanically induced crack direction

Figure 7-49. Translaminar Compression Fractures; Unidirectional 0-Degree Laminate

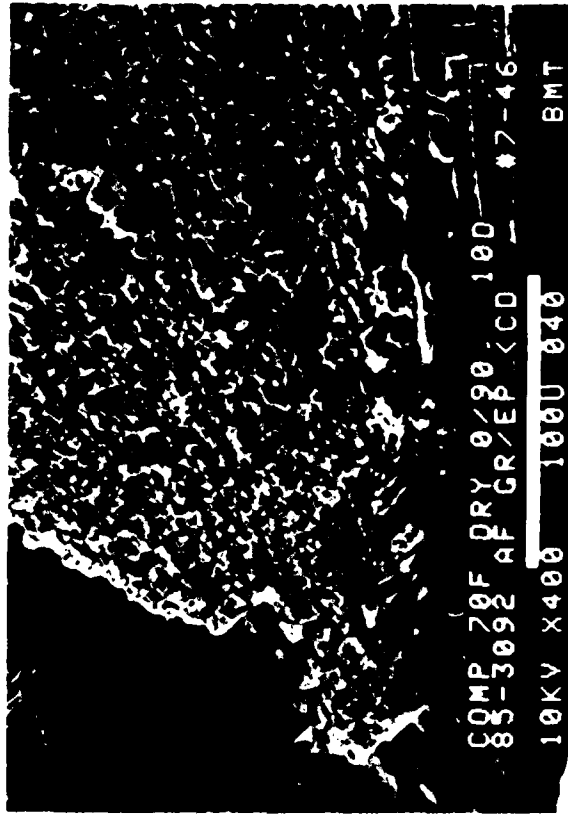


50X

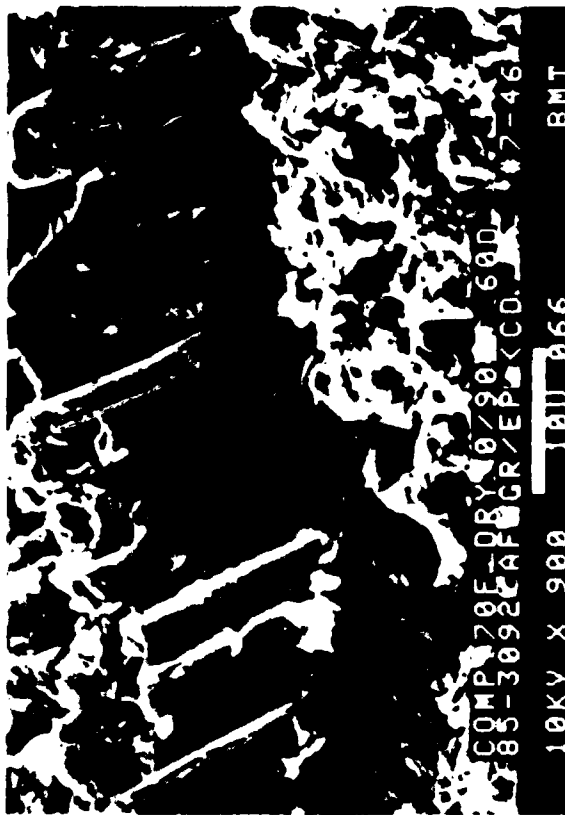
← Mechanically induced crack direction →



2000X



400X



900X

Figure 7-50. Translamellar Compression Fractures; 0/90-Degree Laminate



500X

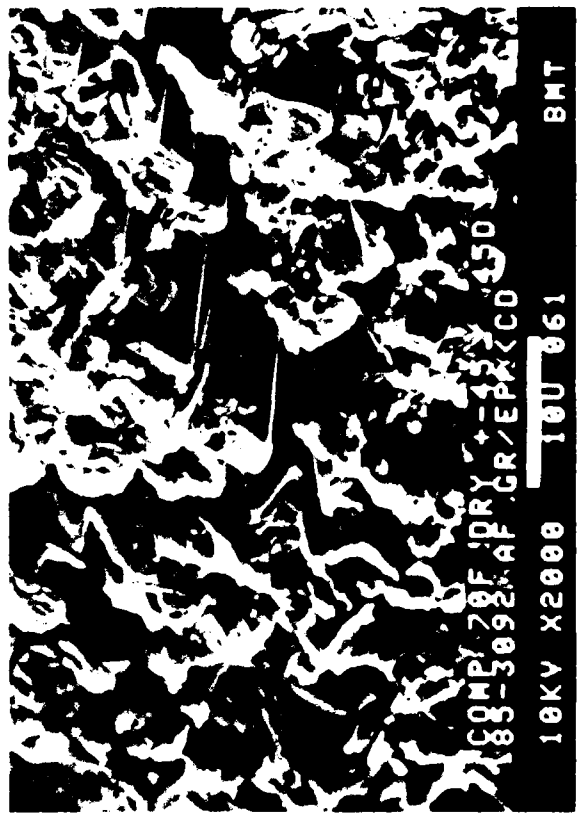
← Mechanically induced crack & region



2000X



400X



2000X

Figure 7-51. Translamellar Compression Fractures; +45/-45-Degree Laminate

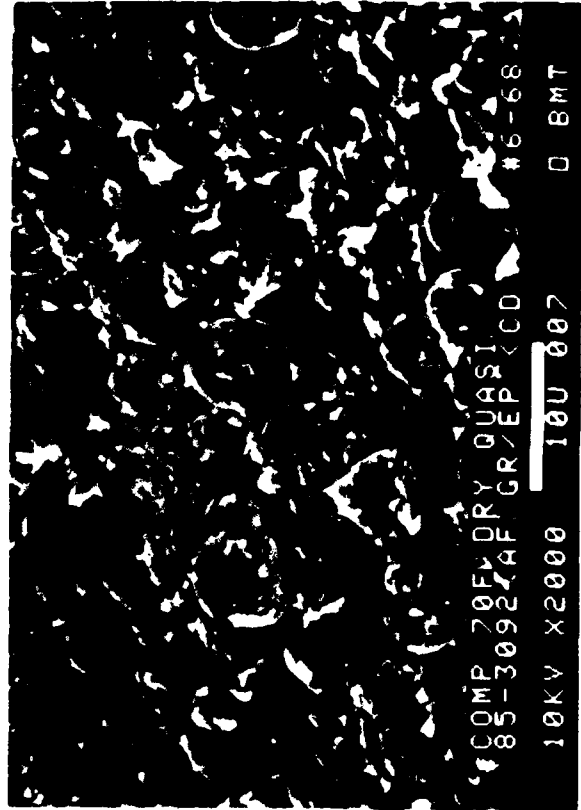
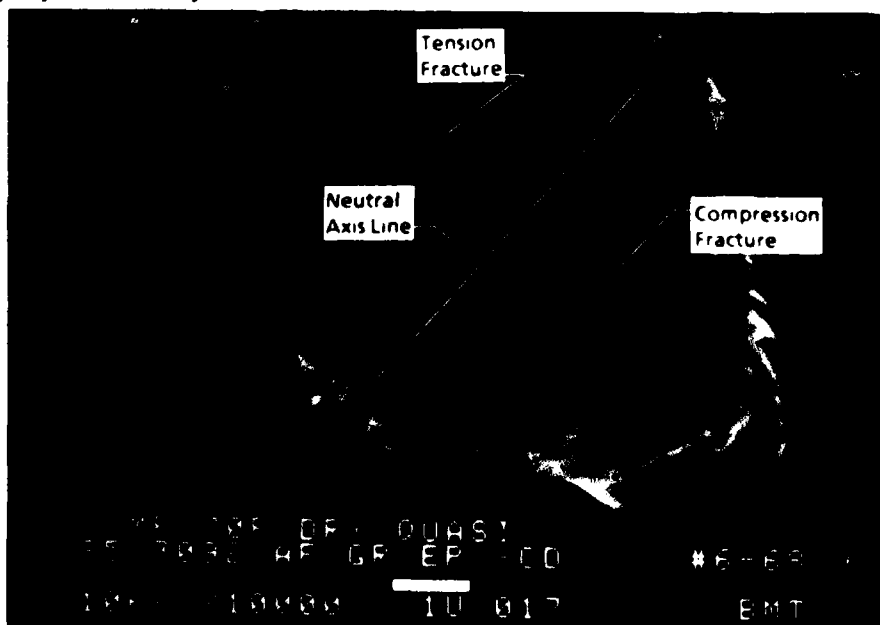


Figure 7-52. Translamellar Compression Fractures; Quasi-Isotropic Laminate

revealed a combination of fiber buckling, fiber-end fracture, resin-matrix fracture, and postfailure damaged regions. In the upper and lower right photomicrographs in each series, extensive fiber-end damage and many fractured resin particles can be seen. This obliteration of fracture surface features was attributed to postfailure abrasion between mating fracture surfaces.

Detailed investigation of the fiber fracture morphology shows that fiber microbuckling extends over the majority of the fracture surface. Compression microbuckling, evidenced by local buckling of individual fibers, creates dual-flexural fiber fracture. Under compressive flexure, fracture occurs at each antinode of a buckle, with each fracture separated by approximately 5 to 10 fiber diameters. This feature is best represented in the bottom photomicrographs of Figure 7-50. Examination of the fiber ends reveals a distinct line separating two different fracture morphologies. Radial lines indicative of tensile fracture conditions are evident on one side of this line. On the other side, there is a smooth morphology. This dual fracture morphology is direct evidence of flexure at the buckle antinode, with radial and smooth sides representative of tensile and compressive fracture, respectively (Figure 7-53). For each individual fiber the direction of flexure and fiber failure occurs normal to the neutral axis line formed between these two fracture features. However, when comparing the antinode fractures for a given fiber, the direction of flexural failure was found to be opposite for each antinode. Thus, for flexural microbuckling compression fractures, it appears that a singular crack direction cannot be determined. It can be deduced, however, that individual fiber fracture does propagate perpendicularly to the neutral axis lines found on the fiber ends.



7.53. Typical Fiber End Fracture; Representative of Fiber Flexure Fracture

10,000X

Upon inspection of multiple fiber features, the neutral axis lines were parallel to one another, indicating that fiber microbuckling occurs on a local scale in a concerted manner and in a unified direction (see lower left photomicrographs of each series). However, the direction of fiber microbuckling in these localized regions varies widely throughout the fracture surface. In many cases, there appeared to be a slight tendency for the neutral axis lines of these regions to be oriented parallel to the direction of induced crack propagation. Therefore, individual fiber fractures and their anti-nodes are oriented normal to the direction of macroscopic crack propagation. This condition indicates that flexural collapse and fracture propagation on a local scale occur transverse to the gross crack direction. This dichotomy may reflect the reduced buckle stability of plies in the transverse direction due to either 1) the direction of crack propagation, or 2) the geometry of the specimen or layups examined. The first of these two possibilities suggests that the direction of crack propagation could be fractographically established from these neutral axis lines. In contrast, the second suggests that the direction of microbuckle failure depends solely upon the configuration and lateral stability of its plies. For this latter possibility, the direction of microbuckle failure is independent of the direction of crack propagation. Therefore, the orientation of neutral axes may not be useful in determining the direction of crack propagation.

8.0 SUMMARY AND CONCLUSIONS

This document is an interim summary of efforts to establish a Compendium of Postfailure Analysis techniques for Composite Materials. This portion of the program reviewed and evaluated existing failure analysis techniques, developed detailed procedural guidelines, and investigated and developed fractographic methods for the analysis of simple causes of composite failure. The results of these interim efforts will be the cornerstone of the remaining program. This interim document establishes how, and in what order, an investigator should approach and carry out a failure analysis. This fundamental information will be refined by examining failure conditions that more closely simulate real-world "complex" conditions, then it will be assembled into an instructional Compendium of Postfailure Analysis Techniques for Composite Materials. This final compendium and its evaluation on three failed components should provide the basis to ultimately develop a widely disseminated handbook on failure analysis.

As illustrated in the Introduction and Objectives (see Figure 1-1), this program involves five tasks that verify and expand Boeing's existing metals and composites failure analysis capabilities. This interim report summarizes Tasks 1 through 3. The bulk of the program's investigative effort, these tasks were to establish:

- o A summary of literature's diagnostic techniques for inclusion in the compendium
- o A detailed set of procedural guidelines (FALNs)
- o Fractographic techniques to determine the direction mode, thereby the origin of failure.

Task 1, Literature Search and Diagnostic Technique Selection, addressed the first two of these objectives. Literature from 1978 to the present was examined for applicable techniques in four disciplines: nondestructive evaluation, fractography, stress analysis and materials characterization. Additionally, certain expertise sites were visited to clarify and more accurately define methods for failure analysis investigations. This review revealed the following:

1. There are several techniques for analyzing material characteristics and for nondestructively evaluating failed composite materials. Most of these techniques had been developed by application to manufacturing and production problems, but these problems bear a distinct similarity to those of postfailure analysis. For this reason, the application of most of these techniques to failed components should be relatively straightforward; and most were sufficiently mature for direct incorporation into the compendium.
2. Fractography techniques were not sufficiently mature for direct incorporation. In general, both the literature and visited experts described an emerging, still-immature technology. To date, a study aimed at addressing the specific requirements of a failure analysis has only been partially investigated. Specific problems included author disagreement about findings and interpretations, and studies having such a general nature that applicability was extremely limited.
3. A wide variety of stress analysis methods were examined in the literature search activities; they generally fell into either the individual-ply or laminate-level categories. Individual-ply analysis typically evaluated the stress at which first-ply fracture occurs, while laminate-level analyses examined the critical load for catastrophic laminate fracture. Both categories appeared to have their weak and strong aspects, including the ability to evaluate in-plane and out-of-plane damage, environmental effects, and the accurate prediction of failure onset. In this regard, the maturity of these techniques was found to depend on the level of detail and number of contributory conditions being considered as part of a failure analysis—The lower the level of detail and the fewer of contributory conditions considered, the more mature the technique.

Detailed FALN's were developed in Task 1 for each of the four major diagnostic techniques examined—nondestructive evaluation, stress analysis, materials characterization and fractography—and are contained in this report. For each discipline the FALN gives the logical steps of analysis and the corresponding methods for determining cause of failure. Particular emphasis was placed on minimizing a premature destruction of evidence and on building an analysis sequence in which information builds and directs further analyses.

Tasks 2 and 3 aimed at developing fractographic methods by which the direction, mode, and subsequent origin of fracture could be determined. Although these investigations are still underway, certain relationships have been established thus far. Specific ones include: failures produced under interlaminar mode 1 (tension) and mode 2 (shear), translaminar failures produced under conditions of mode 1 (tension) and compression, and the effect of environment on these failure conditions. Examination of these specimens revealed several methods for identifying the load state, direction and origin of fracture:

- o Mode 1 interlaminar fractures were identified by their flat fracture topography. Fracture direction could be identified by examining the direction and orientation of river mark coalescence and microflow.
- o Mode 2 interlaminar fractures were identified by a rough, hackled fracture morphology. In some cases, the direction of crack growth could be identified by the direction of hackle tilting and orientation. However, further work in this area will be necessary to establish confidence in this finding.
- o Translaminar tension fractures were identified by their rough, tiered appearance with fiber pullout and undamaged fiber ends. For this type of failure the direction of crack propagation correlated with the direction of individual fiber end fracture.
- o Translaminar compression fractures were typically identified by a flat overall fracture topography. At a more detailed level, fractures of this type also were found to exhibit pronounced surface damage and fiber microbuckling. Conclusive identification of the direction of these fractures could not be made.

9.0 REFERENCES

Written permission has been obtained from the publishers for the use of figures or quoted material from the following sources:

9.1 SOURCES FOR MATERIAL CITED AND FIGURES USED

9.1.1 Fractography (Section 4.3)

1. Miller, A. G., and Wingert, A. L., "Fracture Surface Characterization of Commercial Graphite/Epoxy Systems," ASTM STP 696, Edited by R. B. Pipes, 1979, pp. 223-273.
2. Clements, L. L., and Adamson, M. J. "Failure Morphology of (0 deg.) 8 Graphite/Epoxy as Influenced by Environment and Processing," NASA-TM-81318, August 1981.
3. Purslow, D., "Some Fundamental Aspects of Composites Fractography," Composites, October 1981.
4. Adams, D. F., "Analysis of the Compression Fatigue Properties of a Graphite /Epoxy Composite," 1981 Advances in Aerospace Structures and Materials, Proceedings of the Winter Annual Meeting, published by American Society of Mechanical Engineers, 1981, pp. 43-49.
5. Freeman, S. M., "Damage Progression in Graphite-Epoxy by a Depleting Technique," AFWAL-TR-81-3157, December 1981.
6. Morris, G. E., "Determining Fracture Directions and Fracture Origins on Failed Graphite/Epoxy Surfaces," ASTM STP 696, Edited by R. B. Pipes, 1979, pp. 274-297.
7. Liechti, K. M., et al., "SEM/TEM Fractography of Composite Materials," AFWAL-TR-82-4085, September 1982.

8. Kline, R. A., and Chang, F. H., "Composite Failure Surface Analysis," Journal of Composite Materials, Vol. 14, October 1980, pp. 315-324.
9. Sinclair, J. H., "Fracture Modes in High Modulus Graphite/Epoxy Angleplied Laminates Subjected to Off-Axis Tensile Loads," Rising to the Challenge of the 80's; 35th Annual Conference and Exhibit, published by Society of the Plastics Industry, Inc. 1980, pp. 12-C1 to 12-C8.
10. Johannesson, T., Sjoblom, P., and Seldon, R., "The Detailed Structure of Delamination Fracture Surfaces in Graphite/Epoxy Laminates," Journal of Materials Science 19, 1984, pp. 1171-1177.
11. Donaldson, S. L., "Fracture Toughness Testing of Graphite/Epoxy and Graphite/PEEK Composites," Composites, April 1985.
12. Robertson, R., et al., "The Stacked Lamellar Texture on the Fracture Surface of Fibre Composites," Journal of Materials Science 20, 1985, pp. 2801-2806.
13. Robertson, R., et al, "Fracture in Epoxy Matrix Resins," Composites Science and Technology 22, 1985, pp 197-207.
14. Browning, C. E., et al., "A Four-Point Shear Test for Graphite/Epoxy Composites," Composite Materials, ASTM Proceedings, Philadelphia, Pennsylvania, 1983.

9.1.2 Stress Analysis (Section 4.4)

15. Craddock, J. N. and Champagne, P. J., "A Comparison of Failure Criteria for Laminate Composite Materials," Structures, Structural Dynamics and Materials Conference, published by American Institute of Aeronautics and Astronautics, 1982, pp. 268-278.
16. Crossman, F. W., "Analysis of Free Edge Induced Failure of Composite Laminates," First USA-USSR Symposium on Fracture of Composite Materials, Sijthoff and Noordhoff International Publishers, 1979, pp. 291-302.

17. Herakovich, C. T., "On Failure Modes in Finite Width Angle Ply Laminates," Advances in Composite Materials; Proceedings of the Third International Conference on Composite Materials, Vol. 1, Pergamon Press, 1980, pp. 425-435.
18. Chamis, C. C., and Smith, G. T., "CODSTRAN: Composite Durability Structural Analysis," NASA-TM-79070, 1978.
19. Bathias, C., Esnault, R., and Pellas, J., "Application of Fracture Mechanics to Graphite Fibre-Reinforced Composites," Composites, Vol. 12, July 1981, pp. 195-200.
20. McGarry, F. J., Mandell, J. F., and Wang, S. S., "Fracture of Fiber-Reinforced Composites," Polymer Engineering and Science, Vol. 16, No. 9, September 1976, pp. 609-613.
21. Awerbuch, J., et al., "Determination Characteristics and Failure Modes of Notched Graphite Polyimide Composites at Room and Elevated Temperatures," NASA-CR-159375, August 1980.
22. Daniel, I. M., "The Behavior of Uniaxial Loaded Graphite/Epoxy Plates with Holes," Proceedings of the Second International Conference on Composite Materials, published by the Metallurgical Society of AIME, 1978, pp. 1019-1034.
23. Mikulas, M. M., "Failure Prediction Techniques for Compression-Loaded Composite Laminates with Holes," Selected NASA Research in Composite Materials and Structures, NASA Conference Publication 2142, August 1980.
24. O'Brien, T. K., "Analysis of Local Delaminations and Their Influence on Composite Laminate Behavior," NASA-TM-85728, January 1984.
25. Webster, J. D., "Flaw Criticality of Circular Disbond Defects in Compressive Laminates," NASA-CR-164830, June 1981.
26. Wilson, D. W., Gillespie, J. W., York, J. L., and Pipes, R. B., "Failure Analysis of Composite Bolted Joints," NASA-CR-163732, July 1980.

27. Starnes, J. H., et al., "Failure Characteristics of Graphite-Epoxy Structural Components Loaded in Compression," NASA-TM-84552, September 1982.
28. Wu, E. M., "Failure Analysis of Composites with Stress Gradients," First USA-USSR Symposium on Fracture of Composite Materials, Sijthoff and Noordhoff International Publishers, 1979, pp. 63-76.
29. McLaughlin, P. V., and Dasgupta, A., "BILAM: A Composite Laminate Failure Analysis Code Using Bilinear Stress Strain Approximations," UCRL-15371, October 1980.

9.1.3 Nondestructive Evaluation (Section 4.5)

30. Phelps, M. L., "In-Service Inspection Methods for Graphite-Epoxy Structures on Commercial Transport Aircraft," NASA-CR-165746, November 1981.
31. Reynolds, W. N., "Nondestructive Testing (NDT) of Fiber-Reinforced Composite Materials," SAMPE Quarterly, Vol. 16, No. 4, July 1985, pp. 1-16.
32. Schramm, S. W., Daniel, I. M., and Hamilton, "Evaluation of Sensitivity of Ultrasonic Detection of Disbonds in Graphite/Epoxy to Metal Joints," 36th Annual Conference, Reinforced Plastics/Composites Institute, published by The Society of the Plastics Industry, Inc., February 16-20, 1981.
33. Ulman, D. A., and Hennecke, E. G., II, "Nondestructive Evaluation of Damage in F. P./Aluminum Composites," Composite Materials: Testing and Design, ASTM STP 787, 1982, pp. 323-342.
34. Bar-Cohen, Y., et al., "Acoustic Backscattering Imaging of Subcritical Flaws in Composites," Materials Evaluation, Vol. 40, August 1982.
35. Moran, T. J., et al., "High-Resolution Imaging of Microcracks in Composites," Materials Evaluation, Vol. 43, April 1982.
36. Baumann, K. J., Kennedy, W. H., and Herbert, D. L., "Composite Tomography X-ray Scanning NDE of Graphite/Epoxy Coupons," Journal of Composite Materials, Vol. 18, November 1984.

37. Sendeckyj, G. P., and Maddux, G. E., "Comparison of Holographic, Radiographic, and Ultrasonic Techniques for Damage Detection in Composite Materials," ASTM-STP-696, Edited by R. P. Pipes, 1979, pp. 26-44.
38. Reifsnider, K. L., et al., "Defect Property Relationships in Composite Materials," AFML-TR-76-81, (Part III), June 1978.
39. Soni, S. R., "Failure Analysis of Composite Laminates with a Fastener Hole," Joining of Composite Materials; Proceedings of the Symposium, published by the American Society for Testing and Materials, 1981, pp. 145-164.
40. Gibbons, M. N., and Stinchcomb, W. W., "Fatigue Response of Composite Laminates with Internal Flaws," Composite Materials: Testing and Design, ASTM STP 787, 1982, pp. 305-322.
41. Teagle, P. R., "The Quality Control and Nondestructive Evaluation of Composite Aerospace Components," Composites, Vol. 14, No. 2, April 1983.
42. Bar-Cohen, Y., and Crane, R. L., "Nondestructive Evaluation of Fiber-Reinforced Composites with Acoustic Backscattering Measurements," Composite Materials, ASTM-STP-787, 1982, pp. 343-354.
43. Raatz, C. F., "Nondestructive Inspections," Airliner, October-December 1985.
44. Duke, J. C., Jr., "Nondestructive Evaluation of Composite Materials: A Philosophy, An Approach, and An Example," Composite Materials: Quality Assurance and Processing, ASTM-STP-797, 1983, pp. 75-95.

9.1.4 Materials Characterization (Section 4.6)

45. Wickham, A. A., Rice, D. D., and DuBois, R. J., "Chemical Analysis of Advanced Composite Prepregs and Resins," 24th National SAMPE Symposium and Exhibition, Vol. 24, 1979, pp. 506-521.
46. May, C. A., "Composite Matrix Quality Assurance - An Art Becomes a Science," 24th National SAMPE Symposium and Exhibition, Vol. 24, 1979, pp. 390-403.

47. Crozier, D., Morse, G., and Tajima, Y., "The Development of Improved Chemical Analysis Methods for Epoxy Resins," SAMPE Journal, September/October 1982, pp. 17-22.
48. Rogers, A. K., Tajima, Y. and Young, R. C., "The Development of a Material Specification for 177°C (350°F) Curing Graphite/Epoxy Composites," Composite Materials: Quality Assurance and Processing, ASTM-STP-797, Edited by C. E. Browning, 1983, pp. 15-28.
49. Tung, C. M., and Dynes, P. J., "Chemorheological Characterization of B-Stage Printed Wiring Board Resins," Composite Materials: Quality Assurance and Processing, ASTM-STP-797, Edited by C. E. Browning, 1983, pp. 38-53.
50. Chen, J. S., Hunter, B. A., and Katsumoto, M. T., "Development of Quality Assurance Methods for Epoxy Graphite Prepreg," NASA CR-3531, March 1982.
51. Carpenter, J. F., "Test Program Evaluation of Hercules 3501-6 Resin," N00019-77-C-0155, May 1978.
52. Sewell, T. A., "Quality Assurance of Graphite/Epoxy by High-Performance Liquid Chromatography," Composite Materials: Quality Assurance and Processing, Edited by C. E. Browning, 1983, pp. 3-14.
53. Mones, E. T., Walkup, C. M., Happe, J. A., and Morgan, R. J., "The Characterization of Diaminodiphenyl Sulfone (DDS) Cured Tetraglycidyl 4,4' Diaminodiphenyl Methane (TGDDM) Epoxies," 14th National SAMPE Technical Conference, Vol. 14, 1982, pp. 89-100.
54. Stark, E. B., Ibrahim, A. M., and Seferis, J. C., "Experimental Analysis of the Network Structure for the High-Performance TGDDM-Novalac-DDS Epoxy Matrix System," 28th National SAMPE Symposium and Exhibition, Vol. 28, 1983, pp. 581-589.
55. Carpenter, J. F., "Physiochemical Testing of Altered Composite 3501-6 Epoxy Resin," 24th National SAMPE Symposium and Exhibition, Vol. 24, 1979, pp. 446-457.

56. Munns, T. E., and Seferis, J. C., "Coupling of DSC and Dynamic Mechanical Experiments for Probing Processing-Structure-Property Relationships of Catalyst Modified High-Performance Epoxy Matrices," Analytical Calorimetry, Vol. 5, Edited by J. F. Johnson and P. S. Gill, Plenum Press, 1984, pp. 1-12.
57. Chu, H. S. and Seferis, J. C., "Network Structure Description and Analysis of Amine-Cured Epoxy Matrices," The Role of the Polymeric Matrix in the Processing and Structural Properties of Composite Materials, Edited by J. C. Seferis and L. Nicolais, Plenum Press, 1983, pp. 53-125.
58. Young, P. R., Stein, B. A., and Chang, A. C., "Resin Characterization in Cured Graphite Fiber Reinforced Composites Using Diffuse Reflectance - FTIR," 28th National SAMPE Symposium and Exhibition, Vol. 28, 1983, pp. 824-837.
59. Burroughs, P., and Leckenby, J. N., "Analysis of Composite Materials by Dynamic Thermomechanometry (Dynamic Mechanical Analysis)," Composite Structures: Proceedings of the First International Conference, Applied Science, 1981, pp. 438-449.
60. Chu, H. S. and Seferis, J. C., "Dynamic Mechanical Experiments for Probing Process-Structure-Property Relations in Amine-Cured Epoxies," Polymer Composites, Vol. 5, No. 2, 1984, pp. 124-140.
61. Baumgartner, W. E., and Lemming, H., "Cure Monitoring and Properties Assessment of Graphite Epoxy Composites Using Dynamic Mechanical Test Methods," 22nd National SAMPE Symposium and Exhibition, Vol. 22, 1977, pp. 650-662.
62. Putter, S., Buchanan, D. L., and Rehfield, L. W., "Influence of Frequency and Environmental Conditions on Dynamic Behavior of Graphite/Epoxy Composites," Composite Materials: Testing and Design (Sixth Conference), ASTM-STP-787, Edited by I. M. Daniel, 1982, pp. 414-424.
63. Jackson, W. T., "Critical Evaluation of Several Methods for Determining Fiber Fraction of Cured Graphite/Epoxy Composites," 23rd National SAMPE Symposium and Exhibition, Vol. 23, 1978, pp. 160-174.

64. Chang, T. D., Carr, S. H., and Brittain, J. O., "Studies of Epoxy Resin Systems, Part B: Effect of Crosslinking on the Physical Properties of an Epoxy Resin," Polymer Engineering and Science, Vol. 22, No. 18, 1982, pp. 1213-1220.

9.2 ADDITIONAL REFERENCES WITH ABSTRACTS

The following section summarizes additional references reviewed as part of the Task I literature search but not directly referenced in the text of this document. In many cases these works were not referenced in order to avoid encumbering the reader with a long list of authors whose work yielded similar results. In other cases, certain reference were not discussed because of the limited applicability of their results.

9.2.1 Fractography

1. Charentenay, F. X., et al., "Analysis of Mechanical Damage Growth in Notched Carbon-Epoxy (+45 or -45 deg) Laminates," Progress in Science and Engineering of Composites; Proceedings of the Fourth International Conference on Composite Materials, Vol. 1, published by Japan Society of Composite Materials/North Holland, 1982, pp. 625-631.

The damage growth in notched coupons of (+ or - 45 deg)2s carbon-epoxy laminates has been analyzed in details by microscopic observation of section. Main cracks initiated by the notch grow parallel to the fiber and induce in adjacent plies small cracks. Delamination occurs by mode III crack propagation initiated by the sets of main and induced cracks. Fractographic observations are consistent with this mechanism.

2. Bradley, W. L., et al., "Composite Materials for Structural Design," AFOSR-TR-82-1018, March 1982.

Research activities related to advanced fiber reinforced plastics are reported in detail for the final year of the initial contract on the continuing composites program at Texas A&M. Work was initiated or continued in the areas of fracture, delamination, fatigue, and residual stresses in elastic and viscoelastic composites. Delamination fracture toughness is investigated using macroscopic measurements of fracture toughness to determine critical energy release rate for crack

propagation and is interpreted in terms of microscopic mechanisms of fracture determined from careful examination of the fracture surface using a scanning electron microscope. Additional experimental work in compression-induced delamination and delamination under complex load histories is presented. Analytical methods are developed for prediction of the mechanical state and energy release rate for delamination and used in the investigation of tensile coupons with various amounts of delamination and matrix degradation due to microcracking. A viscoelastic crack growth theory for nonlinear media was developed earlier in the program and this work is being extended to develop a damage theory of laminates. An investigation of the effects of moisture and temperature on residual stresses in composite laminates is continuing. Solution forms which relate curvatures in unsymmetric cross-ply laminates to temperature excursions and moisture content, including viscoelastic effects, were formulated and programmed.

3. Sinclair, J. H., et al., "Compression Behavior of Unidirectional Fibrous Composites," NASA-TM-83833, 1982.

The longitudinal compression behavior of unidirectional fiber composites is investigated using a modified Celanese test method with thick and thin test specimens. The test data obtained are interpreted using the stress/strain curves from back-to-back strain gages, examination of fracture surfaces by scanning electron microscope, and predictive equations for distinct failure modes including fiber compression failure, Euler buckling, delamination, and flexure. The results show that the longitudinal compression fracture is induced by a combination of delamination, flexure, and fiber tier breaks. No distinct fracture surface characteristics can be associated with unique failure modes. An equation is described which can be used to extract the longitudinal compression strength knowing the longitudinal tensile and flexural strengths of the same composite system.

4. Wells, J. K., et al., "The Construction and Use of Toughness Maps in a Fracture Analysis of the Micromechanics of a Composite Failure," AF-AFOSR-3644-78, February 1981.

Analytical expressions are presented which predict the debonding and pull out lengths observed in brittle fiber composites. These characteristic lengths are combined with models of four toughening mechanisms to calculate the work of fracture of a composite.

5. Mao, T. H., et al., "Crack Propagation in Fibrous and Particulate Composites," CUED/C-MATS/TR-89-1981, November 1981.

Crack propagation in particulate and fibrous composites was studied by direct observation of advancing cracks in the scanning electron microscope, coupled with mechanical measurements on double-torsion specimens. The results give insight into the strain field at the crack tip, the mechanism of crack advance, and the origins of the toughness of composites.

6. Francis, P. H., et al., "Damage Mechanisms and Failure in 3-D Carbon-Carbon Composites," Southwest Research Institute, Report Number SWRI-02-4982, San Antonio, Texas, February 1979.

Mechanical property characterization tests were conducted on specimens from a three-dimensional, cartesian orthogonally woven carbon-carbon (C-C) material. Tests consisted of tensile and rail shear, which were conducted at room temperature, and compression tests conducted at room temperature up to 2165°C (3930°F). Stress-strain characteristics and acoustic emission instrumentation were employed to infer the mechanics of the fracture initiation process. In addition, a specially developed axial loading stage integral to SWRI's ETEC scanning electron microscope facility was used to view and videotape the crack initiation and development processes. As a result of these studies, a tentative model is described to explain the mechanics of failure in 3-D C-C composites.

7. Kline, R. A., et al., "The Effects of Interlaminar Microcracking on Composite Behavior," Advanced Composites: Proceedings of the Conference, published by Technology Conferences, 1979, pp. 171-182.

Interlaminar microcracking is a particularly important problem in the fabrication of graphite-epoxy composites. In this study, specimens with this type of defect, introduced during processing, were examined. Mechanical testing of these components indicated that a reduction in strength can be expected for materials with such processing defects under certain loading conditions. After the testing was completed, the surfaces of the failed specimens were examined with a scanning electron microscope. This study revealed the presence of delaminated regions along the ply boundary where no evidence of features which characterize composite deformation could be observed.

8. Hampey, J. M., "The Effects of Jet Exhaust Blast Impingements on Graphite-Epoxy Composites," Master's Thesis, Naval Postgraduate School, Monterey, California, June 1981.

The effect of jet exhaust blasts on graphite epoxy composites (Hercules 3501-6/AS4) is examined. The material degradation of the composites is determined by means of the short beam shear test. The jet exhaust tests were designed to test the worst case conditions for an F-18 aircraft operating off an aircraft carrier. Results indicate that the composites show no significant property changes if the temperature is maintained less than 230°C. At temperatures in excess of these, strength degradation occurs. It was also observed that when strength degradation occurs, obvious discoloration and delamination of the composite are evident.

9. Whitcomb, J. D., "Experimental and Analytical Study of Fatigue Damage in Notched Graphite/Epoxy Laminates," NASA-TM-80121, June 1979.

Both tension and compression fatigue behaviors were investigated in four notched graphite/epoxy laminates. After fatigue loading, specimens were examined for damage type and location using visual inspection, light microscopy, scanning electron microscopy, ultrasonic C-scans, and X-radiography. Delamination and ply cracking were found to be the dominant types of fatigue damage. In general, ply cracks did not propagate into adjacent plies of differing fiber orientation. To help understand the varied fatigue observations, the interlaminar stress

distribution was calculated with finite element analysis for the regions around the hole and along the straight free edge. Comparison of observed delamination locations with the calculated stresses indicated that both interlaminar shear and peel stresses must be considered when predicting delamination. The effects of the fatigue cycling on residual strength and stiffness were measured for some specimens of each laminate type. Fatigue loading generally caused only small stiffness losses. In all cases, residual strengths were greater than or equal to the virgin strengths.

10. Starnes, J. H., et al., "Failure Characteristics of Graphite-Epoxy Structural Components Loaded in Compression," NASA-TM-84552, September 1982.

Failure characteristics of compressively loaded graphite-epoxy components are described. Experimental results for both strength-critical laminates and structural components with postbuckling strength are presented. Effects of low speed impact damage and circular holes on compressive strength are discussed. Delamination and shear crippling failure mechanisms that limit the performance of strength-critical laminates are described. Transverse shear and skin-stiffener separation failure mechanisms that limit the performance of components with postbuckling strength are also described. The influence of matrix properties on compressive strength improvements for impact damaged laminates is discussed. Experimental data and results from a failure analysis for strength-critical laminates with cutouts are discussed and compared with impact damage results. Typical postbuckling test results are compared with analytical predictions.

11. Browning, C. E., et al., "A Four-Point Shear Test for Graphite/Epoxy Composites," Composite Materials: Quality Assurance and Processing: Proceedings of the Symposium, American Society for Testing and Materials, 1983.

Graphite/epoxy composite thin beam 16-ply and thick beam 50-ply short beam shear (SBS) specimens, and thin beam 16-ply and slightly thicker, 24-ply four-point shear (FPS) test specimens, were tested to failure and the data gathered were statistically analyzed. In addition, fractured surfaces were examined with SEM. The FPS specimen was found to be

an effective alternative to the thin beam SBS specimen, consistently producing interlaminar shear failure modes and corresponding failure surfaces, together with a reasonable data distribution, while retaining such attractive features of the thin-beam SBS specimen as small dimensions, ease of machining, and simplicity of method.

12. Morris, G. E., et al., "Fractographic Studies of Graphite/Epoxy Fatigue Specimens," Damage in Composite Materials: Basic Mechanisms, Accumulation, Tolerance and Characterization, American Society for Testing and Materials, 1982.

Techniques have been developed which employ scanning electron microscopy (SEM) to identify failed epoxy component topographic features (hackles) characterizing overload failures, in fracture origin and direction studies of graphite/epoxy laminates. The hackle interpretation technique is presently employed to trace hackles back to fracture origin locations on the fracture surfaces of graphite/epoxy test coupons and structures which have failed in tension, and the technique is then expanded to include fatigue-tested, cross plied graphite/epoxy specimens. Arrest mark patterns, or striations, have been associated with tension-compression fatigue crack propagation in some of the test specimens; these striations are different in appearance from hackles, and therefore present a promising topographic feature for the differentiation of tension-compression fractures from overload fractures in graphite-epoxy composites.

13. Cruse, T. A., et al., "Fractographic Study of Graphite-Epoxy Laminated Fracture Specimens," Report SM-72-24 (A), Carnegie Mellon University, Pittsburg, Pennsylvania, December 1972.

No abstract available.

14. Beck, B., et al., "Investigation of Adhesive Adherend and Fiber/Matrix Interactions, Part B: SEM/ESCA Analysis of Fracture Surfaces," NASA-CR-169798, January 1983.

Adhesion was studied with emphasis on the characterization of surface oxide layers, the analysis of fracture surfaces, and the interaction of

matrices and fibers. A number of surface features of the fractured lap shear samples were noted in the SEM photomicrographs including the beta phase alloy of the Ti 6-4 adherend, the imprint of the adherend on the adhesive failure surface, increased void density for high temperature samples, and the alumina filler particles. Interfacial failure of some of the fractured lap shear samples is invariably characterized by the appearance of an ESCA oxygen photopeak at 530.3 eV assigned to the surface oxide layer of Ti 6-4 adherend. The effect of grit blasting on carbon fiber composites is evident in the SEM analysis. A high surface fluorine concentration on the composite surface is reduced some ten fold by grit blasting.

15. Ingraham, J. A., et al., "Scanning-Electron Microscopy Study of Argon-Plasma-Treated and Untreated Peel-Test Kevlar 49/Epoxy Laminates," Report DE83-003856 UCID-19607, California University, Lawrence Livermore Lab., Livermore, October 1982.

Two hundred watt RF argon plasma treatment of Kevlar fibers for four minutes increases the fiber/epoxy interfacial bonding. However, as a consequence of this increase in fiber-matrix bonding, the fiber is readily fibrillated during laminate deformation and failure.

16. Purslow, D., et al., "Composite Fractography Without an SEM - The Failure Analysis of a CFRP I-Beam," Composites, Vol. 15, No. 1, January 1984.

This paper describes the fractographic analysis of a typical aerospace structural element made from CFRP. The methods of fracture characterization and failure sequencing are described in detail and the cause of ultimate failure successfully determined using low-power optical microscopy only.

17. Purslow, D., et al., "The Effect of Environment on the Compression Strength of Notched CFRP - A Fractographic Investigation," Composites, Vol. 15, No. 2, April 1984.

Compression strength tests were carried out on notched $0^{\circ} \pm 45^{\circ}$ CFRP coupons under various environmental conditions. In addition, the

fracture of a number of specimens was arrested to minimize post-failure damage and thus facilitate fractographic analysis. The investigation revealed three basic environment-related failure modes. Significant compressive notch sensitivity occurred only under hot-wet conditions and, apart from this condition, laminates in which axial plies were distributed singly were weaker than those in which the 0° plies were in groups of two or three.

18. DaSilva, J. L. G., et al., "Flexural Studies of Carbon Fibers," Journal of Materials Science, Vol. 19, 1984, pp. 3201-3210.

Fracture faces of several commercially available carbon fibres have been examined in the scanning electron microscope (SEM) after tensile and flexural failure. There are marked differences between the faces obtained after flexural failure and those produced after tensile failure, in the case of all the PAN-based fibres studies. In contrast, there is very little difference between the fracture faces for the two modes of failure in a mesophase-pitch-based fibre. The circular cross-section PAN-based fibres of all types are more flexible and less brittle than both a high modulus bilobal cross-section PAN-based fibre and the mesophase-pitch-based fibre. These fracture studies indicate that the Reynolds-Sharp failure mechanism operates in both tensile and flexural modes so that fibres containing sheet-like structures will be more brittle and inflexible than those containing more highly inter-linked random structures.

19. Donaldson, S. L., "Fractography of Mixed Mode I-II Failure in Graphite/Epoxy and Graphite/Thermoplastic Unidirectional Composites," AFWAL-TR-84-4186, June 1985.

The notched off-axis tensile test and the notched three rail shear test were used to produce states of in-plane loading varying from pure Mode I (crack opening) to Mode II (forward shearing). The two material systems tested were Fiberite T300/1034C graphite/epoxy and Imperial Chemical Industries graphite reinforced polyetheretherketone thermoplastic composite (APC-1 PEEK).

Using a scanning electron microscope, a detailed examination of the resulting fracture surfaces was conducted. Results at magnification levels of 100X and 800X are presented. Very distinct changes can be observed in each material as the load ratio changes. In addition, for a fixed mixed mode load ratio, large differences can be seen in the matrix deformation patterns between the two material systems. Of particular interest are ductile spike formations seen in the highly shear loaded PEEK specimens. These observations provide some insight as to the increased toughness seen at higher Mode II ratios, and the increased toughness seen in the thermoplastic system.

20. Clements, L. L., et al., "Influence of Quality Control Variables on Failure of Graphite Epoxy Under Extreme Moisture Conditions," NASA-TM-81246, October 1980.

Tension tests on graphite/epoxy composites were performed to determine the influence of various quality control variables on failure strength as a function of moisture and moderate temperatures. The extremely high and low moisture contents investigated were found to have less effect upon properties than did temperature or the quality control variables of specimen flaws and prepreg batch to batch variations. In particular, specimen flaws were found to drastically reduce the predicted strength of the composite, whereas specimens from different batches of prepreg displayed differences in strength as a function of temperature and extreme moisture exposure. The findings illustrate the need for careful specimen preparation, studies of flaw sensitivity, and careful quality control in any study of composite materials.

21. Clements, L. L., et al., "Deformation and Failure Mechanisms of Graphite Epoxy Composites," NASA-CR-166328, September 1981.

The mechanisms of deformation and failure of graphite epoxy composites under static loading were clarified. The influence of moisture and temperature upon these mechanisms were also investigated. Because the longitudinal tensile properties are the most critical to the performance of the composite, these properties were investigated in detail. Both

ultimate and elastic mechanical properties were investigated, but the study of mechanisms emphasized those leading to failure of the composite. The graphite epoxy composite selected for study was the system being used in several NASA sponsored flight test programs.

22. Matsumoto, D. S., "Fatigue Initiation in a Short Glass Fibre Composite," Journal of Materials Science, Vol. 2, 1983, pp. 7-11.

No abstract available.

23. Hertzberg, P. E., et al., "Effect of Matrix Resin on the Impact Fracture Characteristics of Graphite-Epoxy Laminates," NASA-CR-165784, January 1982.

This report presents the results of an investigation into the effect of resin chemistry on basic impact-energy-absorbent mechanisms exhibited by graphite-epoxy composites. Impact fracture modes and microscopic resin deformation characteristics were examined for 26 NASA-impacted graphite-epoxy laminates with different resin chemistries. Discrete specimen fracture modes were identified through cross-sectional examination after impact and subsequently compared with measured glass transition temperatures, cure cycles, and residual impact capabilities. Details of microscopic resin deformation mechanisms and their overall relationship to impact loading conditions, voids, and resin content also were characterized through detailed scanning electron microscopic examination of separated fracture surfaces.

24. Purslow, D., "Fractographic Analysis of Failures in CFRP," Characterization, Analysis and Significance of Defects in Composite Materials, AGARD Proceedings No. 355, July 1983.

A wide-ranging fractographic research program, from the fundamental characterization of test coupon fractures to the failure analysis of full-scale aerospace components, has been undertaken in Materials and Structures Department, RAE.

This paper describes work on unidirectional CFRP test coupons in which a known mode of failure had been produced, the modes being longitudinal

and transverse tension, compression and shear. From a fundamental understanding of the character of the different modes and of the mechanisms of fracture propagation it is shown how the qualitative significance of "micro-defects" occurring in good quality laminates may be assessed. The defects considered are fibre faults, fibre-matrix bond strength, fibre distribution, fibre alignment and voids and inclusions; these are illustrated and their individual and collective significance discussed.

9.2.2 Stress Analysis

25. Hashin, Z., et al., "Analysis of Composite Materials - A Survey," ASME Transactions, Journal of Applied Mechanics, Vol. 50, September 1983, pp. 481-505.

The present investigation has the objective to provide an analysis of composite materials from the applied mechanics and engineering science point of view. The elastic properties are considered, taking into account statistically isotropic composites and fiber composites. Aspects of thermal expansion and moisture swelling are discussed along with visco-elastic properties, steady state conduction through a composite material, and the analysis of failure of composite materials. Attention is given to static failure in the case of one stress component, static failure caused by combined stress, the fatigue failure of unidirectional fiber composites, and the failure of laminates.

26. Wilson, D. W., et al., "Analysis of Shearout Failure Mode in Composite Bolted Joints," Composite Structures: Proceedings of the First International Conference, Applied Science Publishers, 1981, pp. 34-49.

A semi-empirical shearout strength model has been formulated for the analysis of composite bolted joints with allowance for the effects of joint geometry. The model employs a polynomial stress function in conjunction with a point stress failure criterion to predict strength as a function of fastener size, edge distance, and half spacing. The stress function is obtained by two-dimensional plane-stress finite element analysis using quadrilateral elements with orthotropic material properties. Comparison of experimentally determined shearout strength

data with model predicted failures has substantiated the accuracy of the model.

27. Masters, J. E., "An Experimental Investigation of Cumulative Damage Development in Graphite Epoxy Laminates," Ph.D. Thesis, Virginia Polytechnic Institute and State University, 1981.

The results of an experimental investigation of cumulative damage development in laminated graphite epoxy plates are discussed. The general approach was to apply nondestructive test techniques to interrogate the specimens during loading. Principal results reported were obtained through the use of a surface replication technique. The goal was to define the physical mechanisms which lead to ultimate failure of the material. Two quasi-isotropic graphite epoxy laminates were subjected to quasi-static tension and tension-tension fatigue. The unnotched AS/3501-5 laminates had stacking sequences of 0/90/ + 45/ - 45s and 0/ +45/ -45/90s. Damage development in the form of transverse cracking in all off-axis lamina, longitudinal cracking and delamination was monitored throughout the tests. Results of the study include a detailed description of the chronology of events leading to failure of the two specimen types. A characteristic damage state indicates that, with increased loading, transverse cracks develop in all off-axis lamina until a uniform crack spacing is attained.

28. Wilson, D. W., et al., "Failure Analyses of Composite Bolted Joints," NASA-CR-163732, 1980.

The complex failure behavior exhibited by bolted joints of graphite epoxy (Hercules AS/3501) was investigated for the net tension, bearing and shearout failure modes using combined analytical and experimental techniques. Plane stress, linear elastic, finite element methods were employed to determine the two dimensional state of stress resulting from a loaded hole in a finite width, semiinfinite strip. The stresses predicted by the finite element method were verified by experiment to lend credence to the analysis. The influence of joint geometric parameters on the state of stress and resultant strength of the joint was also studied. The resulting functional relationships found to exist

between bolted joint strength and the geometric parameters were applied in the formulation of semiempirical strength models for the basic failure modes. A point stress failure criterion was successfully applied as the failure criterion for the net tension and shearout failure modes.

29. Tennyson, R. C., et al., "Failure Analysis of Composite Laminates Using a Tensor Polynomial Strength Criterion," Proceedings of Army Symposium on Solid Mechanics, 1982 - Critical Mechanics Problems in System Design, September 1982.

This report presents a summary of the work done on the development of the cubic form of the tensor polynomial strength criterion for composite laminates. The capability of this model to accurately predict multi-mode failures for a range of laminates under various load conditions is demonstrated, and the results compared to quadratic model predictions. Both symmetric and nonsymmetric laminates have been considered. Furthermore, the effect of nonlinear shear stress/strain behavior is included to provide some insight as to its role in determining the strength of laminates. Of particular interest is the application of this criterion to the strength analysis of laminates containing circular holes.

30. Wu, E. M., et al., "Failure Analysis of Composites with Stress Gradients," First USA-USSR Symposium on Fracture of Composite Materials; Proceedings, published by Sijthoff and Noordhoff International Publishers, 1979, pp. 63-76.

In technical applications of composites, there exists a need to analyze composite strength in terms of stress gradients such as cracks, cutouts, and concentrated loads. Traditional continuum stress analysis cannot fully reconcile the interaction of the stress gradient and the local heterogeneity of fiber matrix and lamination. We present an adaptation of the statistical strength theory to analyze the effect of stress gradients by explicit relation to the intrinsic strength variability of the composite. This method is suitable for failure analysis of composites under a general state of stress without employing an arbitrary averaging parameter.

31. Goree, J. G., et al., "Fracture and Crack Growth in Orthotropic Laminates," NASA-CR-157424, October, 1978.

An approximate solution is developed for the determination of the interlaminar normal and shear stresses in the vicinity of a crack in a three dimensional composite containing unidirectional linearly elastic fibers in an infinite linearly elastic matrix. In order to reduce the complexity of the formulation, certain assumptions are made as to the physically significant stresses to be retained. These simplifications reduce the partial differential equations of elasticity to differential-difference equations which are tractable using Fourier transform techniques. The potential for damaged or debonded zones to be generated by an embedded crack is discussed, and stress concentration factors for fibers near the crack are given. Detailed comparisons are made between the present solution, the analogous two dimensional problem, and corresponding shear-lag models.

32. Wurzel, D., "Optimization of Composite Laminates," Materials and Processes - Continuing Innovations: Proceedings of the Twenty-eighth National SAMPE Symposium and Exhibition, published by Society for the Advancement of Material and Process Engineering, 1983, pp. 9-19.

In order to arrive at minimum weight designs, the directional properties of laminated composites have been matched to given stress resultants for in-plane loading. Optimum laminate strength was determined by the first ply failure envelope, on the basis of the quadratic interaction failure criterion. Such an optimization can be easily accomplished, given an understanding of the concept of principal stress and strain directions, together with the matching of ply and stress ratios and the use of programmable, hand-held calculators. Attention is given to results for T300/5208 graphite-epoxy, where the total laminate thickness can be reduced for the cases of nonisotropic cross-ply or angle-ply configurations, but not for quasi-isotropic laminates. Multiple loading is also considered.

33. Chamis, C. C., "Simplified Composite Micromechanics Equations for Strength, Fracture Toughness and Environmental Effects," SAMPE Quarterly, July 1984.

A unified set of composite micromechanics equations of simple form is summarized and described. This unified set includes composite

micromechanics equations for predicting (1) ply in-plane uniaxial strengths; (2) through-the-thickness strength (interlaminar and flexural); (3) in-plane fracture toughness; (4) in-plane impact resistance; and (5) through-the-thickness (interlaminar and flexural) impact resistance. Equations are also included for predicting the hygrothermal effects on strength, fracture toughness and impact resistance. Several numerical examples are worked out to illustrate the ease of use of the various composite micromechanics equations.

34. Jurf, R. A., "Interlaminar Fracture of Composite Materials," CCM-85-05, Center for Composite Materials, University of Delaware, 1985.

Interlaminar fracture characteristics of a graphite/epoxy composite material (AS1/3501-6) are investigated under the opening, shearing and mixed mode conditions. The Arcan test fixture was modified to accommodate the composite specimen containing an embedded interlaminar crack. Both critical stress intensity factor and strain energy release rate data were determined and the quadratic interaction for mixed mode behavior was compared to experimental data. Results of over sixty tests showed that the test fixture yielded results which compare favorably with results from contemporary test fixtures. Critical fracture parameters for the opening and shearing modes were shown to differ by a factor of 9.1. Further, the test results showed general agreement with the quadratic interaction relation.

35. Chamis, C. C., et al., "Mechanical Behavior and Fracture Characteristics of Off-Axis Fiber Composites II - Theory and Comparisons," NASA-TP-1082.

The mechanical behavior and stresses inducing fracture modes of unidirection high-modulus graphite-fiber/epoxy composites subjected to off-axis tensile loads were investigated theoretically. The results are compared with experimental data. The investigation included the use of composite mechanics, combined-stress failure criteria, and finite-element stress analysis. The results led to the formulation of criteria and convenient plotting procedures for identifying, characterizing, and quantifying these fracture modes.

36. Irvine, T. B., et al., "Progressive Fracture of Fiber Composites," NASA-TM-83701, October 1983.

Refined models and procedures are described for determining progressive composite fracture in graphite/epoxy angleplied laminates. Unique Lewis Research Center capabilities are utilized including the Real-Time Ultrasonic C-Scan (RUSCAN) experimental facility and the Composite Durability Structural Analysis (CODSTRAN) computer code. CODSTRAN is used to predict the fracture progression based on composite mechanics, finite element stress analysis, and fracture criteria modules. The RUSCAN facility, CODSTRAN computer code, and scanning electron microscope are used to determine durability and identify failure mechanisms in graphite/epoxy composites. Results indicate that RUSCAN/CODSTRAN is an effective method of studying progressive fracture of composites.

37. Whitcomb, J. D., "Experimental and Analytical Study of Fatigue Damage in Notched Graphite Epoxy Laminates," NASA-TM-80121, June 1979.

Both tension and compression fatigue behaviors were investigated in four notched graphite/epoxy laminates. After fatigue loading, specimens were examined for damage type and location using visual inspection, light microscopy, scanning electron microscopy, ultrasonic C-scans, and X-radiography. Delamination and ply cracking were found to be the dominant types of fatigue damage. In general, ply cracks did not propagate into adjacent plies of differing fiber orientation. To help understand the varied fatigue observations, the interlaminar stress distribution was calculated with finite element analysis for the regions around the hole and along the straight free edge. Comparison of observed delamination locations with the calculated stresses indicated that both interlaminar shear and peel stresses must be considered when predicting delamination. The effects of the fatigue cycling on residual strength and stiffness were measured for some specimens of each laminate type. Fatigue loading generally caused only small stiffness losses. In all cases, residual strengths were greater than or equal to the virgin strengths.

38. Anstice, P. D., et al., "Hygrothermal Aging Effects on the Micromechanics of Crack Extension," AFOSR-TR-80-1244, 1980.

Hygrothermal aging effects and the micromechanisms of crack extension in glass fibre and carbon fibre composites are described. A new collection of failure data based on direct observation of fibres debonding, breaking and pulling out of a cracked epoxy matrix is presented. The data are summarized in cumulative probability diagrams which provide a convenient means for the comparison of fracture behavior of composite systems. These diagrams also demonstrate the effects of changes in environment and time in a given experiment in a manner useful for the failure analysis of a fibrous composite.

9.2.3 Nondestructive Examination

39. Henneke, E. G., II, et al., "Review of the State-of-the-Art of Nondestructive Evaluation of Advanced Composite Materials," Virginia Polytechnic Institute, Blacksburg, 1979.

A review of the literature on the nondestructive testing of advanced composites is presented. The report is categorized according to the reinforcing filament in the composite system. A number of nondestructive evaluation methods have proven suitable for detecting specific types of flaws in composites: fiber-matrix debonds, delaminations, matrix crazing, fiber misalignments, resin-rich or resin-poor regions, etc. However, the literature is lacking, in general, any definitive conclusions concerning the effect these detected defects have upon the mechanical properties of the composite, such as stiffness, strength, residual strength, or expected lifetime. (ERA citation 08:002750)

40. Sullivan, P. G., and Davis, L. W., "Nondestructive Testing Methods for Graphite/Aluminum Composites," Nondestructive Evaluation and Flaw Criticality for Composite Materials, ASTM STP 696, Edited by R. B. Pipes, 1979, pp. 339-354.

No abstract available.

41. Pettit, D. E. "Characterization of Impact Damage in Composite Laminates," Nondestructive Evaluation and Flaw Criticality for Composite Materials, ASTM STP 696, Edited by R. B. Pipes, 1979, pp. 101-124.

The potential application of the Holskan 400 as a laboratory tool to monitor and characterize impact damage in graphite/epoxy composite material was evaluated. Impact damage in 16- to 32-ply-thick material was examined. A number of modifications were made to the basic Holskan system and the unit evaluated in terms of impact damage characterization ability and ease of operation in a laboratory environment. The results showed several of the modifications to be needed to provide a system with the desired capability and ease of operation.

42. Henneke, E. G., II, and Jones, T. S., "Detection of Damage in Composite Materials by Vibrothermography," Nondestructive Evaluation and Flaw Criticality for Composite Materials, ASTM STP 696, Edited by R. B. Pipes, 1979, pp. 83-95.

A new nondestructive inspection method, vibrothermography, has been studied here to determine its degree of application to the investigation of damage in composite materials. Subsurface damaged regions containing delaminations, relatively large matrix cracks, or matrix crazing are easily located by the method. A three-dimensional anisotropic heat-conduction model, solved by a finite-difference method, has shown that the surface heat patterns monitored by thermography represent accurately the geometry and extent of the subsurface heat source.

43. Dance W. E., and Middlebrook, J. B., "Neutron Radiographic Nondestructive Inspection for Bonded Composite Structures," Nondestructive Evaluation and Flaw Criticality for Composite Materials, ASTM STP 696, Edited by R. B. Pipes, 1979, pp. 57-71.

Neutron radiography was found to be effective as a nondestructive inspection technique for detection of bondline voids/defects in a variety of composite structures. Radiographic data are presented in this paper from typical structures for which the neutron radiographic inspection

technique offers advantages over more conventional inspection techniques. Complex composite joints such as box beam members, for example, are difficult to inspect by ultrasonic techniques, and the X-ray attenuation coefficients of the different materials in composite/metal combinations differ in such a manner as to yield very little nondestructive inspection (NDI) information regarding the integrity of the bond. Accurate bondline defect information was achieved in such structures utilizing a transportable californium-252 (^{252}Cf) neutron radiography system containing approximately 2 mg of ^{252}CF isotope. Through techniques developed at Vought Corp. Advanced Technology Center, resolution of simulated bondline voids as small as 0.127 mm (0.005 in.) diameter in laminated graphite/epoxy specimens was achieved. It is expected that continuing improvements in imaging techniques, and in mobility of neutron sources for radiography, will spawn wide usage of the neutron technique for nondestructive inspection of complex wing joints, control surfaces, and other airframe structures.

44. Heyman, J. S., and Cantrell, J. H., Jr., "Effects of Material Inhomogeneities on Ultrasonic Measurements: The Problem and a Solution," Nondestructive Evaluation and Flaw Criticality for Composite Materials, ASTM STP 696, Edited by R. B. Pipes, 1979, pp. 45-56.

Most ultrasonic measurements of materials involve the generation of an acoustic wave and the propagation of that wave from a transducer through a coupling medium to a specimen under test. After interacting with the specimen, the wave propagates through the coupling medium to a receiving transducer and is converted to an electrical signal. The information presented to the observer by the electrical signal depends on each element of the system.

In this paper, we examine the role that the receiving transducer plays in ultrasonic measurements. The phase-sensitive nature of conventional receiving transducers has for the most part, been neglected in nondestructive evaluations. This is shown to lead to significant data misinterpretation.

A new acoustoelectric transducer (AET) has been developed which is phase insensitive. Comparative data obtained with both conventional and AET transducers are presented and discussed. The AET is shown to produce more accurate measurements for the cases investigated.

45. Liber, T., Daniel, I. M., and Schramm, S. W., "Ultrasonic Techniques for Inspecting Flat and Cylindrical Composite Specimens," Nondestructive Evaluation and Flaw Criticality for Composite Materials, ASTM STP 696, Edited by R. B. Pipes, 1979, pp. 5-25.

Ultrasonic techniques are discussed for inspection and evaluation of flat and cylindrical composite specimens. Immersion ultrasonic techniques are described using a 5-MHz broad-band focused transducer in the pulse-echo mode. Two types of recording methods are employed, conventional pen-lift C-scanning and analog scanning, augmented with photographs of oscilloscope traces of the pulse at selected locations. The complete scanning system is described, including a fixture for scanning tubular specimens. The techniques discussed are applied to monitoring flaw growth in graphite/epoxy coupons of $(0/\pm 45/90)_s)_2$ and $(0_2/\pm 45)_2s$ layups with four types of initial flaws subjected to fully reversed spectrum fatigue loading. The flaws investigated are (1) circular hole, (2) embedded film patch, (3) internal ply gap, and (4) surface scratches. It was found that, in general, flaw growth is greater in specimens of $(0/\pm 45/90)_s)_2$ layup than in those of $(0_2/\pm 45)_2s$ layup. The residual tensile strengths for the preceding specimens, determined after four lifetimes of fatigue testing, are not significantly lower than the initial strengths.

10.0 ACRONMYS

AES	auger electron spectroscopy
BOP	buckling of panels
CLS	cracked lap shear
CODSTRAN	composite durability structural analysis
DCB	double cantilever beam
DDS	diaminodiphenyl sulphone
DIB	di-iodo-butane
DMA	dynamic mechanical analysis
DR-FTIR	diffuse reflectance-Fourier transform infrared spectroscopy
DSC	differential scanning calorimetry
EDX	SEM/microprobe energy dispersive X-ray analysis
ENF	end-notched flexure
ESCA	electron spectroscopy for chemical analysis
FALN	failure analysis logic network
FEP	fluorinated ethylene propylene
GPC	gel permeation chromatography
GR-EP, GR/EP, GR/E	graphite-epoxy
HPLC	high-pressure liquid chromatography
IR	infrared
MMF	mixed-mode flexure
MTS	mechanical testing systems
NASTRAN	NASA structural analysis program
NDE	nondestructive evaluation
NTIS	National Technical Information Service
PGC	pyrolysis-gas chromatography
PGC/MS	pyrolysis-gas chromatography/mass spectroscopy
SEM	scanning electron microscopy
SIMS	secondary ion mass spectroscopy
STAGS	structural analysis of general shells
STEM	scanning transmission electron microscopy
TEM	transmission electron microscopy
T _g	glass transition temperature

TGDDM-DDS tetraglycidyl diaminodiphenyl methane-diaminodiphenyl sulphone
TMA thermomechanical analysis
TTU through-transmission ultrasonics
VIPASA vibration and instability of plate assemblies including shear and anisotropy
WDX SEM/microprobe wavelength dispersive X-ray analysis
XPS X-ray photoelectron spectroscopy

ENM

IP - 86

DTIC